Spikes, synchrony, sequences and *Schistocerca's* sense of smell

David C. Sterratt

Doctor of Philosophy
University of Edinburgh
2001

Declaration

I declare that this thesis was composed by me and that the work contained therein is my own, except where explicitly stated otherwise in the text.

26th October 2001

(*David C. Sterratt*)

Acknowledgements

I would like to thank:

My supervisors. David Willshaw and Bruce Graham allowed me freedom to follow my own interests, but provided guidance, help, proofreading and encouragement when needed.

The Caledonian Research Foundation whose stipend supported me for three years.

My officemates. Gert Westermann, Will Lowe and Sarah Gingell made work in the office a pleasure. The time spent in enjoyable discussions at best tangentially related to work has probably been recouped in terms of time saved by knowing more about Neuroscience, UNIX, C/C++, Biology, Neural Networks, Statistics, and having grammatical queries resolved. Even if it hasn't been recouped, the friendship of my officemates and the atmosphere of mutual support helped me through the more depressing moments.

Other colleagues in Cogsci/CNS/ANC such as Stephen Eglen, the local emacs guru, Nicola van Rijsbergen who organised the Temporal Encoding Workshop with me, and the residents of 1 Buccleuch Place who shared in the delights of rat infestations and building works.

The secretarial staff in Cogsci/CNS/ANC. Betty Hughes, Dyane McGavin, Rosanna Maccagnano, Emma Black and Fiona Jamieson have been unfailingly helpful and cheerful.

Thomas Wennekers who has engaged in helpful discussions and commented on my work.

Laura who has suffered my ever-shifting but ever-imminent deadlines, has consoled me and encouraged me, and has done far more than her share of housework.

Abstract

This thesis starts from the assumption that individual neuronal action potentials (spikes) have computational and dynamical significance. Two of the types of activity that networks of spiking neurons can engage in are sequences and synchrony. The first part of the work reviews the role spikes, sequences and synchrony play in coding, dynamics and learning in the nervous system and models of the nervous system. Models of spiking neurons, especially the spike response model (SRM), feature strongly, as do synfire chains, a form of spatiotemporal sequence.

A methodology chapter deals with the problem of efficient simulation of networks of threshold-fire neurons such as integrate-and-fire (IF) neurons and SRM neurons. I show that networks of SRM neurons can be simulated with larger time steps than are required for numerical integration of equivalent networks of IF neurons. I extend an interpolation method for more accurate simulation of IF neurons to noiseless and stochastically-firing SRM neurons, and show that a network of noiseless, interpolated SRM neurons can be simulated with larger time step than the equivalent network of interpolated IF neurons.

Synfire chains can be learned with a temporal learning rule and a supervised training protocol. I extend previous analyses of the speed of recall of a synfire chain by (a) explicitly including the speed at which the synfire chain was trained and (b) performing an analysis on a synfire chain comprising discrete neurons rather than starting from a continuum approximation. I conclude that synfire chains can be recalled much faster than the speed at which they were trained.

The final part of the thesis is a modelling study of a system that incorporates spikes, sequences and synchrony, the olfactory system of the locust *Schistocerca gregaria*. Building the model leads to the problem of setting the mean weights in a network of reciprocally-connected excitatory and inhibitory spiking neurons on the basis of the desired oscillation time period and phase lead of the excitatory neurons over the inhibitory neurons. The solution to this problem includes a generalisation of a locking theorem from the literature to certain types of networks with nonuniform connections. Finally, I integrate the theoretically-determined mean weights into the locust model and present simulation results from it.

Contents

List of Notation

β ..... The inverse temperature of the escape rate function $\tau^{-1}(h)$. *Page 36*

c ..... The synchrony coefficient of the starting activity of the uniformly connected network. *Page 91*

C ..... The membrane capacitance. *Page 25*

Δ^{ax} ..... The axonal transmission delay. *Page 41*

Δ^{dend} ..... The dendritic transmission delay. *Page 41*

$\delta(\cdot)$ ..... The Dirac δ-function. *Page 31*

$\varepsilon(t)$ ..... The PSP function of a neuron. *Page 32*

$\eta_i(t)$ ..... The refractory potential of an SRM neuron. *Page 32*

$\gamma_i(t)$ ..... The PSC function of ith IF neuron. *Page 31*

$\Gamma(t)$ ..... The potentiation function. *Page 41*

$\mathcal{G}_l$ ..... The set of neurons in the lth group *Page 158*

$\overline{g}_{\mathrm{L}}$ ..... The leakage conductance *Page 26*

$\overline{g}_{\mathrm{Na}}$ ..... The sodium conductance *Page 26*

$\overline{g}$ ..... The maximum synaptic conductance. *Page 29*

$h_i^{\mathrm{ref}}(t)$ ..... The refractory potential of SRM neuron i. neuron. *Page 32*

$h_i^{\mathrm{syn}}(t)$ ..... The synaptic potential of SRM neuron i. *Page 32*

I^{ext} ..... The external input current. *Page 25*

I^{mem} ..... The membrane current. *Page 25*

I^{syn} ..... The synaptic current. *Page 25*

J_{ij} ..... The weight (synaptic efficacy) from the jth to the ith neuron. *Page 6*

$\kappa(t^{\text{post}}, t^{\text{pre}})$ .... The value of the PSP evoked in a postsynaptic neuron that fired t^{post} ago by a presynaptic neuron that fired t^{pre} ago. *Page 34*

μ ..... Index of a pattern. *Page 49*

N ..... The number of neurons in a network. *Page 4*

n ..... The number of neurons in a node of a synfire chain. *Page 189*

N_R ..... The number of neurons recorded from. *Page 189*

ν ..... Index of a pattern. *Page 49*

P ..... The number of links in a synfire chain. *Page 189*

$P^{\text{F}}[t; \delta t]$ ..... The probability of an SRM neuron firing in the time interval $[t, t+\delta t]$. *Page 36*

$P_2^{\text{F}}[t, t^{(1)}]$ ..... The instantaneous probability of an SRM neuron spiking at time t having last spiked at $t^{(1)}$. *Page 36*

S_i ..... The activation value of the ith unit in a Hopfield network *Page 6*

Σ ..... The synchrony measure of an exatly-solved network of spiking neurons. *Page 92*

$\hat{\Sigma}$ ..... The synchrony measure of a simulated network of spiking neurons. *Page 92*

T ..... Length of time summed over when calculating the membrane potential. *Page 91*

τ ..... Alpha-function time constant. *Page 29*

τ_0 ..... The time constant of the escape rate function $\tau^{-1}(h)$. *Page 36*

τ_1 ..... The first time constant of a double exponential EPSC or EPSP. *Page 91*

τ_2 ..... The second time constant of a double exponential EPSC or EPSP. *Page 91*

$\tau^{-1}(h)$ ..... The escape rate function of a neuron. *Page 36*

τ_{m} ..... The membrane time constant. *Page 30*

ϑ ..... The threshold of a neuron. *Page 30*

$t_i^{(f)}$ ..... The fth last firing time of the ith neuron. *Page 29*

V ..... The membrane potential of a neuron. *Page 30*

V_{K} ..... The potassim reversal potential *Page 26*

V_{L} ..... The leakage reversal potential *Page 26*

V ..... The membrane potential. *Page 25*

V_{Na} ..... The sodium reversal potential *Page 26*

V^{rev} ..... The synaptic reversal potential. *Page 29*

ξ_i^μ ..... The activity of the ith neuron in the μth pattern of a sequence. *Page 49*

List of Abbreviations

AL ..... antennal lobe

ANN ..... artificial neural network

CF ..... contextual field

CNS ..... central nervous system

CPG ..... central pattern generator

EPSC ..... excitatory postsynaptic current

EPSP ..... excitatory postsynaptic potential

GABA ..... γ-aminobutyric acid

IF ..... integrate-and-fire

IPSP ..... inhibitory postsynaptic potential

ISI ..... interspike interval

JPSTH ..... joint peri-stimulus time histogram

KC ..... Kenyon cell

LFP ..... local field potential

LGN ..... lateral geniculate nucleus

LN ..... local neuron

LPL ..... lateral protocerebral lobe

LTD ..... long term depression

LTP ..... long term potentiation

MB ..... mushroom body

NMDA..... *N*-methyl-D-aspartate

OB..... olfactory bulb

PN..... projection neuron

PSC..... postsynaptic current

PSP..... postsynaptic potential

PSTH..... post stimulus time histogram

PTSP..... precisely timed spike pattern

RF..... receptive field

RK2 ..... second order Runge-Kutta integration

RN..... receptor neuron

SRM..... spike response model

STDSP ..... spike timing dependent synaptic plasticity

STM..... short term memory

V1..... primary visual cortex

Chapter 1

Introduction

How does the nervous system compute? What is the neural code? In the 1920s, Adrian and Zotterman (Adrian, 1928) showed that the phenomenon of electrical *spikes* is an important element of the code. Spikes are spatially- and temporally-localised travelling pulses in the membrane potential. They all have very similar amplitudes and shapes and can travel long distances through nervous tissue. Although not all neurons spike, the vast majority of neurons in vertebrate nervous systems produce spikes, as do a good proportion in invertebrate systems. How does the nervous system use these spikes?

One school of thought says that spikes are simply a consequence of the need to propagate information over long distances and that the nervous system has to work around this need. In this picture — called *rate coding* — the nervous system averages the number of spikes over space and time to produce a firing rate, which it then interprets.

The other school of thought takes the point of view that whatever the evolutionary origin of spikes, the nervous system tries to make as much use of them as possible, and averaging over lots of them is simply wasteful. Advocates of *temporal encoding* argue that the timing of individual spikes both in single neurons and across populations can encode information and be used for processing. They also tend to argue that rate-coders have not developed

> ...the flavour of thinking needed to exploit the possibilities of temporal organization. It is perhaps closest in kinship to the dying art of railway planning, in which awareness of the organizing (or disorganizing) power of small changes in timing used to be a dominant intuition. (MacKay, 1962, p. 44)

There is strong evidence for both types of coding in different parts of the nervous system. Indeed, rate coding is not incompatible with certain forms of temporal coding. I side with the temporal encoders, however, in believing that the flavour of thinking

necessary to exploit the possibilities of temporal coding and processing has not been sufficiently developed.

Although the rate versus temporal *coding* debate has been very vigorous, the rate versus temporal divide goes further. It has been shown theoretically that the *dynamics* of networks of spiking neurons are much richer than those of traditional artificial neural network (ANN) units. Recent experiments have shown that *learning* at synapses depends on the timing of individual pre- and postsynaptic spikes, rather than their firing rates, as was thought previously.

1.1 Aim of the thesis

The initial aim of my thesis was to discover more about how the timing of spikes can be used to *process* or *encode* information. However, as time as gone on, the aim of the thesis has shifted towards the *dynamics* of networks of spiking neurons and how they *learn*.

We might regard the processing and encoding aspects of neural networks — the neural code — as the holy grail of brain research and the question of the mechanics underlying processing and encoding as subsidiary. However, I believe there are conceptual problems with studying the theory of encoding in central systems directly. I believe that studying the dynamics and learning presents a much more tractable way into the problem.

1.2 Overview of the thesis

The first three main chapters are mainly review chapters, although I will also introduce some technical prerequisites for the later chapters.

Chapter 2 deals with *spikes*. I begin with the history of the spike, or action potential. I then move onto the various ways in which the nervous system might interpret the spiking activity of other neurons, in other words, how spikes might encode information. Models of spiking neurons play an important role in this thesis. Accordingly, a large amount of chapter 2 is devoted to models of spiking neurons from the very realistic Hodgkin-Huxley model to the less realistic integrate-and-fire model. The spike response model is a flexible model that can lie more or less anywhere between these two models. I go on to review recent work that shows that, contrary to the prevailing view for the last twenty-five years, the precise timing of individual spikes is important for learning. I will consider briefly how the dynamics of networks of spiking and rate-based neurons

differ, and then go onto consider the difficult issue of what constitutes "coding".

In chapter 3 I consider *sequences*. By sequences I mean sequences of patterns, or, equivalently, *spatiotemporal* patterns. It is clear that networks that produce and recognise sequences must exist in nature. I review some of the work done on learning and recalling various types of spatiotemporal patterns. This turns out to be very related to some classic ANN models. A particular type of spatiotemporal pattern is the synfire chain. I describe synfire chains and weigh the experimental evidence for and against them. Although the evidence for them is not conclusive, synfire chains still merit the theoretical study of their dynamics and learning; I go on to review the work so far.

Chapter 4 deals with the final theme of this thesis, *synchrony*. Synchrony often occurs with, and is confused with, oscillations; I try to explain the difference between the two. I consider there to be two main forms of synchrony: stimulus-locked synchrony and stimulus-independent synchrony. The former type of synchrony has been observed in the auditory system and is uncontroversial. The role of the latter type is less clear and has been the subject of much speculation. There is also a good deal of experimental evidence that is consistent with the idea that synchrony encodes the parts of distributed representations which belong together — the binding problem. I will present some of the work on how both rate-based and spike-based models synchronise and desynchronise and introduce a useful theorem that will be particularly relevant later on in the thesis.

Chapter 5 is methodological in nature. In it, I extend work done on simulating integrate-and-fire neurons more efficiently to spike response model neurons. I also extend the method to cope with a certain kind of noise. Although this chapter stands on its own, I use the methods developed in it for simulations later on in the thesis.

The next four chapters are the theoretical and modelling parts of the thesis.

In chapter 6 I investigate sequence learning. In particular, I investigate how the speed at which a synfire chain was learned affects its speed of recall. I conclude that such sequences will be recalled much faster than they were learned.

The motivation behind chapter 7 is to investigate how spikes, sequences and synchrony interact in a real system. The olfactory system of the desert locust *Schistocerca gregaria* provides an intriguing example of such a system. Although there is a good deal of network-level physiological data from the system, the mechanism of the activity of the locust olfactory system is unknown. This justifies building a "bottom-up" model of the locust olfactory system, which I do on the basis of the detailed anatomy and physiology presented earlier in the chapter. In the course of building the model I encounter a problem of how to set the values of one group of parameters, the mean

weights between different types of units. There are, however, some unused physiological constraints, which should constrain the mean weights.

Solving this problem turns out to be somewhat involved, so I devote the whole of chapter 8 to it. In the process of doing so I generalise the locking theorem due to Gerstner et al. (1996b), which states under what conditions *uniform* networks of spiking neurons synchronise, to certain types of *nonuniform* networks. The solution to the problem reveals some unexpected results about the time period and relative phase of firing of groups of excitatory and inhibitory neurons.

In chapter 9 I integrate the theoretical results of the previous chapter into the model developed in chapter 8.

Finally, in chapter 10, I list what has been achieved in this thesis, what implications this has for neuroscience, and suggestions for further work.

1.3 Artificial neural networks

This section gives an overview of some of the artificial neural network (ANN) ideas and terminology used later on in the thesis. I outline the elements common to all ANNs in section 1.3.1. Section 1.3.2 deals with recurrently-connected neural networks and how they can be trained to store patterns. In section 1.3.3 I describe feedforward networks and how they can be trained using the delta rule and the backpropagation rule. Hertz et al. (1991) provide extensive coverage of the ideas presented in this section.

1.3.1 The elements of artificial neural networks

Artificial neural networks comprise *units* linked by *connections*. Each unit has a *state* or *activation* associated with it; this may be binary or real-valued. In general the activation of each unit could be a nonlinear (and possibly stochastic) function of all of the activations of all units in the network at all previous points in time. In practice, simpler models provide enough complexity to study.

Common to all the ANNs presented here is the modelling of connections by a real-valued or binary weight and calculation of the *input* to each unit as the weighted sum of the activations of other units in the network. We can represent this in the equation

$$h_i(t) = \sum_{i=1}^{N} w_{ij} x_j(t) - \vartheta_i \ , \tag{1.1}$$

where $h_i(t)$ is the input to the ith unit in a network of N neurons at time t, $x_i(t)$ is the activation of each unit, w_{ij} is the weight of the connection from the jth to the ith

unit and the optional term ϑ_i is the *threshold.*

The activation of each unit can be computed from its input either deterministically or stochastically. In the deterministic case, it is a function of the input:

$$x_i(t+1) = g(h_i(t)) \ . \tag{1.2}$$

The *activation function* $g(\cdot)$ is often a nonlinear function such as a sigmoid $g(x) = 1/(1+\exp(-2\beta h))$. It may be a Heaviside (step) function

$$\Theta(x) = \begin{cases} 0 & x < 0 \\ 1 & x \geq 0 \end{cases} \ . \tag{1.3}$$

In this case the unit is one when the input $\sum_j w_{ij}x_j$ exceeds the threshold ϑ_i and is 0 otherwise. In the stochastic case, the units are generally binary-valued and the probability of a unit being on is a function of its input.

Artificial neural networks come in a variety of different architectures. *Feed-forward* networks can be described as a number of layers, with the units of each layer projecting to units in the next. The first layer serves as an input layer and the final one as an output layer. Networks in which there at least one loop of connections are called *recurrent* networks.

Recurrent networks are dynamic: given starting unit activations, the state of the network (as described by the activations of all its units) does not necessarily remain static. As with all dynamical systems, the state of the network will either relax to a steady state (stable attractor), cycle periodically through a number of states (limit cycle) or follow an aperiodic orbit in state-space (chaotic attractor). The way in which the units are updated may affect the dynamics and is therefore important. When the network is updated *synchronously* (for example Little, 1974) the activation of all units is calculated from the activations of all units at the previous time step. In *asynchronous* update (for example Hopfield, 1982), units are chosen at random and updated from the current activations in the network. By recasting the update of the activation of each unit as a differential equation, the network can be updated *continuously* (for example Hopfield, 1984).

1.3.2 The Hopfield Model

Hopfield (1982) studied how to store binary patterns in a fully-connected, recurrent network comprising binary units and asynchronous update. A similar network with synchronous update had been studied earlier (Little, 1974; Little and Shaw, 1978), but the network came to prominence after Hopfield's analysis.

The network is described as above, except that in the following I will use the statistical Physics convention of denoting the activation of unit i by S_i and the weights by J_{ij}. The activations can take the values $+1$ or -1, and are analogous to nuclear spins and the weights are analogous to magnetic coupling between nuclear spins. As before, each unit receives an input h_i that depends on the weighted activity of the other units and the threshold is 0:

$$h_i(t) = \sum_{i=1}^{N} J_{ij} S_j(t) \ . \tag{1.4}$$

Each of P patterns μ is described by a vector with elements ξ_i^μ. Its elements can take the values 1 or -1 and there are equal numbers elements with either value. The weights are set using the learning rule:

$$J_{ij} = \frac{1}{N} \sum_{\mu} \xi_i^\mu \xi_j^\mu \ . \tag{1.5}$$

This rule is broadly based on the ideas of Hebb (1949) in that pre- and postsynaptic activity lead to potentiation of a synapse.

Hopfield (1982) showed that the learning rule tends to lead to the deterministic version of the network with asynchronous update settling into stable *attractor states* where the activations of the units of the network are closely aligned with one of the patterns. If the network is initialised so that its activity is similar to one of the patterns (this could mean a degraded version of the pattern or part of the pattern), the network will tend to relax towards the complete pattern. Amit et al. (1985a,b) studied a version of the network that used stochastic units whose randomness was controlled by a pseudo-temperature. Their rigourous statistical mechanical analysis showed that: asynchronous update and synchronous update lead to similar results; that if the units are too noisy (that is high pseudo-temperature), the network activity is completely disordered; and that at low pseudo-temperatures (that is, less noisy units) superpositions of patterns are also stable states of the network. Furthermore, they shoed that the *capacity* of the network (the number of patterns that can be stored before the stored patterns become unstable) was about $0.14N$

In the deterministic case, we can see why the attractor states should be stable by a simpler signal-to-noise analysis (Hertz et al., 1991). Suppose the network is in the state corresponding to pattern ν, so that $S_i = \xi_i^\nu$. The activation will be given by

$$h_i^\nu = \frac{1}{N} \sum_j J_{ij} S_j \tag{1.6}$$

$$= \frac{1}{N} \sum_j \sum_\mu \xi_i^\mu \xi_j^\mu \xi_j^\nu \tag{1.7}$$

$$= \xi_i^\nu + \frac{1}{N} \sum_j \sum_{\mu \neq \nu} \xi_i^\mu \xi_j^\mu \xi_j^\nu \ . \tag{1.8}$$

The final term is called the crosstalk term. For uncorrelated patterns, it will be distributed binomially around a mean of zero with a standard deviation of $\sqrt{\frac{P}{N}}$. For small numbers of patterns the activation of units that should be on (activity of 1) will be close to 1 so these units will remain on as their activation is positive. Similarly, units that should be off will remain off. For higher numbers of patterns, the spread of activation will be greater, and the lower tail of the distribution centred on activation of 1 will creep below zero, meaning that some units that should be on will be turned off. Similarly, some units that should be off will be turned on, and above a critical value of P/N the recall of patterns will become unstable. The capacity calculated using this method is similar that of Amit et al. (1985b).

1.3.3 Feedforward neural networks

Another type of network architecture is connected in a feedforward fashion, rather than recurrently. The simplest, one layer, feedforward network comprises input units with activities x_j which are connected by weights w_j and an output unit whose activity is

$$y = g\left(\sum_j w_j x_j\right) \ , \tag{1.9}$$

where the function $g(x)$ is a squashing function, typically a threshold function or a sigmoid function.

When the squashing function is a threshold function, the network is known as a *perceptron*. One application of the perceptron is as a classifier of patterns into one of two groups. To set the weights of the perceptron so it acts as a classifier, it is trained on a set of pairs of input vectors x_j^μ and their desired classifications t^μ. At each time step the weights are incremented by an amount

$$\Delta w_j \propto -(y^\mu - t^\mu) x_j^\mu \ . \tag{1.10}$$

This rule, known as the *delta* rule, says that if the input is positive and the target value is greater than the actual output, the weight should be increased so as to increase the output. The amount the weight is increased is proportional to the discrepancy between the target and the output and to the size of the input, since it is more important to alter the weights from the input units that give the greatest contribution to the output.

The perceptron is rather limited as a classifier, as it can only separate certain types of patterns, namely those that are linearly separable. To separate more complex groups

of patterns, we can add a *hidden layer* between the input and output layers containing units with activities u_i. The weights from the first layer to the hidden are v_{ij} and the weights from the hidden layer to the output layer are w_{ij}. The weights from the hidden layer to the output layer can be trained as before. With sigmoidal units, change in the weights upon presentation of a pattern μ is

$$\Delta w_{ij} \propto -\underbrace{(y^\mu - t_i^\mu) y_i^\mu (1 - y_i^\mu)}_{\delta_i^\mu} u_j^\mu \ . \tag{1.11}$$

However, there are no target values for the weights from the input layer to the hidden layer, so the same rule cannot be used there. The solution to this problem is the *backpropagation* algorithm (Rumelhart et al., 1986). The learning rule for the units from the input to hidden layers is given

$$\Delta v_{jk} \propto -\left(\sum_i w_{ij} \delta_i^\mu \right) u_j^\mu (1 - u_j^\mu) x_k^\mu \ . \tag{1.12}$$

Here, for each hidden unit, we have replaced the difference between the target and desired value by the sum of error terms from the output units of that hidden unit (the first term in brackets). Hence the error has been backpropagated.

All the forms of learning discussed so far have been *supervised* learning, in which the knowledge of the inputs and the corresponding desired outputs is known to the learning rule. The complement to supervised learning is *unsupervised* learning. Here there are no desired outputs presented at the same time as the inputs; the learning rule simply works on the activities of the output units caused by the inputs and the current weights. Networks trained in an unsupervised fashion learn to pick out different statistical features of the input vectors, depending on the network architecture and the learning rule.

An example of an unsupervised network is a one-layer network like the perceptron described above, but with a linear activation function $g(x) = x$. If this network is trained with a Hebbian learning rule

$$\Delta w_i \propto x_i y \ , \tag{1.13}$$

then it learns to find the first principal component of a set of data points with zero mean.

Chapter 2

Spikes

Since the starting point of much of the work in this thesis is the action potential, or spike, it seems appropriate to start off by focussing on spikes. This introductory chapter deals with how spikes encode information, how spiking neurons can be modelled, how networks of spiking neurons learn, and how networks of spiking neurons behave.

Before dealing with spikes, it is necessary to know what neurons and synapses are. I outline this in slightly historical fashion in section 2.1. In section 2.2 I give a brief historical overview of the spike.

Individual spikes can offer many possible ways of encoding information, learning synaptic strengths and embodying network dynamics. Despite this, most research since Adrian first recorded action potentials has focussed on the time-averaged firing rate of neurons rather than their individual spikes. Section 2.3 gives a working definition of rate codes and temporal codes, and presents some temporal codes found naturally.

Models of spiking neurons are useful for a number of reasons, not least because they allow us to investigate the dynamics of networks of neurons. In section 2.4 I focus on models of spiking neurons, starting from the most complex and realistic point neuron model, the Hodgkin-Huxley model, going to arguably the simplest model, the IF model, and ending up with a simple extension of the IF model that can be used to model neurons approaching the complexity of the Hodgkin-Huxley model.

Recent work has shown that the timing of individual spikes is important for learning and synaptic adaptation. Section 2.5 explains how, and relates the modern temporal learning rule to Hebb's rule.

The dynamics of networks of spiking neurons are potentially much richer than those of graded response units. For example, they may synchronise on a millisecond timescale and can support sequences of precise firing patterns. Section 2.6 will outline these possibilities and present the results of recent theoretical work on network synchrony

and the response of population firing rate to input.

2.1 Neurons and synapses

This section gives a short overview and history of the neuron and its logical counterpart, the synapse. Unless otherwise stated this information is based on Shepherd (1994).

In 1865 Otto Dieters made first observations of neurons in which their defining features were apparent. Figure 2.1 shows a modern cartoon picture of a group of neurons. The central part of a neuron is the cell body or *soma.* From the soma protrude two types of *processes.* The first type are thin and branch many times. Because of their similarity to branches they became known as *dendrites*; all the dendrites are sometimes referred to as the dendritic arborisation. The second type is a single, unbranched tube called an *axon* (originally it was known as the "axis cylinder").

Dieters' observation did not, however, make it clear that the neuron was a single cell. One theory — the reticular theory — held that the nervous system must be continuous like arteries and veins of the blood system. Techniques for staining single cells came in 1885 when Camillo Golgi discovered how to stain individual neurons in tissue. Santiago Ramón y Cajal took up these methods, and worked to stain many cells in the nervous system. He believed in the *neuron doctrine*, namely that the entities he was staining were individual cells, that nerve signals passed through the dendrites and axons, and that signals passed between cells where axons and dendrites met. In 1891 evidence from Cajal's anatomical preparations finally established the neuron doctrine and Wilhelm Waldeyer coined the term *neuron* for nerve cell.

As with all cells, neurons have an electrical potential difference across their membrane called the *membrane potential.* It arises from the permeability of the membrane to different types of ions and the ionic pump that maintains differences in the concentrations of various ions on either side of the membrane. In contrast to other cells, the membrane potential in neurons can vary quickly, allowing neurons to pass signals. The permeability of the membrane to ions is due to many types of *channels.* In neurons, these channels change their permeability in response to the membrane potential, certain types of ions and neurotransmitters, thus endowing neurons with complex computational properties.

Traditionally, the membrane potential is measured with respect to the external medium. At rest the potential is negative. Increasing the potential makes it *less* negative and such a change is called a *depolarisation.* Making the potential *more* negative is called *hyperpolarisation.*

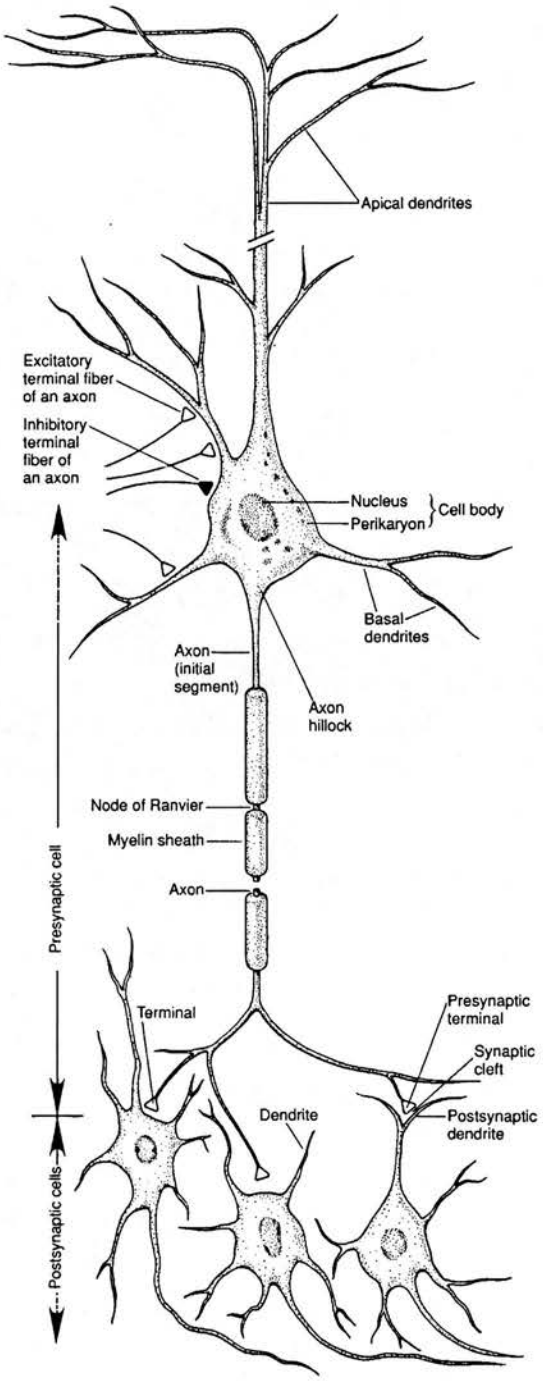

Figure 2.1: The neuron. From Kandel et al. (1995).

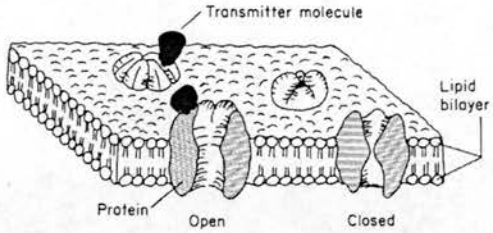

Figure 2.2: Section of cell membrane. The membrane is made up of a *lipid bilayer* that is somewhat permeable to ions. Distributed over the membrane are *ion channels* that can be open or closed to different ions. Their opening and closing can be controlled by the membrane potential, ionic concentrations and neurotransmitters. From Brodal (1992).

In 1897 Sherrington coined the term *synapse* for a connection from one nerve cell to another. His work in spinal reflexes led him to believe that synapses only work in one direction. This idea, which agreed with Cajal and van Gehuchten's theory that the dendrites and soma of neurons are its receptor parts and the axon is its effector part, became known as the *Law of Dynamic Polarisation.*

Synapses can be electrical or chemical. Electrical synapses are direct electrical connections between neurons that allow charge to flow directly. They can be bidirectional or unidirectional (an exception to the Law of Dynamic Polarisation). They are not very common in the vertebrate nervous system.

The vast majority of synapses in the vertebrate nervous system are *chemical synapses.* In chemical synapses there is a clear distinction between the *presynaptic* and *postsynaptic* terminals of the neuron. Inside the presynaptic terminal are many vesicles (sacks) of neurotransmitter. On depolarisation of the presynaptic terminal region, vesicles dock with the membrane wall, releasing neurotransmitter into the synaptic cleft. The neurotransmitter then diffuses across the cleft to the postsynaptic terminal where it docks with receptors sensitive to that neurotransmitter. Some of these receptors directly cause channels to open, and other receptors release second messengers into the postsynaptic terminal, that, in turn, dock with channels. The open channels allow ions to flow into or out of the postsynaptic neuron, thereby changing the postsynaptic membrane potential.

Synapses that allow through ions that tend to depolarise the membrane are known as *excitatory* synapses as extensive depolarisation leads to propagation of nerve impulses. Synapses that allow through ions that cause hyperpolarisation are called *inhibitory* synapses. Receptors are classified according to the neurotransmitters to which they are

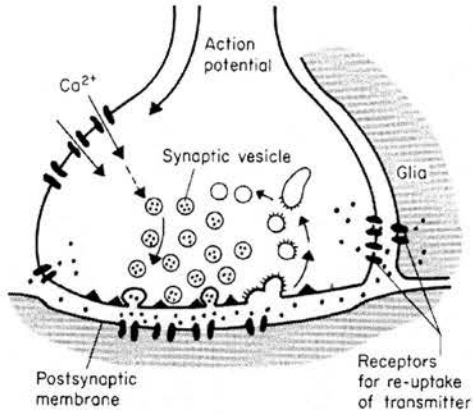

Figure 2.3: The chemical synapse and spike transmission. The synapse comprises a *presynaptic terminal* and a *postsynaptic terminal*, separated by the *synaptic cleft*. Neurotransmitter is stored in *vesicles* in the presynaptic terminal. When a spike arrives at the presynaptic terminal, it causes calcium ions to flow in. The calcium causes the vesicles to move to the presynaptic membrane, where they dock with the membrane and release their neurotransmitter into the cleft. The neurotransmitter diffuses across the cleft. When it arrives at the postsynaptic membrane it causes channels to open. From Brodal (1992).

sensitive. For example acetylcholine receptors are sensitive to acetylcholine. Receptors can be further subdivided according to different substances that activate them. For example nicotinic acetylcholine receptors are sensitive to nicotine but not muscarine whereas muscarinic acetylcholine receptors are sensitive to muscarine but not nicotine.

2.2 The action potential

In 1791 Luigi Galvani showed that frog muscles could be stimulated by electricity (Shepherd, 1994). This finding led to the belief that nerves communicated by "animal electricity". In the 1840s Carlo Matteuci and Emil du Bois Reymond established that nerve impulses involve real electricity. However, nerves are not just like electrical wires, as Herman von Helmholtz demonstrated in 1850 when he discovered that nerve impulses propagate relatively slowly. This implied that an active biological mechanism supported the propagation of nerve impulses, and led to the name *action potential* for the nerve impulse.

At the time these experiments were performed very little was known about the microscopic structure of the nervous system, so of necessity the measured quantities

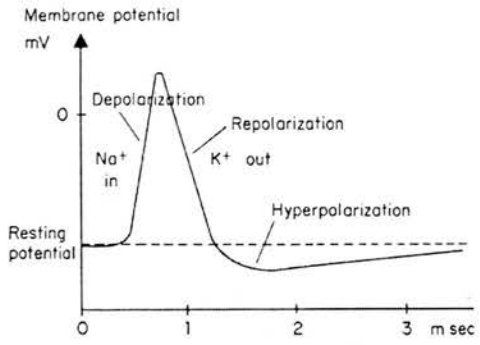

Figure 2.4: The action potential.

were the macroscopic properties of nerve fibres. Although the neuron doctrine became established at the end of the nineteenth century, it took another 20 years before the activity of single neurons was recorded. The limiting factor was lack of methods of low noise amplification (Rieke et al., 1997).

Adrian and Zotterman developed these methods. Their work (summarised by Adrian, 1928) showed that a characteristic response of sensory neurons (cutaneous receptors) to stimuli is a sharp depolarisation localised within about 1 ms of time. This characteristic response was the correlate of action potential, and became known as the *spike*, due to its appearance in a recording trace. They found that spikes are always similar in size and shape. This means that the only information the rest of the nervous system has from spiking sensory neurons is the times of their spikes.

Since then, spikes have been observed in many different types of cells in the nervous systems of vertebrates and invertebrates. They are generated in (or near) the soma of nerve cells, and propagate at a steady rate down their axons with no attenuation. Thus they provide a way of communicating over long distances in the nervous system. The Hodgkin-Huxley model (see section 2.4.1) describes the mechanism of propagation which relies on active, voltage-dependent, conductances in the cell membrane.

Although we believe action potentials are the dominant mode of communication between neurons, they are not the only mode. For example, receptors and horizontal and bipolar cells in the retina communicate by graded response potentials. One disadvantage of graded response potentials is that their amplitude decays after propagating short distances, so they are not suitable for long distance communication in the central nervous system (CNS).

2.3 Spike codes

If the timing of spikes is the main method of neuronal communication, how do they encode the information that neurons process? In section 2.3.1 I introduce the ideas of interpreting neuronal spiking activity as rate codes or temporal codes. In general, to make sense of a neuron's spikes, the experimenter and other neurons in the nervous system have to perform some sort of averaging. Section 2.3.2 defines three types of average and introduces a frequently-used experimental measure. This allows me to define the difference between rate codes and temporal codes more rigourously in section 2.3.3. In section 2.3.4 I present some examples from the nervous system where the timing of spikes does convey information. Up until this point, I will have been using the term "coding" rather loosely. Section 2.3.5 presents my thoughts on the definition of coding. I have not found a satisfactory general definition of coding in the nervous system, nor have I been able to produce one myself. However, I do reach the conclusion that network models are a valuable method of exploring the ways that neurons use spikes to process information.

2.3.1 Rate codes and temporal codes

Adrian and Zotterman (Adrian, 1928) found that frog cutaneous receptors responded with more spikes when the load on them was increased. Thus was born the idea of *rate coding*, the idea that the firing rate of neurons encodes information. The idea that rate coding is the main or only way that neurons encode information has been the dominant paradigm in electrophysiology since Adrian and Zotterman's discovery (Barlow, 1972; Rieke et al., 1997). Neurophysiologists have used it to elucidate much of the function of visual, olfactory, somatosensory and central systems. For example, the notion of feature selectivity in the visual system was found on the basis of rate coding.

Although rate codes have much explanatory power, sequences of spikes (spike trains) could encode much more information by using the *timing* of spikes, as a simple example shows. Consider a 100 ms long spike train. If we assume that the temporal resolution of the nervous system is about 2 ms, and that the maximum neuronal firing rate is 500 Hz, then there are 50 possible positions for spikes. Using a rate code the spike train could convey 51 different pieces of information, from zero spikes to 50 spikes. A code that uses the full potential of the spike train could encode up to 2^{50} pieces of information by treating the spike train as a binary number.

2.3.2 Averaging and spike train statistics

This section is intended as an introduction to the spike train analysis that is used in this thesis. For more comprehensive reviews, see Rieke et al. (1997) or Koch and Segev (1998), chapter 9.

When Adrian talked about a firing rate, he meant the number of spikes occurring in a certain period of time divided by the length of the time period. In other words he averaged the spike train across time. However, to obtain a rate we can also average across more than one neuron or more than one trial of an experiment. Thus there are three main ways of averaging, each of which roughly corresponds to a conventional meaning of the word "rate" (Gerstner, 1998):

Time averaging: Count the number of spikes in a time window and divide by the length of time to give a rate.

Trial averaging: Repeatedly measure spike trains produced under the same conditions to produce an average spike train.

Population averaging: Average the number of spikes across a population.

These averages are not mutually exclusive. For example, we can repeatedly count the number of spikes in a given time window after presenting a stimulus (time and trial averaging). Or we can count the number of spikes produced by a population of neurons in a given time window (time and population averaging).

One very useful combination of averages is time averaging in a sequence of small time bins and trial averaging (figure 2.5). When the origin of the time axis is locked to the occurrence of a stimulus, the resulting vector of spike counts is known as the post stimulus time histogram (PSTH) (Perkel et al., 1967a). The histogram is sometimes smoothed with a kernel such as a Gaussian (Richmond et al., 1987). We can think of the PSTH being the discrete approximation to an underlying "time-dependent rate" (Rieke et al., 1997).

On its own, the PSTH does not tell us about the relationship between spike times in a spike train. For example, in bursting neurons the firing rate might remain constant over a long time scale but the timing of spikes could be correlated on a short time scale within spike trains. To uncover features like this in the spike train, we must look at higher order statistics of spike trains.

The *autocorrelation* matrix, denoted by $C(t, t')$ is the next highest order statistic of spike trains. If the spike train is represented by $S(t)$, then the autocorrelation matrix

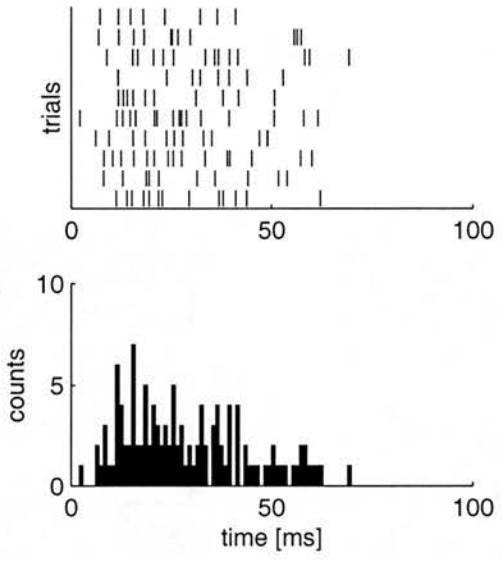

Figure 2.5: The post stimulus time histogram (PSTH). The top panel shows spike trains elicited in response to a stimulus at time 0. The bottom panel shows the PSTH resulting from counting the number of spikes in 1 ms bins.

is given by

$$C(t,t') = \langle S(t)S(t') \rangle \ , \tag{2.1}$$

where $\langle \cdot \rangle$ represents trial averaging. In principle, the $S(t)$ could be a function comprising delta functions at the spike times; however in practice it will be a vector of spike counts in time bins centred on t. Therefore the autocorrelation matrix will have the same number of rows and columns as there are time bins in the spike trains. Figure 2.6 gives examples of autocorrelation matrices generated by an integrate-and-fire model neuron (see section 2.4.4) with *stationary* and *nonstationary* spike trains.

Stationarity is a property of a stochastic point process, that is a process where indistinguishable events happen at randomly distributed points in time. It means that "the underlying probability distributions governing the times of occurrence of the point events do not vary with respect to an arbitrary translation of the time axis" (Perkel et al., 1967a, p. 395). Spike trains are examples of point processes and in the context of spike trains stationarity implies that the underlying firing rate must be constant. Spike trains that are not stationary are *nonstationary.*

We can make an important simplification if we assume that the spike train is sta-

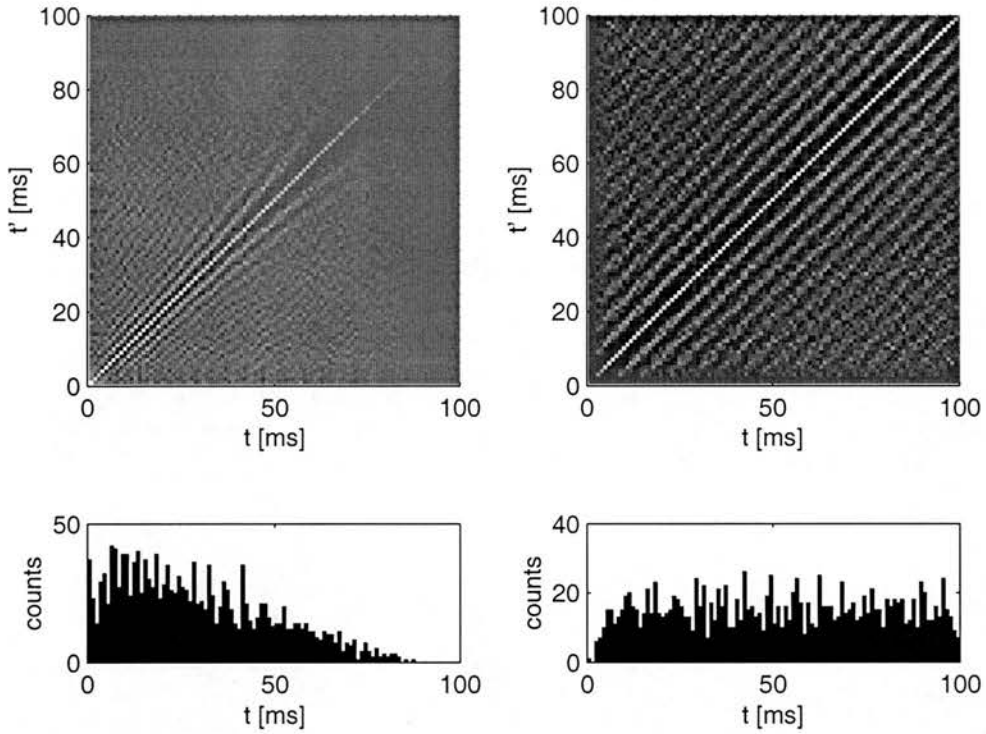

Figure 2.6: Two examples of the autocorrelation matrix of a randomly-generated spike train. The top panels are the autocorrelation matrices $C(t, t')$. The bottom panels contain the corresponding PSTH. *Left*: A non-stationary spike train. It is non-stationary, since the rate $r(t)$ is not constant. The matrix is not constant along its leading diagonals as it would have to be for $C(t, t') = C(t - t')$. *Right*: A stationary spike train. Here $r(t)$ is almost constant and there are the value of the matrix along the leading diagonals is almost constant. The spike trains were generated injecting current into a noisy integrate-and-fire (IF) model neuron. The membrane time constant of the neuron was 10 ms and its threshold was 1 (normalised units). The current decayed from 3 (normalised units) initially to 0 100 ms later in the non-stationary case and was held at 2 in the stationary case. The number of trials averaged over was 100.

tionary. Then (see Rieke et al., 1997, for a derivation) we can write

$$C(t,t') = C(t-t') \ . \tag{2.2}$$

We can see that this is the case in the correlation matrix corresponding to the stationary spike train in figure 2.6, since the value of the correlation matrix is constant along diagonals with a gradient of one.

Perkel et al. (1967a) named the quantity $C(t)$ normalised by the average firing rate the *autocorrelation function.* It is often referred to simply as the autocorrelation, and sometimes is called the *autocorrelogram.* Although it might be confused with the autocorrelation matrix, I shall also refer to it as the autocorrelation. In its normalised form, it gives the probability of a spike at $t+\tau$ given a spike at t and is sometimes referred to as the *conditional rate.* It is also common to subtract the square of the mean rate from $C(t)$ to give a function that tends to zero as t tends to infinity (Koch and Segev, 1998). For simplicity, I will deal with unnormalised quantities in this section.

Since the probabilities are stationary we can average over time to obtain a better estimate: $C(\tau) = \langle \overline{S(t+\tau)S(t)} \rangle$ (the horizontal bar denotes time averaging). This states explicitly that we are averaging over trials; in practice, there may be enough data to make averaging over trials unnecessary. We can express the time-averaged part of $C(t)$ as the more familiar conventional autocorrelation function[1]:

$$C(t) = \int_{-\infty}^{\infty} S(t+\tau)S(\tau)d\tau \ . \tag{2.3}$$

If we trial average over the activities of two neurons i and j we obtain the *cross-correlation* matrix (or function of two variables) $C_{ij}(t,t') = \langle S_i(t)S_j(t') \rangle$. Vaadia et al. (1995) call the cross-correlation matrix the joint peri-stimulus time histogram (JPSTH). By either name, the matrix has the same number of rows and columns as there are bins. As with the autocorrelation, if both spike trains are stationary the cross-correlation will depend only on the time difference between the t and t' and we can write the it as a function of the time difference, that is $C_{ij}(t,t') = C_{ij}(t-t')$. It is this function that is typically referred to as the cross-correlation function (Perkel et al., 1967b). As with the autocorrelation, the cross-correlation is often constructed from data using time-averaging.

The differences between time-averaging and trial averaging and between stationary and non-stationary spike trains are worth emphasising. There may be information in

[1]It is not clear whether the term autocorrelogram might refer to the purely time-averaged part of the autocorrelation (see, for example, Engel et al. 1990), though the terms autocorrelation and autocorrelogram seem to be used quite interchangeably.

the cross-correlation *matrix* that is missed in the cross-correlation *function* (Vaadia et al., 1995).

The interpretation of the cross-correlation is not always straightforward. A flat cross-correlation is a fairly good indication that the spike times between neurons are independent, since if we were to measure spike times from random instants in time (not necessarily spike times) we would see a flat distribution. A cross-correlation with one or more bumps in it indicates that the firing times of the two neurons are dependent on each other.

There are more measures of correlation of spike trains of different or the same neuron. For example the interspike interval (ISI) is similar to the correlation function, except that only interval between adjacent firings of the neurons are included.

2.3.3 The distinction between rate codes and timing codes

So far, I have used the terms rate code and temporal code rather loosely. The distinction between the two is, however, not obvious and there is not yet unanimity in the literature as to what counts as a temporal or rate code. Ultimately, the question is more one of semantics than of fact — what matters most is the methods by which spike trains from single neurons and populations of neurons are generated and analysed. Nevertheless, it is illuminating to consider the question briefly.

One approach is to look at encoding of time-varying stimuli in spike trains. Dayan and Abbott (2001) make the distinction between an *independent spike code*, in which the spike train is an inhomogeneous Poisson process generated from the time-dependent firing rate which is in turn a function of the stimulus, and a *correlation code*, in which the spikes are not encoded independently. An example of a correlation code would be if interspike intervals were used to encode information. It seems intuitive that an independent spike code should count as a rate code.

(In the case of an independent spike code, the autocorrelation would be flat in the case of a constant stimulus. In the case of a correlation code with interspike interval coding, we would expect to see peaks in the autocorrelation separated by the interval corresponding to the stimulus quantity.)

Dayan and Abbott argue that the issue of temporal versus rate coding arises when we come to measure the spike times of the spike train in order to extract the maximum amount of information from it. The resolution at which we have to look at the spikes determines whether we are dealing with a temporal code or a rate code. So, for example, if we have to measure spikes with millisecond precision, the code would count

as temporal, whereas if it suffices to measure spikes within a window tens of milliseconds long, the code would be a rate code. The problem with this definition is that it is not clear where the dividing line between temporal and rate lies. Furthermore, the resolution will depend on the frequency spectrum of the stimulus. If a signal with high-frequency components generated spike trains according to an independent spike code, we would require high temporal precision (at least as great as the inverse of the Nyquist frequency) in order to decode the spike train. Yet the spike train would have been generated in a way which intuitively feels like a rate code.

One solution to this problem is to compare the frequency spectra of the stimulus and spike train (or trial-averaged rate) (Theunissen and Miller, 1995). If frequency components of the response greater than the highest frequency present in the stimulus are required to extract maximal information from the spike train, the code counts as a temporal code; otherwise it is a rate code.

A problem with this definition of rate code is that it leads to decoding strategies that appear to be temporal being counted as rate codes. In the stimulus-reconstruction technique (Bialek et al., 1991; Rieke et al., 1997) the stimulus is estimated from a spike train by convolving the spikes with a filter constructed by comparing large amounts of stimulus and spike train data (see figure 2.7). This filter can be negative and vary sharply with time. Furthermore, the filter could quite short relative to the average interspike interval — there might only be a couple of spikes in the duration of one filter. The timing of spikes would therefore seem to be quite important — if they were randomly shifted by a fraction of the average interspike interval, we would expect the effect on the estimation to be much more catastrophic than it ought to be for a rate code. However, according to the definition of Theunissen and Miller, this counts as a rate code since convolution in the time domain is equivalent to multiplication in the frequency domain, so no frequency components of the spike train higher than the highest component in the (estimated) stimulus are used to decode the spike train. Another absurdity in this definition is that spike trains that have been generated using a form of correlation code can still be decoded adequately using a single filter, and therefore count as a rate code (Rieke et al., 1997).

Although somewhat paradoxical, I will stick with this distinction. It still leaves codes where nonlinear convolution (that is, using a filter that depends on the timing of two or more spikes) to count as "temporal codes".

So far, only single-neuron codes have been discussed. An important question is how to decode populations of neurons. Dayan and Abbott (2001) define an *independent-*

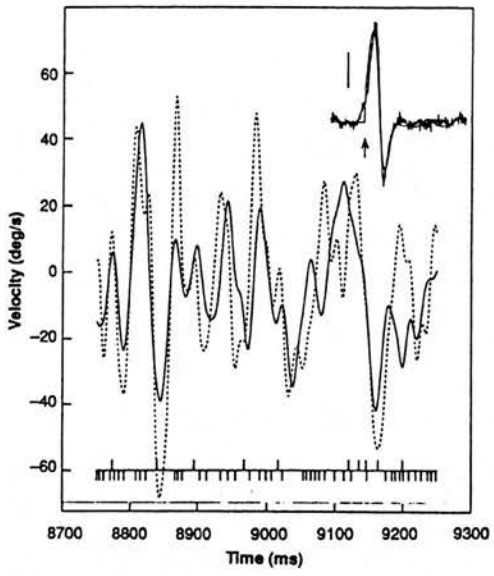

Figure 2.7: The reconstruction (solid line) of the time-dependent angular velocity signals (broken line) obtained by filtering the spike train of an H1 cell in the blowfly (*Calliphora erythocephela*) visual system. The upward spikes represent the response to the stimulus and the downward spikes represent the response to the negative of the stimulus. The reason for these two recordings is the asymmetric response of H1 cells. *Inset:* The filter used to reconstruct the response. From Bialek et al. (1991).

neuron code as one in which the spike trains of different neurons can be combined without taking into account correlations between different neurons. When correlations do have to be taken into account, the code is a *population-correlation code.* Synchrony and oscillations do not by themselves constitute a population correlation code; this is only the case if significant amounts of information can be shown to be conveyed by the correlations.

2.3.4 Examples of temporal codes

There are many different possible temporal codes, for example interval codes, latency codes, filtering codes and population synchrony codes (Bullock, 1993). Some of these codes involve decoding the output from more than one neuron and the codes do not always mutually exclude each other. Nevertheless, experimentalists have discovered systems in which interpreting the spike trains in ways other than the time-averaged rate provides more information about the stimulus. Here are some examples.

An example where the stimulus is aperiodic is the fly visual system, where the timing of spikes H1 cells encode the velocity of the visual field (Bialek et al., 1991; Rieke et al., 1997). The stimulus-reconstruction technique (see previous section) was used to estimate the stimulus from the timing of spikes in H1 cells (see figure 2.7).

Coding using spike timing does not seem to be limited to the vertebrates or systems with dynamic stimuli. In the locust olfactory system (to be discussed in detail in chapter 7) the excitatory neurons at the second stage of processing appear to encode odour identity with the spatiotemporal pattern of activation of excitatory neurons over a period of about 1 s (Laurent, 1996; Laurent and Davidowitz, 1994). In addition to the spatiotemporal pattern, oscillations are imposed on the activity. The oscillations seem to be important for refining the representation of the odour, as when they are pharmacologically abolished honeybees find it harder to discriminate between similar odours.

To conclude this section, there is now ample evidence for systems in which the timing of spikes in one neuron or across a population of neurons encodes more information than a time-averaged or population-averaged rate.

2.3.5 On the definition of coding

This section is rather tangential to the thesis, since the focus of the thesis is more on the way networks of spiking neurons work rather than what they encode. However, at this point it is worth noting that I have been using the terms *coding* and *rate code* and

temporal code rather loosely. Theunissen and Miller (1995) define the *coding problem* as follows:

> Deciphering the neural code at any particular location within a neural system can be reduced to three interconnected tasks, representing a qualitative characterization of the observed stimulus-response characteristics of the neurons under study. The first task is to determine the quantity and qualitative nature (such as the specific parameters characterizing a complex sensory stimulus) of the information encoded in the spike trains of the neuron or neuronal ensemble under study. The second task is to determine the nature of the neural symbols with which that information is encoded — that is, all of the information encoded in the *mean firing rates* of the cells, or is some significant proportion of the information encoded in more complex statistical features of the spike train *patterns*? The third task is to define relevant, objective measures of significance with which the information and neural symbols are correlated.

They define the second of the tasks — determining the nature of the neural symbols — as the *encoding problem.* I believe that deciphering the neural code in this way is reasonably tractable near the sensory periphery, but will be impossible in central systems. As Peter Dayan (personal communication) has pointed out, the problem lies with the first of the tasks, determining the stimulus-response characteristics of central neurons. Neurons deeper in the nervous system code for more than one thing. Although we might be able to find out one aspect it appears to code for, it is very likely that the cell is coding for many more things.

Is it possible to extend the definitions of encoding and decoding from the sensory periphery to central systems? Unless there is a direct behavioural route from perception to action we will not be able to tell exactly what sensory information the system encodes; there is no obvious "stimulus". It might be argued that we could proceed iteratively: If we know what all of a cell's presynaptic neurons are encoding, then we should be able to manufacture inputs to it that encode known information. This would certainly not be easy. In particular the procedure demands that we know all of the information a neuron encodes, and we are almost bound to "lose" features the further up the system we go. A more fundamental objection is that unmeasurable internal states — for example memory states — might also count as part of the stimulus.

Perhaps we could treat the stimulus of a particular neuron as the activity of all of its presynaptic neurons. In this case we would need to know the distribution of firing patterns of the neuron and its presynaptic neurons *in vivo* in order to decode the output spike train. We might be able to apply the stimulus reconstruction technique to

reconstruct the input spike trains (the stimulus). In many cases we might expect this to fail, since the neuron could be extracting features rather than trying to maximise information transmission. Also, this would not tell us what information the spike train stimulus represented in the first place.

An alternative approach for the cerebral cortex (and possibly other central systems) is to make the assumption that it behaves as a generalised computer and to investigate the modes of computation between the fundamental computing units. That is, assume that there are some underlying internal state variables that represent activation in a class of ANN that are represented by spike trains. For example, the firing delay of a neuron could represent activation in a feedforward network (Maass, 1997, 1996). Each hypothesis generates conditions that neurons must meet for that hypothesis to be true. For example if quantities are encoded in some way in the timing of spikes, neurons they project onto must be sensitive to these timings in order to use the information. Therefore, logically, we may be able to weed out some hypotheses experimentally, but we will not able to prove that any hypothesis is the true description of encoding.

Hypotheses about encoding are tied up hypotheses about the fundamental computing units. So we must hypothesise about what the activity of neurons encodes and the fundamental computing units themselves. Some hypotheses are:

- Groups of neurons could be the fundamental unit (Shadlen and Newsome, 1994). They would communicate by weighting each other's mean firing rates much as the neurons in many types of ANN analogue quantities. Some groups of neurons might serve as short term memory units (Amit, 1995).

- The time delay of spikes represents analogue activation of an ANN and neurons compute by producing appropriately delayed spikes on the basis of input spikes (Maass, 1997).

- Activity runs through chains of neurons which represent features. These chains can be dynamically linked to represent multi-featured objects and concepts (Bienenstock, 1995).

All these theories presuppose that the code is fairly uniform throughout at least large parts of the cerebral cortex. This is not an unreasonable assumption given the fairly uniform nature of the cerebral cortex. Also, the hypotheses are not be mutually exclusive; the different modes could operate in different areas of the cerebral cortex. I will return to some of these theories later on.

2.4 Models of spiking neurons

As a large part of this thesis will be on modelling networks of spiking neurons, now seems an appropriate time to introduce models of spiking neurons. I will proceed to present the membrane potential equation, the biophysical foundation of all spiking neuron models, in section 2.4.1. The classic realistic neuron model that uses the membrane potential equation as its basis is the Hodgkin-Huxley model, described in section 2.4.2. In section 2.4.3 I will discuss the ways of coupling together spiking neurons. The simplest spiking neuron model is the integrate-and-fire model, which I describe in section 2.4.4. In section 2.4.5 I describe a recent derivative of it, the spike response model. This model has the advantage of analytical tractability, and can easily incorporate noise.

2.4.1 The membrane potential equation

At the heart of the most realistic neuron models lies the membrane potential equation. It is derived by treating the soma or a dendritic or axonal segment of a cell as an electrical circuit comprising a resistor, a capacitor and a current source (see figure 2.8). This idea goes back at least as far as Lapicque (1907). The components are coupled in parallel, and represent: the resistance of the membrane, R, to current flow; the capacitance (the ability to store charge) of the membrane, C; the membrane current I^{mem} flowing into the cell through channels in the membrane; any synaptic current I^{syn} flowing through channels controlled by other neurons; and possibly an external current I^{ext}, injected by the experimenter. Together, these factors induce a membrane potential V that changes with time. From Kirchoff's first law and the relationship between current flowing into a capacitor and the voltage across it, we obtain the fundamental equation of excitable membranes:

$$C\frac{dV(t)}{dt} = -\frac{V(t)}{R} + I^{\text{mem}}(t) + I^{\text{syn}}(t) + I^{\text{ext}}(t) \ . \tag{2.4}$$

The differences between the neuron models using this equation are all in the membrane current term $I^{\text{mem}}(t)$.

2.4.2 The Hodgkin-Huxley model

The classic neuron model using this equation is the Hodgkin-Huxley model of the squid giant axon (Hodgkin and Huxley, 1952). Here the membrane current $I^{\text{mem}}(t)$ is the total current flowing through sodium, potassium and "leakage" channel conductances.

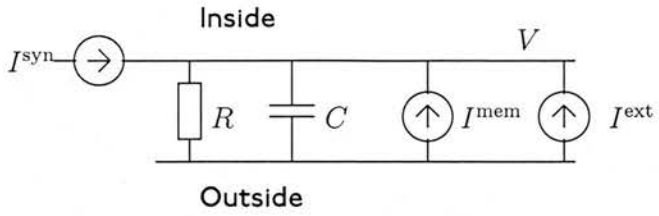

Figure 2.8: The membrane circuit. The lower line represents the outside of the neuron and has a potential of 0 mV. The upper line represents the inside of the cell and has a potential of V mV.

The current through the sodium conductance is $\overline{g}_{\text{Na}} m^3 h(V(t) - V_{\text{Na}})$ where $\overline{g}_{\text{Na}}$ is the maximum sodium channel conductance, m and h are state variables, $V(t)$ is the membrane potential and V_{Na} is the sodium *reversal* potential. The state variables are the solutions of rate equations of the form

$$\frac{dm}{dt} = \alpha_m(V)(1 - m) - \beta_m(V)m \ , \tag{2.5}$$

where the functions $\alpha_m(V)$ and $\beta_m(V)$ are found empirically by voltage-clamp[2] experiments. Each state variable ranges between zero and one, and we can imagine that they represent the probability that one of a number of "gates" that make up the channel is open. Thus we can view the sodium channel as comprising three m-type gates and one h-type gate, all of which have to be open in order for the channel to conduct. (Hodgkin and Huxley found the powers to raise the state variables to empirically and then proposed the explanation in terms of gates.)

The potassium channel conductance is proportional to one state variable n raised to the power four and has a maximum conductance of $\overline{g}_{\text{K}}$ and a reversal potential of V_{K}. The leakage current represents voltage-independent channels with conductance $\overline{g}_{\text{L}}$ that will tend to drive the membrane towards the resting potential V_{L}. Putting together the various currents gives the membrane current component of the Hodgkin-Huxley equation:

$$I^{\text{mem}}(t) = \overline{g}_{\text{Na}} m^3 h(V - V_{\text{Na}}) + \overline{g}_{\text{K}} n^4 (V - V_{\text{K}}) + \overline{g}_{\text{L}}(V - V_{\text{L}}) \ . \tag{2.6}$$

The Hodgkin-Huxley model accounts very well for the data from the squid giant axon. (For other types of neurons, different channel types and combinations of channel

[2]These experiments involve clamping the membrane potential at various voltages by controlling the current fed into the neuron by an intracellular electrode. Small changes in the voltage result in the conductances settling to a value that depends on the voltage. The time constant of the settling can be measured, and along with the new value of the state variable can give an estimate of the value of $\alpha(V)$ and $\beta(V)$ for a particular depolarisation.

types are needed.) Once all the functions and constants are known, the four coupled differential equations (one in V and the other three in the state variables m, h, and n) can be solved numerically. Injection of delta pulses of current into the model results in a discontinuous (step) increase in membrane potential. If this increase is below a certain level (known as the *threshold initial depolarisation*, Tuckwell, 1988b), the membrane potential decays directly back to its resting level. If the increase is above the threshold initial depolarisation, the membrane potential will rise steeply (or *depolarise*) to about 40 mV, then return quickly to resting potential (*repolarise*), overshoot the resting potential (thus *hyperpolarising* the membrane) and gradually return to the resting potential. This process is known as an *action potential* and the sharply rising and falling parts of it occur within about 1 ms.

The reason why action potentials are generated can be understood as follows. When a external current causes the membrane potential to rise the value of m increases (sodium channels open). The dependence of m on the membrane potential is roughly sigmoidal. As the membrane potential reaches the sharply rising part of this sigmoid curve, many sodium channels start to open. As the sodium reversal potential is much higher than the resting potential, the voltage increases further causing more sodium channels to open. This snowball effect produces a sharp rise in the membrane potential. The slower potassium channels (the n state variable) start to open soon after this rise and allow current to flow out of the neuron because of the low potassium reversal potential. Also the inactivating variable h decreases as voltage increases, adding to the effect. The membrane potential quickly swoops back down to its resting level, overshooting somewhat to hyperpolarise the neuron. For a period, it is impossible to generate a new spike by injecting current (absolute refractory period); thereafter the trigger voltage required to spike is higher than from the resting state (relative refractory period). Eventually all the state variables return to their resting states and the membrane potential returns to its resting level.

The equations can be extended and solved to show that spikes tend to propagate along axons or dendrites at a fairly constant rate determined by the passive parameters of the axon such as the membrane resistance, the internal resistance and the membrane capacitance, as well as the active parameters such as $\alpha_m(V)$ and $\beta_m(V)$.

Although these equations were designed to deal with the squid axon, they can in principle be extended to deal with any neuron in nervous system by including different types of channels. As well as voltage-dependent channels, as modelled by Hodgkin and Huxley, non-voltage mediated effects (such as the effect of calcium concentration) can

also be built into such models.

A further generalisation of the Hodgkin-Huxley model is to models of neurons with spatial structure. In compartmental models, the neuron is split up into many compartments which are assumed to be at the same potential throughout. Current can flow between compartments as well as through the membrane. With an extra term to describe the current from other compartments and extra terms to describe the effect of different conductances, equation (2.6) and equations of the form of (2.5) apply to each compartment. Neurons can be simulated to levels of realism constrained only by computational resources and physiological knowledge. It is also possible to simulate networks of compartmental neurons, though computational limitations tend to dictate that each neuron has fewer compartments.

Although the Hodgkin-Huxley model is realistic, it is also rather complex and can only be solved analytically in a handful of cases (Tuckwell, 1988b). Consequently, there have been a number of attempts to simplify it. One approach is to reduce the number of differential equations by making approximations and reducing the number of variables. FitzHugh-Nagumo neurons (FitzHugh, 1961) exemplify this method. Kepler et al. (1992) have proposed a systematic way of reducing conductance-based models.

Although in the Hodgkin-Huxley model there is no well-defined threshold potential at which an action potential is produced, the "point of no return" is similar under a variety of input conditions. Another class of models, *threshold-fire* models, use this observation as well as the fact that the time course of spikes is always similar. Furthermore, in the region below the threshold voltage the behaviour of the membrane potential is a fairly linear function of input current; the nonlinearities created by the voltage-dependent conductances only come into play when the neuron spikes. Therefore it is possible to simplify the model by leaving out the voltage-dependent conductances and simply making the neuron spike when the membrane potential crosses a threshold. After spiking, the membrane potential is reset to its resting potential. There may also be an enforced refractory period during which the neuron cannot fire and a relative refractory potential during which the threshold is higher than normal so that the neuron is less likely to fire.

Although the former class of models are interesting, they do not simplify things as much as using threshold models does. As we will see, some threshold-fire models are quite a good approximation to Hodgkin-Huxley neurons, and by extension to real neurons. I will therefore concentrate on two of these models, the integrate-and-fire (IF) model (Lapicque, 1907; Tuckwell, 1988a) and the SRM (Gerstner, 1991). Before doing

so, I will discuss models of synapses.

2.4.3 Synaptic dynamics

The synaptic current can be modelled to varying degrees of realism. In general, the synaptic current from the jth to the ith neuron is given by

$$I_{ij}^{\text{syn}}(t) = g_{ij}(V_j, t)(V_i(t) - V_{ij}^{\text{rev}}) \tag{2.7}$$

where V_{ij}^{rev} is the postsynaptic reversal potential and $g_{ij}(V, t)$ is the synaptic conductance. The synaptic conductance may depend on a number of factors.

In very realistic models, the conductance $g_{ij}(V_j, t)$ is the solution of differential equations with terms depending on the presynaptic voltage. Ermentrout (1998) calls such synapses *gated* synapses.

A simpler way of modelling the conductance is to trigger a function of time alone whenever a spike arrives at the synapse:

$$g_{ij}(t) = \overline{g}_{ij} \sum_f s_j \left(t - t_j^{(f)}\right) \ , \tag{2.8}$$

where $s_j(t)$ is a synaptic gating variable, $\overline{g}_{ij}$ is the maximum synaptic conductance for the synapse and $t_i^{(f)}$ is the fth last firing time of neuron i. (We can therefore describe the spiking activity of a neuron i by the set of firing times $\left\{t_i^{(f)}\right\}$.) A typical gating variable is given by the alpha function (figure 2.9):

$$s(t) = \frac{t}{\tau} e^{-\frac{t}{\tau}} \Theta(t) \ , \tag{2.9}$$

where $\Theta(t)$ is the Heaviside (step) function (see section 1.3.2 for definition) and where τ is the time constant of the conductance. In this case the time course of the conductance change does not depend on the presynaptic membrane potential and we say the synapse is *ungated*. In either cases, the combination of conductance and voltage produces a postsynaptic current (PSC).

The maximum conductance $\overline{g}_{ij}$ may depend on the previous history of the synapse. In a somatic whole-cell recording from layer V pyramidal neurons from rats in slice Tsodyks and Markram (1997) discovered *synaptic depression*: the EPSP amplitude in response to a spike train in a presynaptic neuron decreased in size during the spike train. The underlying mechanism for this behaviour is that the spike train releases vesicles docked at the presynaptic terminal faster than they can be replenished. This phenomenon is known and modelled in other systems, for example inner hair cells of the cochlea (Meddis, 1986).

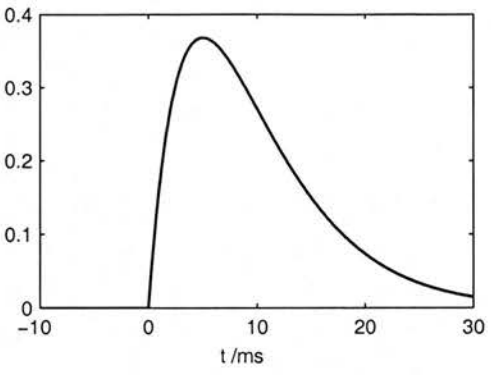

Figure 2.9: The alpha function $t/\tau e^{-t/\tau}$ with $\tau = 5\,\text{ms}$.

2.4.4 The integrate-and-fire model

The integrate-and-fire (IF) neuron is the simplest of the threshold-fire neuron models. It is based on the membrane potential equation (2.4) with the membrane potential currents omitted. However, when the membrane potential V hits the threshold ϑ the neuron fires and the membrane potential is reset. Most often the neuron is reset to its resting potential though sometimes the reset can be noisy, and the membrane potential differs somewhat from this value. Without loss of generality, I set the resting potential to 0 mV in this thesis.

Often we rewrite the membrane potential equation (2.4) by multiplying by R to give

$$\tau_{\text{m}} \frac{dV_i}{dt} = -V(t) + R\left(I_i^{\text{syn}}(t) + I_i^{\text{ext}}(t)\right) \quad , \tag{2.10}$$

where $\tau_{\text{m}} = RC$ is the *membrane time constant.*

With this very basic model of one IF neuron, it is possible to derive results such as the firing frequency of a neuron for a given constant input current. To model a network of spiking neurons, we can connect IF neurons with gated or ungated synapses. These can be simulated easily and relatively analytically tractable (see, for example, Ermentrout, 1998; van Vreeswijk et al., 1994).

We can simplify the ungated synapse further since in IF models, the voltage is by definition in a relatively small range between the resting potential and the threshold. As the reversal potential for excitatory synapses is usually much bigger than the threshold this means that is not unreasonable to approximate the voltage part of (2.7) as a constant and deal with a fixed *current* time course, $\gamma(t)$ for excitatory synapses. This is not true for inhibitory synapses, as their reversal potential is closer to the threshold,

and the voltage factor in (2.7) will vary by at least a factor of two between resting potential and the threshold. As the inhibitory current is most important when the membrane potential is near threshold, we can approximate the driving potential by the difference between the threshold and reversal potential for the inhibitory synapse. This may lead to unphysiologically negative potentials, but the effect should not be too great near to the threshold. The approximation will be more valid if the membrane potential hovers close to the threshold. I call this the *voltage-independent* or *current-based* ungated synaptic model. The equation for the membrane potential reads in full:

$$\tau_{\mathrm{m}}\frac{dV_i}{dt} = -V(t) + R\left(\sum_j J_{ij}\sum_f \gamma(t - t_j^{(f)}) + I_i^{\mathrm{ext}}(t)\right) \quad . \tag{2.11}$$

Here the dimensionless quantity J_{ij} replaces the maximum conductance and $\gamma(t)$ is the form of the current and has the units of amps.

2.4.5 The spike response model

Gerstner (1991) first introduced the SRM and it has been presented subsequently in a number of papers (see, for example, Gerstner and van Hemmen, 1992; Gerstner et al., 1993a; Gerstner and van Hemmen, 1994a). In fact the SRM comes in two flavours, which I will call the *simple* and *extended* versions. In section 2.4.5.1 I will take the approach of the introduction of Gerstner, 1998 by deriving the simple SRM from the IF model. Section 2.4.5.2 presents the small modification to the simple SRM necessary to make the extended SRM, which is equivalent to a renewal process. In section 2.4.7 I weigh the advantages and disadvantages of the SRM.

2.4.5.1 The simple spike response model

We can represent the reset of the IF neuron more rigourously than in the previous section by using delta functions. Following Gerstner (1998), we can add an extra reset current to the right hand side of (2.11):

$$-C\vartheta\sum_{f=1}^{\infty}\delta(t - t_i^{(f)}) \quad . \tag{2.12}$$

This term expresses the effect of an infinitesimally short pulse of current leaving the neuron when it fires. The effect of this term when integrated is to reset the membrane potential to 0 mV (the resting potential) whenever there is a spike. Mathematically, we show this by solving the equation

$$\tau_{\mathrm{m}}\frac{dV_i}{dt} + V_i = -RC\vartheta\sum_{f=1}^{\infty}\delta(t - t_i^{(f)}) \tag{2.13}$$

to give

$$V_i(t) = -\vartheta \sum_{f=1}^{\infty} \Theta(t - t_i^{(f)}) \exp\left(-\frac{t - t_i^{(f)}}{\tau_{\rm m}}\right) \ . \tag{2.14}$$

We can extend this approach by integrating the other current terms. Since (2.11) is a linear differential equation, we can add the solutions to give the membrane potential as a function of time:

$$V_i(t) = \sum_{j=1}^{N} J_{ij} \sum_{f=1}^{\infty} \varepsilon(t - t_j^{(f)}) + \sum_{f=1}^{\infty} \eta_i(t - t_i^{(f)}) + V_i^{\rm ext}(t) \ , \tag{2.15}$$

where

$$\varepsilon(t) = \frac{R}{\tau_{\rm m}} \int_0^t \gamma(t - t') e^{-\frac{t'}{\tau_{\rm m}}} dt' \ , \tag{2.16}$$

$$\eta_i(t) = -\vartheta \Theta(t) \exp\left(-\frac{t}{\tau_{\rm m}}\right) \ , \tag{2.17}$$

and

$$V_i^{\rm ext}(t) = \frac{R}{\tau_{\rm m}} \int_0^{\infty} I_i^{\rm ext}(t - t') e^{-\frac{t'}{\tau_{\rm m}}} dt' \ . \tag{2.18}$$

We can interpret the function $\varepsilon(t)$, which has the dimensions of volts, as a postsynaptic potential (PSP) function. The kernel $\eta(t)$ also has the dimensions of volts, but it has no interpretation in conventional physiological terms. I shall return to it shortly.

This integrated IF equation (2.15) is the basis for the SRM. In the conventional notation of the SRM, each model neuron has a membrane potential $h_i(t)$. This is a sum of the *synaptic potential* $h_i^{\rm syn}(t)$, the *refractory potential* $h_i^{\rm ref}(t)$ and the *external potential* $h_i^{\rm ext}(t)$:

$$h_i(t) = h_i^{\rm syn}(t) + h_i^{\rm ref}(t) + h_i^{\rm ext}(t) \ . \tag{2.19}$$

This notation derives from the conventional notation for artificial autoassociative neural networks (Hertz et al., 1991). These networks may be viewed as systems of coupled atomic spins (denoted by S_i) which sum to produce a local magnetic field h_i. I shall use this notation when dealing with SRM neurons in the rest of this thesis.

We can identify $h_i(t)$ with $V_i(t)$ in (2.15), $h_i^{\rm syn}(t)$ with the first term on the right hand side of (2.15), $h_i^{\rm ref}(t)$ with the second term on the right hand side of (2.15) and $h_i^{\rm ext}(t)$ with $V_i^{\rm ext}(t)$. To summarise, this gives us:

$$h_i^{\rm syn}(t) = \sum_{j=1}^{N} J_{ij} \sum_{f=1}^{\infty} \varepsilon(t - t_j^{(f)}) \tag{2.20}$$

$$h_i^{\rm ref}(t) = \sum_{f=1}^{\infty} \eta_i(t - t_i^{(f)}) \ . \tag{2.21}$$

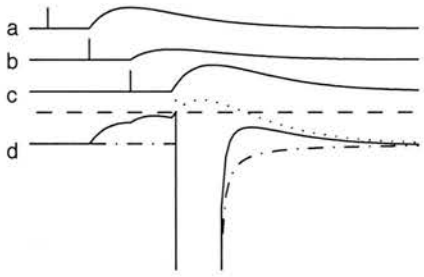

Figure 2.10: The membrane potentials in an SRM neuron. The top three lines, labelled a, b and c, represent the spikes and EPSPs in presynaptic neurons a–c. They sum in neuron d, whose total membrane potential is denoted by the lowest solid line. It is clearly a weighted sum of the membrane potentials a–c, and when it reaches the threshold (horizontal dashed line), neuron d spikes. Its total membrane potential then falls to $-\infty$ for a while (the absolute refractory period) before converging on the summed EPSPs. The dotted line denotes the summed EPSP input and the dash-dotted line denotes the refractory potential.

Figure 2.10 shows an example of the time courses of the different potentials in an SRM neuron.

In the SRM, the functions $\eta(t)$ and $\varepsilon(t)$ need not be the integrals of currents weighted by decay as in (2.16) and (2.17); they can be more general. This is especially useful for the kernel $\eta(t)$, which we refer to as the *refractory function.* We can use this function to model the absolute and relative refractory properties of the neuron, as well as the reset. For example, one possible choice is the rectangular hyperbola

$$\eta(t) = \begin{cases} 0 & t \leq 0 \\ -\infty & 0 < t \leq \tau_{\text{abs}} \\ \frac{\eta_0}{t-\tau_{\text{abs}}} & \tau_{\text{abs}} < t \end{cases} . \tag{2.22}$$

This kernel simulates the absolute refractory period of τ_{abs} with an infinitely negative potential and the relative refractory period with a finitely negative potential.

We can use the refractory function to model phenomena such as after-depolarising potentials and the associated burst firing tendencies of neurons (Gerstner and van Hemmen, 1994b).

2.4.5.2 The extended spike response model

A simplification is to consider only the last F spikes of neuron i so that

$$h_i^{\text{ref}}(t) = \sum_{f=1}^{F} \eta_i \left(t - t_i^{(f)}\right) \quad . \tag{2.23}$$

With a refractory function with a form like (2.22), if F is greater than 1, the neuron remembers more than one spike and tends to adapt its firing rate. In the case where $F = 1$, the neuron only remembers its last firing event. This means we can classify it as a *renewal process* (Gerstner, 1995) and therefore use the properties of renewal processes in derivations. Unfortunately, the resulting simplified SRM is not formally equivalent to the IF model any more, even with the correct kernels (2.16) and (2.17).

An extension to the SRM rectifies this problem. Gerstner (1995) made the PSP kernel a function of two variables, where the extra variable is the last time of spiking of the *post*-synaptic neuron. Thus the synaptic potential becomes

$$h_i^{\text{syn}}(t) = \sum_j J_{ij} \sum_f \kappa(t - t_i, t - t_j^{(f)}) \ , \tag{2.24}$$

where $\kappa(s,t)$ is the value of the PSP evoked in a postsynaptic neuron that fired s ago by a presynaptic neuron that fired t ago. To get back to the IF model, we can set (Gerstner, 2000)

$$\kappa(s,t) = \begin{cases} \varepsilon(t) & s < 0 \\ \varepsilon(t) - \varepsilon(t-s)e^{-s/\tau_{\text{m}}} & s \geq 0 \end{cases} \ , \tag{2.25}$$

where $\varepsilon(t)$ is defined as in (2.16) and is always zero for negative arguments. If the presynaptic neuron has fired after the postsynaptic neuron, that is $t < s$, the second term in the equation is 0 since its argument is negative and the PSP is given by $\varepsilon(t)$. If, however, the presynaptic neuron has fired before the postsynaptic neuron, that is $t > s$, the second term is not zero. At the time of firing, that is when $t = 0$, the two terms cancel out, effectively resetting the membrane potential to zero.

The contribution due to the external current will also depend on the last postsynaptic firing time too:

$$V^{\text{ext}}(t, t_i) = \frac{R}{\tau_{\text{m}}} \int_0^{t-t_i} I_i^{\text{ext}}(t - t') e^{-\frac{t'}{\tau_{\text{m}}}} dt' \ . \tag{2.26}$$

This is just the same as (2.18), except for the upper limit of the integration, which is $t - t_i$ rather than infinity. Since this external potential depends on $t - t_i$ alone, and since we accomplish the reset by the boundary conditions on the integrals, there are no explicit current spikes to integrate to obtain $\eta(t)$. Since $V^{\text{ext}}(t, t_i)$ depends only on

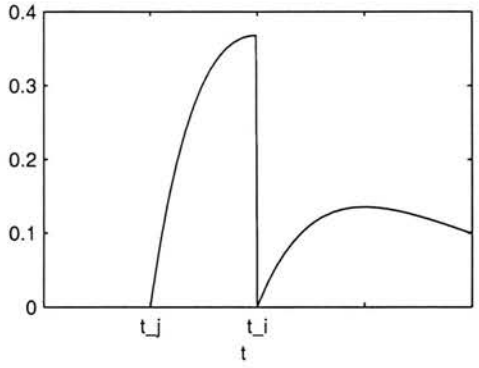

Figure 2.11: The extended alpha function $\kappa(t - t_i, t - t_j)$. The potential increases from the presynaptic firing time t_j until the postsynaptic neuron fires at t_i. Then the potential is reset, and integration begins again.

$t - t_i$ it is formally equivalent to $\eta(t)$ and we can equate the two; it is conventional to do so (Gerstner, 1995, 2000). In the case of constant current injection, that is $I^{\text{syn}} = I_0$, we can solve the integral (Gerstner, 1995) to give

$$\eta(t) = RI_0(1 - e^{-t/\tau_{\text{m}}}) \ . \tag{2.27}$$

2.4.5.3 Noise in the spike response model

Gerstner (1998, 2000) outlines three types of noise that could affect IF neurons and by extension SRM neurons.

Noisy threshold: There is not a fixed threshold, but rather a region of membrane potential in which a spike is triggered.

Noisy reset: The neuron has a fixed threshold, but is reset to a random value around a mean. This results in the next spike being earlier or later than it would have been had there been a deterministic reset.

Noisy integration: Noise is added to the current in equation (2.11).

In the rest of this thesis I will concentrate on the first of these three. The reason for this is mainly ease of analysis and implementation in a SRM network, though the second has also been used in analysis (Gerstner, 2000). The third would be difficult, if not impossible to implement in an SRM network, and is also hard to deal with analytically (Gerstner, 1998).

To implement the noisy threshold, we imagine that the neuron has a probability of firing per unit time that increases with the membrane potential. We can express the firing probability as

$$P^{\mathrm{F}}(h;\delta t) = \tau^{-1}(h)\delta t \ , \tag{2.28}$$

where $\tau^{-1}(h)$ is the *escape rate* and δt is a infinitesimal time interval. A typical choice for the escape rate is based on the kinetic reaction constant (Gerstner and van Hemmen, 1992):

$$\tau^{-1}(h) = \frac{1}{\tau_0} e^{\beta(h-\vartheta)} \ , \tag{2.29}$$

where β is the inverse temperature and gives a measure of the noise and where τ_0 characterises the rate at threshold. For large β, the escape rate $\tau^{-1}(h)$ changes from 0 to infinity as h increases past ϑ, and the function effectively implements a deterministic threshold. For small β, there is a finite probability of firing when the membrane potential is below threshold and firing is not guaranteed when it is above. Therefore spike times can be earlier or later than they would have been if produced deterministically.

Given that a spike has fired at time $t^{(1)}$, it is useful to know the probability of it firing at some time t, later than $t^{(1)}$. Following Gerstner and van Hemmen (1994a) I denote this $P_2^{\mathrm{F}}(t|t^{(1)})$. In any particular infinitesimal time period δt at time t the probability of firing is equal to the probability that the neuron has not yet fired times the probability that the neuron fires in that time segment:

$$P_2^{\mathrm{F}}(t|t^{(1)}) = S(t|t^{(1)})P^{\mathrm{F}}(h(t)) \ , \tag{2.30}$$

where $S(t|t^{(1)})$ is the *survivor function* (Perkel et al., 1967a) and where $t \geq t^{(1)}$. The survivor function represents the proportion of neurons at time t that have not fired since $t^{(1)}$. Since the spiking probability only depends on the membrane potential, the survivor function is the product of the probabilities of the neuron not firing at successive time steps. With n time steps of length $\delta t = (t - t^{(1)})/n$, taking the limit as $n \to \infty$ gives

$$S(t|t^{(1)}) = \lim_{n\to\infty} \prod_{i=0}^{n} \left(1 - \tau^{-1}\left(h\left((t-t^{(1)})i/n\right)\right)\delta t\right) \ . \tag{2.31}$$

In this limit of $\delta t \to 0$ each term of the product is a linear approximation of an exponential function $\exp\left(-\tau^{-1}\left(h\left((t-t^{(1)})i/n\right)\right)\delta t\right)$. Substituting in this exponential function simplifies the equation as we can convert the product into a summation in the argument of the exponential:

$$S(t|t^{(1)}) \ = \ \exp\left(\lim_{n\to\infty} \sum_{i=0}^{n} -\tau^{-1}\left(h\left((t-t^{(1)})i/n\right)\delta t\right)\right) \tag{2.32}$$

$$= \exp\left(-\int_{t^{(1)}}^{t} \tau^{-1}\left(h(t')\right) dt'\right) \quad . \tag{2.33}$$

One immediate use of this expression for the survivor function is in simulations with discrete time steps. In each time step of length Δt, we assume that the membrane potential is constant. The expression for the firing probability is then one minus the probability that the neuron does not fire in the interval Δt:

$$P^{\mathrm{F}}(h;\Delta t) = 1 - S(t+\Delta t|t) = 1 - \exp\left(-\tau^{-1}(h)\Delta t\right) \quad . \tag{2.34}$$

Here the survivor function means something slightly different to before, as it is not fixed on a spike time, but rather an arbitrary time.

There are many more applications for the survivor function, including calculating the ISI distribution and in general network activity calculations (see, for example, Gerstner and van Hemmen, 1992; Gerstner, 1995, 2000).

2.4.6 Relationship between the neuronal models

We have already seen that the Hodgkin-Huxley model, the IF model and the SRM are all derived from the membrane potential equation (2.4). Furthermore, we have seen that the SRM model can be derived from the IF, and so can be seen as a generalised version of the IF model, but that when used in a limited form (the simple SRM remembering finite numbers of its own spikes) cannot function as an IF neuron.

Kistler et al. (1997) have shown that the extended SRM with appropriately chosen kernels and threshold resembles the output of a Hodgkin-Huxley model by injecting the same noisy current into both models. The simple SRM does not do so well, and a simple IF model does even worse.

2.4.7 Advantages and disadvantages of the spike response model

What is to be gained by integrating the IF model neuron to create the SRM? I see two main advantages of the SRM:

- It is more general than the IF model so that neurons with arbitrary biological kernels can be simulated (section 2.4.6, Kistler et al., 1997).

- It is analytically tractable, offering general results which may be solved for arbitrary biological functions and constants. The SRM has proved a useful tool in studying general population dynamics of networks of neurons (Gerstner and van Hemmen, 1992; Gerstner et al., 1993a; Gerstner, 1995, 2000) especially in

locking and stability phenomena. Some of the results later on in this thesis will also demonstrate its analytical utility.

In the form presented here it also has disadvantages:

- It is not as general as IF models with voltage-dependent PSCs (Gerstner, 1995).
- In analysis it is more awkward to feed it currents that are arbitrary functions of time as they should be integrated first, and not all functions are integrable.

The simulations of Ermentrout (1998) and Gerstner (1998) suggest that the loss of detail due to the first point is acceptable. Ermentrout simulated the membrane conductance at a gated synapse in response to a single spike and approximated its time course with a sum of exponentials type alpha function. The waves of activity produced in two IF neuron networks, one with synaptic conductances generated by gated channels and one with the explicit approximated conductances gave indistinguishable results.

2.5 Spike learning

Do individual spikes play a role in learning, or are only time- or population-averaged rates important? Hebb's rule itself does not explicitly specify the timing of spikes, though causality is implicit in it. The long term potentiation (LTP) paradigm implicitly deals with rates averaged over a time window of hundreds of milliseconds. Section 2.5.1 outlines Hebb's rule and the classical LTP results, which I refer to as rate-dependent synaptic plasticity. Later theoreticians have examined the idea of spike timing dependent synaptic plasticity (STDSP), where the timing of individual spikes affects the synaptic strength. Recent experiments have confirmed that the timing of individual pre- and postsynaptic spikes is important in potentiating or depressing synapses. I outline the theoretical and experimental aspects of STDSP in section 2.5.2. I shall return to the functional implications of the STDSP later. In section 3.2 I will discuss synfire chains, which can be seen as a special case of sequences. In chapter 6 I will investigate how the temporal learning rule affects aspects of the recall of sequences.

2.5.1 Hebb's rule and rate dependent synaptic plasticity

Hebb (1949) proposed that features were represented by groups of concurrently active neurons, which he called *cell assemblies*[3]. To explain how cell assemblies formed, he proposed the well-known learning rule:

[3]This contrasts with the localist, "pontifical" or "cardinal" cell coding championed by (Barlow, 1972).

> When an axon of cell A is near enough to excite a cell B and repeatedly or persistently take part in firing it, some growth process or metabolic change takes place in one or both cells such that A's efficiency, as one of the cells firing B, is increased. (p. 62)

Precise time scales are not mentioned in Hebb's rule, although there is a notion of causality: cell A must be active before cell B in order to contribute to its firing. In principle, the learning rule could take account of how much individual presynaptic spikes contribute to the firing of the postsynaptic cell. If, however, both cells are firing persistently (say at a constant rate) then we could argue that individual spikes are not particularly important and that firing rates adequately describe the activity of both neurons. This is the idea of rate-dependent synaptic plasticity.

The Hebb rule has been used as the basis of much theoretical work on neural networks. Heteroassociative networks (Willshaw et al., 1969), autoassociative networks (Hopfield, 1982) and the backpropagation learning rule for feedforward networks (Rumelhart et al., 1986) all use abstractions of the Hebb rule to learn.

The experimental phenomenon of LTP in hippocampal slices has confirmed Hebb's proposal (see Bliss and Collingridge, 1993, for a review). In the original LTP experiments an extracellular electrode stimulated a group of presynaptic neurons with 50 or so high frequency (order of 100 Hz) current pulses. Strong pulses caused a long-term (order of hours) increase in the synaptic efficacy, whereas weak pulses caused no or only a short-lasting change in the synaptic efficacy. This property was called *cooperativity* because the inputs from many fibres have to cooperate to effect learning. However, when the weaker inputs were paired with stronger ones, the synapses corresponding to the weaker inputs were strengthened in the long term, showing that LTP was *associative*. Finally, only those synapses that had been presynaptically activated were potentiated, showing that LTP was *input-specific*.

The explanation for the LTP results was that sufficiently strong inputs were required to depolarise the postsynaptic neuron enough. Only when both post- and presynaptic neurons were active concurrently was the synapse potentiated. This was later confirmed experimentally by pairing postsynaptic and presynaptic depolarising pulses at 1 Hz.

It is worth noting that traditional LTP does not control the timing of both pre- and postsynaptic spikes. It appears that the assumption of rate-dependent synaptic plasticity is implicit in traditional LTP.

2.5.2 Spike timing dependent synaptic plasticity

Recent work has suggested that the timing of individual spikes can change synaptic strengths, a phenomenon we can call spike timing dependent synaptic plasticity (STDSP).

Gerstner et al. (1993b) hypothesised that information about the postsynaptic neuron firing could reach the synapse by means of backpropagated activity from its soma. Were this activity localised in time and space (as is a conventional spike), the synapse would receive very precise information about the firing time of the postsynaptic neuron. Precise information about the firing time of the presynaptic neuron could come from concentration of neurotransmitter in the synaptic cleft. Supposing there was some way of putting together these two pieces of information, when a backpropagating spike arrived at the synapse, the synapse would be potentiated in proportion to the amount of neurotransmitter there. Thus individual pairs of spikes could potentiate the synapse and the amount of potentiation could depend on the time difference between pre- and postsynaptic spikes. Figure 2.12 shows the principle graphically. Allowing for axonal and dendritic delays, this means that when presynaptic spikes precede postsynaptic ones by a short time the synapse is potentiated, whereas all other spike combinations do not alter its strength. Gerstner et al. (1993b) proposed that the time window for potentiation was identical to the time course of the neurotransmitter concentration, which they modelled with a $\sim$1 ms wide Gaussian.

The evidence from mammalian cortical pyramidal (Markram et al., 1997), developing frog retinotectal (Zhang et al., 1998) and rat hippocampal (Bi and Poo, 1998) synapses has confirmed the hypothesis that synapses can be potentiated by pairs of pre- and postsynaptic spikes and that the amount of potentiation depends on the interval between the spikes. The main differences to the prediction are: firstly that appropriately-timed spikes can depress the the synapse; and secondly that the time window in which spikes can affect the synaptic weight is of the order of 20 ms, an order of magnitude greater. When a presynaptic spike arrives shortly (within about 20 ms) before a postsynaptic one, the synapse is potentiated and when the converse is true it is depressed. Figure 2.13 shows how the amount of potentiation depends on the relative timing of the pre- and postsynaptic spikes.

The evidence of Bi and Poo (1998) suggests that only relatively weak synapses that can be potentiated, whereas synapses with any strength can be depressed. This is consistent with the maximum synaptic strength being limited.

Neither LTP or long term depression (LTD) occurs when the postsynaptic neuron

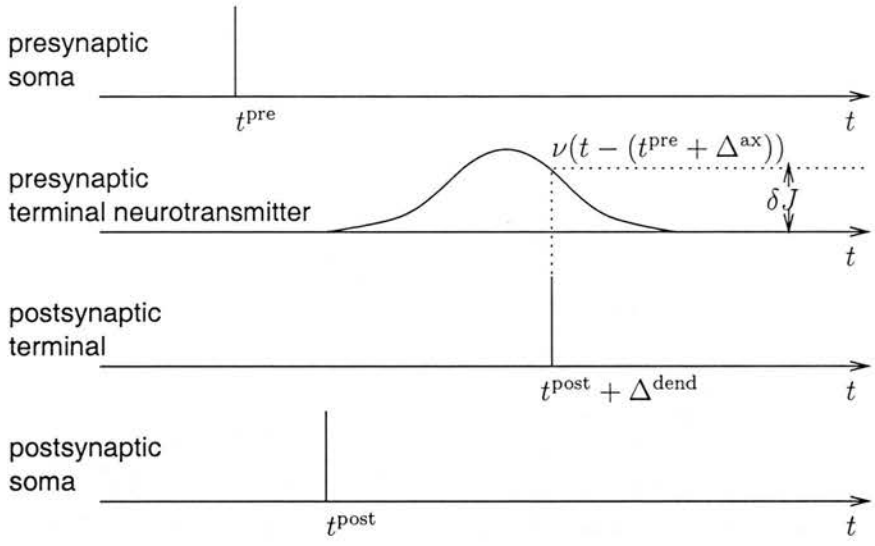

Figure 2.12: The mechanism of potentiation. The presynaptic neuron fires at time t^{pre} and reaches the presynaptic terminal Δ^{ax} later, causing neurotransmitter to be released according to the function $\Gamma(t)$. Meanwhile, the postsynaptic neuron has fired at time t^{post} and a spike from its soma has taken Δ^{dend} to get to the postsynaptic terminal. The amount of potentiation δJ is equal to the concentration of neurotransmitter at the presynaptic terminal when the postsynaptic backpropagated spike arrives.

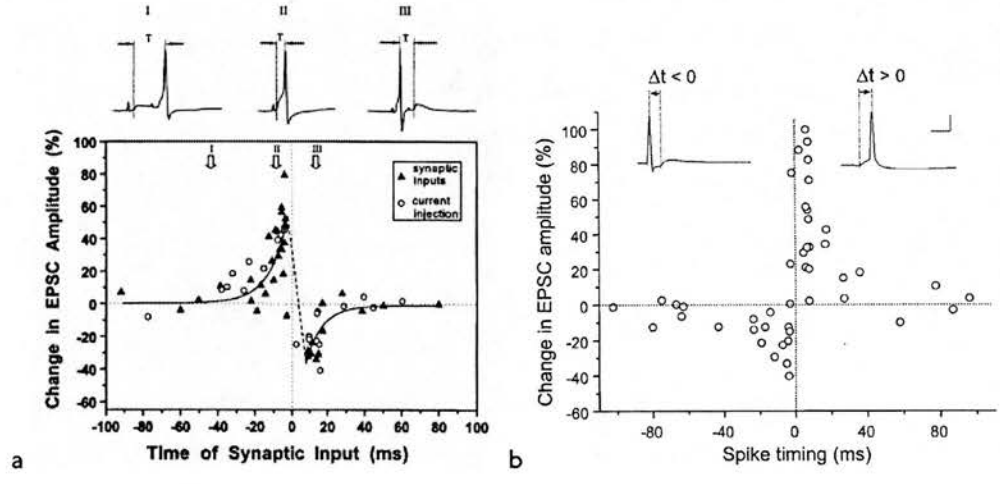

Figure 2.13: *a.* The temporal learning rule in frog retinotectal cells. The time of from the presynaptic spike to the postsynaptic spike is plotted along the abscissa; negative times indicate the presynaptic neuron fired before the postsynaptic one. The change in the EPSC amplitude is plotted on the ordinate. (From Zhang et al., 1998.) *b.* The temporal learning rule in glutamatergic rat hippocampal cells. Same interpretation of axes as *a.* except that the abscissa is reversed. (From Bi and Poo, 1998.)

expressing the γ-aminobutyric acid (GABA) subtype of glutamate channels. This suggests that the synaptic strengths from excitatory neurons to inhibitory neurons are not changed by this particular mechanism.

Both LTP and LTD depend on glutamate receptors of the N-methyl-D-aspartate (NMDA) subtype being activated, as when NMDA channels were pharmacologically blocked, no potentiation can take place. When L-type Ca^{2+} channels in the postsynaptic neurons are pharmacologically blocked, LTD cannot be induced and the extent of LTP is reduced. As NMDA receptors allow in Ca^{2+}, this implies that the mechanism of potentiation depends on the spatiotemporal patterns of Ca^{2+} in the postsynaptic cell (Bi and Poo, 1998). This is consistent with the implication of Ca^{2+} in the induction of traditional LTP (Bliss and Collingridge, 1993).

The cellular mechanism of potentiation is not fully understood at present. However, the mechanism does seem to involve backpropagated action potentials, as postulated by Gerstner et al. (1993b). In cortical pyramidal neurons (Stuart and Sakmann, 1994) and hippocampal CA1 neurons (Spruston et al., 1995) spikes propagate actively back to the postsynaptic synapse from the soma, opening L-type Ca^{2+} channels .

Other types of STDSP have been found between different types of neurons in different systems (Abbott and Song, 1999). One is the complete opposite of the rule just described in that presynaptic spikes before postsynaptic spikes lead to depression and whereas when they occur after postsynaptic spikes, the synapse is potentiated.

Regardless of the potentiation mechanism, the resulting learning rule can be expressed as follows. If t_i is the firing time of the postsynaptic neuron, t_j the firing time of the presynaptic neuron and Δ^{dend} the dendritic delay to the backpropagating spike, the learning rule

$$\delta J_{ij} \propto \Gamma\left((t_i + \Delta_{ij}^{\text{dend}}) - (t_j + \Delta_{ij}^{\text{ax}}), J_{ij}\right) \ , \tag{2.35}$$

expresses the change in synaptic efficacy for a pair of spikes in the spike trains of the two neurons. The *potentiation function* $\Gamma(t, J)$ expresses the relationship between temporal separation of spikes, the current strength of the synapse and potentiation or depression. We can combine all the small changes δJ_{ij} over a period of activity in the network. Since weight strengths cannot increase infinitely, the dependence of $\Gamma(t, J)$ on the weight should be such that it converges on a steady value. For small numbers of paired spikes, we may be able to ignore the weight-dependence of the potentiation function.

2.6 Spike dynamics

Wilson and Cowan (1972) assumed that the population rate in groups of interacting neurons was the appropriate variable to be working with. From this assumption they derived integral equations for the population activity in interacting excitatory and inhibitory groups. As the integral equations were difficult to work with, they transformed them into differential equations by a "time coarse-graining" procedure. They then applied phase plane analysis to the equations and found oscillating and stable solutions and hysteresis states, depending on the input to the system and the connections strengths within and between the groups. The oscillations displayed by the system led to the name *Wilson-Cowan oscillator.*

Wilson-Cowan oscillators can serve as a model of a cortical column. When connected together, as columns in a sheet of cortex are, they can synchronise (König and Schillen, 1991) or desynchronise with each other (Schillen and König, 1991). (See also section 4.3.1.)

The decay time constant of the activity limits the speed at which Wilson-Cowan oscillators can respond to input. As it is normally of the order of 10 ms, this means Wilson-Cowan oscillators will miss very short time scale temporal phenomena.

Similarly, the response speed of many artificial neural network (ANN) models is limited by time constants. Most ANN models implicitly use time or population rates as the fundamental measure of activation. The time evolution of the systems may be one-step (for example heteroassociative memories, feedforward networks), may proceed by stochastic update (Hopfield, 1982), or by differential equations (Hopfield, 1984). In the differential equation evolution the time constant limits the response speed of the network.

The dynamics of networks of spiking neurons are potentially much richer than those of graded response units. For example, they may synchronise on a millisecond timescale (see chapter 4), or can support sequences of precise firing patterns (see chapter 3). Over the past decade, theoretical work has uncovered the conditions required for network synchrony and asynchrony and has investigated the learning of sequences.

Studying networks of spiking neurons can also confirm and clarify assumptions about rate coding, as does the recent work (Spiridon and Gerstner, 1999; Gerstner, 2000) that shows that the population firing rate of networks of spiking neurons can respond surprisingly quickly to rapid changes in input. Many of these results are generalisations of previous work with phase oscillators and coupled differential equations.

2.7 Summary

Although neurons can communicate by graded response potentials and by extracellular neurotransmitter diffusion, the dominant method of communication is the action potential, or spike. A spike is a sharp increase in the membrane potential localised within about 1 ms of time. Individual spikes could offer many possible ways of encoding information, learning synaptic strengths, and embodying network dynamics. Despite this, most research since Adrian first discovered action potentials has focussed on the time-averaged firing rate of neurons rather than their individual spikes.

Part of the reason for this is that the number of possible spike codes is overwhelming; interval codes, latency codes, filtering codes, population synchrony codes and sequential patterns are all possibilities. Some of these codes involve decoding the output from more than one neuron and the codes do not always mutually exclude each other. Nevertheless, experimentalists have discovered systems in which interpreting the spike trains in ways other than the time-averaged rate provides more information about the stimulus. Examples include the mammalian auditory system, the fly visual system and the locust olfactory system.

The membrane potential equation is the biophysical basis of all spiking neuron models. In a complex model, such as the Hodgkin-Huxley model, channels that depend on voltage and ionic concentration account for the neuron's sub-threshold and spiking dynamics. A simpler model, such as the IF model, concentrates on the subthreshold dynamics and produces spikes only when the membrane potential reaches threshold. By using the fact that PSPs are fairly well stereotyped functions of time, the nonlinear channel dynamics can be completely omitted, thus simplifying the model further. It is from this simplified IF model neuron that the SRM neuron can be derived straightforwardly by integrating with respect to time. This "integrated IF neuron" has the advantage of ease of analysis, particularly with a escape rate firing noise model. It can also be generalised to model arbitrary PSPs and refractory properties.

Hebb's rule postulates that when a presynaptic neuron contributes towards a postsynaptic neuron's firing, the synapse between the two is strengthened. Under the assumption that the timing of individual spikes is unimportant, this rule can be formulated in terms of firing rates (rate-dependent synaptic plasticity). A number of artificial neural network models implicitly make this assumption. "Classic" LTP confirms Hebb's rule. However, the timing of individual spikes is not controlled, so it is not clear whether a rate-based description of activity would be appropriate. Recent work has shown that the timing of individual spikes can affect synaptic plasticity. A typical form of spike

timing dependent synaptic plasticity (STDSP) in glutamatergic neurons is that when the presynaptic neuron fires before the postsynaptic neuron, the synapse is potentiated, whereas if the postsynaptic neuron fires first, the synapse is depressed. Spikes further apart in time are less effective at inducing either potentiation or depression; the time window is about 20 ms wide.

The dynamics of networks of spiking neurons are potentially much richer than those of graded response units. For example, they may synchronise on a millisecond timescale, or can support sequences of precise firing patterns. Over the past decade, theoretical work has uncovered the conditions required for network synchrony and asynchrony and has investigated the learning of sequences. Studying networks of spiking neurons can also confirm and clarify assumptions about rate coding, as does the recent work that shows that the population firing rate of networks of spiking neurons can respond surprisingly quickly to rapid changes in input. Many of these results are generalisations of previous work with phase oscillators and coupled differential equations.

Chapter 3

Sequences

Sequences of patterns abound in nature. Animals must be able to recognise sequences, such as the movement of a predator or the sequence of sounds corresponding to a phoneme, and produce sequences, such as motor movements.

The neural substrate of sequence generation has been studied theoretically for a long time. Sequence recognition has also been explored theoretically, for example in the hippocampus (Levy, 1996). However, these models use rate-based neurons which implicitly assume that individual spikes are not important.

Another type of neural sequence is one where the spikes in individual neurons repeat in a precise order. I call this kind of sequence *spatiotemporal firing patterns*. Spatiotemporal firing patterns are closely related to *synfire chains*, a concept proposed by Abeles (1991) to account for various aspects of cortical activity. This chapter is intended as a comprehensive review of spatiotemporal firing patterns and synfire chains. I am not aware of a review of this scope in the literature.

In section 3.1 I will describe neural network models that store spatiotemporal patterns, from a simple modification of the Hopfield network to a network of spiking neurons trained with temporal learning rule. In section 3.2 I will describe synfire chains and in section 3.3 I will describe the relationship between spatiotemporal firing patterns and synfire chains.

There has been some theoretical work on the dynamics of synfire chains. Section 3.4 lists the various types of instability that synfire chains are subject to. Some of them are common to stable attractor networks, such as the capacity constraint. Others, such as those caused by strongly correlated patterns close together in the sequence, are peculiar to temporal networks.

To further motivate the study of synfire chains, I present some of the possible functions of synfire chains in section 3.5. These range from being a short term memory

to implementing finite state automata.

In section 3.6 I will present the evidence for and against synfire chains. This is a controversial area, as to detect synfire chains, sparse data has to be interpreted appropriately. The experimental evidence for spatiotemporal patterns in the mammalian cortex is suggestive but not conclusive. Nevertheless, the idea of spatiotemporal sequences and synfire chains does not seem implausible, and I conclude that study of their dynamics is worthwhile.

An important question is how spatiotemporal firing patterns can be learned. Section 3.7 explains how an asymmetrical temporal learning rule in conjunction with a supervised learning protocol can be used to train generalised synfire chains. This method of training has been investigated implicitly and is relevant to the idea of copying synfire chains. Attempts to encourage synfire chains to self-organise with an asymmetric temporal learning rule have not been very successful.

3.1 Spatiotemporal patterns

An obvious extension of neural networks that store static patterns (see section 1.3.2) are networks that store sequences of patterns. As each pattern can be thought of as being spread across space and the patterns are spread across time, we can view a sequence of patterns as a *spatiotemporal pattern*. (This is not to say that all spatiotemporal patterns are sequences of patterns.)

Simple, small networks that reproduce sequences of patterns have been studied for many years in the form of central pattern generators (CPGs) (see Shepherd, 1994, for an overview). They are the neural circuits that underly rhythm generation in motor systems. Although they do store sequences of patterns, they cannot be trained to recall arbitrary patterns spread across large numbers of neurons. It seems reasonable to suppose that higher areas of the nervous system need to be able to perform this task. For example, episodic memory sequences consist of arbitrary sequences of different memories, each of which we may suppose corresponds to a pattern of neuronal activation.

Amari (1972) investigated the behaviour of networks of threshold neurons with $-1/+1$ activations that were connected by a weight matrix:

$$J_{ij} = \frac{1}{N} \sum_{\mu} \xi_i^{\mu+1} \xi_j^{\mu} \ . \tag{3.1}$$

His analysis indicated that with synchronous update, it was possible for such networks to store sequences of patterns defined by ξ_i^{μ}. This is similar to the system studied later

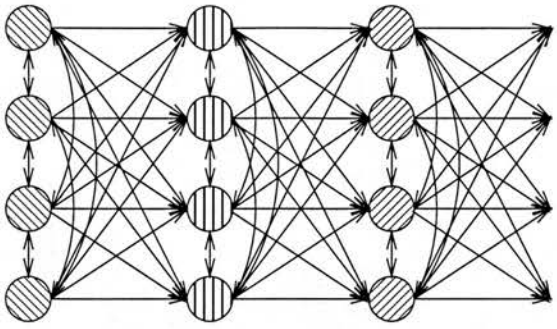

Figure 3.1: Schematic diagram of the connectivity of a Hopfield-style sequence network. The differently-shaded circles represent neurons belonging to different patterns in a network. In a Hopfield-style network neurons of one pattern are connected to each other and to the next pattern.

by Herrmann et al. (1995) by mean field methods.

Hopfield (1982) suggested a method of learning a sequence of patterns by modifying the learning rule for the standard Hopfield network so that the neurons of one pattern also activate the next pattern in the sequence:

$$J_{ij} = \frac{1}{N} \sum_{\mu} (\xi_i^\mu \xi_j^\mu + \lambda \xi_i^{\mu+1} \xi_j^\mu) \ , \tag{3.2}$$

where ξ_i^μ is the activity of the ith neuron in the μth pattern of a sequence and λ is a parameter that determines how strong the weights from one pattern onto the next pattern are. Figure 3.1 shows the connectivity schematically and figure 3.2 shows the type of output we would expect from this network with asynchronous update. Implicit in this rule is the spike timing dependent synaptic plasticity (STDSP) described in section 2.5.2 since the asymmetric part of the weight matrix depends on the activity of the network at two different points in time.

When presented with a pattern ξ_i^ν, we expect the activation of the units h_i^ν to be given by

$$h_i^\nu = \frac{1}{N} \sum_{\mu j} (\xi_i^\mu \xi_j^\mu \xi_j^\nu + \lambda \xi_i^{\mu+1} \xi_j^\mu \xi_j^\nu) \tag{3.3}$$

$$= \xi_i^\nu + \lambda \xi^{\nu+1} + \frac{1}{N} \sum_j \sum_{\mu \neq \nu} (\xi_i^\mu \xi_j^\mu \xi_j^\nu + \lambda \xi_i^{\mu+1} \xi_j^\mu \xi_j^\nu) \ . \tag{3.4}$$

For *uncorrelated* adjacent patterns, the third term (the crosstalk term) in (3.4) should be small compared to the first terms. For $\lambda < 1$, ξ_i^ν determines the sign of h_i^ν, and so pattern ν is stable. For $\lambda > 1$, pattern $\nu + 1$ will dominate the sign of h_u^ν, and

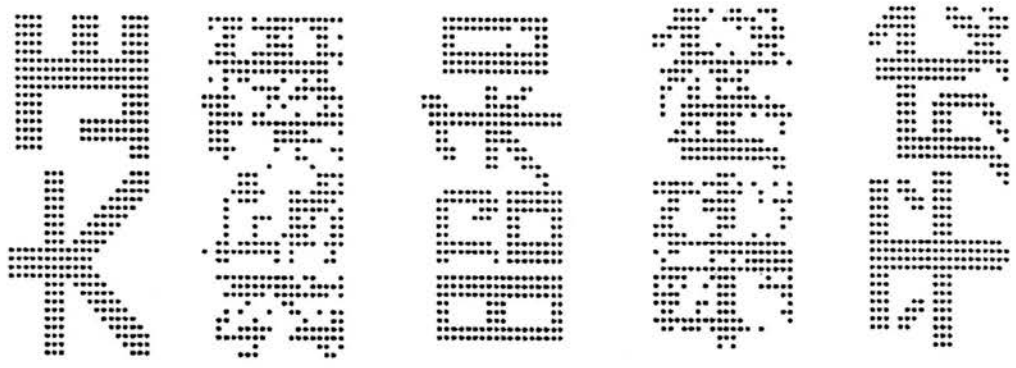

Figure 3.2: Example of the type of sequence expected from a temporal Hopfield network with asynchronous update. Each grid of dots represents the activity of neurons at one time step. In fact this sequence was produced using a different type of weight matrix to Hopfield's original equation (3.2) by Nishimori et al. (1990).

so the network becomes unstable to the attractor for the next pattern. With *asynchronous* update, the rule was not very successful at reproducing learned sequences (Hertz et al., 1991). It is, however, possible to achieve spatiotemporal pattern recall with asynchronous update with a somewhat complicated learning rule that requires potentiation or depression of connections between patterns that are any distance apart (Nishimori et al., 1990). This aspect of the rule detracts from its biological plausibility.

Braitenberg (1978; reviewed in Palm, 1990) proposed the idea of a *Gedankenpumpe* or thought-pump. With a similar set of weights to this above, by lowering and raising the threshold periodically it could be possible to store and reproduce a sequence of patterns. If the network is recalling one pattern, lowering the threshold will cause other neurons to ignite — probably those that belong to the next pattern in the sequence, as they will have most input from the currently-active group. Once the second pattern is fully active, its recurrent excitation should be sufficient to keep it firing when the threshold is raised again. The original pattern might die because of refractory effects. The thalamus could control neuronal excitability in the cortex, thus acting as an effective periodic change in threshold (Palm, 1990).

Levy (1996) has investigated learning of sequences of patterns in networks of sparsely-connected McCulloch-Pitts threshold neurons with synchronous update. Global shunting input and recurrent inhibition help to control activity levels in the network. Rather than using prespecified weights, as in a Hopfield network, learning occurs online. The learning rule is a simplified temporal Hebbian rule. Whenever a neuron is active,

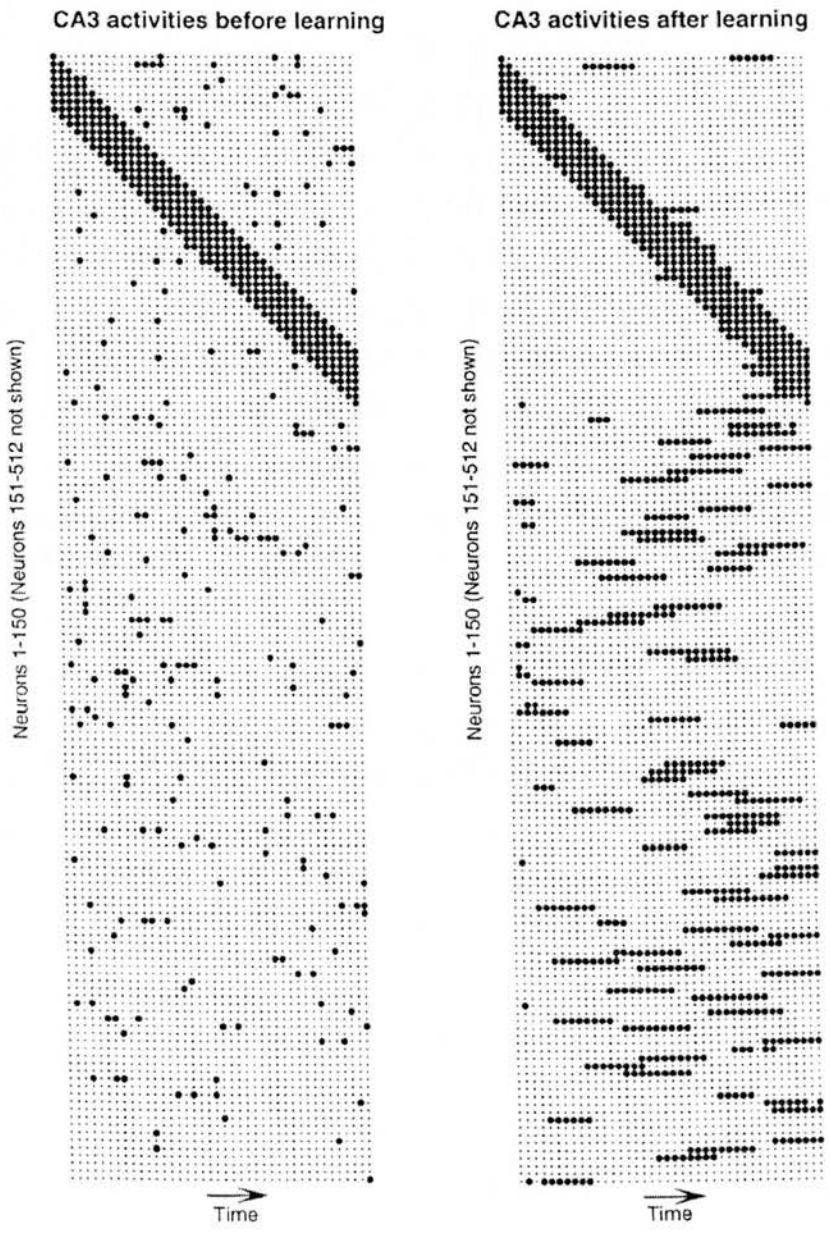

Figure 3.3: Pattern storage in Levy's (1996) network. In both diagrams, each vertical column represents the activity of the network at one time step. *Left.* The network is trained by activating a subset of adjacent neurons and shifting the group on each time step (visible as the diagonal stripe at the top). Adjacent patterns are therefore highly correlated. *Right.* The network recalls the sequence of patterns when prompted by the first in the sequence.

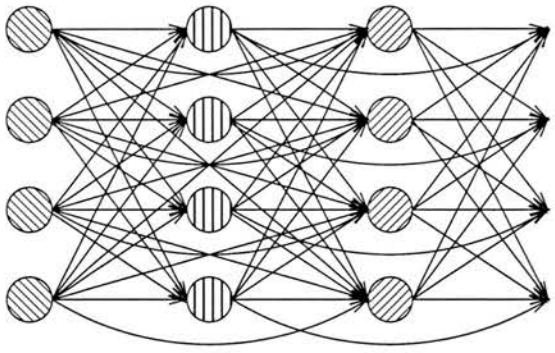

Figure 3.4: Schematic diagram of spatiotemporal pattern connectivity.

all weights from presynaptic neurons decay by a fraction and connections from all presynaptic neurons that were active on the previous time step are strengthened. The network is trained by presenting part of the network with sequences of patterns. Adjacent patterns in the network can be quite correlated (see figure 3.3). Sequence recall proceeds by activating the first pattern or first few patterns in a sequence.

Herz et al. (1988) developed Hopfield's idea in a different direction. They assumed there are many connections with different delays between each pair of neurons and that learning occurs only when the spike in the presynaptic neuron occurs at exactly the axonal delay before the spike in the postsynaptic neuron. Thus their potentiation function was effectively a delta function. They showed that sequences of patterns could be learned with this rule. This rule will lead to there being connections from neurons in one pattern to neurons in the next *and subsequent* patterns, as shown in figure 3.4.

The previous work used rate-based or binary neurons. Gerstner et al. (1993b) applied a similar sort of learning rule in a network of SRM neurons:

$$J_{ij} = \frac{1}{N} \sum_{\mu} \sum_{\nu} \xi_i^{\mu} \xi_j^{\nu} \Gamma(\mu - \nu) \ . \tag{3.5}$$

This rule leads to a similar connectivity to the Herz et al. (1988) model, as shown in figure 3.4. Typical patterns produced by the network are shown in figure 3.5. The patterns were quite uncorrelated, though sometime neurons could fire more than once during the same spatiotemporal pattern.

Although the weights determine the patterns and the order in which they are recalled, the magnitude of the threshold determines whether and how fast the patterns may be recalled for a given set of weights. If it is too high no units will ever fire; if it is too low the units will be firing at the maximum frequency allowed by their refractory period. For values between these extremes, the threshold has the effect of controlling

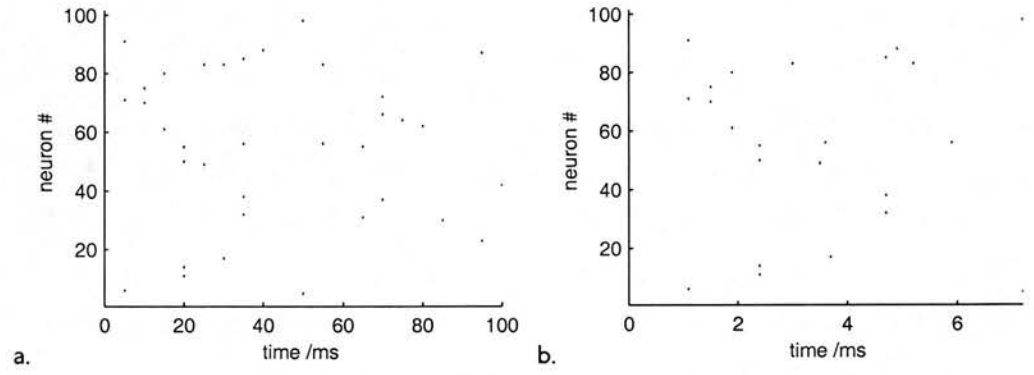

Figure 3.5: Recall of a stored spatiotemporal pattern. *a.* Part of a spatiotemporal pattern used to train the weights of a network according to an abstraction of the temporal learning rule of Zhang et al. (1998). *b.* Output from the trained network on presentation with the first four patterns. Parameters will be discussed in chapter 6.

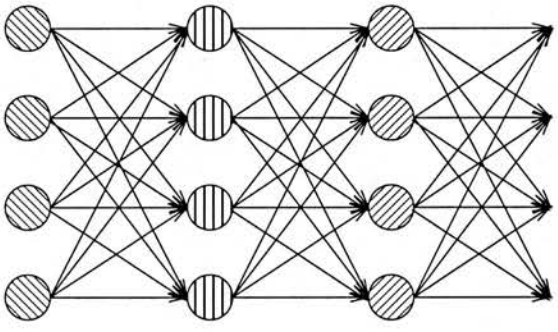

Figure 3.6: Schematic diagram of synfire chain connectivity.

the speed of recall since each unit fires when the membrane potential crosses the threshold while rising. The membrane potential will cross a lower threshold sooner, causing activity to propagate faster.

3.2 Synfire chains

Abeles (1991) proposed *synfire chains* to account for a number of phenomena in the primate neocortex:

Precisely timed spike patterns: In experiments from various areas of the cortex, there appeared to be more repeating precisely timed spike patterns within the same neuron and across different neurons than would be expected with neurons firing independently at the same rate.

Connectivity and processing: The anatomy of the neocortex is strongly recurrent whereas processing appears to be feed-forward and hierarchical (Abeles, 1991).

Low firing rate: Cortical neurons fire at around 1–5 Hz. Abeles' calculations and those of other workers indicated that even with inhibition, neurons in randomly-connected networks could not fire stably at this rate unless there was external excitation.

The experimental evidence for precisely timed spike patterns is now disputed (see section 3.6) and the low firing rates can be accounted for theoretically by fast, strong inhibition (Amit and Brunel, 1997). Despite this, synfire chains are an interesting theoretical concept with testable predictions and have not been disproved. I shall go on to describe them and how they account for the data.

The term "synfire chain" refers to a combination of an anatomical structure and a mode of propagation through that structure. The word "chain" refers to a sequence of groups of neurons (known as *nodes* or *pools*) embedded in a neural network. This sequence is defined by diverging and converging connections between adjacent nodes (see figure 3.6). It is possible for the same neuron to appear twice or more in different nodes of the same chain and the neurons of the same node do not have to be physically close to each other. The word "synfire" refers to the mode of activity propagation through the chain. Under certain conditions (see section 3.4), the neurons of each node fire almost synchronously and send their spikes to the next node. The neurons of this node fire almost synchronously, and so activity propagates along the chain. This mode of propagation is called *synfire propagation.*

The first of Abeles' experimental phenomena, precisely timed spike patterns, is explained by the fact during synfire propagation there should be very little dispersion (1–3 ms) in a node's firing times and the delay between any pair of nodes' mean firing times should be the same whenever activity passes through the chain. Thus, during prolonged recordings from two or more neurons in the same chain (though not necessarily the same node) the same patterns of intervals between the neurons firing on a 1–3 ms time scale should recur. As it is possible for the same neuron to belong to different nodes in the same chain, there may even be repeated patterns in one neuron.

The second phenomenon is explained by the ordered connectivity of the synfire chain embedded in a network of randomly-connected neurons. Thus the connectivity can appear to be recurrent, whereas the processing — or at least activity propagation — appears to be feed-forward.

The stability argument is more subtle. First of all, Abeles considered a randomly-

connected patch of cortex containing 20000 neurons with 25% connectivity. He concluded that with only excitatory neurons, activity will either saturate or die out, depending how many neurons are initially active. This is because a certain number of presynaptic spikes are required to activate a postsynaptic neuron. The probability of a neuron receiving at least this number of connections from a group of active neurons increases as the size of the active group increases. If the group is below a critical size, fewer neurons will be activated than were originally active and the activity dies out. If it is above the critical size, more neurons will fire and the number of neurons firing snowballs. Abeles reckoned that with inhibition it is difficult to obtain the low firing rates present in the cortex without external excitation.

The cortex does receive tonic inputs from other areas of the brain (most notably the thalamus), which could provide the external excitation that would account for the low firing rates. Notwithstanding this solution, Abeles proposed another. Chains of diverging and converging connections with somewhat strengthened synapses superposed on the background connectivity could keep activity low. In each node of the chain there would be fewer neurons than the critical number that causes the network activity to snowball, but activity would propagate within the chains, thereby maintaining activity. However there was a problem if the activity propagated asynchronously through the chain. The number of neurons concurrently activated in a number of successive nodes might exceed the critical number and lead to explosion of the activity. There were two approaches to this problem:

1. anatomical separation of nodes; that is, remove the background random connections; and

2. synchronous transmission; that is, minimise the temporal overlap between nodes firing.

The second solution is adopted in synfire chains.

3.3 Spatiotemporal patterns and synfire chains

At this point it is worth noting that there is a strong connection between spatiotemporal patterns and synfire chains.

Firstly, there is a link between the activity patterns in a synfire chain and a spatiotemporal pattern. We can regard the neurons of each node in a synfire chain as a pattern; thus synfire propagation is the same as recalling a sequence of patterns synchronously.

There is also a link between the connectivity in networks supporting synfire chains or spatiotemporal patterns. We can define the set of neurons comprising the μth node analogously to the set of neurons comprising the μth pattern: ξ_i^μ. Since only adjacent nodes in a synfire chain are connected, the weight matrix in a network in which one synfire chain was embedded would be

$$J_{ij} = \frac{1}{N} \sum_\mu \xi_i^{\mu+1} \xi_j^\mu \ . \tag{3.6}$$

This equation is a special case of the general spatiotemporal pattern weight matrix (3.5). The anatomy of synfire chains is thus a special case of the more general spatiotemporal pattern connectivity, since there can be only connections between *adjacent* patterns.

These similarities suggest that synfire chains might be learned with the same mechanism as is proposed for spatiotemporal patterns, namely a temporal learning rule. In this case, a useful generalisation to the concept of synfire chains is to have non-adjacent connections as well as adjacent connections. The reason for this is that if the learning rule has a sufficiently broad temporal spread, the firing of nodes several stages apart may trigger learning.

3.4 Dynamics

In this section I will outline a number of factors that affect the recall of synfire chains without venturing too much into mathematics, which I will do in the course of explaining the derivations in chapter 6.

There are five possible instabilities in the propagation of synfire chains that constrain the weights, threshold, sparseness and number of links stored in a network of fixed size. In section 3.4.1 I discuss the instability I call *temporal coherence.* It was first investigated by Abeles (1991), who referred to it as "dynamical stability". The terminology of the last four instabilities is due to Wennekers (1999a). *Asynchronous background instability* (section 3.4.2) and *chain death due to fluctuating potentials* (section 3.4.3) are both consequences of a capacity analysis of the network in the limit of a large network. *Cross excitation* (section 3.4.4) and *chain death due to refractoriness* (section 3.4.5) occur in networks where the asymptotic analysis breaks down.

Although the weight matrix specifies the order in which activity passes through nodes, it does not determine the frequency or speed at which nodes are recalled. Section 3.4.6 discusses the factors that affect the speed.

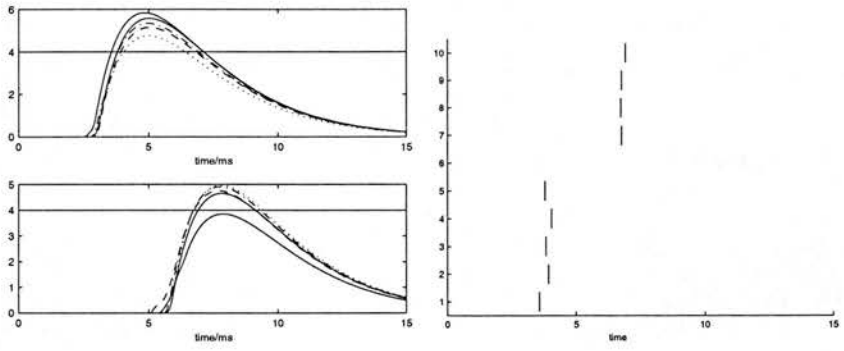

Figure 3.7: Demonstration of temporal coherence and chain death due to fluctuating potentials. *Left.* Plots of the membrane potentials of neurons from the first node (upper) and second node (lower) in a synfire chain. The threshold of 4 is labelled by a solid horizontal line. *Right.* Corresponding raster plots (the neurons of the first node are labelled 1–5; those of the second are 6–10). The variation in weights and delays between the two groups of neurons causes dispersion in the firing times of the second node and causes one of the neurons (6) not to fire, because its membrane potential does not reach threshold.

3.4.1 Temporal coherence

Although the term "synfire" indicates the firing is synchronous, in fact there will be always some temporal dispersion of the firing times within a node (see figure 3.7). Does this temporal dispersion increase rapidly or stabilise as activity propagates down the chain? Abeles (1991) argued qualitatively that under cortical conditions, activity would stabilise, being robust to small amounts of jitter in the firing times of neurons. Herrmann et al. (1995) and Hertz (1999) confirmed this quantitatively in the case where the rise time of the EPSP is small compared to the temporal jitter. They found that synfire propagation is stable, given a large enough average connectivity, large enough nodes, an appropriate shape of EPSP and small enough fluctuations around the average connectivity level, thresholds and EPSP size.

Aertsen et al. (1996; Diesmann et al., 1996, 1999) reached similar conclusions in a simulation study. They used the concept of *pulse packets*, the probability density of an active neuron as a function of time. They found the mean response of an IF neuron with a noisy membrane potential to input pulse packets parameterised by the total number of spikes and temporal dispersion. They characterised the output similarly and thus were able to find a neural transmission function that gives the relationship between the height and width of incoming and outgoing pulse packets. From the neural transmission function they determined a parameter range in which synfire transmission

is stable, that is, for which the pulse packet width does not increase. This led to conditions for minimum width and connectivity of chain. They estimated 100 spikes — that is 100 neurons in a node — were needed for stable transmission. A drawback of this analysis is that it deals with transmission in the mean (Diesmann et al., 1999). A particular input activity pattern drawn from the mean distribution might not be sufficient to fire the next node in the chain, especially on the margins of stability as calculated with pulse packets. This will tend to reduce the stable parameter range.

3.4.2 Asynchronous background instability

The weight matrix (3.6) makes clear that synfire chains can be thought of as an associative memory. As with all associative memories, synfire chains can only store a finite number of patterns before recall breaks down. Herrmann et al. (1995) exploited the similarity with an autoassociative network of sparse 0/1 patterns studied by Tsodyks and Feigel'man (1988). The update of the network was synchronous, so that at each time step the activity of the network corresponded to those neurons that would have fired in a synfire chain with the same connectivity at the same time step. There was inhibition to control the activity of the network and the activation function of the network was a step function which implemented a threshold.

They used mean field analysis to obtain fixed point equations for the activity of the network and the overlap of the patterns. Stability analysis showed that for a given capacity of the network, if the threshold is below a certain level, the activity level explodes. In the limit of large network size, the cells that fire are uncorrelated with the simultaneously active synfire patterns. This gives rise to the name *asynchronous background instability* (Wennekers, 1999a).

(Bienenstock (1995) and Hertz (1999) calculated the capacity using a simpler signal to noise calculation.)

3.4.3 Chain death due to fluctuating potentials

The equations of Herrmann et al. (1995) show that if the firing thresholds are high, and the variance of the potentials in a node are also high due to a large number of stored patterns, then some neurons in a node may fail to fire causing activity to die out (see figure 3.7). Wennekers (1999a) calls this instability *chain death due to fluctuating potentials.*

3.4.4 Cross excitation

In small networks the asymptotic analysis (Herrmann et al., 1995) breaks down because the background noise between cells is not independent. In this case there may be exceptionally large overlaps between nodes that might erroneously activate other nodes if the threshold is low (Wennekers, 1999b).

3.4.5 Chain death due to refractoriness

Overlap of nodes is responsible for chains dying when there is a high threshold and a refractory period. This is because if two nodes that are close together in the sequence overlap strongly, many of the neurons in the second node will be refractory when their turn to fire comes because they will have recently fired (Wennekers, 1999b).

3.4.6 Speed of recall

In the original picture of synfire chains, the speed at which nodes fired was considered to be constant. However, as explained in section 3.1 in the context of spike-based spatiotemporal patterns, the speed of recall can be modulated by changing the threshold or, equivalently a control input (Arnoldi and Brauer, 1996; Wennekers and Palm, 1996). To recap, the lower the threshold, the sooner the membrane potential in a given neuron will reach the threshold, and therefore the faster activity will propagate.

Arnoldi and Brauer (1996) have investigated this phenomenon with simulations and others (Wennekers and Palm, 1996; Wennekers, 1999b; Ermentrout, 1998) and have analysed a somewhat more general system where connections are not restricted to neighbouring nodes.

Changing the recall speed could be a useful property for recalling patterns (for example motor sequences) at variable speeds. It could also be used to synchronise the activity of two synfire chains, as Bienenstock's (1995) model requires. Arnoldi and Brauer (1996) showed this was possible using weak inter-chain excitatory connections. Variable speed of recall also has interesting implications for the detection of synfire chains (see section 3.6).

3.5 Coding

This section describes a number of proposals as to how synfire chains could process information.

3.5.1 Synfire chains as spatiotemporal pattern memory

As pointed out in section 3.3, we can think of synfire chains as a special case of a spatiotemporal pattern memory in which the patterns are retrieved synchronously. The nervous system certainly needs to be able to produce sequences of patterns, for example motor patterns or episodic memory patterns in the hippocampus (Levy, 1996). Whether or not the patterns need to be produced synchronously is an open question. Nevertheless, the possibility seems reasonably likely and it therefore seems worthwhile to investigate the properties of synfire chains that might relate to pattern storage.

Wennekers and Palm (2000) and Wennekers (1999b) have shown that a slight modification to synfire chains allows them to act as sequence recognisers. The trick is to set up the synfire chain so that it needs extra activation at each node to allow it to propagate. The extra activation comes from the scalar product of stored weights and an input pattern as in a conventional associative network. Again, it is not known whether the brain uses this method of pattern recognition.

3.5.2 Synfire chains as reverberating short term memory

The end of a synfire chain can be connected back to its beginning to create a loop. In this structure, once a node is activated, activity will *reverberate* around the loop (Abeles et al., 1993). This state can be regarded as a stable attractor. Thus, the network can act as a short term memory (STM) or working memory state. It should be possible to store a number of loops in a group of neurons. Inhibitory input could be responsible for quenching the activity.

It is possible to build networks of spiking neurons that store stationary attractors (Gerstner and van Hemmen, 1992) by means of purely excitatory connections. In these networks the recall can be either asynchronous or synchronous. However, firing rates are unrealistically high and the ISI histograms of individual neurons are not distributed exponentially, because they fire almost periodically. It is difficult to keep the activity at realistic levels with inhibitory neurons without quenching the activity of the network completely.

3.5.3 Synfire chains as transmission mechanism

Synfire chains could be a mechanism for transmitting activity across long distances in the cortex (J. Murre, personal communication), though given the long range connections that exist in the cortex this seems unlikely.

3.5.4 Synfire chains as multilayer perceptrons

Abeles (1991) proposed that synfire chains are equivalent to multilayer perceptrons (see section 1.3.3). This is true insofar as synfire chains exhibit feed-forward propagation of activity. However, on their own, synfire chains do not *process* information; the activation at each node is always the same (or similar) on each pass of activity through the chain. By contrast, the activations in the units of a multilayer perceptron depend on the input pattern.

Would it be possible to modify the synfire chains to implement multilayer perceptrons? There would need to be a number of possible routes through a particular chain that would lead to a different output at the final node. Although I cannot prove that it would be impossible, the problem of learning indicates this would an unpromising line of research. Learning would require the backpropagation algorithm, which requires feedback from all layers higher than a certain layer back to that layer. Although spike timing dependent synaptic plasticity (section 2.5.2) might allow this, it is not clear that the error would be propagated properly.

3.5.5 Synfire chains as primitive features

Bienenstock (1995) proposed that synfire chains represent primitive features. He wanted to show that representations in the neocortex could be built up *compositionally*, that is recursively, out of previously constructed entities. For compositionality to work, there needs to be some way of binding entities dynamically. Therefore, if synfire chains represent primitive features, it should be possible to bind them dynamically by some mechanism. Narrower synfire chains could be dynamically linked by weak connections to form broader chains thereby allowing recursive representations.

A proposed linking mechanism is to synchronise the activity of two activated chains. Bienenstock (1995) proposed that this could be achieved by weak connections from the node of one chain to the next node of another chain and vice versa.

Using simulations, Abeles et al. (1994) showed how weak connections could be learned between synfire chains embedded in a random, sparsely-connected network. The basic training protocol was to activate a pair of synfire chains simultaneously and if activity successfully propagated to end of both chains, apply Hebbian learning to the inter-chain connections. The synaptic modification was stronger for smaller time intervals between pre- and postsynaptic cells, consistent with the experimental evidence (section 2.5.2). After sufficient training synfire activity in one chain activated the chain it had been paired with.

Although these simulations certainly demonstrated the possibility of learning synfire chains dynamically, it is not clear how dependent the result was on various aspects of the simulations. Such aspects include: the particular neuron model (refractory IF neurons with various channels); the activity-dependent dynamic threshold; and the weight decay factor. A further questionable aspect was the connectivity. Each synfire chain in a pair was embedded in a sub-network containing both excitatory and inhibitory connections[1], but the links between these sub-networks were purely excitatory. This obviously restricts the generality of the result, although arguments could probably be made about the pattern of excitatory and inhibitory cortical connectivity.

I can not think of a knock-down theoretical argument against using synfire chains as primitive features and synfire binding, although perhaps a careful look at the numbers of synfire chains required for the theory might prove instructive.

3.5.6 Synfire chains as finite state automata

Wennekers (1999b) has shown that slightly modified synfire chains can be arranged so as to implement finite state automata. The slight modification is to add an extra gating input to nodes, similar to the one needed to make a sequence-recogniser. This effectively allows a node to act as an AND gate, thereby allowing nodes to be excited only when they receive the correct external and internal input. Thus the nodes and external inputs of a finite state automaton can be implemented. The model can be extended to implement a non-deterministic finite state automaton.

This result is interesting as it shows that synfire chains can compute. However, it is worth noting that relatively simple systems such as time-discrete, binary threshold neurons can implement finite state automata.

3.6 Experimental evidence for synfire chains

Synfire chains are a nice theoretical construct, but do they exist? In section 3.6.1 I summarise the evidence for synfire chains. I outline some criticisms of the methods and data in section 3.6.2. Finally, in section 3.6.3, I discuss the arguments for and against.

[1] An interesting point is that when fully trained, the total activity of the assemblies was also correlated. Due to the inhibitory-excitatory connections, the overall activity was oscillatory, with the period being regular in the case of moderate learning, and irregular in the fully trained network. Abeles et al. (1994) speculated that the stimulus-dependent, oscillatory, synchronised activity found experimentally (Gray et al., 1989; Gray, 1994) might be a consequence of this process, which they call *synfire binding*.

3.6.1 The evidence for synfire chains

As mentioned in section 3.2, the synfire hypothesis predicts precise time locking (1–3 ms) between cells recorded from within the same node. We might expect it to be difficult to find synchronous firing of neurons experimentally, as the chain will probably be very sparse, so there will be an extremely low probability of finding neurons in the same node. However, the (constant speed) synfire hypothesis also predicts that there will be precisely timed spike patterns (PTSPs) between neurons on a timescale of hundreds of milliseconds, due to the small dispersion of activity. Repeated spatiotemporal patterns in one or more neurons would therefore provide indirect evidence for synfire chains.

Early attempts at finding patterns in spike trains of single neurons (Marczynski and Sherry, 1971; Marczynski et al., 1980) used the pattern of interspike time interval increases and decreases rather than the precise temporal patterns to determine whether neurons were producing unusual spike patterns. Marczynski and others found above-chance patterns of increases and decreases in the caudate nucleus of unanaesthetised, immobilised cats (Marczynski and Sherry, 1971) and in the hippocampal neurons of cats during rapid eye movement and motionless quiet wakefulness but not during slow wave sleep (Marczynski et al., 1980).

Dayhoff and Gerstein (1983a,b) proposed a method for detecting excess temporal patterns within a neuron by comparing counts of "words" (that is patterns of ISIs) in the recording with the null hypothesis numbers of spikes created by shuffling the ISI histogram of the recording. They also proposed a template method for determining how many of each pattern was present. Put together, these two methods allowed them to discover above-chance numbers of repeating temporal patterns in over 50% of cells in the Crayfish claw control system and 50% of neurons from the striate cortex of lightly anaesthetised cats, albeit at a very low resolution of about 50 ms.

Lestienne and Strehler (1987) found evidence for excessive numbers of repeating doublets and triplets of spikes at a time resolution of 0.14 ms in 100 ms time windows of activity recorded from neurons in the monkey visual cortex.

Abeles and Gerstein (1988) developed an efficient pattern-matching algorithm based on the idea on representing the spike train by punched holes in a piece of paper. When a copy of one spike train punched tape is pulled past the another, excessive patterns are evident when more holes than usual align. The amount by which the tape has been pulled is the interval between the two spikes in a PTSP. This is in fact the same as performing a cross correlation analysis on the spike trains and looking for large peaks. They also developed a significance test that worked quite well for stationary

and near-stationary spike trains but failed on spike trains with considerably varying rates.

Villa and Abeles (1990) found evidence for spatiotemporal firing patterns in the auditory thalamus of an anaesthetised cat using this algorithm. Abeles et al. (1993) used the same pattern-matching algorithm to discover excessively-repeating PTSPs in the frontal cortex of behaving monkeys. They found an excess of repeating PTSPs in 1, 2 or 3 neurons in 30–60% of cases, allowing for a timing jitter of 1–3 ms. For a given behavioural condition there were many different patterns, though one pattern did not correspond to more than one behavioural condition. In 13 out of 20 cases the elevated firing rate above 40 Hz was mainly associated with repeated spatiotemporal patterns. The most marked excess patterns mainly comprised one or two units. The repeated activity in one or two units was interpreted as *reverberations* in the synfire chain, that is recurrent connectivity.

Prut et al. (1998) have matched recordings from the premotor and prefrontal ares of monkeys performing a task with various aspects of that task. They found evidence that suggests the identity of the PTSP correlates to the behavioural state. Furthermore, the time-dependent firing rate did not provide a better description of the behavioural state than the PTSPs.

3.6.2 Criticism of the evidence for synfire chains

There are three main criticisms of the evidence for synfire chains.

3.6.2.1 The "null hypothesis" criticism

PTSPs can occur by chance as well as by design. Whether the number of PTSPs detected in an experiment are significant or not depends on the null hypothesis used to determine how many PTSPs would be expected to occur by chance. The simplest null hypothesis is a uniform Poisson process with the same firing rate as the neurons recorded from. The expected number of PTSPs depends in a highly nonlinear way on the firing rate. When using a uniform Poisson null hypothesis, it is therefore important to make sure that the variation in the firing rate is small over the firing period. For variable firing rates the minimum null hypothesis should be a nonuniform Poisson process based on an estimate of the time-dependent rate.

Oram et al. (1999) have gone one step further in their search for PTSPs across triplets and quadruplets of lateral geniculate nucleus (LGN) and primary visual cortex (V1) neurons in the awake fixating rhesus monkey. Their "spike matched" null hypoth-

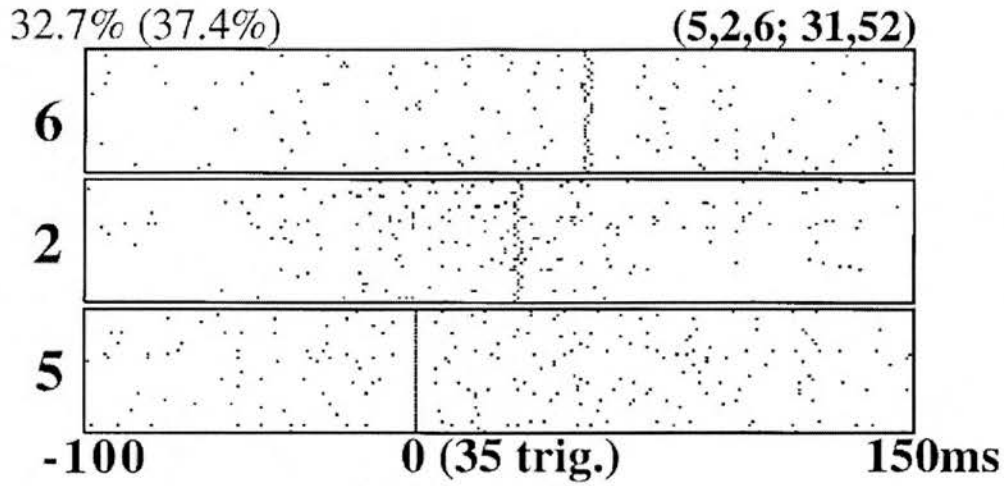

Figure 3.8: An example of a precisely timed spike pattern (PTSP). Each box contains a number of spike rasters from trials in a different neuron; the same trial from each neuron is plotted at the same height in each box. The rasters have been aligned so that the PTSP is evident. The PTSP is a triplet: its first spike is at time 0 in neuron 5; its second is in neuron 2 at 31 ms later; and its final spike is 52 ms later in neuron 6. The second and third spikes are not perfectly aligned; this reflects the jitter allowed in the pattern-matching algorithm. From Prut et al. (1998).

esis is based on a nonuniform Poisson process but additionally matches the number of spikes on a trial-by-trial basis and matches the ISI histogram by removing short intervals that occur less frequently in the neural data because of refractory properties of the neurons. They found that the number of PTSPs in their data was not significantly different from the number predicted by the "spike matched" null hypothesis. Other possible null hypotheses, including uniform Poisson and nonuniform Poisson, underestimated the number of PTSPs actually produced. The number of PTSPs was correlated almost perfectly with the spike count, indicating that the number of PTSPs might not convey any more information than the time-averaged rate. Information theoretic analysis bore this out: the number of PTSPs conveyed only a third of the information carried by the spike count, and even a combined spike count and number of PTSPs code did not convey any more information than the rate.

3.6.2.2 The "correlation with behaviour" criticism

Another criticism (Shadlen and Newsome, 1994) of the experiments of Abeles et al. (1993) is that they made no attempt to correlate the identity of the PTSPs with the current behaviour or state of the animal. The experiments of Prut et al. (1998) answer

this criticism and show that the identity of the PTSP does correlate to the behavioural state.

3.6.2.3 The "too many single-spike patterns" criticism

One puzzling aspect of the frontal cortex data is the preponderance of three-spike patterns made up from the firing times of one or two units rather than three units. If the units that make each node are chosen from a uniform distribution we would expect to observe far more triplets from different neurons than from the same neuron (see appendix A.1). In fact, we see almost the opposite, with the percentages of 1, 2 and 3 unit triplets being 70%, 29% and 1% respectively (Abeles et al., 1993) and 24%, 43% and 24% respectively (Prut et al., 1998). Therefore, either the assumption of uniform participation must be wrong, or there may be some bias in the measurement and detection of the repeating patterns. Abeles et al. (Abeles et al., 1993; Prut et al., 1998) believe the distribution of participation is strongly non-uniform and that the synfire chains are circularly connected so that activity *reverberates* around them. This would tend to favour single unit recordings more than the uniform case, since activity would certainly return back to the neuron. However, the patterns should then all have the same intervals, which they appear not to.

3.6.3 Discussion

The "null hypothesis" criticism of Oram et al. (1999) is the most convincing of the criticisms of evidence for synfire chains. However, it does not rule out synfire chains conclusively.

Firstly, none of the possible functional roles of synfire chains mentioned in section 3.5 predicts that the *number* of times a PTSP appears conveys information. Rather they predict that the same PTSPs should appear in different trials, and that their *identity* should be correlated with behavioural or cognitive states. Secondly, the results of Oram et al. (1999) are from visual areas rather than frontal areas. It may be that synfire chains exist in frontal areas and not in visual areas. Finally, a factor which no experiments have taken into consideration is that of variable speed of synfire chains. If, as suggested in section 3.4.6, the speed of recall is variable, then the intervals between neurons in successive nodes in a chain will not be constant, and the chain will be impossible to detect using current methods. Although it is not inconceivable that new methods could be developed to detect chains propagating at variable speeds, they will have to be much more sophisticated that today's methods. This does not mean that synfire chains are

unfalsifiable in principle, though it may prolong the debate between the proponents and opponents of synfire theory.

It is also worth noting that although synfire chains are one possible cause of excessive PTSPs, another mechanism could produce the same effect. Therefore, experiments to determine the existence and coding properties of excessively repeating PTSPs can only prove that synfire chains do not exist.

To conclude, there are two answers to the question "do synfire chains exist in the mammalian brain" depending on where we look. In visual areas, the answer is "probably not" and in frontal and auditory areas it is a cautious "possibly". Despite this, I believe that there is still enough doubt about the existence of synfire chains to make their theoretical study worthwhile. More ideas about how they might function could lead to more precise, testable hypotheses.

3.7 Learning

In this section I will review work done on learning synfire chains. I believe that as with conventional neural networks, there are two possible methods of learning synfire chains: supervised and unsupervised. In section 3.7.1 I will review work done on learning synfire chains might form in an unsupervised fashion from a network with random connections due the random activity of the network and a suitable learning rule. In section 3.7.2 I discuss aspects of supervised learning.

3.7.1 Unsupervised learning

If the identity of the neurons of a node does not convey any meaning we might expect the synfire chains to self-organise. (An example where the identity does not matter is the "synfire chains as primitive features" scenario discussed in section 3.5.) Abeles (1991) argued heuristically that synfire chains should be able to self-organise from a randomly-connected network. Hertz and Prügel-Bennett (1996) explicitly modelled the Hebbian learning of synfire chains, using synchronously updated, leaky IF neurons with shunting inhibition proportional to total activity. There was initially random 25% connectivity and weights were randomly distributed. They adjusted the parameters of the weight distribution and the inhibition so that the level of background activity was stable. They then tried to make synfire chains self-organise by using a Hebbian rule with a one-step time delay and by repeatedly presenting a stimulus to the same small group of neurons. This protocol alone did not cause synfire chains to form, though with various strategies it is possible to learn 20 nodes. These strategies included sequential

stimulation of groups of neurons, a more abrupt nonlinear learning rule, adaptive inhibition, normalisation of presynaptic weights and an adaptive threshold. The main limit on learning seemed to be as the random connectivity changed, the spontaneous activity became unstable. Hertz (1999) suggests that short-term synaptic modification (Tsodyks and Markram, 1997) might improve synfire chain self-organisation.

3.7.2 Supervised learning

Another possibility for learning synfire chains is that there is some external network with connections to the network in which the synfire chain is to be learned. Possible teacher-student pairs are the hippocampus and the neocortex (McClelland et al., 1995) or the motor cortex and the basal ganglia.

Excitation from the external network could activate groups of neurons in the target network in the same order repeatedly. If this happens enough times while a temporal learning rule is in operation, we would expect to end up with a weight matrix similar to the prespecified one (3.5) given earlier in the chapter. With the exception of the preceding section, we have thus been considering supervised learning throughout this chapter.

In section 3.4.6 I discussed how the speed of *recall* could vary as a function of the threshold and other parameters. If we are explicit about supervised learning, another, hitherto neglected speed comes in to play, namely the *training speed.* This is speed (or frequency) at which the patterns are presented to the network by the external network. In chapter 6 I will present analysis that explicitly considers the training speed.

3.8 Summary

Sequences in their most general form encompass a progression of activity from one state to the next. Although this could be in the form of firing rates, such as dynamic attractor networks, a spike-based alternative is spatiotemporal firing patterns. Spatiotemporal firing patterns can be learned with an asymmetrical temporal learning rule and recalled by activating the first few neurons in the pattern.

Synfire chains are the name given to the neural substrate and activity pattern of one particular form of spatiotemporal spiking pattern. Here the neurons are organised into a sequence of groups known as nodes. When activity propagates down the chain, activity within each group is synchronous. In the original conception of synfire chains, there were only connections between adjacent groups. Synfire chains help keep activity constant in a system without requiring unrealistically fast inhibition.

Synfire chains have many possible functions, including spatiotemporal pattern memory, reverberating short term memory a transmission mechanism, primitive features and a basis for implementing finite state automata.

Synfire chains or spatiotemporal firing patterns manifest themselves as precise, repeated time intervals in single and multiunit recordings. There are algorithms to discover precise, repeated time intervals in spike train data, but the statistics of showing that there are a significant number of repeated time intervals are disputed. The experimental evidence for spatiotemporal patterns in the mammalian cortex is suggestive but not conclusive. Nevertheless, the idea of spatiotemporal sequences and synfire chains does not seem implausible, so study of their dynamics is worthwhile. Less precise sequences are present in many other systems, for example the mammalian hippocampus and the locust olfactory system. Studying synfire chains might throw up results applicable to less synchronised systems.

There has been some theoretical work on the dynamics of synfire chains. There are simple arguments that show the conditions on the variance of the weights, time delays and neuronal noise in order to obtain temporally coherent pulses of activity at each node. A network of neurons can only support a certain number of synfire chains before activity becomes unstable, as with a standard Hopfield network. The firing threshold can be set higher to prevent this instability, but if it is set too high, chains will fail because the potential is not sufficient to reach the firing threshold. In small networks, exceptional overlaps between nodes in different chains are more likely, causing activation to spread from one chain to another. A similar problem arises when overlap occurs between nodes close together as many neurons may be in a refractory state when they are due to fire.

Attempts to encourage synfire chains to self-organise with an asymmetric temporal learning rule have not been very successful. "Supervised" learning has been investigated implicitly and is relevant to the idea of copying synfire chains. The speed of propagation of synfire chains can be controlled by the threshold.

I will present my work on this in chapter 6.

Chapter 4

Synchrony

The purpose of this chapter is to introduce some of the experimental evidence for, function of and mechanisms underlying synchronous activity in the nervous system.

Oscillations and synchrony are ubiquitous in nervous systems. Although they often occur together, they are distinct concepts. Section 4.1 gives an definition of synchrony and oscillations in terms of their detection using cross-correlation functions, already discussed in chapter 2.

Synchrony has been proposed as a way of encoding certain types of information. Section 4.2 gives examples of how synchrony appears to encode information in the visual, auditory and olfactory modalities. Neuronal firing can be locked to the time course of a stimulus or can be synchronised with other neurons. One potential use of synchrony that has received much attention in recent years is as a mechanism to bind together distributed representations in the nervous system.

In section 4.3 I review theoretical work on the dynamics of synchrony in networks of graded response and spiking neurons and with purely inhibitory or excitatory connections. For a network with a certain type of uniform connectivity, the SRM encountered in chapter 2 provides a way of deriving a general condition on whether a network will remain in a synchronous state.

4.1 Synchrony and oscillations

A working definition of synchrony is that different neurons fire within a few milliseconds of each other. The cross-correlation function (see section 2.3.2) is one way of showing whether neurons are firing synchronously over a period of time. In the case of a pair of neurons firing synchronously, we would expect to see a single large peak in the cross-correlation function at a time lag of zero.

What we would see in the rest of the cross-correlation function would depend on

the nature of the neurons' activity. If, in addition to firing synchronously, the neurons were firing fairly periodically, we would expect to see bumps in the cross-correlation away from the centre peak. This is the case of *synchronous oscillations*, the subject of a great deal of research in recent years (see section 4.2.3.2). Despite the research interest, synchrony can also occur without oscillations. In this case, there will just be a peak at a time lag of zero against a fairly constant background at other time lags.

The converse of synchrony without oscillations is oscillations without synchrony. This could occur when recording from two neurons that are firing periodically at the same frequency, but with a phase lag between them. The locust olfactory system (to be discussed in chapter 7) is an example of where there are oscillations, though not synchrony between neurons of different classes.

4.2 Synchrony codes

This section presents a selection of codes involving synchrony. It is by no means exhaustive; for a more comprehensive review see Gray (1994). Perhaps the most straightforward type of synchrony code is one in which the neural response is synchronised to a stimulus. In section 4.2.1 I present evidence that shows that such a code exists in the auditory system. Synchrony need not be stimulus-locked; in section 4.2.2 I present an example from the auditory system where synchrony represents the presence or absence of a quality in the stimulus. Section 4.2.3 deals at some length with a controversial proposed use of synchrony as a solution for the binding problem, the problem of indicating to the nervous systems which parts of distributed representations belong to the same object. In section 4.2.4 I describe how synchronous oscillations also seem to refine representations of odours in the locust olfactory system.

4.2.1 Stimulus-locked synchrony in the auditory system

Figure 4.1 shows how in the mammalian auditory system, neurons in the auditory nerve lock their firing to the periodicity of sounds impinging on the ear (Kiang, 1980). This information is used by the CNS to determine phase differences between the ears (Carr, 1993). The firing rate of neurons in the auditory nerve encodes the intensity of stimuli. Thus the firing of the auditory nerve is a dual code.

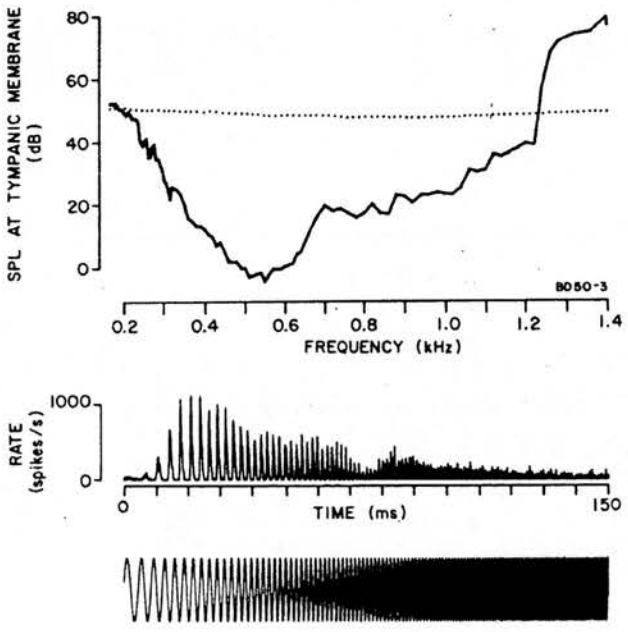

Figure 4.1: Auditory nerve fibre locking to a stimulus. The *bottom trace* shows the stimulus presented, a swept tone ranging in frequency from 0.2 kHz to 1.4 kHz. The *middle trace* shows the post stimulus time histogram (PSTH) of the neuron's discharges averaged over 960 repetitions of the stimulus. It is clear to see that at lower frequencies the auditory nerve discharges are locked to the stimulus amplitude. The *top graph* is a tuning curve based on the discharge rate of one neuron from the cat auditory nerve. The solid line indicates the sound pressure level of a pure tone at the frequency on the abscissa required to elicit an increase in firing rate of 10 spikes per second. The dotted line indicates the level of the sound of the swept tone shown in the bottom trace. From Kiang (1980).

4.2.2 Synchrony in the auditory system

Another example from the auditory system, though further from the periphery, comes from deCharms and Merzenich (1996), who recorded from two locations of the primary auditory cortex of marmoset monkeys. Firing rates in response to no stimuli were the same as the firing rates in the tonic part of a prolonged stimulus. But during the tonic part of the continuous stimulus the correlation between the two neurons increased. The correlation was not stimulus-locked, so seemed to originate from the network dynamics of the system.

4.2.3 Binding by synchrony

This section deals with a controversial theory, that of binding by synchrony. Section 4.2.3.1 outlines the binding problem and the theory developed to solve it. Evidence from the visual system that appears to support this theory is presented in section 4.2.3.2. In section 4.2.3.3 I present theories of how binding by synchronisation might be extended in central systems. Finally, I end with some of the criticisms of the binding by synchrony theory in section 4.2.3.4.

4.2.3.1 The theory

While developing a theory of translation-invariant shape recognition, Milner (1974) encountered the problem of how the nervous system represents *primitive unities*, that is, parts of an object that belong together. The psychological analogue of this is known as the *binding problem*, and has been discussed since the time of the Gestalt psychologists. To solve this problem, he suggested:

> If adjacent, or nearly adjacent, cells interact when excited, in such a way as to synchronize and perhaps intensify each other's activity, this could provide the unifying characteristic that ties the elements of a figure together. At subsequent levels of the pathway, impulses from the cells fired by one whole would arrive as synchronous volleys, whereas impulses from different figures would have a random temporal relationship to each other. (p. 526)

Thus stimuli could induce synchrony and this synchrony can be read-out at higher levels of the nervous system because groups of neurons firing synchronously are more effective at making other neurons fire than asynchronously firing groups.

Independently, von der Malsburg (1981) put forward the *correlation theory* of brain function. In a similar vein to Milner, he suggested the correlations between cellular signals on a 2–5 ms time scale served to mark those signals as belonging together.

He also proposed synaptic modulation on a fast (millisecond) timescale, as well as conventional long term synaptic plasticity. The fast plasticity provides a mechanism for separating concurrently activated assemblies by changing the effective connectivities between the cells in each assembly.

4.2.3.2 Experimental evidence from the visual system

Evidence in favour of the correlation theory in the visual system has accumulated. Figure 4.2 illustrates the key result, stimulus-dependent synchronisation. When two cells in primary visual cortex with non-overlapping receptive fields (RFs) are excited by different parts of something that is perceived as the same object, the cells synchronise their activity. If each cell is responding to a different object, their responses are uncorrelated (Gray et al., 1989). In fact the strength of correlation depends on the Gestalt coherence of the object. The neurons with non-overlapping RFs are most correlated when stimulated with different parts of the same moving bar, are somewhat less correlated when the bar was split in the centre, but the two parts were collinear, and showed no correlation when the different parts of the bar moved in opposite directions.

This synchrony occurs in the context of oscillations. Gray et al. (1989) showed the spiking activity of neurons in the same column of the cat visual cortex oscillated synchronously in the gamma frequency range of 40–60 Hz. The synchronous oscillations can occur within columns and between columns (Gray et al., 1989; Eckhorn et al., 1988), between different brain areas (Eckhorn et al., 1988) and between hemispheres (Engel et al., 1992). Singer and Gray (1995) comprehensively review all this work. Engel et al. (1990) discusses the basis of the methodology of these investigations, auto- and cross-correlation histograms.

The substrate for the oscillations was postulated to be due to the lateral connections between neurons in the visual cortex (Engel et al., 1992). This is because the inputs to either side of the visual cortex remain segregated after the optic chiasm, so it would be not be possible for common input from the thalamus to synchronise the activity. When the corpus callosum was cut, synchronisation was abolished, confirming this theory. However, the synchronisation could be due to feedback activity from later stages of the visual system, which would also be abolished by severing the corpus callosum (Bugmann, 1997).

Another possibility is that the synchronisation is established early in the processing system. Neuenschwander and Singer (1996) found that synchrony could be evoked in the retina. In retinal ganglion cells in anaesthetised cats, stationary and moving light

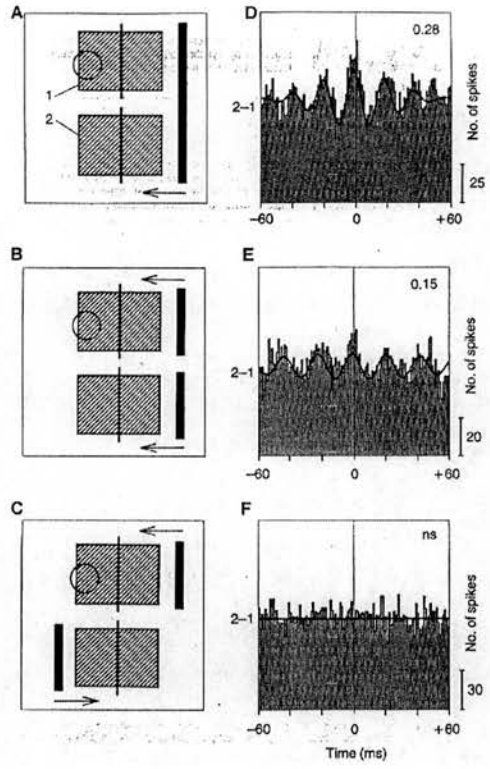

Figure 4.2: The Gestalt criteria of continuity and common fate are satisfied by synchronous firing between cells with different RFs but similar orientation preferences. Multiunit recordings were taken from two sites in area 17 of the cat visual cortex separated by 7 mm. *A–C.* The thick vertical bars represent the stimuli and the arrows show their direction of movement. The shaded rectangles correspond to the visual fields of the recorded neurons, with the thin vertical bars indicating their preferred orientation. The circle marks the centre of the visual field. *D–F.* The corresponding cross-correlograms of recorded activity. The number in the upper right corner is a measure of correlation strength, where "ns" stands for "not significant". The scale bars indicate the number of spikes. (From Engel et al., 1992.)

stimuli evoked oscillatory responses in the frequency range of 61–114 Hz. There was stimulus-dependent synchronisation between cells as far as 20° of visual angle apart. They also found oscillatory correlations in the 35–125 Hz range between cells in LGN of anaesthetised cats. The oscillations could be coherent between hemispheres, but not between eyes, indicating that the retinal oscillation drives the LGN oscillations. Although the LGN oscillations could be due to feedback from higher visual areas such as area 17 and area 18 this seems less likely because of the difference in frequency range (30–60 Hz as opposed to 60–120 Hz).

4.2.3.3 Central systems

Phillips and Singer (1997) proposed that synchronisation plays an important role in a general scheme of cortical computation. They suggested that the basic cortical processor has receptive field (RF) and contextual field (CF) inputs. The RF inputs are meant to represent external information, are feedforward and largely determine the output of the processor. By contrast, the CF inputs are lateral or recurrent and serve to modulate the output of the processor rather than changing it directly. They help improve the coherence of the information passed forward, so that similar pieces of information will tend to reinforce each other (coherent Infomax). Phillips and Singer suggest that the synchronous oscillations implement the CF inputs to neurons.

The idea of synchronous oscillation has been proposed to deal with consciousness and attention (Crick and Koch, 1990; Singer, 1994). One possibility is that a saliency map or "spotlight of attention" could promote synchronous oscillations in areas of the primary visual cortex to make them more salient to higher levels of processing. Crick and Koch (1990) speculate about the number of oscillations in the brain. One global oscillation would be of little use since there could be a "best set" of fast firing neurons that would not need to be reinforced by oscillations. Oscillations might overlap and interfere with each other to different extents. There might be between about 4–7 coherent cycles in the brain at one time, and if these cycles correspond to attention or memory states they could explain the limits on human attention and memory.

4.2.3.4 Criticism of binding by synchrony

Wilson and Bower (1991) modelled the visual cortex using fairly realistic spiking neurons and anatomy. There were local inhibitory connections and longer distance excitatory connections. They presented continuous stimuli (like the bars used in the experiments) and found fairly weak 40 Hz auto- and cross-correlations locally within stimuli.

The extent of correlation was determined by longer distance excitatory circuits, the correlation length in objects being limited to twice the distance of the long-distance connections. Furthermore, where synchrony did occur, it was only possible to find a phase difference of zero between neurons by averaging over trials; there was no common phase difference for within-trial phase locking as in the experiments. Wilson and Bower felt that this presented a challenge to the theory of binding by synchrony, since it would not be possible for one large object to be represented by neurons firing at the same phase.

Amit (1997), in replying to Phillips and Singer (1997), criticises the idea that synchronisation is a necessary physiological solution to a cognitive problem, the binding problem. The solution is dependent on the correct parameters, and so it is not a necessary one. He also questions the amount of synchronisation required, and claims that the observed amounts are not great compared to the amounts seen in random networks (Amit and Brunel, 1997).

Golledge et al. (1996) criticise synchrony by binding on a number of counts. From a physiological viewpoint, they doubt whether neurons can be coincidence detectors and they note that it is more difficult to get synchrony between single unit recordings than it is to get oscillations. Golledge et al. argue most convincingly from a psychophysical basis. Experiments show that feature binding is very fast and indicate that object recognition requires only 20-30 ms of neural activity. This does not leave much time for binding with 40 Hz cycles. Furthermore most information from a spike train is available from the first 50 ms, that is only two cycles of 40 Hz. Less convincingly, they argue that the oscillations could be due to chance. This, they claim, is because a high level of firing implies a high level of synchronous firing by chance. As an alternative, they propose a spatial-attentional mechanism via the dorsal stream. Most radically they propose that the binding problem is not a problem because animals do not have to deal with as much information as we think. Therefore there is space in the cortex for information to reconverge physically in the system. This seems to be an incarnation of the grandmother or "cardinal" cell hypothesis (Barlow, 1972) and is a difficult argument to prove or disprove either way, as we do not have an exact figure on the amount of information a brain has to deal with, nor do we know what the possibilities of non-synchrony-based computation are.

Gray (1999) provides a comprehensive overview of the temporal correlation hypothesis and the debate surrounding it.

4.2.4 Refining the odour in the olfactory system

In the locust and honeybee olfactory systems, oscillations in the second stage of processing appear to be necessary for fine discrimination between similar odours (Stopfer et al., 1997). Chapter 7 covers this in more detail.

4.3 Synchrony dynamics

In this section I will review theoretical work on synchrony in networks of graded response neurons and networks of spiking neurons. The earliest models of network synchrony were based on graded response units such as the Wilson-Cowan oscillator. I discuss them in section 4.3.1 along with some of their applications. More recently, the synchronisation of networks of spiking neurons have been studied. I will summarise the variety of different systems studied and try to draw out some general principles in section 4.3.2. Finally, in section 4.3.3, I will present the *locking theorem* due to Gerstner et al. (1996b) that unifies the plethora of models to some extent. It also demonstrates the analytical utility of the SRM (see chapter 2).

4.3.1 Rate-based synchrony

As the stimulus-dependent synchrony results appeared from the late 1980s onwards (see section 4.2.3.2), interest grew in modelling them. As the oscillations occurred between cortical columns, the fundamental unit of the models was a cortical column. The Wilson-Cowan oscillator (Wilson and Cowan, 1972, see section 2.6) and similar *relaxation oscillators* with excitatory and inhibitory groups provided the model of a cortical column.

In order to model the synchronisation and desynchronisation necessary for binding and segmentation by synchrony, these oscillators have been connected together in a number of ways. For example, Wang and coworkers (Campbell and Wang, 1996; Wang, 1996) use local excitatory-excitatory connections between excitatory and inhibitory units arranged in a two-dimensional grid representing a visual area. They use fast synaptic plasticity (von der Malsburg, 1981; von der Malsburg and Schneider, 1986) as a normalisation mechanism to achieve synchrony between neurons in connected regions and a global inhibitor to prevent accidental synchronisation. The global inhibition is supposed to represent either general inhibitory activity from within the cortex, or thalamic inhibition. The network can segment up to five objects simultaneously present in the scene.

A different approach was taken by König and Schillen (König and Schillen, 1991; Schillen and König, 1991). Their model had short-range inhibitory connections and longer-range excitatory connections between units. The connections had time delays and there was no fast synaptic plasticity or global inhibitor. The units responded preferentially to bars of different orientations and were arranged topographically, similar to parts of a hypercolumn in the early visual system. With the correct time delays and connection weights, a bar with orientation between two of the orientation detectors synchronised the activity between them. However, two orthogonal bars each of which was close to one of the orientation detectors made the activity of the orientation detectors desynchronise (figure 4.3).

Similar models with excitatory-inhibitory neuronal units have been applied to binding and segmentation in the visual (Schillen and König, 1994; von der Malsburg and Buhmann, 1992) and auditory (Wang and Brown, 1999) systems.

These models suggest that binding and segmentation by synchrony is possible with a variety of different architectures (global inhibitor, different excitatory and inhibitory connection radii) and synaptic mechanisms (fast synaptic plasticity). As models of potential mechanisms and as engineering systems (for example Wang and Brown, 1999) they are interesting. However, as models of the visual system, I believe they are not sufficiently constrained to make predictions about the true mechanisms of synchronisation. As Gerstner and van Hemmen (1994b) have pointed out, spikes are a more fundamental quantity to use than firing rates, and spike-based synchronisation may turn out to be quite different to rate-based synchronisation.

4.3.2 Spike-based synchrony

Is synchrony different with spiking units? Since the late 1980s, theoretical work has been done on the synchronous properties of networks of spiking neurons connected by purely excitatory and purely inhibitory neurons. The basic units of these networks are IF or SRM neurons or mathematical abstractions of them. They are linked by pulses, like spikes. The PSC function associated with each spike can be delta function (which causes a step increase in potential), decaying exponential or alpha function.

Although the individual units in such systems can be thought of as IF neurons, they tend to be called *oscillators* since when IF neurons are sufficiently tonically activated they fire regularly. As the spikes are a form of pulse, this class of models is known as *pulse-coupled oscillators*. Furthermore, the units are sometimes not pure IF neurons, but rather abstractions of them that allow different kinds of analysis.

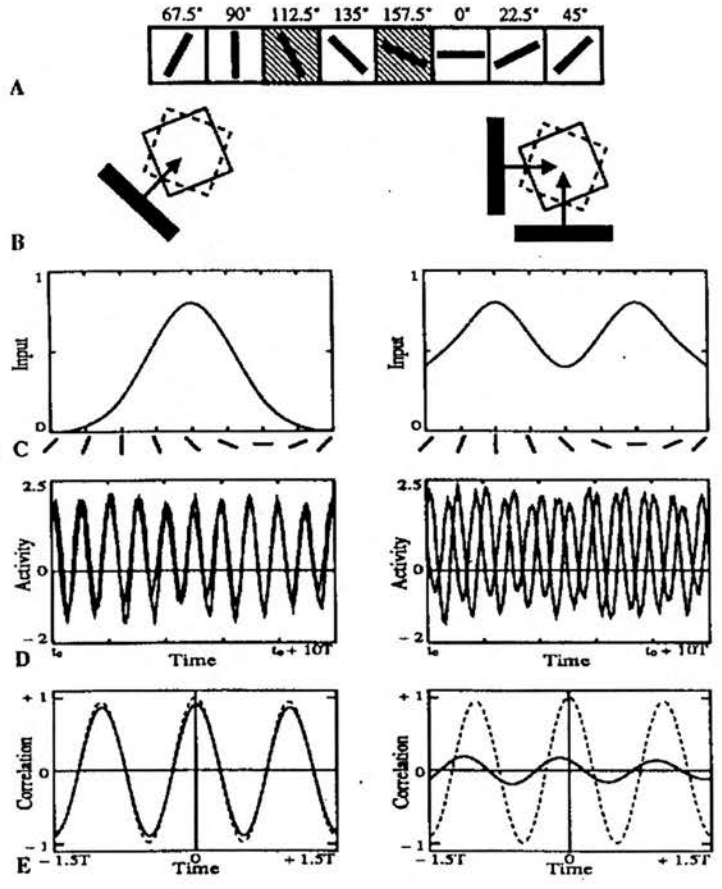

Figure 4.3: Stimulus-dependent assembly formation in the König and Schillen model. The top part of A represents the orientation sensitivity of feature detectors. The highlighted detectors are the ones that the recordings come from. When a bar of orientation between the two detectors is presented (lower part of A, left) the input across the detectors is as shown in the top, left-hand part of B, and the activity of the oscillators is synchronised as shown by the time traces (middle part of B) and cross-correlation function (lower part of B). When the two bars with orientations on either side of the selected orientation units are presented, the outputs are desynchronised (right column of A and B). ((from Schillen and König, 1991).)

In section 4.3.2.1 I will discuss networks of such neurons connected by excitatory synapses, in section 4.3.2.2 I will describe the properties of networks connected by inhibitory synapses, and in section 4.3.2.3 I will discuss the effect of delayed connections.

4.3.2.1 Networks of excitatory neurons

Mirollo and Strogatz (1990) used an oscillator model to show that networks of IF neurons coupled by purely excitatory infinitesimally short pulses with no time delays will synchronise from almost any starting configuration. Interestingly, this mathematical result applies to many other biological systems, providing an explanation for the synchronisation of firefly flashes and the synchronisation of the mensuration period in groups of women.

The results can be extended to networks connected by arbitrarily-wide pulses and excitatory, normalised weights with time delays (Gerstner, 1996). Here the network is guaranteed to converge on a phase-locked (though not necessarily synchronous) state.

Hopfield and Herz (1995) considered models of pulse-coupled IF neurons with tonic input that differed in two respects to the model of Mirollo and Strogatz. Firstly, the network comprised a lattice of neurons with each neuron connected to its four nearest neighbours. Secondly, the rules for update during synchronous spikes were different. Since the coupling between neurons is by delta function currents, when one neuron fires it leads to a step increase in membrane potential in other neurons connected to it, and may cause these neurons to fire at the same time. This is a idealisation of the behaviour of real neurons as one neuron cannot force another neuron to fire simultaneously. Hopfield and Herz attempted to make this situation more realistic by assuming that if a neuron i had caused a neuron j to fire at the same time, then i should receive a spike back from j and would have its membrane potential increased. Furthermore, in one variant of their model, they assumed that synaptic currents were long compared to the action potential, and that some of the current invoked in j by i would persist after the action potential, and therefore that j's membrane potential should not be reset to zero. In contrast, Mirollo and Strogatz assumed that the membrane potential is set to zero regardless of whether other neurons were firing at the same time.

Both models studied by Hopfield and Herz converge on (approximately) periodic solutions with synchronised clusters of neurons that occur at fixed phases in the cycle. The model in which current persists during an action potential eventually converges on a global solution. The other model does not converge to a globally synchronised state. Hopfield and Herz also studied non-leaky IF models and a model, based on earthquake

Study	Unit	J	Δ	γ	N	Synchrony
Mirollo and Strogatz (1990)	IF	E, g	0	δ	∞	Synchrony.
Hopfield and Herz (1995)	IF	E, l	0	δ	$10^3 \times 10^3$	Synchrony when synaptic currents persist through spike; otherwise synchronised clusters.
Tsodyks et al. (1993)	IF	E, g	0	e	∞	Synchrony.
van Vreeswijk et al. (1994)	IF	E, g	0	α	2	Partial synchrony for short PSC. time constant; antisynchrony for longer time constants
van Vreeswijk (1996)	IF	E, g	0	α	∞	Partial synchrony for short PSC. time constant; antisynchrony for longer time constants
Smith et al. (1994)	IF	I, g	0	2	δ	Antisynchrony.
van Vreeswijk et al. (1994)	IF	I, g	0	α	2	Synchrony for all PSC time constant; additionally antisynchrony for faster time constants.
van Vreeswijk (1996)	IF	I, g	0	α	∞	Synchrony for long PSC time constant; multi-cluster synchrony for shorter time constants; in the limit antisynchrony.
Smith et al. (1994)	IF	I, g	+	δ	2	Synchrony.
Gerstner and van Hemmen (1993)	SRM	E, g	+	e	∞	Partially asynchronous state stable for all delays; above a critical delay, a completely synchronous state is also stable.
Gerstner (2000)	SRM	E/I, g	+	e	∞	Yes, depending on weights.

Table 4.1: Summary of synchrony results. The column headed J shows whether the weights were excitatory (E) or inhibitory (I) or global (g) or local (l). The column headed by Δ shows whether the delays were zero (0) or finite (+). The column headed γ shows whether the PSC was a delta (δ), decaying exponential (e) or alpha (α) function. The column headed N shows the size of the network, with ∞ referring to a large network.

models, which has synaptic responses that are proportional to the membrane potential of the presynaptic neuron (see also Herz and Hopfield, 1995).

Tsodyks et al. (1993) analysed a network of tonically-excited IF neurons connected uniformly by pulse connections and exponentially-decaying PSCs. In the stable, synchronously-firing, periodic state they could write a mean field expression for the current. By substituting this into the equation for the voltage, they found various types of behaviour of the system. For small values of input current there are stable, periodic solutions, with the phase of the firing decreasing with increasing input. Above a critical input current, there is no stable firing; neurons will advance faster than the below-critical current time period. Thus if the current applied to neurons is inhomogeneous, with some neurons receiving more than the critical amount and others receiving less, the population will split into two groups: the below-critical current one firing periodically and the ones with current above the critical value firing more rapidly and not phase-locked.

The next stage of complexity is to use neurons connected with alpha-function PSCs. Van Vreeswijk et al. (1994) studied pairs of IF neurons so connected and showed that excitatory connections could induce anti-synchrony depending on the time constant of the alpha function. Van Vreeswijk (1996) extended these results to infinitely-large networks of IF neurons. With excitatory connections, the network fires completely asynchronously with long enough time constants, and below a critical time constant it starts to fire increasingly synchronously as the time constant decreases.

4.3.2.2 Networks of inhibitory neurons

For purely inhibitory, infinitesimally short pulse coupling a pair of IF neurons fire in anti-synchrony (Smith et al., 1994). Van Vreeswijk et al. (1994) studied a similar network but with alpha function PSCs. They showed that the synchronous state was stable for all PSC time constants, though with shorter time constants the network could also fire stably in antiphase.

Van Vreeswijk (1996) found that this result generalised to a large network. Slow connections completely synchronised the network. Below a critical time constant, the neurons break into two or more synchronised clusters, tending to complete asynchrony as the time constant tends towards zero.

4.3.2.3 The effect of delays

All the analysis summarised so far had no time delays. Smith et al. (1994) studied a pair of IF neurons coupled by delta-pulse postsynaptic potentials with and without coupling delays. In contrast with the zero-delay network, non-zero delays produced a finite basin of attraction for synchronous firing.

Gerstner and van Hemmen (1993) showed in a network of SRM neurons with effectively exponential PSCs (alpha function PSPs) that complete synchrony was locally stable with long enough delays. However, a partially asynchronous state with oscillating network activity was also possible for all delays. The level of noise in the network determined how asynchronous the state was.

4.3.3 A unified framework for spike-based synchrony

The SRM model has proved the basis for a general theory of synchrony in networks of spiking neurons. Gerstner and van Hemmen (1993) investigated purely asynchronous (incoherent) and synchronous network states of homogeneously-connected networks of SRM connected by arbitrary PSP functions.

In noiseless networks asynchronous states are very rarely purely asynchronous, often being susceptible to oscillations in the overall activity (figure 4.4). Gerstner et al. (1993a) looked at a perturbation of the asynchronous state and derived general conditions for the stability of the perturbation. Gerstner (1995) applied this condition to a homogeneously-connected network with an alpha function PSP (decaying exponential PSC). He found that in a noiseless network the asynchronous state was often unstable to oscillations in the overall activity. Noise served to stabilise the asynchronous states.

Under certain conditions purely synchronous states can exist. Gerstner et al. (1996b) generalised earlier results (Gerstner et al., 1993a; Gerstner, 1995) to prove the *locking theorem*:

Theorem 4.1 *In a spatially homogeneous network of spiking neurons with standard dynamics, a necessary and, in the limit of a large number n of presynaptic neurons ($n \to \infty$), also sufficient condition for a coherent oscillation to be asymptotically stable is that firing occurs when the postsynaptic potential arising from all previous spikes is increasing in time.*

(*Standard dynamics* means that the refractory potential $\eta(t)$ is always rising.)

The left-hand graph in figure 4.5 shows the conditions for synchrony. The synaptic potential from all other neurons in the network (solid line) and the neuron's own re-

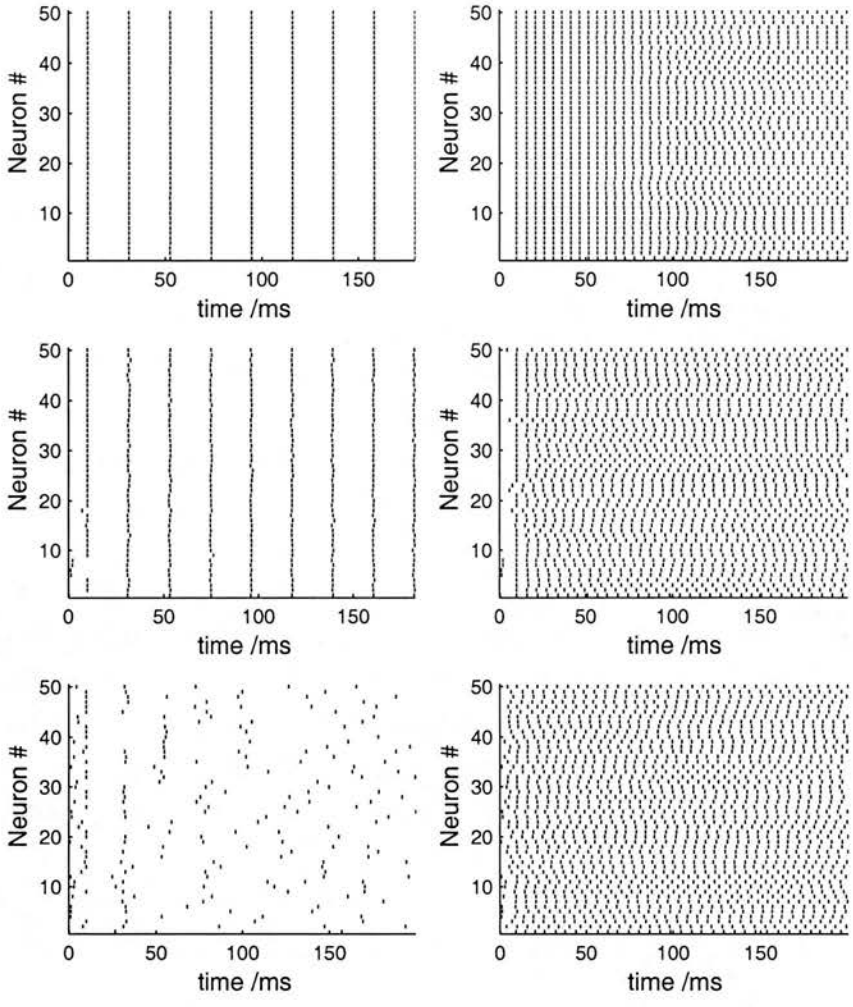

Figure 4.4: Differing levels of synchrony in the network activity. The six spike rasters show the spiking activity of networks with refractory functions and delays of the left and right graphs of figure 4.5 with increasing amounts of noise ($\beta = 1000, 15, 8$). Synchronous parameters: $\Delta = 20\,\text{ms}$, $\eta_0 = 10$. Asynchronous parameters: $\Delta = 2.5\,\text{ms}$, $\eta_0 = 1$. Other parameters: $F = 1$, $N = 100$, $\tau = 2\,\text{ms}$, $J = 1/N$, $\tau_{\text{abs}} = 4\,\text{ms}$. See equation (2.22) for meaning of τ_{abs} and η_0

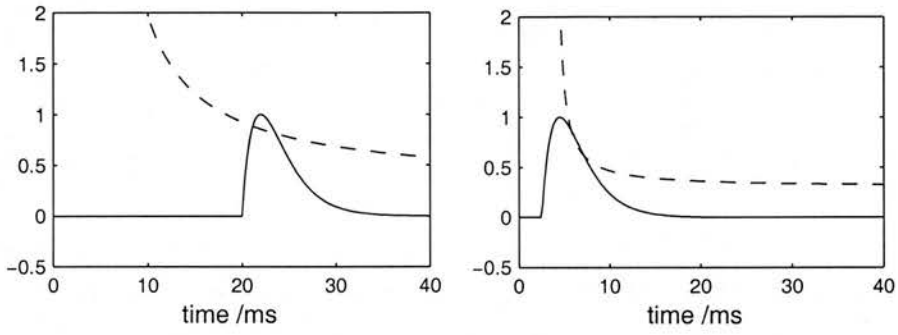

Figure 4.5: The conditions for synchrony and asynchrony in the network. The graphs show the synaptic potential (solid line) and refractory potential plus threshold that a neuron experiences after firing at time 0. As the text explains, the situation in the left hand graph will tend to lead to complete synchronisation.

fractory potential (dashed line) are depicted. Under normal circumstances, the neuron will fire when the refractory potential meets the synaptic potential, in this case about 22 ms after the neuron last fired. Suppose now the neuron fires a little later than normal on one cycle. Presuming that all other neurons have fired normally, the synaptic potential the neuron sees will be the same. However, as it has fired later, its refractory potential will be shifted to the right. Thus it will fire a little later than all the other neurons, but, due to the slope of the refractory function and the synaptic potential, the delay relative to the other neurons will be less than on the previous cycle. Hence small perturbations in firing times should be corrected for. By contrast, in the situation on the right any small perturbations will be accentuated due to the relative slopes of the synaptic potential and the refractory potential. The difference between the two cases is that in the first, the synaptic potential is rising when the neuron is due to fire, whereas in the second, it is falling when the neuron is due to fire.

In chapter 8 I will use a generalised version of this theorem to find conditions for synchrony in inhomogeneous networks.

4.4 Summary

The purpose of this chapter has been to introduce some of the experimental evidence for, function of and mechanisms underlying synchronous activity in the nervous system.

Synchrony in neural systems is roughly defined as different neurons firing within a few milliseconds of each other. It can be detected over a period of time using the cross-correlation. Synchronous firing is possible when activity is oscillating, but does

not require oscillations. Oscillations are possible when there is not complete synchrony, for example in the case of two groups of neurons that fire synchronously within groups, but where the activity oscillates between the groups.

In the auditory nerve, spikes are locked to the phase of the stimuli. Synchrony has been proposed as a way of encoding whether neurons with different receptive fields are responding to the same object (the binding problem). Evidence consistent with this hypothesis comes from the visual modalities. Here the synchrony often occurs in conjunction with mass activity oscillations in the gamma frequency range. Synchronous oscillations also seem to play a role in the locust olfactory system, where it has been shown that when 20 Hz oscillations are abolished, fine scale odour discrimination is impaired.

There is an extensive literature on the dynamics of synchrony. The models vary in abstraction and biological realism. Basic units range from compartmental models, through spiking neurons to relaxation oscillators based on the Wilson-Cowan model that represent cortical columns containing inhibitory and excitatory populations. The SRM has been used to show that the condition for synchrony of a homogeneous population is that each neuron's synaptic potential should be rising as it fires. This allows synchrony with both purely excitatory and purely inhibitory connections.

Although the binding by synchrony theory is disputed, it is clear that synchrony and synchronous oscillations are important, and studying their mechanisms is still interesting.

Chapter 5

Simulating networks of threshold-fire neurons

Models of spiking neurons have featured as mathematical tools in this thesis already. Later on, I will use them as the units for simulations of large networks of neurons. It is clearly desirable to make the simulations as efficient as possible. This chapter deals with the methodological problem of simulating networks of threshold-fire neurons such as integrate-and-fire (IF) and spike response model (SRM) neurons efficiently.

To simulate networks of IF neurons directly, differential equations coupled by current pulses must be integrated numerically using an algorithm such as the Runge-Kutta algorithm (Press et al., 1992). An important question when integrating differential equations is how large the time step can be before the accuracy of the integration becomes unacceptable. By contrast, no integration is required to simulate networks of SRM neurons. We might therefore expect the time step to be much less important, though, as we will see below, this is not the case.

Hansel et al. (1998) investigated the question of how the size of the time step in a network affects accuracy in a network of IF neurons. The network's synchronisation properties were particularly sensitive to the time step. Despite this sensitivity, it was possible to find the spiking times of the network to arbitrary accuracy using an "exact method" that incorporated the Newton-Raphson algorithm. Hansel et al. found that with both the simple Euler and Runge-Kutta integration methods a very small time step was required to reproduce the synchronisation properties discovered using the exact method. This was because the discrete simulation time step meant the firing times were also discrete, which lead to a considerable reduction in the accuracy. The accuracy for a given time step could be improved by removing the discreteness by linearly interpolating the membrane potential between time steps to find the firing time. For second order Runge-Kutta integration (RK2) the simulation time step could be increased by a factor

of ten without impairing performance.

As shown in chapter 2, SRM neurons with the appropriate PSP and refractory functions are integrated IF neurons. Therefore simulating a network of such SRM neurons is equivalent to simulating a network of IF neurons with a "perfect" integration method. However, the time step will still be important since it makes the possible firing times discrete. How much better is the accuracy with SRM neurons than with IF neurons integrated with RK2? Can the interpolation method of Hansel et al. (1998) be applied to SRM neurons, and if so, how does it change the performance? I address these questions in section 5.1.

Hansel et al. (1998) suggested that their work could be extended by investigating the effect of noise on the simulation. In section 5.2 I develop an interpolation method for SRM neurons with noisy thresholds.

Finally, in section 5.3, I state the conclusions arising from this chapter.

5.1 Deterministic simulation using SRM neurons

In section 5.1.1 I will describe the network model used by Hansel et al. (1998), the measures used to assess the simulation performance and the simulation method itself. The results, presented in section 5.1.2, show that the simple SRM is more accurate for a given time step than the IF model, though not by much. Finally, in section 5.1.3, I summarise the performance in terms of CPU cycles, and discuss whether the extended SRM could do any better.

5.1.1 Method

The benchmark network comprises $N = 128$ completely connected excitatory neurons. Hansel et al. (1998) simulated each neuron as an IF neuron whose membrane potential evolves according to (2.11) with constants[1] $\tau_{\mathrm{m}} = 10\,\mathrm{ms}$ and $R = 10\,\mathrm{k}\Omega$. The threshold and external current are the same for all neurons; $\vartheta = 20\,\mathrm{mV}$ and $I_i^{\mathrm{ext}} = 2.30\,\mu\mathrm{A}$. The weights have the units of charge (nC) and are uniformly set to $J_{ij} = J^{\mathrm{syn}}/N$. The EPSC function[2] is given by

$$\gamma(t) = \frac{1}{\tau_1 - \tau_2}\left(e^{-\frac{t}{\tau_1}} - e^{-\frac{t}{\tau_2}}\right) , \tag{5.1}$$

[1] Some of these units should be intensive instead of extensive since we are dealing with areas of membrane. For example, mVcm^{-1} instead of mV. However to simplify things I will imagine we have a unit area of membrane and deal with the extensive units.

[2] In the limit $\tau_2 \to \tau_1$ this double exponential function approximates the alpha function $t/\tau_1 \exp(-t/\tau_1)$.

with synaptic time constants $\tau_1 = 3\,\text{ms}$ and $\tau_2 = 1\,\text{ms}$.

The starting conditions of the IF neurons are

$$V_i(0) = RI^{\text{ext}}\left(1 - \exp\left(-c\frac{i-1}{N}\frac{T}{\tau_\text{m}}\right)\right) \quad , \tag{5.2}$$

where

$$T = -\tau_\text{m} \ln\left(1 - \frac{\vartheta}{RI^{\text{ext}}}\right) \tag{5.3}$$

is the firing period of an isolated neuron receiving only constant external input I^{ext} and where the coefficient $0 < c < 1$ controls the initial degree of synchrony. If $c = 0$ the neurons all fire at the same time; if $c = 1$ uncoupled neurons would fire uniformly throughout the first period T.

To convert the IF formulation into the simple SRM formulation we need to integrate the synaptic current according to (2.16). This yields the EPSP kernel

$$\varepsilon(t) = \frac{R}{\tau_1 - \tau_2}\left(\frac{\tau_1}{\tau_1 - \tau_\text{m}}e^{\frac{-t}{\tau_1}} - \frac{\tau_2}{\tau_2 - \tau_\text{m}}e^{\frac{-t}{\tau_2}} + \frac{\tau_\text{m}(\tau_1 - \tau_2)}{(\tau_1 - \tau_\text{m})(\tau_2 - \tau_\text{m})}e^{\frac{-t}{\tau_\text{m}}}\right) \quad . \tag{5.4}$$

The starting conditions present something of a problem to the SRM since we cannot integrate it from a particular membrane potential. Instead we must fix the external voltage $V^{\text{ext}}(t)$ so that the membrane potential passes through the prescribed values at $t = 0$. As the current is constant we should be able to use the solution of (2.18), appropriately shifted by $c(i-1)T/N$:

$$V_i^{\text{ext}}(t) = RI^{\text{ext}}\left(1 - \exp\left(-\frac{t}{\tau_\text{m}} - c\frac{i-1}{N}\frac{T}{\tau_\text{m}}\right)\right) \quad . \tag{5.5}$$

The refractory potential is given by (2.17). As the SRM is of the simple variety, all spikes of a neuron could contribute to its refractory potential.

One important measure of the performance of the network is how well it matches the synchronisation of the "exactly" solved network. To compare the synchrony we need a measure of synchrony. Hansel et al. (1998) compared the time-averaged variance of the population activity

$$\overline{\left(\frac{1}{N}\sum_{i=1}^{N} V_i(t)\right)^2} - \left(\overline{\frac{1}{N}\sum_{i=1}^{N} V_i(t)}\right)^2 \tag{5.6}$$

with the population average of time-averaged variance of single cell activity

$$\frac{1}{N}\sum_{i=1}^{N}\left(\overline{(V_i(t))^2} - \left(\overline{V_i(t)}\right)^2\right) \tag{5.7}$$

to create a synchrony measure

$$\Sigma = \frac{\overline{\left(\frac{1}{N}\sum_{i=1}^{N} V_i(t)\right)^2} - \left(\overline{\frac{1}{N}\sum_{i=1}^{N} V_i(t)}\right)^2}{\frac{1}{N}\sum_{i=1}^{N}\left(\overline{(V_i(t))^2} - \left(\overline{V_i(t)}\right)^2\right)} \quad . \tag{5.8}$$

When the activity of the network is completely asynchronous, the numerator (5.6) of this expression is equal to zero, since the population activity at every time step is the same. In the completely synchronous state $V_i(t) = V(t)$ and both the numerator (5.6) and denominator (5.7) are equal, so $\Sigma = 1$. In fact there are size effects, so the measure Σ is not exact even with 128 neurons (Hansel et al., 1998). Fortunately this is not important as we only need the measure to compare between simulations. To distinguish between the synchrony of the exactly solved network and the simulated networks, Σ is taken to be the "exact" synchrony measure and $\hat{\Sigma}$ refers to the synchrony of one of the simulations with varying time steps. In all of the simulations, Σ and $\hat{\Sigma}$ were found by sampling every 1 ms from 5–10 s.

The fractional error in the synchronisation is defined

$$E_\Sigma = \left| \frac{\hat{\Sigma} - \Sigma}{\Sigma} \right| \tag{5.9}$$

and gives a measure of how well the simulations match the exact solution. Another useful measure is the error on the population firing rate,

$$E_\mathrm{r} = \left| \frac{\hat{r} - r}{r} \right| \ , \tag{5.10}$$

where

$$r = \sum_{i=1}^{N} \overline{r_i(t)} \ , \tag{5.11}$$

and where the time average is over the time period 5–10 s of the exact solution and $\hat{r}$ is defined by analogy with $\hat{\Sigma}$.

I have replicated the "exact" integration method of Hansel et al. (1998) using the SRM equations implemented in a C++ program. The procedure is to find the first threshold crossing times of all neurons using the Newton-Raphson technique (Press et al., 1992). The neuron with the earliest spike time has a spike added to its set of spikes at that time, and then the procedure is repeated from the time of the latest spike. In practice, the neurons always fire spikes in numerical order, so we only need to find the spike time of the next neuron in the sequence when a neuron spikes.

I have implemented the SRM version of the simulated network in a C++ program. The program to solve the network by Newton-Raphson was based on this code. The same code was also used as a base for an interpolated version of the simulation. In this version, the membrane potential of each neuron $h_i(t)$ is remembered at each time step. When the membrane potentials are next calculated, Δt later, any firing times are

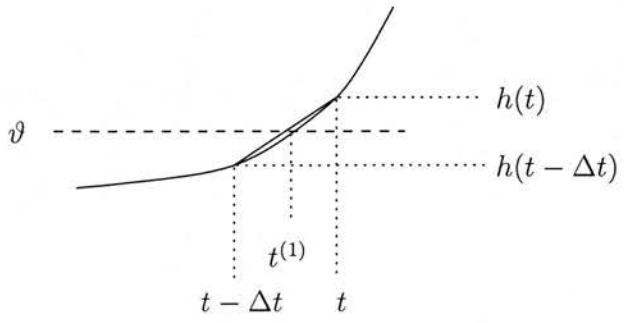

Figure 5.1: The interpolation method.

found by interpolation:

$$t_i^{(1)} = t - \Delta t + \frac{\vartheta - h(t)}{h(t-\Delta t) - h(t)} \Delta t \ . \tag{5.12}$$

Figure 5.1 shows the interpolation method graphically.

As with the exact solution the firing order should be the same as the numerical order of the neuron labels. Hence there is no need to check that no other neurons have fired between t and $t + \Delta t$ before adding a spike to a neuron's spike set. In a more realistic simulation the delays would be longer than the interval Δt and so there would be no need to update neurons synchronously.

5.I.2 Results

Figure 5.2 shows the synchronisation of the network as function of coupling strength J^{syn} as determined by (a) an uninterpolated simulation with varying time steps Δt and (b) the exact method. The results agree[3] with those of Hansel et al. (1998) in that the coherence decreases with increasing coupling strength, with a transition point around $J^{\text{syn}} = 8$. As we would expect, the approximation gets much better with smaller time steps.

Figure 5.3 shows the synchronisation of the network as function of coupling strength J^{syn} as determined by (a) an interpolating simulation with varying time steps Δt and (b) the exact method. Also shown are the corresponding results of Hansel et al. (1998) for an interpolating network solved by RK2. The results agree[4] with those of Hansel et al. (1998) in that the coherence decreases with increasing coupling strength, with a

[3] My units seem to be a factor 10 out compared to those of Hansel et al.. I have not been able to determine whether the fault is mine or theirs.

[4] Hansel et al. (1998) show similar results for the uninterpolated (standard) Euler algorithm but do not show the equivalent results for standard RK2. As I want to present reasonably fair comparisons, I only show the results of Hansel et al. (1998) that used RK2.

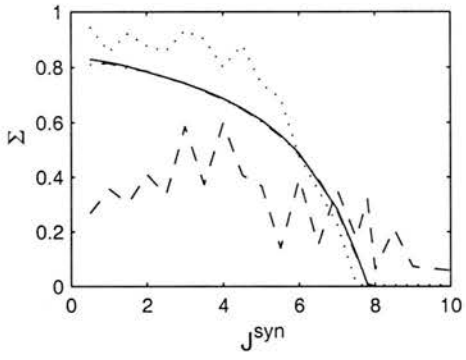

Figure 5.2: Coherence Σ as a function of the coupling strength J^{syn} for the standard SRM algorithm. Solid line: exact integration; dashed line: $\Delta t = 1\,\text{ms}$; dotted line: $\Delta t = 0.1\,\text{ms}$; dash-dotted line: $\Delta t = 0.01\,\text{ms}$.

transition point around $J^{\text{syn}} = 8$. As we would expect, the approximation gets much better with smaller time steps.

Figure 5.4 shows the relative error on the firing rate E_{r} as a function of the time step for both the SRM and IF models. The curves for the SRM model are not as smooth as those for the IF model. This is because of quantisation at very low errors. The average firing rate with $J^{\text{syn}} = 6$ is about 70 Hz. Since the sampling time is 5 s, the total number of spikes fired by the population is $70 \times 5 \times 128 = 44800$. The smallest possible absolute error is one spike, so the minimum non-zero fractional error should therefore be $1/44800 \approx 2 \times 10^{-5}$, which corresponds to the plateau in figure 5.4. It is not clear how Hansel et al. (1998) achieve a minimum fractional error of 10^{-10} as the scale of their figure implies they did. This would require simulations that were 10^5 times longer.

Although I have not fitted curves, from the logarithmic graph it looks as though the power dependence for the standard SRM is about 1.0 and the power dependence for the steeply falling part of the interpolated curve is about 2.0. This seems to agree with the IF results. It means that with the standard SRM network the error depends approximately linearly on the time step, whereas with the interpolated SRM network, the error has a quadratic dependence on the time step.

Figure 5.5 shows the relative error on the firing rate E_{r} as a function of the time step for both the SRM and IF models. Here there is no inherent quantisation, so we might expect both curves to decrease continuously as the time step decreases. This is indeed the general trend, though there are bumps in both curves. My curve does

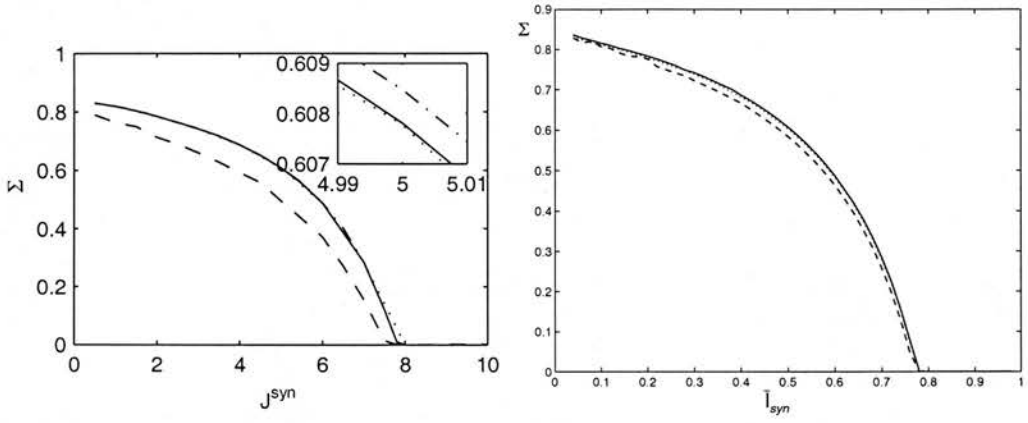

Figure 5.3: *Left.* Coherence Σ as a function of the coupling strength J^{syn} for the interpolated SRM algorithm. Solid line: exact integration; dashed line: $\Delta t = 1\,\text{ms}$; dotted line: $\Delta t = 0.1\,\text{ms}$; dash-dotted line: $\Delta t = 0.01\,\text{ms}$. *Left inset:* Detail of the curves to show detail of $\Delta t = 0.1\,\text{ms}$, $\Delta t = 0.01\,\text{ms}$ and exact curves. *Right.* The same curves for the interpolated IF network solved with RK2 (taken from Hansel et al., 1998, figure 7). Solid line: exact integration; dashed line: $\Delta t = 0.25\,\text{ms}$; dotted line: $\Delta t = 0.1\,\text{ms}$.

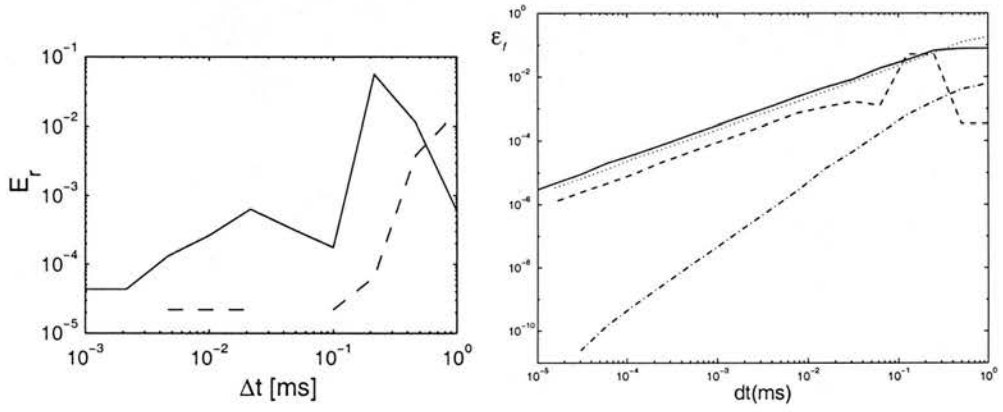

Figure 5.4: *Left.* Relative error on the firing rate E_{r} as a function of the time step for the standard (solid line) and interpolated (dashed line) SRM algorithms. $J^{\text{syn}} = 6$. Other parameters same as in figure 5.2. The dashed line disappears when the error is 0 due to the logarithmic scale. The line is level around $\Delta t = 10^{-2}$ because of the quantisation inherent in the spike count. See text for more details. *Right.* The equivalent measure for IF neurons solved with various algorithms (Hansel et al., 1998). Solid line: standard Euler; dotted line: Euler with interpolation; dashed line: standard RK2; dash-dotted line: RK2 with interpolation. It is not clear why this curve does not show the quantisation effect my curves do.

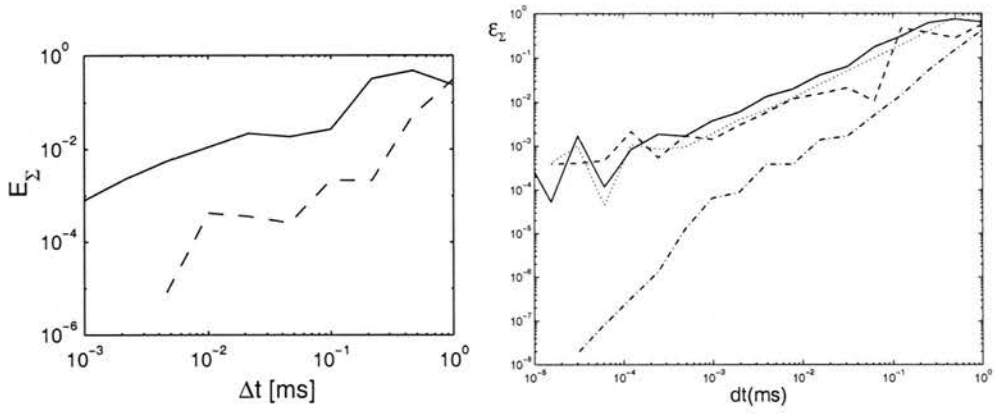

Figure 5.5: *Left.* Relative error on the coherence E_Σ as a function of the time step for the standard (solid line) and interpolated (dashed line) SRM algorithms. $J^{\text{syn}} = 6$. Other parameters same as in figure 5.2. *Right.* The equivalent measure for IF neurons solved with various algorithms (Hansel et al., 1998). Solid line: standard Euler; dotted line: Euler with interpolation; dashed line: standard RK2; dash-dotted line: RK2 with interpolation.

Method	Δt [ms] for 10% on Σ	Δt [ms] for 1% on Σ
IF Standard Euler	0.031	0.0020
IF Interpolated Euler	0.061	0.0010
IF Standard RK2	0.062	0.0039
IF Interpolated RK2	0.25	0.063
SRM Standard	0.14	0.014
SRM Interpolated	0.67	0.26

Table 5.1: Minimum time step allowed for the different methods. The Euler and RK2 values are from Hansel et al. (1998).

not extend to such small time intervals as does that of Hansel et al. (1998), though the error is generally less than theirs in the region I investigated. Table 5.1 shows the minimum time steps required for 10% and 1% accuracies found by interpolating between data points in figure 5.5. Both the standard and interpolated SRM methods do better than their IF/RK2 counterparts on both measures. The factor of improvement ranges between 2.3 for the standard 10% case and 4.1 for the interpolated 1% case.

5.1.3 Discussion

I have shown that using the SRM to simulate the activity of a network of all-to-all connected spiking neurons is more accurate for a given time step than integration of the IF model by either the Euler or second order Runge-Kutta integration methods.

Method	CPU per Time step [s]
SRM Standard	9.6×10^{-3}
SRM Interpolated	9.7×10^{-3}

Table 5.2: CPU time per time step for the SRM integration scheme with $J^{\text{syn}} = 6$ and $\Delta t = 0.01$ ms.

The factor of the speed-up ranges between about two and four. This is less than the approximately order of magnitude improvement gained by using interpolation rather than uninterpolated SRM or RK2 simulation.

The CPU time per time step for $J^{\text{syn}} = 6$ and $\Delta t = 0.01$ ms on a SUN ULTRA 5 MODEL 333 is shown in table 5.2. There is no significant time difference between the interpolated and standard cases. It appears to be about two orders of magnitude *greater* than the CPU time per time step found by Hansel et al. (1998) on a HP9000 (MODEL 819.K200). The SPECfp95 benchmark[5] suggests that the SUN is about twice as fast as the HP machine (18 versus 8.85). Thus the discrepancy could be due to a systematic difference in the algorithms or programming differences or programming errors.

Running the program through a profiling program showed that the vast bulk of the time was spent calculating exponential functions. However this can only account for a factor of two in the difference of execution speed, as the following considerations show. Suppose that in each method, we only look at spikes produced in the last τ^{int} seconds. At each time step with the IF method we need to calculate the currents caused by all spikes in the last τ^{int}, which, at a firing rate of r, comes to $2Nr\tau^{\text{int}}$ exponentials, since the EPSC function $\gamma(t)$ contains two exponentials. For the simple SRM we need to calculate $3Nr\tau^{\text{int}}$ exponentials to find the EPSPs $\varepsilon(t)$ for all neurons, and additionally the program must calculate $Nr\tau^{\text{int}}$ exponentials for the refractory functions $\eta(t)$. So in theory the simple SRM method should take twice as long for a time step. This reduces the computational advantage over the RK2/IF method, though there is still some advantage.

Could the extended SRM do any better? Another way of writing the equation for the kernel $\kappa(s,t)$ is

$$\kappa(s,t) = \begin{cases} \frac{R}{\tau_{\text{m}}} \int_0^t \gamma(t-t') e^{t'/\tau_{\text{m}}} dt' & t < s \\ \frac{R}{\tau_{\text{m}}} \int_0^s \gamma(t-t') e^{t'/\tau_{\text{m}}} dt' & t \geq s \end{cases} . \tag{5.13}$$

The solution of either integral is a weighted sum of three exponentials, like (5.4). Since only one integral needs to be evaluated, the number of exponentials required per time

[5] `http://www.specbench.org/osg/cpu95/results/cfp95.html`

step comes down to $3Nr\tau^{\text{int}}$, a factor of 1.5 greater than the IF/RK2 method.

One potential algorithmic difference between my simulations and those of Hansel et al. (1998) is that they could have calculated PSPs by solving differential equations rather than using exponential functions. This approach was used by Destexhe et al. (1994) with synaptic conductances, where it had the advantages of requiring only two state variables per synapse and the calculation of a single exponential per time step. The computational requirements of the method for the network described in this chapter would be similar, and considerably smaller than remembering the times of all spikes within the time window τ^{int} and computing three exponentials per spike. This could account for the differences in speed between the two algorithms.

5.2 Stochastic simulation using SRM neurons

Can we extend the interpolation simulation method to noisy neurons? Section 5.2.1 shows that we can in the case of threshold noise. I have not been able to find a benchmark task, so there is no way to compare the performance of the interpolated noisy simulation with an uninterpolated one. I discuss alternative ways of testing the method in section 5.2.2.

5.2.1 Method

The interpolation method can be extended to deal with noise caused by exponential escape rate (2.29). The problem is to find a random time of firing $t+\Delta t^{(1)}$ and the value of the membrane potential at t and $t+\Delta t$. To do this, we need to find the cumulative probability of a spike from t onwards, that is $1-S(t'|t)$, where $S(t'|t)$ is the survivor function introduced in section 2.4.5.3. If we can compute the inverse of this function, we can give this function a random number chosen uniformly from $[0,1]$ to produce a random time of firing.

The interpolated membrane potential function is

$$h(t') = h(t) + (t'-t)\dot{h}(t) \ , \tag{5.14}$$

where

$$\dot{h}(t) = \frac{h(t+\Delta t) - h(t)}{\Delta t} \tag{5.15}$$

is the gradient of the membrane potential around t. Substituting this into (2.32), the definition of the survivor function, gives

$$S(\Delta t^{(1)} + t, t) = \exp\left(-\int_t^{t+\Delta t^{(1)}} \tau^{-1}\left(h(t) + (t'-t)\dot{h}(t)\right)dt'\right) \ . \tag{5.16}$$

Integrating (5.16) with the escape rate (2.29) substituted in yields

$$S(\Delta t^{(1)} + t, t) = \exp\left(\frac{1}{\tau_0 \beta \dot{h}(t)} \exp(\beta h(t) - \vartheta)\left(e^{\beta \dot{h}(t) \Delta t^{(1)}} - 1\right)\right) \quad . \tag{5.17}$$

Although the cumulative probability is $1 - S(\Delta t^{(1)} + t, t)$, since the random number is to be chosen randomly from $[0, 1]$, we can find $\Delta t^{(1)}$ as a function of the random number S. After some rearrangement, we arrive at

$$\Delta t^{(1)} = \frac{1}{\beta \dot{h}(t)} \ln\left(1 - \tau_0 \beta \dot{h}(t) e^{\beta(\vartheta - h(t))} \ln S\right) \quad . \tag{5.18}$$

This equation forms the basis for implementing noisy interpolation. However, it needs modification as there are some values of $h(t)$ and $\dot{h}(t)$ for which it has no solution as the argument of the outer logarithm is negative. For $\dot{h}(t) > 0$ this cannot happen as $\ln S$ is always negative. Physically, if the membrane potential is rising, the neuron *must* fire at some point in the future, so there must be a solution. For $\dot{h}(t) < 0$ there may not be a solution, depending on the value of S and $h(t)$. This is because if the membrane potential is decreasing there is a finite chance it will never fire and so there can be no solution. The implementation deals with this by calculating the argument of the outer logarithm first. The probability of the neuron not firing is just the probability of the argument being negative, so if the argument is negative no spike is produced. If the argument is positive it is passed to the outer logarithm and a spike time is found as normal. Finally, in the case $\dot{h}(t) = 0$ the formula is not valid, and (5.17) must be reintegrated for constant $h(t)$. This yields

$$\Delta t^{(1)} = -\ln S e^{\beta(\vartheta - h)} \tag{5.19}$$

and is bound to have a solution.

5.2.2 Discussion

I have implemented the above algorithm in C++, though I have not evaluated its performance against the standard noisy method. To do this I need to find a suitable benchmark task. Although the benchmark task used by Hansel et al. (1998) and by me in this chapter might be suitable, it would be better to have a task for which an analytical solution is known. This is because the integration method would not work in a stochastic model. An alternative would be to compare the performance of the interpolated and standard method with the standard method at very small time steps. I have not done this due to the simulation time that would be required.

Although I have no firm evidence that this is the case, I would guess that we can extrapolate from the deterministic case to the stochastic case, and use time steps two to four times longer than we would do in the uninterpolated simulations. There are two arguments in favour of this position. Firstly Hansel et al. (1998) suggested that noise might effectively smooth out the discontinuities caused by discrete time steps. Secondly, noise tends to desynchronise networks anyway (see section 4.3.3), so any synchronisation will probably not be as sensitive as the synchronisation in the benchmark network used in this chapter.

5.3 Conclusions

One advantage of simulating the IF model over more complex models (for example, compartmental models) is that it is faster. However, with a standard integration method, the speed of simulation may be deceptive, as discrete spike times introduce errors. As Hansel et al. (1998) have shown, this can be largely alleviated by linearly interpolating the membrane potential between time steps to calculate firing times.

In this chapter I first investigated whether deterministic SRM neurons are more efficient in simulation than deterministic IF neurons. I summarise the conclusions of this investigation below.

- For deterministic simulations without interpolation, the SRM method can achieve the same accuracy as the IF/RK2 method with time steps that are between two and three and a half times longer.
- The interpolation method can be applied to the SRM model.
- For deterministic simulations with interpolation, the SRM can achieve the same accuracy as the interpolated IF/RK2 method with time steps that are between two and a half and four times longer.
- However, this advantage is reduced by the additional calculation of exponential functions required in the SRM model.
- The extended SRM would require fewer exponentials in simulation, and would retain the advantages of the simple SRM over integration of IF neurons.
- I have shown how the interpolation method can be extended to noisy SRM neurons with an exponential escape rate, although I have not evaluated the algorithm. This must remain the subject of further work.

5.4 Summary

Threshold firing models, such as the IF model and the SRM, should require a smaller simulation time step than Hodgkin-Huxley type models since the subthreshold dynamics are much slower than the spiking dynamics. However, Hansel et al. (1998) have shown that the level of synchronisation of a group of homogeneously-connected neurons requires a very small time step to simulate accurately using IF neurons and Euler integration and RK2. The problem arises because neurons can only fire at multiples of the simulation time step, which disturbs the delicate synchronisation properties. By interpolating the membrane potential between time steps to find the firing times, the time step can be reduced by an order of magnitude without affecting the accuracy.

I tested the idea that SRM neurons would not need such small time steps as IF neurons solved using RK2 both with and without interpolation. In order to do this I programmed a SRM simulator that included interpolated and uninterpolated simulation methods. The results were indeed better than using IF neurons with RK2, but only by a factor of two to four. The simulation times were also much longer than expected, though this could have been due to computing PSP functions using exponential functions rather than by differential equation methods, which would probably have been faster.

Finally, I extended the interpolation simulation method to noisy SRM neurons with an exponential escape rate. Although I have not evaluated the algorithm, I believe that it could be used safely with time steps two to four times longer than conventional noisy SRM simulation would require.

Chapter 6

Sequences: recall speed of supervised synfire chains

In this chapter I will concentrate on one aspect of the dynamics and biological plausibility of synfire chains.

As explained in chapter 3, spatiotemporal patterns or synfire chains may be learned in the presence of a suitable temporal learning rule by activating each node or group of neurons in turn. This is a form of supervised learning where the supervisor is other groups of neurons, possibly directly activated by sensory neurons. Such a system might be found in the interplay between the neocortex and hippocampus (McClelland et al., 1995), or when learning motor patterns. An important parameter of the training protocol is the training speed, the speed at which nodes are activated.

Also as explained in chapter 3, the speed of propagation of a spatiotemporal sequence or synfire chain will depend on the strength of weights in the chain, the threshold and the excitatory postsynaptic potential (EPSP) function. The refractory properties of neurons are important in ensuring that nodes do not re-excite. This threshold-speed relationship has been previously investigated in simulation (Arnoldi and Brauer, 1996) and by treating neural tissue as a continuum of spike response model (SRM) (Wennekers and Palm, 1996) and integrate-and-fire (IF) model (Ermentrout, 1998) neurons with connections corresponding to idealised temporal learning rules.

In this chapter, I will address the same question, though with differences from the previous treatments. The first difference is that I consider the weight matrix of the synfire chain to have been created by a supervised training protocol with a certain training speed. The second difference is that I first analyse a network comprising discrete neurons rather than starting with a continuum approximation. The continuum approximation is only valid when the time between adjacent patterns being recalled is small compared to the EPSP time constant. The third difference is that I check for

the stability of threshold-speed pairs. The final difference is that I apply the results of the analysis to a realistic temporal learning rule derived from the experimental spike timing dependent synaptic plasticity (STDSP) results presented in chapter 2 as well as the Gaussian learning rule used previously.

In section 6.1 I present an analysis of a network of discrete SRM neurons and confirm that under appropriate conditions it can be approximated by continuous equations similar to those derived in the continuum case (Wennekers and Palm, 1996). In section 6.2 application of both analyses to a temporal learning rule suggested by recent experimental work (Zhang et al., 1998) confirms that the discrete analysis is important at low speeds and that recall may occur faster than training. I discuss the implications of these results for learning synfire chains, suggest possible criticisms and propose how they might be resolved in section 6.3.

This chapter has been published in the proceedings of the ICANN99 conference (Sterratt, 1999).

6.1 Analysis

To derive the speed of propagation for a given threshold I assume an infinitely large network of noiseless neurons in which an infinitely long synfire chain with non-overlapping nodes is to be learned. The network is trained by activating the neurons corresponding to each node in turn at regular intervals $1/v_t$, where v_t is the *training speed* of propagation. The neuron model I use is the simple SRM (section 2.4.5.1).

I assume that the network learns noiselessly according to (2.35), so that: there is no variance in the trained connection strength between a pair of nodes; all neurons are at the same resting potential immediately before firing; and the refractory potential ensures neurons fire only once. The refractory potential can therefore be ignored in the following derivations. For the above reasons, each neuron in a node experiences the same membrane potential, so a node can be treated as a single neuron (with appropriately scaled weights). Consequently, from now on I refer to nodes as though they were neurons. At the end of the training protocol the weight from node j to node i will be:

$$J_{ij} = \Gamma\left(\frac{i-j}{v_t} - \Delta^{\text{ax}} + \Delta^{\text{dend}}\right) \quad . \tag{6.1}$$

Note that I have omitted the dependency on the current weight from (2.35), so there are no weight saturation effects.

Although the weights determine the order of recall of nodes, the magnitude of the threshold determines whether and how fast the nodes may be recalled for a given set of

weights. If it is too high no units will ever fire; if it is too low the units will be firing at the maximum frequency allowed by their refractory period. For values between these extremes, the threshold has the effect of controlling the speed of propagation since each unit fires when the membrane potential crosses the threshold while rising. The membrane potential will cross a lower threshold sooner, causing activity to propagate faster.

Whilst physically the threshold determines the recall speed, mathematically we can calculate the threshold as an explicit function of speed. In the following analysis I consider one node and assume that all previous nodes have fired regularly at speed v, either because of synfire recall, or maybe caused by some forcing mechanism. Thus the recall firing times are $t_i = i/v$, which we can denote as a function comprising delta functions (see also section 2.3.2):

$$S_i(t) = \delta(t - i/v_t) \ . \tag{6.2}$$

Without loss of generality we consider the membrane potential of node 0, which should fire at time 0. If at $t = 0$ all the nodes have fired at the correct times t_i/v there are two conditions that must be fulfilled for propagation to carry on at the same speed. Firstly, the membrane potential of node 0 should be equal to the threshold,

$$h_0(0; v) = \vartheta(v) \ . \tag{6.3}$$

I refer to this as the self-consistency or *threshold* condition (see also section 8.1). Secondly, the membrane potential must be rising:

$$\dot{h}_0(0; v) > 0 \ . \tag{6.4}$$

I refer to this as the *rising potential condition* (again, see section 8.1). I have explicitly included the recall speed v is a parameter of the membrane potential and threshold.

As long as the membrane potential is rising, the first condition ensures that the neuron fires at time $t = 0$, that the next node in the chain will see the same pattern of firing and that activity will continue to propagate stably along the chain. If the membrane potential is falling the node must have fired already, since as long as the threshold is greater than the resting membrane potential and the EPSP function is continuous, the membrane potential will already have risen through the threshold and caused the neuron to fire. If the node has already fired, then at the next node the condition that all previous nodes have fired regularly no longer holds, and that particular speed is not stable.

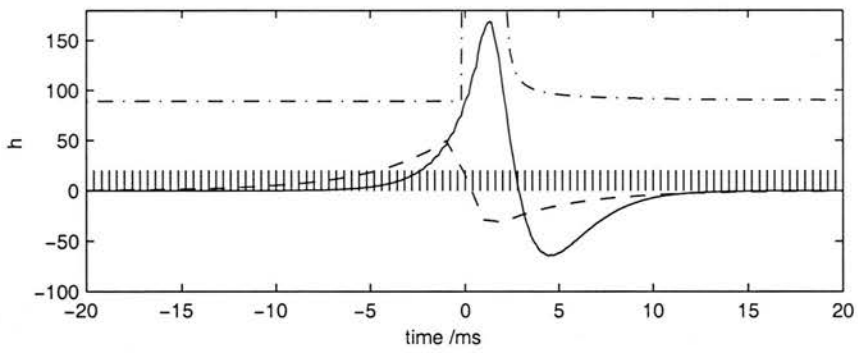

Figure 6.1: The predicted membrane potential and refractory potential. The solid line shows the predicted synaptic potential and the dashed line shows the weights connecting a neuron due to fire at $t = 0$ with neurons due to fire at other times. The vertical spikes indicate the predicted recall firing times that give rise to the synaptic potential. The dash-dotted line is the "threshold minus refractory function" of a neuron that fires at $t = 0$. The synaptic potential touches this line just once, at $t = 0$.

We can write down the membrane potential of an arbitrary node i at time t by substituting the recall firing times in (2.20) to give

$$h_i(t;v) = \sum_{j=-\infty}^{\infty} J_{ij}\varepsilon(t - \Delta^{\mathrm{ax}} - j/v) \ . \tag{6.5}$$

Figure 6.1 gives an example of a predicted membrane potential and a refractory potential that means it only fires once. The membrane potential of node 0 at time 0, and hence the threshold is obtained from (6.5). We can also substitute in the alpha function EPSP

$$\varepsilon(t) = \frac{t}{\tau} e^{1-\frac{t}{\tau}} \Theta(t) \tag{6.6}$$

to obtain:

$$\vartheta(v) = h_0(0;v) = \sum_{j=-\infty}^{\lfloor -v\Delta^{\mathrm{ax}} \rfloor} J_{0j} \frac{-\Delta^{\mathrm{ax}} - j/v}{\tau} e^{1-\frac{(-\Delta^{\mathrm{ax}} - j/v)}{\tau}} \ , \tag{6.7}$$

where the notation $\lfloor x \rfloor$ denotes the highest integer less than x. The upper limit on the sum in (6.7) is due to the Heaviside function part of the EPSP function. Its physical significance is that during recall, at time 0, neuron 0 will have "seen" all neurons which have fired before $t = -\Delta^{\mathrm{ax}}$. If the inter-neuron time interval $1/v$ is less than the axonal delay Δ^{ax} then the firing of at least one neuron will be ignored. To be precise, neuron 0 will see $\lfloor -v\Delta^{\mathrm{ax}} \rfloor, \lfloor -v\Delta^{\mathrm{ax}} \rfloor - 1, \lfloor -v\Delta^{\mathrm{ax}} \rfloor - 2 \ldots$ fire at times $\lfloor -v\Delta^{\mathrm{ax}} \rfloor / v, (\lfloor -v\Delta^{\mathrm{ax}} \rfloor - 1)/v, (\lfloor -v\Delta^{\mathrm{ax}} \rfloor - 2)/v \ldots$

We can also write down the derivative of the membrane potential for the 0th node at time 0 by differentiating equation (6.5) and setting $i = 0$ and $t = 0$:

$$\dot{h}_0(0) = \sum_{j=-\infty}^{\infty} J_{0j}\dot{\varepsilon}(-\Delta^{\mathrm{ax}} - j/v) \ . \tag{6.8}$$

With the alpha function (6.6), the derivative of the EPSP function is[1]

$$\frac{1}{\tau}\left(1 - \frac{t}{\tau}\right) e^{1-\frac{t}{\tau}}\Theta(t) \ . \tag{6.9}$$

We can approximate the discrete equations above by continuous ones in the case where the reciprocal of the speed is much less than the EPSP time constant, that is $1/v \ll \tau$, and the reciprocal of the training speed is much less than the a characteristic time constant τ_{p} of the potentiation function that is $1/v_{\mathrm{t}} \ll \tau_{\mathrm{p}}$. This is because in this case the exponential and linear terms in equations (6.7) and (6.8) are being numerically integrated with step sizes $1/(v\tau)$ and $1/(v_{\mathrm{t}}\tau_{\mathrm{p}})$. In the neocortex the velocity of propagation has been estimated by Ermentrout (1998) as $100\,\mathrm{units\,s^{-1}}$ from experimental data. With $\tau = 1\,\mathrm{ms} = 1 \times 10^{-3}\,\mathrm{s}$ the first condition is not fulfilled. Although this means that the continuous analysis is not strictly applicable, it still gives a rough idea of the behaviour we can expect from the system.

In the continuous case the membrane potential is given by the integration over space rather than summation over neurons:

$$h(x,t) = \int_{-\infty}^{\infty} J(x,x') \int_{t-T}^{t} \varepsilon(t')S(x', t - t' - \Delta^{\mathrm{ax}})dt'dx' \ , \tag{6.10}$$

where, by analogy with (6.2), $S(x,t)$ describes the activity of a continuous node at position x and time t. The continuous equivalent of the assumption (6.2) that the firing time of the neuron is proportional to its position in the chain is

$$S(x,t) = \delta\left(t - \frac{x}{v}\right) \ . \tag{6.11}$$

We replace the discrete weights J_{ij} by a continuous weight function defined between positions x and x', $J(x,x')$. In fact this will depend only on the displacement between positions, $x - x'$. Applying the learning rule (2.35) leads to the equivalent of (6.1),

$$\begin{aligned} J(x,x') = J(x - x') &= \int_{-\infty}^{\infty} \Gamma(t - \Delta^{\mathrm{ax}} + \Delta^{\mathrm{dend}})\delta\left(t - \frac{x - x'}{v_{\mathrm{t}}}\right) dt \\ &= \Gamma\left(\frac{x - x'}{v_{\mathrm{t}}} - \Delta^{\mathrm{ax}} + \Delta^{\mathrm{dend}}\right) \ . \end{aligned} \tag{6.12}$$

[1] Since the derivative of a Heaviside function is a delta function and the product rule of differentiation gives a term $(t/\tau)e^{1-t/\tau}\delta(t)$ which is uniformly zero.

In the limit when $T \to \infty$, and when we substitute (6.11) into (6.10), we obtain

$$h(x,t) = \int_{-\infty}^{\infty} J(x-x')\varepsilon\left(t - \Delta^{\mathrm{ax}} - x'/v\right) dx' \tag{6.13}$$

which is the continuous equivalent of (6.5). Substitution of $(x,t) = (0,0)$ and the EPSP function (6.6) into (6.13) yields

$$\vartheta = h(0,0) = \int_{-\infty}^{-v\Delta^{\mathrm{ax}}} J(-x')\frac{(-\Delta^{\mathrm{ax}} - x'/v)}{\tau} e^{1-\frac{-\Delta^{\mathrm{ax}}-x'/v}{\tau}} dx' \ , \tag{6.14}$$

which is the continuous equivalent of equation (6.7). To complete the correspondence between continuous and discrete analysis, there is also an equivalent of (6.8), found by differentiating (6.13):

$$\dot{h}(0,0) = \int_{-\infty}^{\infty} J(-x')\dot{\varepsilon}\left(-\Delta^{\mathrm{ax}} - x'/v\right) dx' \ . \tag{6.15}$$

These equations are essentially the same as those found previously (Wennekers and Palm, 1996). They yield analytic solutions for some EPSP and potentiation functions, in which case we can find an expression for the threshold-speed relationship.

6.2 Application to realistic potentiation function

The experimentally-based potentiation function (Zhang et al., 1998) displayed in figure 6.2 plots percentage change in the strength of *excitatory* synapses against time delay between pre- and postsynaptic spikes. To treat this function as an absolute synaptic weight and substitute it into (6.1) I assume that each connection initially comprises balanced inhibitory and excitatory components. Training the excitatory connections with the potentiation function results in effectively excitatory and inhibitory connections according to its potentiating and depressing parts.

The experimental function comprises potentiating and depressing exponential sections with a time constant of $\tau_{\mathrm{p}} = 20\,\mathrm{ms}$ joined by a linear portion. The constants used in this chapter are roughly the same as the curves fitted in Zhang et al. (1998), although the linear section is not very well defined. The maximum potentiation $k_{\mathrm{u}} = 52$ occurs at a delay of $t_{\mathrm{u}} = 4\,\mathrm{ms}$ and the maximum depression $k_{\mathrm{d}} = -38$ occurs at a delay of $t_{\mathrm{d}} = -6\,\mathrm{ms}$.

For clarity, I initially consider a simpler version of the experimental function where $t_{\mathrm{u}} = t_{\mathrm{d}} = 0\,\mathrm{ms}$, and $k_{\mathrm{u}} = 1$ and $k_{\mathrm{d}} = -1$. There is therefore a discontinuity at $t = 0\,\mathrm{ms}$. In this case the analytical calculation reveals that for $v/v_{\mathrm{t}} > (\Delta^{\mathrm{ax}} - \Delta^{\mathrm{dend}})/\Delta^{\mathrm{ax}}$,

$$\vartheta(v) = \frac{k_{\mathrm{u}} v\tau e^{\left(1-\Delta^{\mathrm{ax}}\left(\frac{v}{v_{\mathrm{t}}}-1\right)-\Delta^{\mathrm{dend}}\right)}}{\left(\frac{v}{v_{\mathrm{t}}}\frac{\tau}{\tau_{\mathrm{p}}}+1\right)^2} \tag{6.16}$$

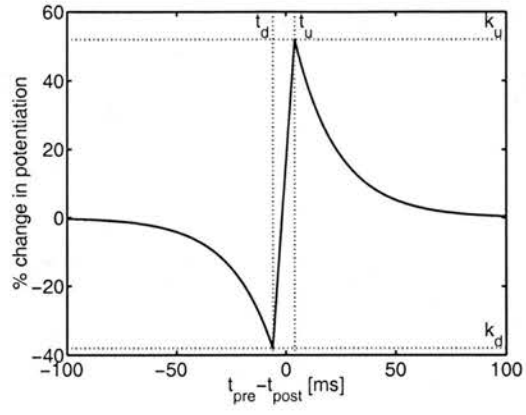

Figure 6.2: The potentiation function derived from experiment. See section 6.2 for explanation of constants.

and

$$\dot{h}(0) = \frac{k_{\mathrm{u}} v e^{\left(1-\Delta^{\mathrm{ax}}\left(\frac{v}{v_{\mathrm{t}}}-1\right)-\Delta^{\mathrm{dend}}\right)}}{\left(\frac{v}{v_{\mathrm{t}}}\frac{\tau}{\tau_{\mathrm{p}}}+1\right)^2}\left(\frac{v}{v_{\mathrm{t}}}\frac{\tau}{\tau_{\mathrm{p}}}\right) \quad . \tag{6.17}$$

This restriction ensures that only the potentiating part of the curve is included in the weights that cause the node to fire. For the rest of this chapter, I assume the training speed is $v_{\mathrm{t}} = 0.1 \times 10^3\,\mathrm{s}^{-1}$ and the delays are $\Delta^{\mathrm{ax}} = \Delta^{\mathrm{dend}} = 1\,\mathrm{ms}$, thus making the restriction $v/v_{\mathrm{t}} > 0$.

Figure 6.3 shows the discrete and continuous threshold-speed relationships determined by substituting the potentiation function in (6.5), (6.8), (6.13) and (6.15) and solving the resulting equations for a training speed $v_{\mathrm{t}} = 0.1 \times 10^3\,\mathrm{s}^{-1}$. The different analyses are in good agreement at higher speeds, though both the speed and stability for a given threshold are markedly different for lower speeds, where the condition $v\tau \ll 1$ breaks down. The cusps in the discrete curve occur when $v = j/\Delta^{\mathrm{ax}}$, where j is an integer, and are due to the effect of a node being able to see the activity of an extra node at these points.

As expected, propagation is only possible for a limited range of thresholds and for higher speeds the speed always increases as the threshold decreases. We might not have expected the speed to increase as the threshold is increased at lower speeds as it does in the continuous analysis. At lower speeds, the synaptic potential reaches the threshold almost at its peak whereas at higher speed solutions for the same threshold the synaptic potential continues to rise well after the node has fired.

A lower bound to the speed in the discrete case is $1/(\Delta^{\mathrm{ax}} + \tau)$, because if the last

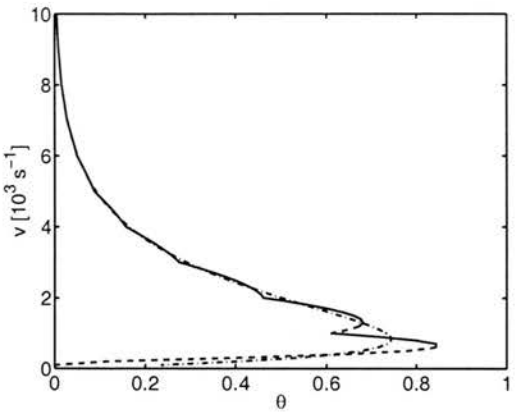

Figure 6.3: Speed-threshold relationship in a simple case where $t_u = t_d = 0\,\text{ms}$, $k_u = k_d = 1$ and $v_t = 0.1 \times 10^3\,\text{s}^{-1}$. Discrete analysis: solid part of curve shows stable solutions and dashed part unstable ones. Continuous analysis: dash-dotted curve shows stable solutions; there are no unstable ones.

node has fired longer than $\Delta^{ax} + \tau$ ago all it sees is the summed tails of several EPSPs. In fact, even if all other nodes have been forced to fire at a speed less than this limit, a node allowed to fire freely will fire on the rising part of the EPSPs, sooner than it "ought" to. This causes the next node to fire after a shorter time interval, and the speed of recall will gradually converge on the stable value for that threshold. By contrast, in the continuous case the neuron will be seeing EPSPs from neurons that have fired only τ ago, and consequently the rising parts of the EPSP functions will balance out the tails that it also sees. We can also see this in equation (6.17) where it is impossible for the derivative to be less than zero.

One of unstable speeds is the training speed itself. Consequently a chain whose connections were learned at v_t will be recalled at much higher speed.

There are some values of the threshold (in the approximate region $[0.6, 0.65]$ for the discrete analysis in figure 6.3) which allow two propagation speeds. Figure 6.2 shows two possible time courses of membrane potential for the same threshold for a discrete calculation and in a continuous analysis.

From (6.16) we can see that it is not just the ratio of v to v_t that determines the threshold as one might have initially thought, but that the speed scales the threshold. We can also see that we must consider v and τ_p separately in contrast to previous work Ermentrout (1998), where the speed scales with the space constant of the weights to a given unit, and therefore with the time constant of the potentiation function. This is because we have used an asymmetric learning function rather than a symmetric one as

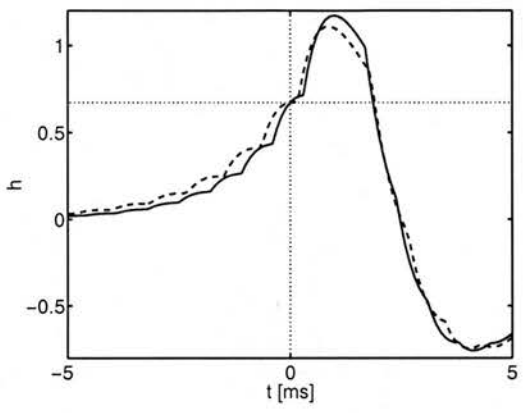

Figure 6.4: Time course of membrane potential for a neuron in the discrete case which fires at $t = 0$ showing how the stable propagation can occur at two speeds for the same threshold ($\vartheta = 0.6728$). Solid curve $v = 1.2\times10^3\,\mathrm{s}^{-1}$; dashed curve $v = 1.4237\times10^3\,\mathrm{s}^{-1}$.

considered previously.

I have solved the analytic threshold and stability equations for the potentiation function with experimentally-determined constants, though presenting the solutions would not be particularly illuminating. The solutions are shown graphically, along with the discrete speed-threshold relationship in figure 6.5. It is broadly similar to the simpler case, although there are some values of ϑ for which the continuous case would be unstable.

6.3 Discussion

In this chapter I have derived equations for the threshold-speed relationship of a generalised synfire chain comprising discrete units trained by a temporal learning rule, derived a continuous approximation to it and applied both analyses to a realistic potentiation function.

The discrete analysis is important as it corresponds better to physical reality than does the continuous approximation to it. On the basis of the continuous approximation alone, the instability of activity at lower speeds would not be predicted. Inclusion of the training speed as an explicit parameter does not simply lead to a scaled version of the previous continuous analysis (Wennekers and Palm, 1996; Ermentrout, 1998) and leads to the surprising conclusion that for low training speeds (less than $(\Delta^{\mathrm{ax}} + \tau)^{-1}$) the recall speed of chains will be higher than the speed at which they were trained. This result raises the possibility that temporal sequences may be trained more slowly

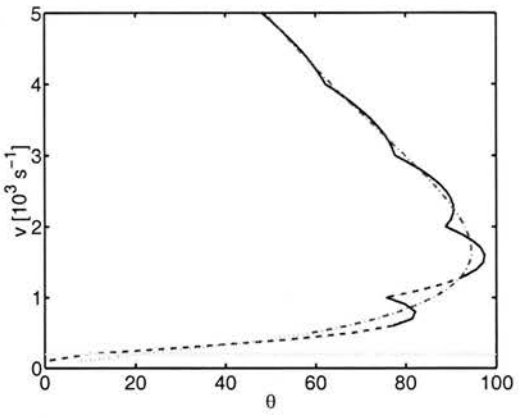

Figure 6.5: Plot of v against ϑ for $\tau = \Delta^{\mathrm{ax}} = \Delta^{\mathrm{dend}} = 1$ and $v_{\mathrm{t}} = 0.1 \times 10^3\,\mathrm{s}^{-1}$ where the weights have been learned with the potentiation function shown in figure 6.2. Discrete analysis: solid part of curve shows stable solutions and dashed part unstable ones. Continuous analysis: dash-dotted curve shows stable solutions and dotted part unstable ones.

than they can be recalled. This possibility could be of significance in learning motor sequences, where if nodes represent actions a slow sequence of movements could be learned and then speeded up (see also Wennekers and Palm, 1996). The effective threshold could be modified dynamically by an external signal that modifies neuronal background activity, thereby causing chains to speed up or slow down and possibly allowing two chains to synchronise their activities, as suggested in some theories of synfire processing (Bienenstock, 1995).

The principle differences between the biologically realistic potentiation function (Zhang et al., 1998) considered in this chapter and the others (for example Gaussian, rectangular) considered previously (Wennekers and Palm, 1996; Ermentrout, 1998) are (a) the longer time constant (20 ms as opposed to 1 ms) and (b) the depression occurring when presynaptic spikes follow postsynaptic ones. The shape of the speed threshold curve remains virtually the same as with a Gaussian curve, though the precise crossover point of the potentiation function affects it. The time course of the membrane potential is similar, though with inhibition after a node has fired. This will tend to turn off a node more quickly than it would had it been trained on a Gaussian learning function, and therefore affects the likelihood of a node re-exciting after firing. Due to the asymmetric learning function the speed does not scale with the time constant of the potentiation function, as in previous work (Ermentrout, 1998).

I am aware of two possible criticisms of this work. The first (pointed out to me be

T. Wennekers) is that I have not taken account of weight saturation effects, as suggested by the experimental evidence (Bi and Poo, 1998). It might be that weight saturation effects combined with repeated activity would lead to an effectively square coupling kernel, as used by Wennekers and Palm (1996). This is true, but it might also be that weight decay effects would tend to weaken distant connections between nodes. In any case, the general discrete analysis will still hold for any potentiation function.

The second criticism is that the assumption of uniform weights and uniform starting potentials is unrealistic. If the training is quite slow, so that only connections between adjacent nodes are potentiated, I expect that this analysis will hold up in most situations where synfire chains are stable (see section 3.4). Nevertheless, it would be interesting to integrate this analysis with the stability analyses mentioned in section 3.4. My preliminary investigations have shown that extending the temporal coherence result (Herrmann et al., 1995; Abeles, 1991) should be quite straightforward. However, extending the previous capacity results (Herrmann et al., 1995; Hertz, 1999; the "asynchronous background instability" and "chain death due to fluctuating potentials" in chapter 3) will not be so easy, since the results are only valid for "pure" synfire chains, that is, synfire chains that only have connections between adjacent nodes. My intuition is that the effect of connections between nonadjacent nodes will be to decrease the stability significantly, since it will result in more connections being potentiated, and therefore more interference between patterns.

Another interesting extension to the work would be to investigate whether the more realistic temporal learning rule allows more successful unsupervised learning of synfire chains than has been achieved previously (Hertz and Prügel-Bennett, 1996).

6.4 Summary

Spatiotemporal patterns or synfire chains may be learned in the presence of a suitable temporal learning rule by activating each node or group of neurons in turn. This is a form of supervised learning where the supervisor is other groups of neurons, possibly directly activated by sensory neurons. Such a system might be found in the interplay between the neocortex and hippocampus, or when learning motor patterns. An important parameter of the training protocol is the training speed, the speed at which nodes are activated. The temporal supervised learning protocol and training speed makes more explicit the assumptions behind previous work.

Previous work on the propagation speed has assumed that the time between pattern recall is small compared to the EPSP time constant, allowing a continuous approxima-

tion to the location of neurons. By contrast, the first analysis presented here uses discrete neurons, and is valid for all recall speeds. The temporal learning rule and the training speed jointly determine the weights between nodes. The threshold controls the speed of propagation through the chain during recall, and can be calculated as a function of recall speed. Some of the slower recall speeds may not be stable as a neuron's membrane potential would be falling as it spiked, which is impossible. There may be thresholds for which two recall speeds are stable. For a realistic learning rule and realistic EPSP functions both effects occur.

In the limit of fast recall the discrete forms of the equations converge on the previously-studied continuous forms. It turns out that the continuous equations do not show the same instabilities at low recall speeds. Thus the discrete analysis corresponds better to physical reality than its continuous approximation.

One implication of this work is that for low training speeds the recall speed of chains will be higher than the speed at which they were trained. This could be significant in the implicit learning of motor sequences where one part of the nervous system (for example the cortex) may be training another part (for example the cerebellum). There is also evidence that the hippocampus "trains" the neocortex; this result might also apply there. The realistic temporal learning rule means that nodes are less likely to fire after their first firing, making the sequences more robust as synfire chains. Due to the asymmetric learning function the speed does not scale with the time constant of the potentiation function, as in previous work.

The major criticisms of this work are that I have not taken account of weight saturation effects or overlapping patterns.

Chapter 7

Synchrony, sequences and *Schistocerca's* sense of smell

The motivation for this chapter is to test out the theoretical ideas of synchrony and sequences in a model of a real biological system. Recent work on the antennal lobe of the locust indicates that it is a suitable system to model. The antennal lobe is the second stage of olfactory processing in the locust and it appears that odours are represented by both synchrony and sequences in it. Although there is a wealth of experimental evidence showing how the codes change under various conditions, the synaptic structure and dynamical mechanisms underlying the dual code are not well understood. Furthermore, the antennal lobe itself is very small, comprising only 830 excitatory and 300 inhibitory neurons. This makes it a more attractive for modelling, as it should be possible, with reasonably simple neuron models, to model the neurons on a one-to-one basis.

We may note that research on locust olfaction has considerable practical applications. Despite advances over the past forty years, locusts are still a major pest in parts of sub-Saharan Africa and South America. They may live for many years in a *solitary* state, being relatively undestructive (Waloff and Green, 1975). In this state their olfactory systems are used to detect food and mates. However, but when the conditions are right — for example sufficient, well-timed rainfall — they swarm together. If the progeny of the swarms remain in swarms a plague is said to be in progress (Waloff and Green, 1975). The locusts are said to be in a *gregarious* phase, and locusts born to gregarious parents are morphologically different from solitary locusts (Bennett, 1975). Special aggregation pheromones are a crucial part of the swarming mechanism, and are therefore an active area of research.

As there is a great deal of similarity of the olfactory systems of both vertebrate and invertebrate species (Hildebrand and Shepherd, 1997), in section 7.1 I will start this

chapter by giving an overview of the anatomy, physiology, coding, learning, memory and plasticity of the first two stages of insect and vertebrate olfactory systems. I will also present some computational models of olfactory systems. In section 7.2 I will provide a detailed review of work on the input odours, the anatomy, physiology and coding in the locust antennal lobe (AL). In section 7.3 I distill from the mass of data the relevant questions that a model should answer. The problem breaks down into explaining the mechanism of the fast oscillations and explaining the mechanism of the slow temporal patterns. Although there are enough constraints to build a general model of the antennal lobe, there are still many undetermined parameters and hypotheses. It may be that two types of model have to be developed and then merged. I take the approach that the simplest model consistent with the data should be constructed before trying out some of the hypotheses. Section 7.4 describes how I build this model. In the course of building the model, I find that although the anatomy determines the connectivity, it does not determine the weights. Rather than spend a long time guessing appropriate weights I decide to attempt to use the constraints provided by the oscillations to calculate a first approximation to the weights. This enterprise turns out to be a small project in itself, and therefore forms a chapter of its own, chapter 8. After this intermission, I will go on to describe the results from the locust model in chapter 9.

7.1 The early olfactory system

There are strong similarities between the early olfactory system in vertebrates and invertebrates (Hildebrand and Shepherd, 1997). Therefore, in this short review of the early olfactory system, I will discuss the vertebrate and invertebrate olfactory systems together.

I will start this review by considering odours, in particular their temporal characteristics as viewed by a flying insect (section 7.1.1). In section 7.1.2 I will present the anatomy of the first two stages of the vertebrate and insect olfactory systems. The related issues of physiology and how the olfactory system encodes odours are considered in section 7.1.3. The topic of section 7.1.4 is learning and memory in the early olfactory system. Finally, in section 7.1.5, I present some existing models of vertebrate and insect olfactory systems.

7.1.1 The nature of olfactory stimuli

Odours comprise mixtures of different molecules. Odour molecules are small volatile compounds with a molecular weight between around 26 and 300 (Mori et al., 1998). Odours occur both singly and in mixtures.

The wind carries the odour molecules from their source, forming an odour plume. Diffusion and turbulence lead to the odour plume having a complex spatiotemporal structure that depends on factors such as wind speed, source size and the landscape (Murlis et al., 1992). This means that an animal sensing an odour plume will encounter odour molecules only intermittently.

In insects the olfactory system has a short sampling time, so the intermittent odour structure is important. Vickers et al. (2001) investigated the spatiotemporal properties of an odour plume 150 cm downstream of an odour source using an electroantennogram measured from an excised antenna. This showed that the intensity and temporal structure of the plume varied significantly over distances of 5 cm from the centre of the plume. The wind speed also changed the structure of the plume: at low wind speeds the electroantennogram measured frequent, high amplitude bursts at the centre of the plume and little activity 5 cm away from it; at higher wind speeds the central activity was smaller, and the peripheral activity greater. The bursts were of the order of tens of milliseconds long.

The number of odour molecules encountered depends on the speed of the animal as well as the odour concentration in the plume. There is therefore no clean concentration gradient to assist the animal in locating a source. Suggested strategies for locating odour sources typically involve moving upwind when in the odour plume, and zigzagging when the plume is lost. However, strategies that utilise the structure of the plume alone have not been ruled out (Murlis et al., 1992).

7.1.2 Anatomy

Olfactory receptor neurons (RNs) are generally located in the antennae of insects or in the sensory epithelium (located within the nasal cavity) of vertebrates (Hildebrand and Shepherd, 1997). In insects, RNs are associated with small hairs (sensilla) on the antennae. The outside surface of a sensillum is waxy so as to absorb odours. Small pores in the surface allow odour molecules to enter and diffuse through the lymph towards the cilia of the RNs. In vertebrates, the mucus of the sensory epithelium plays an analogous role to the lymph. (Hildebrand and Shepherd, 1997)

The RNs project (via the olfactory tract) to a structure called the antennal lobe

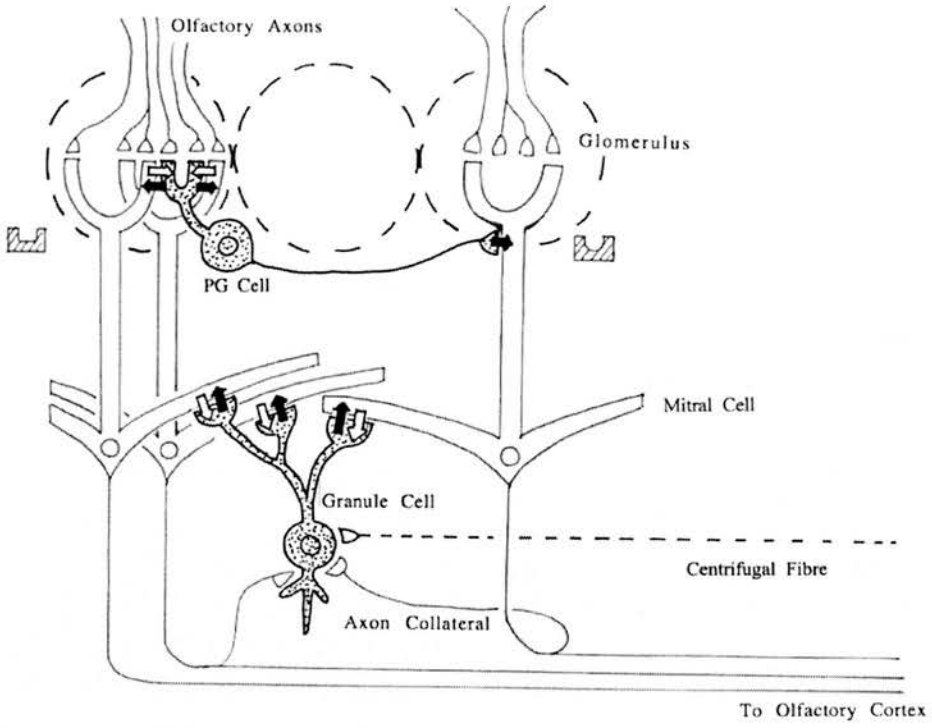

Figure 7.1: Neuronal circuit of the mammalian olfactory bulb. From Mori et al. (1998). Excitatory synapses are represented by open triangles or arrows. Inhibitory synapses are represented by filled arrows.

(AL) in insects or the olfactory bulb (OB) in vertebrates. Besides input fibres from the RNs, the AL or OB comprises various types of projection and intrinsic neurons.

The vertebrate OB is arranged in a number of layers (Shepherd, 1998) located on a segment of sphere or ellipsoid. Figure 7.1 shows the arrangement and connectivity of the OB. The outermost layer contains roughly spherical regions of neuropil called *glomeruli.* They contain preterminal axons and synaptic boutons of RNs, dendritic arborisations from the primary dendrites of mitral and tufted cells (the main projection neurons of the OB) and dendritic arborisations and axons from periglomerular cells. The somata of periglomerular cells surround the glomeruli. The dendritic trees of periglomerular cells arborise in one or possibly two glomeruli and make reciprocal synapses with mitral cell dendrites, while their axons innervate local glomeruli. RNs make type 1 (excitatory) synapses on both mitral and tufted cells and periglomerular cells. Mitral/tufted cells make dendrodendritic type 1 synapses onto periglomerular cells and receive type 2 (inhibitory) inputs from the periglomerular cells (Shepherd, 1998). The next layer

down, the external plexiform layer, contains the secondary dendrites of mitral and tufted cells and the dendritic arborisations of granule cells. There are reciprocal synapses between the granule cell and mitral cell dendrites. The mitral to granule contacts are type 1 (excitatory) whereas the granule to mitral contacts appear to be type 2 (inhibitory). The bodies of the mitral and tufted cells are to be found in the next layer, the mitral cell layer. The mitral/tufted cells send out axons down through the next layer, the granule cell layer, with the axons bunching to form the lateral olfactory tract, which projects to various areas of the olfactory cortex. Also in the granule cell layer are the cell bodies and dendrites of the granule cells and centrifugal afferents from various brain centres.

The organisation of the insect AL (figure 7.2 shows the locust AL) is generally similar to that of the vertebrate OB. There are projection neurons (PNs) that, like mitral and tufted cells, project out of the AL. The intrinsic local neurons (LNs) are analogous to periglomerular and granule cells. Almost all synapses in the AL are located in glomeruli on the periphery of the deutocerebrum.

In contrast with the vertebrate OB, there do not appear to be two types of projection neuron. There also does not appear to be the same geometrical arrangement as in the vertebrate OB. LNs may innervate several glomeruli (unlike periglomerular cells; Galizia and Menzel, 2000a) and do not generally make synapses on PNs outside glomeruli (unlike granule cells). Some insects do not even have a glomerular organisation (Masson and Mustaparta, 1990).

In the locust, the axons of the PNs form a coarse fibre bundle that runs ventro-dorsally through the neuropil of the AL, emerging as the antennoglomerular tract (AGT, also known as the tractus olfactorio glomerulus). The AGT runs to the lateral protocerebral lobe (LPL), with branches to the calyces of the mushroom body (MB). Here the PN axons synapse onto about 50000 excitatory Kenyon cells (KCs) (Laurent, 1996). The KC axons run dorsoventrally, terminating in the α and β lobes of the MB. The MB has been implicated in multimodal associative memory (Strausfeld et al., 1998).

From immunogold histochemical studies of the AL of *Schistocerca americana*, there appear to be connections from RNs to PNs and LNs and reciprocally within and between the PNs and LNs. RNs and PNs are excitatory neurons, whereas LNs are inhibitory (Leitch and Laurent, 1996). Figure 7.3 is a schematic diagram of the network.

Insects have between 2000 and 350000 RNs (Hildebrand and Shepherd, 1997). Typical numbers of RNs are 100000 in locusts (Laurent, 1996), 120000 in worker honeybees (Galizia and Menzel, 2000a), 195000 in the male cockroach *Periplaneta americana* and

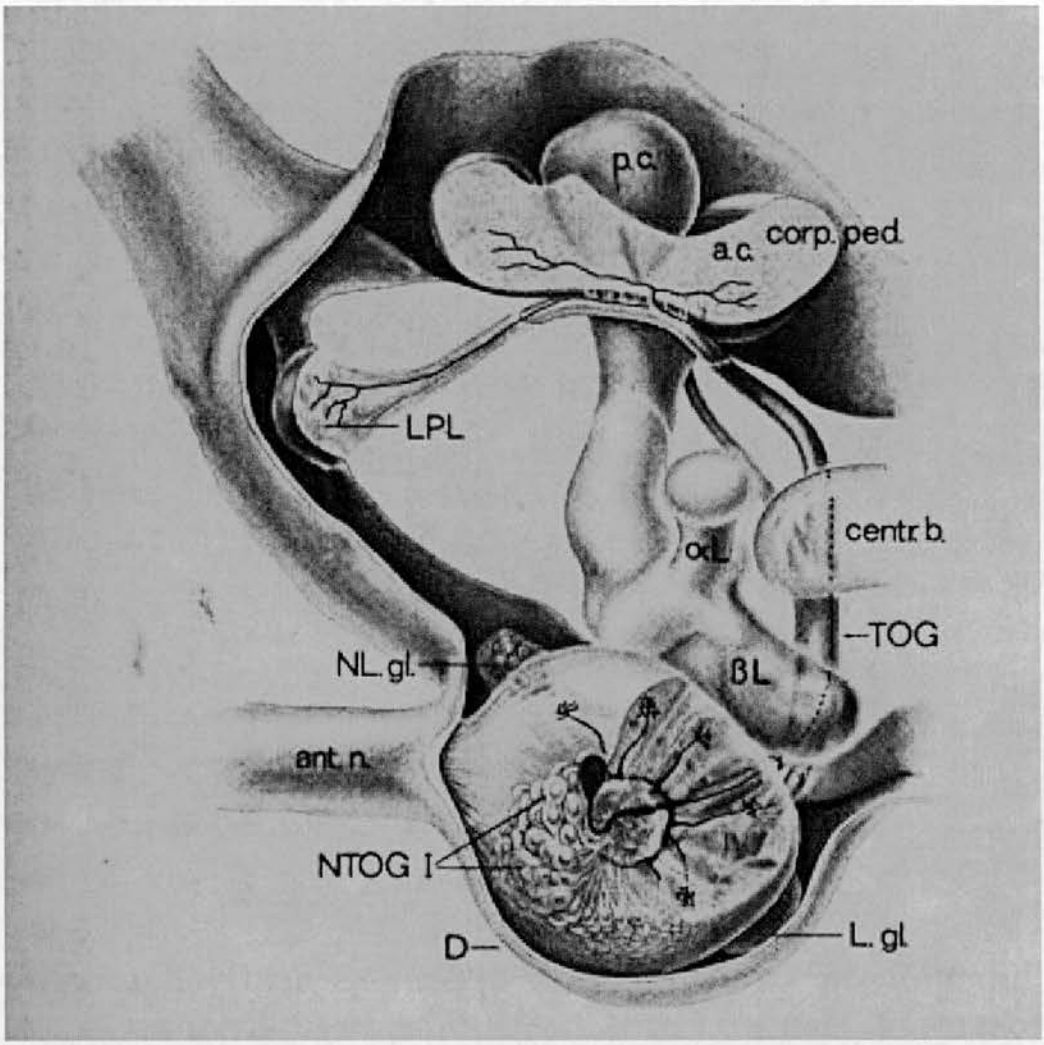

Figure 7.2: Semi-diagrammatic fronto-horizontal view of the right half of the brain of the migratory locust *Locusta migratoria* (from Ernst et al., 1977). *a.c.* and *p.c. corp. ped.* anterior and posterior calyx of the corpus pedunculatum; *ant. n.* antennal nerve; *cent. b.* central body; *D* deutocerebrum; *glom.* glomeruli; *L. gl.* lobus glomeratus of the tritocerebrum; *LPL* lateral protocerebral lobe; *NL. gl.* neurons of the lobus glomeratus; *NTOG I* neurons of type I of the tractus olfactorio-globularis; *TOG* tractus olfactorio-globularis (referred to as the antennoglomerular tract in this thesis); αL α-lobus; βL β-lobus.

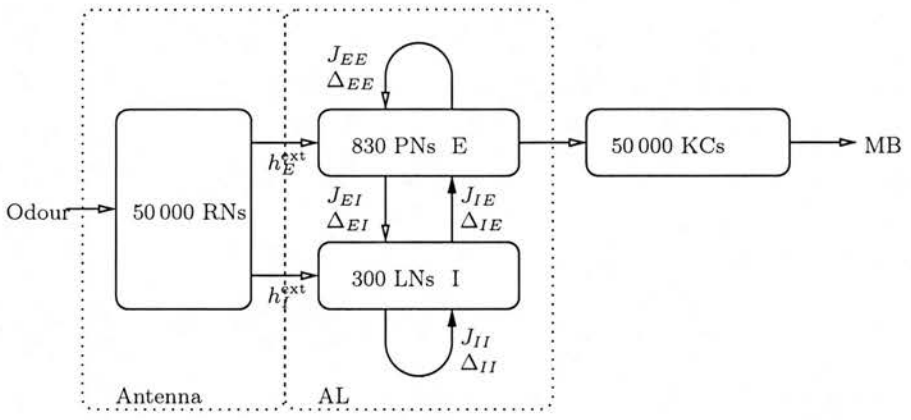

Figure 7.3: Schematic diagram of the first stages of the locust olfactory system. Open arrowheads indicate excitatory connections and closed arrowheads indicate inhibitory connections. See text for abbreviations.

300000 in the moth *Manduca Sexta*. In vertebrates the figure may be an order of magnitude higher, for example 50×10^6 in rabbits (Mori et al., 1998).

The number of glomeruli varies from species to species. In vertebrates it is typically between 1000 and 5000 (Hildebrand and Shepherd, 1997); for the rabbit it is 6300 (Mori et al., 1998). In insects, most species have between around 50 and 200 glomeruli, though a few (locusts and wasps) contain about 1000 (Masson and Mustaparta, 1990). The species with fewer glomeruli are described as macroglomerular whereas those with many glomeruli (for example locusts and wasps) are said to have a microglomerular organisation (Laurent et al., 2001). This is because the glomeruli are larger in species with fewer glomeruli.

The males of some species of insects also have a enlarged glomerular structure referred to as the macroglomerulus (in the case of the *P. americana*) or the macroglomerular complex (MGC; in the case of *M. sexta*). This structure is used for pheremone detection (Hildebrand and Shepherd, 1997). In vertebrates there is an anatomically distinct area of the OB called the accessory olfactory bulb, which is also responsible for pheremone detection (Mori et al., 1998).

In insects, the number of glomeruli a RN projects into depends on the species. For example, in the bee, ant and cockroach, projections are uniglomerular (Masson and Mustaparta, 1990). By contrast in the locust (a microglomerular species) RNs typically project into more that one glomerulus (Ernst et al., 1977; Masson and Mustaparta, 1990). In vertebrates, RN axons do not branch on their way to the glomeruli (Shepherd, 1998), making the projection uniglomerular. The ratio of convergence from RNs to

glomeruli in mammals is typically around 10000:1 whereas in insects it is typically an order of magnitude lower at 1000:1 (Hildebrand and Shepherd, 1997).

In vertebrates it is common for each mitral or tufted cell to innervate only one glomerulus. This pattern is followed in macroglomerular insect species, where the innervation is uniglomerular, but in microglomerular species such as the locust, PNs can innervate more than one glomerulus (Laurent et al., 2001; Ernst et al., 1977). In the rabbit, there are about 1.3×10^5 tufted cells and 6×10^4 mitral cells, giving a glomeruli to projection neuron divergence ratio of about 1:30. In insects, the number of projection neurons is much smaller, for example 260 in *P. americana*, 300 in *M. sexta* (Hildebrand and Shepherd, 1997), 1000 in the honeybee (Faber et al., 1999), and 830 in the locust (Laurent, 1996). In macroglomerular species this gives a typical glomeruli to projection neuron divergence ratio of about 1:2. In a microglomerular species such as the locust, this figure is estimated to be about 1:10.

7.1.3 Physiology and Coding

I will first deal with the physiology and coding of receptor neurons in section 7.1.3.1. In section 7.1.3.2 I will primarily deal with the physiology of the neurons of the AL or OB. It seems convenient to split the discussion of coding in the AL/OB into its spatial features (section 7.1.3.3) and temporal features (section 7.1.3.4).

7.1.3.1 Receptor neurons

The cilia of the RNs contain receptor proteins that are sensitive to odour molecules (Hildebrand and Shepherd, 1997). When the receptors are activated by odour molecules they cause channels to open via a second messenger pathway. In vertebrates, the channels are sensitive to a number of ions, and generally cause a depolarising inward current to flow. This causes the RNs to increase their firing rate above a spontaneous background level. There is more than one type of second messenger pathway. It is not clear if different odours activate different pathways, and therefore cause different membrane currents to flow. RNs generally reduce their firing rate during a prolonged stimulus. This adaptation is also mediated by second-messenger systems. In invertebrates, the RNs may respond to odours with hyperpolarising as well as depolarising receptor potentials. This leads to decreases as well as increases in the spontaneous firing rates (Hildebrand and Shepherd, 1997).

RNs can be sensitive to a range of odour molecules (generalist) or only one type of odour molecule (specialist). In insects, generalist cells tend to respond to food

odours, whereas the specialist cells respond to pheremone components (Hildebrand and Shepherd, 1997). Studies in vertebrates have shown that molecules with the similar functional groups and chain length tend to activate the same generalist cells (Mori et al., 1998).

In vertebrates, a family of odourant receptor genes of about 1000 members encodes the receptors (Mori et al., 1998). The hypothesis that each receptor cell expresses only one type of receptor molecule has yet to be disproved. An individual odourant receptor can bind to molecules with similar structure and chain length. The odour sensitivity range in generalist cells is therefore due to the unspecific nature of the receptor molecules (Mori et al., 1998). In invertebrates, a family of 60 *Drosophila* odourant receptors have been discovered (Gao et al., 2000). *Drosophila* RNs appear to express only one or a few of these receptors. The narrow tuning of RNs in male moth antennae to components of sex pheromones indicates that these cells express only one type of receptor molecule (Hildebrand and Shepherd, 1997).

In invertebrates, there appears to be no temporal patterning of the RN activity other than that inherent in the stimulus (see section 7.1.1). In mammals, the sniff cycle causes a roughly linear rise in firing frequency of receptor cells during inhalation followed by sharp decline as the animal exhales (Li and Hopfield, 1989)

7.I.3.2 AL/OB neurons

In vertebrates, mitral cells are conventional spiking neurons whereas granule cells do not produce action potentials (Shepherd, 1998). When mitral cells fire, the action potential backpropagates through the dendrites, activating excitatory synapses onto spines of granule cells. The resulting EPSP in the granule cell spine causes the inhibitory synapse from the granule cell to the mitral cell to be activated, producing a long-lasting IPSP in the mitral cell. The synaptic interactions within glomeruli are less well characterised, as periglomerular cells are hard to record from (Shepherd, 1998).

In locusts, the PNs are conventionally spiking neurons, whereas the LNs are axonless neurons that produce graded action potentials (Laurent, 1996). Little is known about the electrophysiology of single cells or the synaptic interactions between cells.

7.I.3.3 Spatial features of activation across the AL/OB

In vertebrates, studies measuring 2-deoxyglucose uptake in glomeruli indicate that each odour causes synaptic activation in a particular set of glomeruli, thus forming an "odour image" or "odourtopic map" in the glomerular layer (Shepherd, 1998). The amplitude

of EEG signals from electrodes implanted over the rabbit OB shows a similar map (Freeman and Skarda, 1985). Single unit recordings show that mitral and tufted cells are activated by a limited range of molecules with similar molecular structure (Mori et al., 1998). The distinct odourtopic map can be accounted for by the *one receptor–one glomerulus* hypothesis (Mori et al., 1998). The specificity of the mitral cells follows from the specific activation of glomeruli and the fact that any mitral cell sends its primary dendrite into a single glomerulus. The one receptor–one glomerulus hypothesis is grounded in the finding in mice and rats that receptor cells expressing the same odourant receptor project their axons to two (or more) glomeruli in the OB. Given that there about 1000 odourant receptor genes and about 1800 glomeruli in mice, it seems reasonable to suppose that all the RNs converging on a glomerulus express the same receptor.

A limited range of molecules may decrease mitral cell firing rate below baseline (Mori et al., 1998). These molecules may differ from molecules that excite the cells by having a hydrocarbon chain only one carbon longer. When the granule cell to mitral cell synapses are blocked pharmacologically, the odour-evoked inhibitory responses are greatly reduced. This indicates that they are partly caused by lateral inhibition mediated via the granule cells from mitral cells belonging to neighbouring glomeruli.

In invertebrates, calcium imaging can be used to visualise which glomeruli are active (Galizia and Menzel, 2000a). The activity across a sample of glomeruli correlates with the odour presented. Consistent with the vertebrate results, glomeruli tend to respond to similar molecules. Furthermore, the patterns of activation appear to be largely preserved between different individuals of the same species (Galizia et al., 1999; Galizia and Menzel, 2000a). Recent evidence from *Drosophila* suggests that this glomerular specificity is a result of RNs expressing only one receptor and all RNs expressing the same receptor projecting to the same glomeruli (Gao et al., 2000).

Glomeruli with similar response profiles tend to be neighbours. This suggests a lateral inhibition scheme similar to vertebrates, as in order to sharpen response profiles maximally, glomeruli responding to similar stimuli should inhibit each other laterally. This is appealing in the vertebrate OB, because of the local nature of the granule cells and mitral cell secondary dendrites. However in the insect AL, LNs innervate several glomeruli and their dendrites do not travel from glomerulus to glomerulus, instead converging on the central neuropil (Galizia and Menzel, 2000a). Furthermore, not all neighbouring glomeruli have similar response profiles.

7.1.3.4 Temporal features of activation across the AL/OB

In vertebrates, odour presentation causes high-amplitude bulbar oscillatory activity as measured by EEG electrodes (Freeman and Skarda, 1985). When there is no odour the fast (35–90 Hz) oscillations disappear, though a slow background wave phase locked to the respiratory wave remains.

Laurent and co-workers have investigated responses of the locust AL to approximately second-long pulses of odour (see Laurent, 1996, for a review). PNs appear to represent odours by a spatiotemporal code. This code comprises three main elements (Laurent et al., 1996).

Slow spatiotemporal activity: PN spike trains trial averaged with a time bin of the order of 100 ms have distinct temporal patterns for different odours (figure 7.6). The pattern for a given odour varies between different neurons (Laurent et al., 1996).

Fast global oscillations: The population averaged activities (on a time scale of 1ms) of PNs and LNs show oscillations with a frequency of about 20 Hz (Laurent and Davidowitz, 1994; Laurent et al., 1996). The excitatory PNs lead the inhibitory LNs by one quarter of a cycle (Laurent and Davidowitz, 1994). This frequency and phase seem to be fairly independent of the concentration of the odour. Furthermore, it appears that there is usually only one spike per PN per cycle (Laurent and Naraghi, 1994). Oscillations seem to occur in response to odours that have been presented in the last 10 minutes, and are thus a form of short term memory (Laurent et al., 2001; Anton and Hansson, 1996). See figure 7.8.

Transient synchronisation of active neurons: During the odour presentation, sets of PNs sometimes synchronise their activity precisely at the 20 Hz frequency and sometimes do not. Hence at each point in time neurons fall into three classes: inactive; active and unsynchronised to the global oscillation; and active and synchronised to the global oscillation (Laurent and Davidowitz, 1994; Wehr and Laurent, 1996; Laurent et al., 1996). See figure 7.9.

When ionotropic GABA receptors are antagonised, the first property remains, but the second two disappear (MacLeod and Laurent, 1996). The behavioural implications of this are to disrupt discrimination of very similar odours (Stopfer et al., 1997).

Recently, an alternative role for synchrony without oscillations has been proposed. Christensen et al. (2000) have made extracellular multi-unit recordings from cells in the

macroglomerular complex of *Manduca sexta* in response to short (100 ms) odour pulses reminiscent of naturalistic pheremone signals (Murlis et al., 1992; section 7.1.1). They found a variety of spatial and response profiles and temporal patterns of firing, even within the same glomerulus. They also found that synchronisation between neurons in a 10 ms window could encode whether two components of a pheremone blend were present simultaneously at certain concentrations. This can be seen as support for temporal binding hypothesis (section 4.2.3), but it is context-dependent in that binding may only occur at certain odour concentrations. There was no rhythmic discharge of neurons, in contrast to the findings of Laurent and coworkers (see, for example Laurent, 1996). This raises the question of whether oscillations are simply an epiphenomenon caused by presenting unnaturally-prolonged stimuli and the dynamics of the AL. However, the macroglomerulus could be optimised to perform very fast computations in response to pulses of pheremone; the generalist olfactory system could perform a different, slower, computation involving oscillations (Galizia and Menzel, 2000b). This evidence suggests a dual code in which space indicates odour identity and synchronous timing indicates other features, such as concentration.

7.1.4 Learning, memory and plasticity

Honeybees can be trained to respond to an odour with the proboscis extension reflex; this reflex is directly related to successful learning (Galizia and Menzel, 2000a). We can measure odour discrimination by reinforcing one odour with sugar-water reward and not rewarding another. If the bee can discriminate between the two odours, it will respond only to the positively-reinforced stimulus. Individual components of odours may be presented or a combination of components may be presented when training a honeybee.

Honeybees are able to distinguish mixtures where each component is part of a rewarded and non-rewarded mixture (e.g. AB and CD from BC and AD). Honeybees can generalise from single odours to mixtures of odours as long as the odours are not too similar. For example, when trained with single odour A, the honeybee will respond to AB, unless A and B are very similar. Previously learning a single odour may "block" learning from a mixture. In "blocking" experiments, an odour A is positively reinforced, and then an odour containing A (AB) is also reinforced. If the response to odour B after training is reduced compared to animals trained only on AB, then B is said to be blocked. Blocking has not yet been confirmed in honeybees, although preliminary evidence suggests that it may when odours are similar.

Although glomerular representations of odours are genetically determined (Galizia et al., 1999), associative learning modifies these representations (Faber et al., 1999). After behavioural training using the proboscis-extension task, activity for the rewarded odours increases, activity for the control odor increases to a lesser extent, and activity for unrewarded odours may decrease. It appears that the representations of the rewarded and unrewarded stimuli are decorrelated. The mechanism responsible for this plasticity is not yet known. However, a likely candidate for mediating the reward signal is the VUMmx1 neuron. This neuron increases its firing rate in response to a positively reinforced stimulus and innervates the AL glomeruli and the MB (Hammer, 1993). It thus may provide a signal for learning. Whether the modification occurs by associative presynaptic facilitation or by Hebbian associative plasticity (Kandel et al., 2000) is not known.

The antennal lobe also exhibits short term memory. Stopfer and Laurent (1999) presented sequences of 10 0.25–2 s-long pulses of novel odour separated by intervals ranging from 2.5–20 s to one antenna of a locust. The intracellularly-recorded PN responses to the first odour pulse in a sequence were strong but did not contain any periodic component. In response to later pulses in the sequence, the PN responses were weaker (that is, contained fewer spikes), but became increasingly locked to the 20 ± 5 Hz oscillations in the LFP measured in the MB. Intracellular recordings from LNs revealed no dominant frequency in response to the first pulse, and increasing power in the frequency spectrum around 20 ± 5 Hz to subsequent pulses. Thus it appears that as a stimulus becomes more familiar, PN spikes become more synchronised with each other. This behaviour also happened in response to sequences of pulses with random duration and interstimulus interval, as motivated by odour plume dynamics (section 7.1.1; Murlis et al., 1992). If an odour has not been presented for around 10 minutes, the response to it is no longer oscillatory. Learning generalises to chemically similar odours but not to dissimilar ones: an odour may generate an oscillatory response on the first presentation if a similar odour has been presented within 10 minutes before. The learning does not seem to arise from adaptation of RNs since activating unadapted RNs once responses are oscillatory still leads to oscillatory responses. Thus the mechanism of plasticity is probably local to the AL and could involve descending inputs from the MB. Its function is also unclear, though Stopfer and Laurent (1999) showed that the PN spike intensity was a more reliable indicator of odour identity when taken from later, oscillatory responses than from the first response.

7.1.5 Previous models of olfaction

I will deal with models of the invertebrate olfactory system in section 7.1.5.1 and of the vertebrate olfactory system in section 7.1.5.2.

7.1.5.1 Invertebrate olfactory system

Linster et al. (1993) modelled the insect macroglomerulus using a network with sparse random connectivity comprising receptor, excitatory and inhibitory neurons. The neuron model is a leaky integrating neuron but without membrane potential reset after firing. Spikes are generated stochastically according to a sigmoidal probability function of the membrane potential. EPSCs are modelled by (delta) pulses but the randomly-chosen transmission delays are shorter for excitatory neurons than for inhibitory ones, to reflect faster EPSCs compared to more persistent IPSCs. Receptor neurons are selective to one of two odours. In response to a single odour pulse, neurons respond with a variety of different responses (such as tonic excitation or inhibition or phasic bursts). Which of these is present depends on the proportion of inhibitory neurons and the sparseness of connectivity of the network. Some neurons are selective for one of the two odours whereas others respond to both. The concentration of the odour and its temporal profile is reflected in the amplitude and latency of the response. This is significant as the stimulus profile could depend on distance from an odour (Murlis et al., 1992; section 7.1.1). The network cannot respond to pulsed stimulation above a certain frequency, because of the membrane time constants.

Linster and Masson (1996) modelled the antennal lobe of the honeybee in order to explore the hypothesis that the antennal lobe is used to reduce noise in the signal before sending it to the mushroom bodies to compare with stored odours. The model includes 15 of the 165 glomeruli present in a worker honeybee. Most of the local interneurons in the honeybee AL branch densely in one particular glomerulus (rather than diffusely), rather like periglomerular cells in the vertebrate olfactory system. Based on evidence from the cockroach, they postulated that some of the localised interneurons are excitatory. Feedback excitation from these glomerular-local excitatory cells combined with lateral inhibitory connections between neighbouring glomeruli is responsible for implementing a competitive mechanism that results in glomerular activation either saturating or being silent when presented with an odour. By modulating the lateral inhibition they show how the AL could implement a short term memory. This would present the mushroom bodies with a distinct pattern for a longer period of time. They use the same basic neuron model as Linster et al. (1993) but with firing probability as

a piecewise linear rather than sigmoid function of membrane potential.

Linster and Smith (1997) used the same neuron formalism as Linster and Masson (1996), though with no local excitatory elements. The firing thresholds on the excitatory projection neurons are set so that they fire spontaneously unless inhibited. Receptor neurons synapse onto the inhibitory interneurons. When an receptor neuron is active, it inhibits cells in its own glomerulus, which send inhibition to neighbouring glomeruli. In the resulting competition, the inhibitory neurons activated by the receptor neuron "win", thus leading the projection neurons in neighbouring glomeruli to be released from inhibition (in contrast to the model of Linster and Masson, 1996). A modulatory neuron based on the experimentally-observed VUMmx1 neuron (Hammer, 1993) receives input from projection neurons and a sucrose reinforcement signal and sends back synapses to the inhibitory local neurons. The connections from the excitatory projection neurons are modifiable according to a Hebbian learning rule. When sucrose reinforcement is paired with particular odours, the synapses from the excitatory neurons onto the VUMmx1 neuron are potentiated, thus causing the VUMmx1 neuron to fire when the odour is presented without reinforcement. The model exhibits the psychophysical phenomenon of *overshadowing*: when the network is conditioned to respond to an odour mixture, and then are presented with one component of the mixture, its response is less than if it had been trained on the pure odour. If the synapses from the VUMmx1 neuron to the inhibitory interneurons are also modifiable, the model also exhibits blocking (see section 7.1.4).

Kerszberg and Masson (1995) modelled the honeybee AL in order to determine whether the oscillations observed have cognitive significance. The dendrites of local and projection neurons are modelled as passive compartments and are connected by a mixture of randomly-distributed conductance-based reciprocal and unidirectional synapses. The channels open stochastically as a function of the presynaptic membrane potential and close with an exponentially-decaying function. The spontaneous activity has peaks in the spectrum of the simulated LFP at 100 Hz and 20 Hz. The high-frequency peaks are only present with deterministic thresholds. Activity is quenched with higher thresholds, but the peaks in the spectra remain in the same places. Presenting randomly-distributed inputs to the network with high thresholds leads to the inputs moving the network from a quiescent state to an active one. The network appears to exhibit attractor states. The response frequency is not related to the input frequency.

7.1.5.2 Vertebrate olfactory system

Li and Hopfield (1989) modelled the mitral and tufted cells and granule cells of the OB using rate-based neurons with nonlinear output functions. These were connected together on a 1D ring with each mitral cell receiving inputs from neighbouring granule cells and vice versa. There were reciprocal connections of uniform strength between neighbouring mitral and granule cells, and there were no granule to granule or mitral to mitral connections. The inputs were modelled by a spatial pattern modulated by a temporal envelope corresponding to the sniff cycle. The result is that different odours activate a different set of mitral cells and the activity of these cells oscillates during the active part of the sniff cycle. Mathematical analysis of the system lead to the following predictions. Mitral cells should lead granule cell by quarter of one cycle. The oscillator frequency should be the same everywhere on the bulb. There may be a phase gradient across the bulb. Oscillation activity will rise during inhale and fall during exhale and rides on slow activity which is background baseline shift locked with the sniff cycle. The connection structure determines the type of patterns that the system will oscillate in response to. The initial resting point of the system could be set by descending inputs so that only motivated animals have oscillations.

Li (1990, 1994) incorporated descending control from higher olfactory centres such as the piriform cortex into the model of Li and Hopfield (1989). This input acts to cancel out the oscillations in the OB, thus leading to the adaptation of the OB response. The model was able to account for a number of psychophysical findings concerning odour adaptation and mixing. Li and Hertz (2000) extended the model of Li (1990) by learning odour identity in connections between cortical pyramidal cells and the connections from pyramidal cells onto inhibitory cells. This provides a more principled way of feeding back to cancel the signal.

A different approach of modelling the piriform cortex was taken by Wilson and Bower (1988, 1992). Their model comprised 100 compartmental neurons with realistic channels. Pyramidal cells and feedforward and feedback inhibition were included. They presented the model with bursts of activity in a randomly-chosen subset of the inputs, assumed to have been created by the olfactory bulb. The model exhibited 40 Hz oscillations in response to the inputs. When a number of the synapses were modified according to a Hebbian plasticity rule during exposure to stimuli, the network was able to recall the stimuli when presented with partial stimuli.

Linster and Hasselmo (1997) modelled the OB and descending modulation of it by noradrenergic and cholinergic input from higher olfactory centres using stochastically-

firing leaky integrators (as used by Linster et al., 1993, see previous section). A modulatory cell takes the average of mitral cell activity and feeds it back into periglomerular cells as well as modulating the connection from granule cells to mitral cells. The results show that the modulation make the representation of different odours less overlapping.

7.2 Detailed description of the locust antennal lobe

Various aspects of the anatomy and physiology of the olfactory system of the migratory locust *Locusta migratoria* and the desert locusts *Schistocerca americana* and *Schistocerca gregaria* in the order Orthoptera have been studied in each species, though not all aspects have been studied in one species. Although I have not found a specific reference stating this, people seem to assume that the species are close enough to compare. In this thesis, I assume that the olfactory systems of *L. Migratoria*, *S. gregaria* and *S. americana* have the same anatomical and physiological characteristics, and I refer to them all as "locusts".

In this section I will review in more detail the anatomy (section 7.2.1), physiology (section 7.2.2) and coding (section 7.2.3) in the AL. Unfortunately there is not very much known about the learning and development of representations in the AL; I present what little is known in section 7.2.4.

7.2.1 Anatomy

I will divide up the anatomy of the antenna and AL into its constituent neurons, the RNs, PNs and LNs, and then go onto discuss how they are connected and where they project to after the AL.

7.2.1.1 Receptor neurons

RNs are found in one part of each antenna (the flagellum) (Ernst et al., 1977). They are contained in olfactory organs (*sensilla*), which come in a number of varieties. In the locust there are three types: sensilla trichodea (long hairs); sensilla basiconica (short hairs); and sensilla coeloconica (pit peg) (Masson and Mustaparta, 1990). The sensilla trichodea contain the dendrites of 3 RNs, the sensilla basiconica contain 30–40 RNs and the sensilla coeloconica contain 1–4 RNs (Hansson et al., 1996).

Most RN axons project to the ipsilateral deutocerebrum (that is the AL), but some project to the ipsilateral lobus dorsalis. The axons are found in bundles from adjacent sections of antenna, and go to circumscribed regions. Individual axons can have up to six branches and innervate up to 3 glomeruli of the AL (Ernst et al., 1977).

7.2.1.2 Projection neurons

The ALs of the deutocerebrum of *Locusta migratoria* are dome-shaped with a diameter of 0.5 mm. They comprise the axons from the RNs of the ipsilateral antenna, and the somata and processes of PNs and LNs. The PNs have bigger (20–25 μm) somata located dorsally at the front of the AL, whereas the LNs have smaller (10–12.5 μm) somata situated ventrally at the front of the AL (Ernst et al., 1977).

From the PNs a coarse fibre bundle runs into the neuropil of the AL. Not more than one branch runs from each process at right angles, and then describes a ring-like path around the fibre bundle. From this ring branches arborise at varying depths, and with diameters between 20 and 40 μm (Ernst et al., 1977). Estimates of the number of branches from each ring are 10–25 (Anton and Hansson, 1996) and 10–20 (Leitch and Laurent, 1996). The main process continues out of the AL towards the LPL. Processes of the PNs prefer to innervate glomeruli distant from one another — never adjacent ones (Ernst et al., 1977). From the number of axons in the antennoglomerular tract (AGT), Leitch and Laurent (1996) estimate there are 830 PNs.

7.2.1.3 Local neurons

Processes from the LNs branch several times in the neuropil, with the diameter decreasing at each branch. They "penetrate large sections of the neuropil" (Ernst et al., 1977), perhaps around 25% (my estimate from figures) or may even "occupy the entire neuropil" (MacLeod and Laurent, 1996).

7.2.1.4 Glomeruli and connectivity

The glomeruli are numerous (about 1000) and small (25 μm diameter) compared to other insects (Masson and Mustaparta, 1990). Terminals of the neurons with bigger somata appear to fill the glomeruli, and terminals often overlap (Ernst et al., 1977). Immunogold histochemical studies of the AL of *S. americana* bred in crowded conditions (and therefore presumably in the gregarious phase) indicate that there are synapses from non-GABAergic to non-GABAergic profiles, from non-GABAergic to GABAergic profiles, from GABAergic to non-GABAergic profiles and from GABAergic to GABAergic profiles (Leitch and Laurent, 1996). In addition, some of these synapses are reciprocal.

With additional information about the size of the processes, Leitch and Laurent conclude that all combinations of LNs and PNs are connected. RNs synapse on to PNs and probably onto LNs, but it is not clear whether LNs synapse onto RNs. There are therefore two pathways from the RNs to PNs: a direct one and a multisynaptic one,

via one or more LNs. There is no quantitative information about the synapses of the glomeruli. All glomeruli have about equal numbers of axons (Ernst et al., 1977). In *Locusta migratoria* it is not clear that fibre bundles from the antennae can be assigned groups of glomeruli, as in the cockroach *Periplaneta americana* and ants and honeybees (Ernst et al., 1977).

7.2.1.5 Beyond the antennal lobe

The AGT runs from the AL to the LPL behind the β-lobe and the central body. In the protocerebral neuropil it joins with the tritocerebral bundles and the joint tract is called the tractus olfactorio globularis (TOG) and has about 1200 fibres. There are branches into calyces of corpora pedunculata.

7.2.2 Physiology

I will discuss what is known of the physiology of the RNs, PNs and LNs. The coding issues will be left to the next section.

7.2.2.1 Receptor neurons

Boeckh (1967) recorded the responses of RNs in the sensilla coeloconica of *Locusta Migratoria* to compounds present in plant odours and Kafka (1970) extended this work to around 370 compounds.

RNs fire spontaneously at 0.01–5 Hz with no odour stimulation. When stimulated with odour, they might: (a) not respond at all; (b) fire more frequently (excitation) (c) fire less frequently (inhibition). The excitatory response was a regular but adapting spike train (Kafka, 1970). Figure 7.4 shows excitatory and inhibitory RN spike trains.

The firing rate of excited neurons depends sigmoidally on the logarithm of the odour concentration (Boeckh, 1967; Kafka, 1970). The tuning curves (figure 7.5) are different for different odours in the same neurons and different for the same odour in different neurons. The differences in tuning curve sets could be described by shifts of the whole set of tuning curves between neurons and variance of the thresholds of the curves with respect to a mean for each odour (Kafka, 1970). Thus two different cells could have inverted sensitivity to two odours. Kafka also found an earlier onset of spiking for higher stimulus intensities, as well as frequency dependence.

Hansson et al. (1996) investigated responses of RNs extracellularly in the sensilla of the antennae of *S. gregaria* to pheremone components, other locust-produced odours, and food odours. The large number of action potentials in the trichoid and basiconic

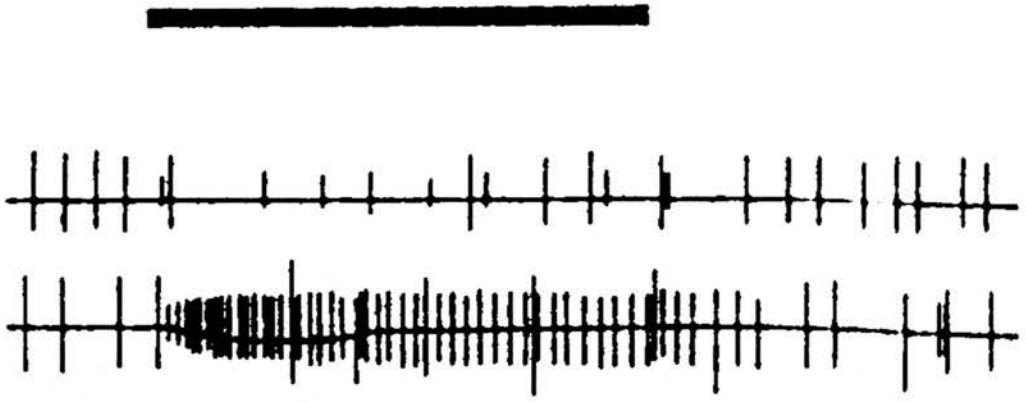

Figure 7.4: Response of two RNs to two odours (from Kafka, 1970). The thick bar indicates the duration of the odour presentations (600 ms). The near-horizontal lines in each trace are the "slow voltage" recorded from the cuticle of the sensilla coeloconica and represent the odour concentration. The large and small spikes on each trace belong to different neurons. Top trace (2-Hexanal): the "small" neuron is excited and the "large" neuron is inhibited. Bottom trace (butyric acid): the "small" neuron is excited more strongly than in the top trace and the "large" neuron is inhibited less strongly.

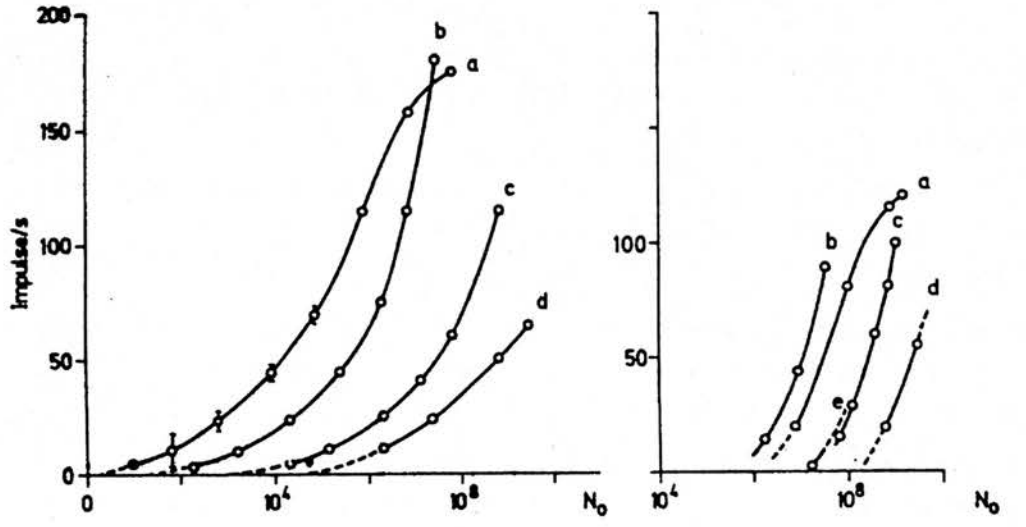

Figure 7.5: Tuning curves of two RNs from different sensilla coeloconica (from Kafka, 1970). Abscissa: estimate of number of molecules arriving at sensilla. Ordinate: average firing frequency during stimulation. *a.* trans-2-hexanal; *b.* trans-2-hexenoic acid; *c.* butyric acid; *d.* propenoic acid *e.* trans-2, trans-4-hexadiene acid.

sensilla prevented unambiguous identification of spiking neurons, so the activity of the whole sensillium was measured. Spontaneous rates ranged between 10–30 Hz, which equates to single unit rates of about 1–3 Hz. Eighty-seven out of 142 RNs responded to at least one of the 12 odours tested. Of the 78 of the 87 responses evaluated, 45 were to one or more components of the pheremone blend, 10 were tuned to the plant odour, and 11 were "generalist" responses. Some sensilla were more narrowly tuned than others. The firing rate of 11 sensilla responding to mixtures of pheremone components increased linearly with log of the concentration of the odours at smaller intensities, though sometimes decreased at higher intensities.

It was possible to deduce single-unit activity from recordings from the coeloconic sensilla. There was no response to any of the odours at the same concentrations as used to screen the basiconic and trichoid sensilla, but there were responses when the concentration was increased by a decade. The RNs were either excited by food odours, inhibited by pheremone components, or excited by food odours and inhibited by pheremone components.

It seems from this study that the coeloconic sensilla are specialised for sensing specific food odours at relatively high concentrations, whereas the trichoid and basiconic sensilla primarily signal pheremones and food odours at lower concentrations.

7.2.2.2 Projection neurons

PNs are spiking neurons. Apart from this, very little seems to be known about the precise physiology of the PNs. For example, I am aware of no current injection experiments performed on them. However, a good deal is known about their behaviour in the network (see section 7.2.3).

7.2.2.3 Local neurons

LNs produce graded-response "spikelets" (Laurent and Davidowitz, 1994) . When observing their influence on hyperpolarised PNs, it looks as though the effective rise time of the IPSPs they produce is about 15 ms.

7.2.3 Coding

As the experimental evidence suggests that, to a first approximation at least, the three components of the code outlined in section 7.1.3.4 can be treated separately, I will discuss the slow spatiotemporal activity, the fast oscillation and the transient synchronisation separately.

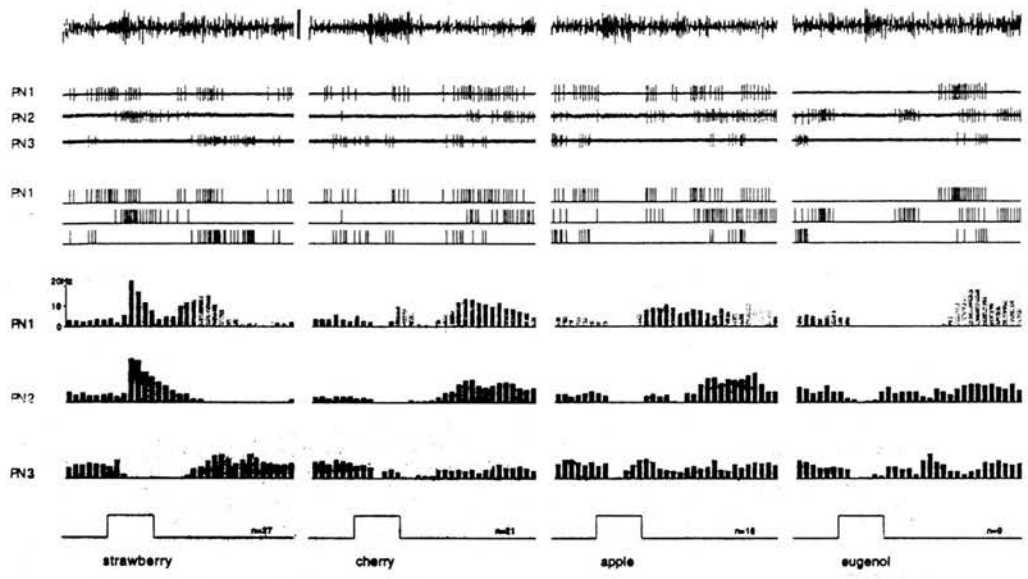

Figure 7.6: The temporal patterning of responses (from Laurent et al., 1996). Simultaneous intracellular recordings of three PNs and the LFP from the ipsilateral MB. Each column corresponds to presentation of a different odour. *Top trace*: LFP recordings from the ipsilateral MB . *Traces 2–4 (from top)*: raw recordings from each of the PNs. *Traces 5–7*: cleaned versions of the raw data. *Trace 8–10*: post-stimulus-time histograms created from n recordings (n given in bottom trace). *Trace 11:* odour pulse and its quality. Each odour pulse lasts 1 s.

7.2.3.1 Slow spatiotemporal activity

About 100 of the 830 PNs respond to any odour tested (over 2 log units of concentration) (Laurent, 1996). Responses by individual PNs to specific odours are reliable over repeated presentations on a timescale of about 10 ms. Responses by individual PNs to different odours are different, and involve periods of firing and/or inhibition (Anton and Hansson, 1996; Laurent et al., 1996). The response to blends of odours cannot be predicted from the response to single odours (Laurent and Davidowitz, 1994).

MacLeod and Laurent (1996) found that antagonising ionotropic GABA receptors with picrotoxin[1] does not destroy these slow spatiotemporal patterns, although the shorter time scale activity does change (see later). MacLeod and Laurent suggest that slow inhibitory mechanisms or temporal structuring of the response of olfactory receptors or a combination of both could be responsible for this. As there seems to be little temporal structuring of input from the RNs (Wehr and Laurent, 1999), the

[1]Picrotoxin also antagonises vertebrate $GABA_A$ receptors.

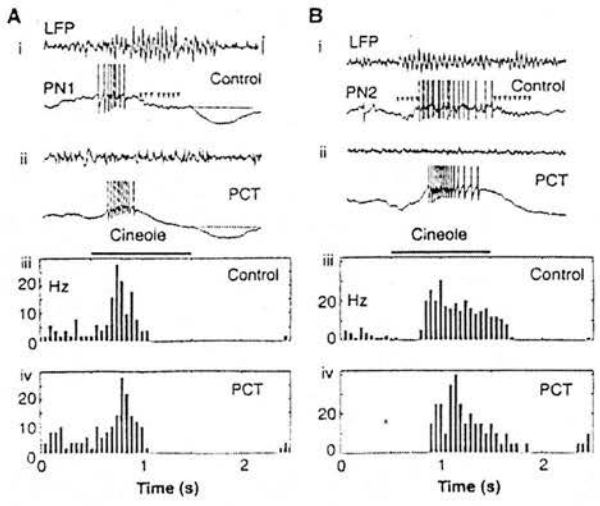

Figure 7.7: Picrotoxin abolishes fast oscillations but spares the slow spatiotemporal patterns of PN activity. The two columns show responses from different PNs to the same odour. *i.* The LFP from the MB and the recording from a single PN in the control case. *ii.* The same responses when picrotoxin was applied to the AL. *iii.* Post-stimulus time histograms in the control case. *iv.* Post-stimulus time histograms in the picrotoxin case. From MacLeod and Laurent (1996).

inhibitory mechanisms seem to be the best explanation for the slow spatiotemporal patterns. Candidate inhibitory mechanisms include histamine, metabotropic GABA receptors and nitric oxide.

7.2.3.2 Fast oscillations

Several pieces of evidence point towards LN and PN population oscillations.

Firstly, the membrane potential of PNs and LNs oscillate at about 20 Hz on presentation of odour (Laurent and Davidowitz, 1994). However, Anton and Hansson (1996) did not obtain the same result in *S. gregaria.* Anton and Hansson suggest that either the different types of stimuli presented (pheremones or complex food odours) or the presentation regime (single or repeated) could account for this. M. Stopfer (personal communication to Anton and Hansson, 1996) and G. Laurent (personal communication) state that membrane oscillations appear much more clearly after multiple presentations. This might account for the differences in the results. MacLeod and Laurent (1996) found that PNs lead LNs by about a quarter period ($96° \pm 53°$).

Secondly, auto-correlations of PN show oscillations at 20 Hz (Wehr and Laurent, 1996). Ablation of the MB calyx does not alter the oscillatory patterns in the AL

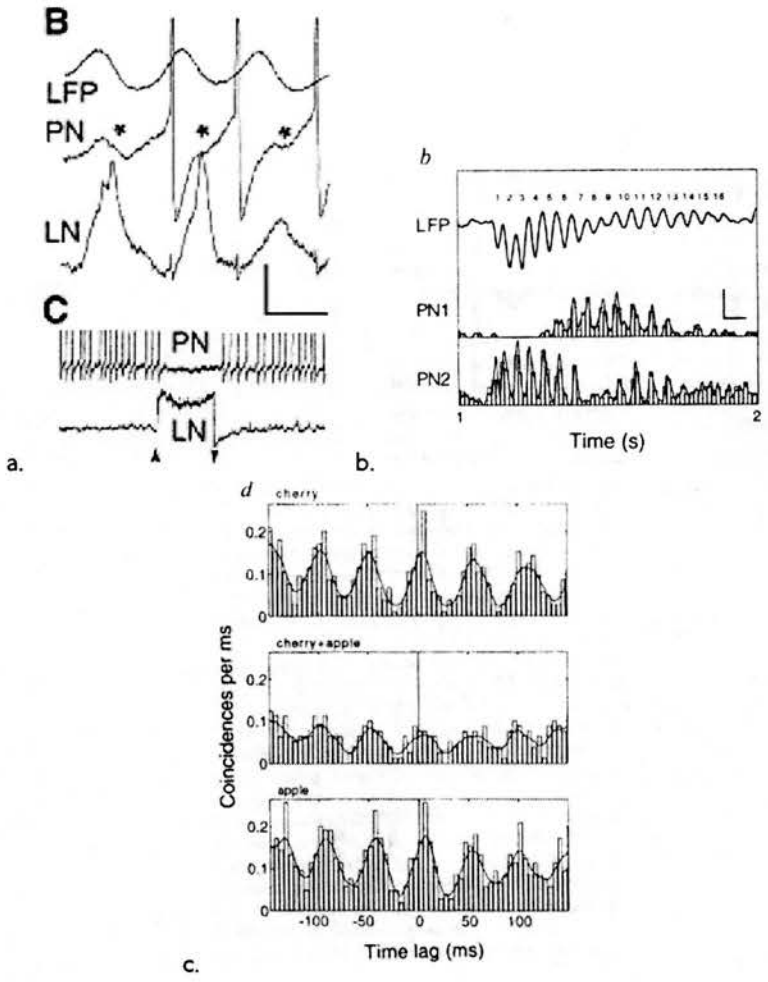

Figure 7.8: Evidence for oscillations. *a.* Simultaneous intracellular recording from a PN and an LN as well as the LFP from the MB during a response to cherry odour. The PN leads the LN by about one quarter of a cycle. From MacLeod and Laurent (1996). *b.* MB LFP and post-stimulus time histograms of activity of two PNs in response to an odour. From Wehr and Laurent (1996). *c.* Cross-correlation of neurons in *b.* showing that the neurons are synchronised with each other for a variety of odours. From Wehr and Laurent (1996).

neurons, indicating that the oscillations are endogenous to the AL (Laurent, 1996) and the inputs from the RNs are not oscillatory (Wehr and Laurent, 1999), so the oscillations are a result of AL connectivity.

In addition to the single unit recordings in the AL, the local field potential (LFP) of the MB often oscillates strongly at 20 Hz when an odour is puffed past the antennae. When pure air is presented there is a small peak at 20 Hz in the LFP power spectrum. The LFP of the AL does not oscillate, but this could be because the glomerular structure of the AL precludes measurement of the coordinated activity of groups of neurons extracellularly. There were some odours which did not cause the MB LFP to oscillate when they were first presented, even at high concentrations. Repeated presentations at (1.5–10 s intervals) did cause oscillations, fitting in with the results from single unit recordings.

Laurent and Davidowitz (1994) found that the LFP recorded from the MB is synchronised both with the PN membrane potential and the PN spikes and LN spikelets. The phase of the spikes does not vary between odours, indicating that it does not code for odour or intensity, as Hopfield (1995) has suggested. The PN spikes occur during the leading phase ($-70^\circ \pm 52^\circ$) of the MB LFP and the onsets of LN spikelets occur at the peak ($16^\circ \pm 26^\circ$) of the LFP.

Antagonising ionotropic GABA receptors with picrotoxin results in a loss of synchronisation as evidenced by the power spectrum of the MB LFP, the autocorrelation of PNs, and the cross-correlation of PNs and the MB LFP (MacLeod and Laurent, 1996).

7.2.3.3 Transient synchronisation of active neurons

Although there are oscillations in population activity, not all active PNs are synchronised with each other and the MB LFP all of the time. Figure 7.9 shows that PNs can be active and phase-locked to the MB LFP or active and not phase-locked. The pattern of phase-locking evolves with time and can be thought of as an additional part of the spatiotemporal code (Laurent et al., 1996).

Further evidence for transient synchronisation comes from cross-correlation analysis with a sliding time window (Laurent and Davidowitz, 1994). In this method a small time window (in this case 200 ms) is placed over two membrane potential (or LFP) traces at a particular point in time. Cross-correlation analysis is then performed on the two sections of trace, producing a 2D curve. The time window is then moved along a small amount (in this case about 20 ms) and the procedure is repeated. Finally all of the 2D cross-correlation plots are "stacked" to make a 3D plot which shows how the

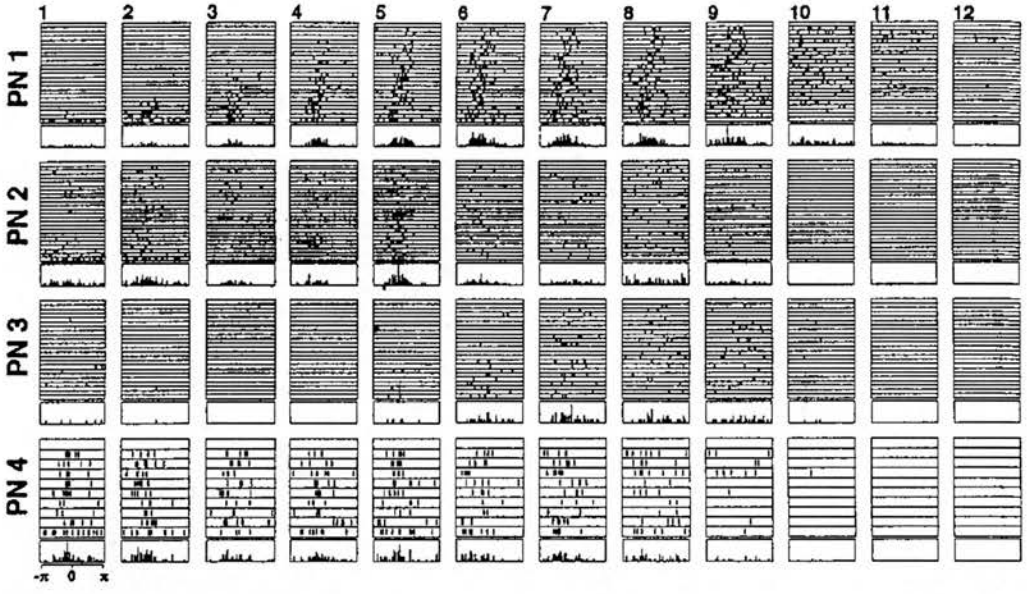

Figure 7.9: The time-course of the phase of PNs (from Laurent et al., 1996). Four different PNs (*PN 1–4*) were recorded from four different animals. For each neuron, each of the large boxes labelled *1–12* corresponds to one "epoch" (that is somewhere between 1/12 and 1/4 seconds) of firing in response to a one second odour pulse. Within each large box each of the upper boxes corresponds to one trial. A vertical line in these boxes corresponds to a PN spike and its horizontal positions reflect the phase of that spike with respect to the MB LFP. The bottom box of each large box contains a histogram with bin size $2\pi/36$ of the spikes in the boxes above.

synchronisation of the recordings changes over time.

Sliding time cross-correlations show distinct, reliable patterns between LN and the LFP recordings from different parts of the MB during an odour presentation (Laurent and Davidowitz, 1994). The same technique also shows transient correlations between the spike trains of PNs, though the cross-correlations must be averaged over several trials to show this structure.

Antagonising ionotropic GABA receptors with picrotoxin destroys the transient synchronisation of PNs with the MB LFP (MacLeod and Laurent, 1996).

7.2.3.4 The code?

Laurent et al. (1996) propose that the evidence can be summarised as a spatiotemporal code. In this code, neurons can be in one of three states: active and not synchronised with the network activity; active and synchronised; and not active. The membership of the groups of neurons in each of these states changes over time. Thus the code is a spatiotemporal one.

7.2.3.5 Behavioural relevance of the code

Stopfer et al. (1997) investigated the honeybee olfactory system to see what the behavioural significance of the synchronisation part of the code is. The reason for using honeybees was that it is easier to train them to do a behavioural task than locusts and their olfactory systems have similar coding properties. Odour puffs lead to a 0.5–1 s long 30 Hz oscillation of the LFP in the MB. AL neurons responded selectively to certain odours and their membrane potentials were phase locked to the LFP in the MB. As with the locust, applying picrotoxin to the whole brain abolished the oscillations, though the slower temporal pattern of projection neurons activity persisted.

Stopfer et al. trained honeybees to discriminate between different odours in a proboscis-extension conditioning task. In this task, control animals are conditioned to extend their proboscises by rewarding a target odour with nectar. The response generalised somewhat so that after conditioning odours similar in molecular structure to the rewarded one also caused proboscis extension, but the spectrum of odours that caused a response was quite narrow. In the test group of animals, picrotoxin was applied 10–45 minutes before conditioning. The discrimination was significantly worse than in the control case. The test honeybees could not distinguish between odours which were similar to the training odour, though still discriminable by the controls. Stopfer et al. concluded that the 20 Hz synchronisation helps to separate odours with

similar representations in the AL so that higher systems can learn from more distinct representations.

7.2.4 Learning properties of the network

As mentioned in section 7.1.4, oscillations appear to be a product of short term memory, with the number of spikes per cycle drops as an odour is presented repeatedly (Stopfer and Laurent, 1999). To start off with, PNs may fire more than one spike per cycle, though after training, the number of spikes is usually less than one per cycle. There has been no investigation of the longer-term synaptic plasticity of the locust AL, as there has in honeybees (Faber et al., 1999).

7.3 Why a model?

Models of biological neural networks are useful for a number of reasons. Firstly, they force us to make explicit the assumptions that can be implicit in verbal explanations and show whether explanations are possible. Secondly, we can study many more aspects of a model than we can of the corresponding real system. For example we can "record" from every neuron in a neural network. Finally, models may have surprising behaviour that might inspire new hypotheses.

Nevertheless, there is necessarily a gap between model and reality, and one should therefore justify why a formal model is better than the biological model, in this chapter the one provided by the locust AL itself. Another criteria for developing a theoretical model is that it is novel. None of the models presented in section 7.1.5 dealt with the spatiotemporal patterns or transient synchronisation present in the locust AL. I believe that the synchronisation of PNs with each other demands a model that uses spiking neurons rather than rate oscillators (Li and Hopfield, 1989) and models the EPSPs and IPSPs realistically (in contrast to current models of the invertebrate olfactory system (for example Linster et al., 1993; Linster and Masson, 1996). I hope in the section to show that a model incorporating more realistic spiking and membrane dynamics could be useful in answering a top-level question, that of the mechanism that underlies the slow spatiotemporal patterns and the fast oscillations.

We can approach this question from the bottom-up or from the top-down. In section 7.3.1 I approach from the top-down and explore possible hypotheses. I take the bottom-up approach in section 7.3.2. Both approaches have advantages and disadvantages. In section 7.3.3 I suggest a synthesis of both approaches as a way forward.

7.3.1 Top-down approach

If we take the top-down approach, we can choose to split the question up logically. If we are not careful, we end up writing a computer program that does exactly what our intuitions and the discussion section of papers say, and therefore does not tell us anything new.

That said, from the evidence presented so far, it looks as though the question can be split into three sub-questions:

1. What is the mechanism of the oscillations?
2. What is the mechanism of the slow temporal patterns?
3. What is the mechanism of the transient synchronisation?

Another reason for splitting the question in this way is that the oscillations are much faster than the slow patterns indicates that the timescales could be separated in an analysis. I suspect that the first two sub-questions need to be answered before the third can be answered.

7.3.1.1 The mechanism of the oscillations

From the experimental evidence, the mechanism of the oscillations appears to depend on relatively fast inhibitory GABA channels. It could be argued that we already understand the mechanisms of coupled groups of excitatory and inhibitory neurons through the Wilson-Cowan oscillator (see section 4.3.1). Therefore we might conclude that the mechanism is obvious and does not need modelling.

However, there are reasons, some of which will become apparent during the bottom-up modelling exercise, for modelling the oscillations. The Wilson-Cowan model does not tell us how to get oscillations of a certain frequency and phase difference between the groups. Furthermore, we are dealing with a relatively small number of spiking neurons.

While there are models and analysis of synchrony in systems of spiking with purely excitatory or inhibitory connections (see section 4.3.2), there does not seem to have been analysis of networks of spiking neurons with both inhibitory and excitatory connections.

7.3.1.2 The mechanism of the slow spatiotemporal patterns

Two possible explanations for the slow spatiotemporal patterns have been put forward already, namely slow, non-GABAergic inhibition and the connectivity structure between PNs.

Since antagonising the LNs seems to leave the spatiotemporal patterns the same with when the LNs are functioning normally, the LNs do not seem to be an important factor in determining the spatiotemporal patterns. That leaves the connectivity between PNs to do the work of producing the spatiotemporal patterns. However the activity of a network with purely excitatory connections is liable to run away. Therefore as yet undiscovered slow inhibitory connections could be used to regulate activity (Laurent and Naraghi, 1994).

There are at least two more possible contributory mechanisms to the slow patterns. Firstly, intrinsic adaption of the PNs could mean that PNs gradually fatigue and have to recover for a period of time. Secondly, synaptic depression (section 2.4.3; Tsodyks and Markram, 1997) would result in synapses fatiguing after being strongly activated.

A third mechanism might be synfire chains since they are offered as an explanation for the fact that activity does not run away in networks with fast excitation and slow inhibition (Abeles, 1991). Could synfire chains be an explanation for the slow temporal patterns?

At first sight, the sequences resemble synfire chains in that there is almost synchronous firing of groups of excitatory units. However, the system differs from synfire chains in two main respects. Firstly, groups that fire at neighbouring time steps overlap strongly, whereas in synfire chains, there is low overlap of neighbouring patterns. Indeed, excessive overlap leads to the breakdown of synfire propagation. The second difference is the timescale. In the locust AL, the time between stages of the synfire chain firing (about 50 ms) is much longer than the rising phase of EPSPs (about 10 ms). In synfire chains, the synchronisation is maintained because the neurons in one node are activated by the rising edge of EPSPs from the previous node. These reasons indicate that synfire chains are not a good description of the slow temporal patterns.

Could then a modified version of synfire chains provide the mechanism? Changing the threshold and refractory function so that neurons can fire multiple times when a node is reached (Gerstner et al., 1993b) would allow the network to produce sequences where the neurons fire more than once on each cycle with the same connectivity patterns. The two other mechanisms above might also contribute to spatiotemporal patterns with synfire-type connectivity.

7.3.2 Bottom-up approach

In the bottom-up approach, we can try to model the system as faithfully as possible making as few assumptions as possible. We then see whether the model responds

similarly to the real one. If not, we try out the next most plausible assumption, and iterate until the model is a perfect replication of the real system. Despite the fact that this method is potentially time-consuming, there is merit in the bottom-up approach. Models constructed using it may constitute a "null hypothesis", a standard model against which other models can be compared.

7.3.3 A synthesis

I shall start by taking a bottom-up approach. The next section will describe a "null hypothesis" model that is fairly well constrained by the anatomy and physiology, yet still has some unknown parameters. Besides being a benchmark model, this will provide the basis for testing the hypotheses mentioned in the previous section. There is still considerable freedom in parameters to explore to see if the possible mechanisms could work.

The model might make some predictions about the behaviour of the system, for example:

- how the representations of different odours are related to each other;
- how the network responds to different concentrations of odour; and
- what sort of learning mechanism could refine the oscillation coherence.

In fact, it will turn out that to fit the bottom-up model to the data, some top-down mathematical modelling comes in useful.

7.4 Model Description

In this section I start the work of building a bottom-up model in earnest. I start by coming up with a simplified way of representing different odours in section 7.4.1. In section 7.4.2 I tackle the anatomy of the model and in section 7.4.3 the physiology.

7.4.1 Odours

Different odours comprise different ratios of molecules. The work of Kafka (1970) shows that molecules can excite or inhibit RNs. Therefore, we would expect presentation of odours to cause a pattern of excitation and inhibition across the RNs. As figure 7.5 shows, the tuning curves to individual molecules are sigmoidal and different RNs can have inverted sensitivity to two different odours. Thus the direction of a firing vector may be quite different for the same odour at different concentrations.

In this modelling study it seems fair to bypass modelling odours directly and concentrate on the inputs to RNs. It also seems fair to ignore the problem of different concentrations and work with different odours at the same concentration. I will assume there is some significance in firing patterns that are similar. This is because we would expect that similar odours (at similar concentrations) produce similar patterns of activity across RNs.

To generate an input pattern to the RNs corresponding to an odour we can generate a random binary vector with 10% ones. To generate an odour uncorrelated with this one we can generate a vector by the same method. To make a correlated odour, we can flip 10% of the bits of the original vector. I model the onset and offset of an odour with a ramp of 50 ms, as do Linster et al. (1993).

7.4.2 Anatomy

The basic units of the model are N neurons, made up of N_{R} RNs, N_{P} PNs and N_{L} LNs. The neurons are connected together by weighted synapses in N_{G} glomeruli. In section 7.2.1 I reviewed the known connection statistics for the AL. In section 7.4.2.1 I will use this data to constrain a randomised connection structure. This does not however determine the weights, which I discuss in section 7.4.2.2. I finish discussing the anatomy by estimating the delays in section 7.4.2.3.

7.4.2.1 Connectivity

In order to describe how to fix the connection strengths, we need clear notation. I will label neurons with their class and a number within that class. Hence there are three series Ri, Pi and Li where i ranges over $1, \ldots, N_{\mathrm{R}}$, $1, \ldots, N_{\mathrm{P}}$ and $1, \ldots, N_{\mathrm{L}}$. To preserve some degree of generality I will use X and Y to refer to one of R, P or L.

The biological data allows for three types of randomness in the connections:

1. the innervation of neurons into glomeruli;
2. the connectivity between neurons projecting into a glomerulus; and
3. the strength of the connections in glomeruli.

I will discuss each in turn.

Innervation of glomeruli Experimental evidence from the locust (see section 7.2.1) constrains the first source of randomness by telling us roughly how many glomeruli each RN, PN and LN innervates. To model this, we first allocate each neuron Xi to a number

N_{R}	5000
N_{P}	830
N_{L}	300
$N_{\mathcal{G}}$	1000
$\min(N_{\mathcal{G}\mathrm{R}})$	1
$\max(N_{\mathcal{G}\mathrm{R}})$	3
$\min(N_{\mathcal{G}\mathrm{P}})$	10
$\max(N_{\mathcal{G}\mathrm{P}})$	20
$\min(N_{\mathcal{G}\mathrm{L}})$	200
$\max(N_{\mathcal{G}\mathrm{L}})$	300

Table 7.1: Anatomical parameters.

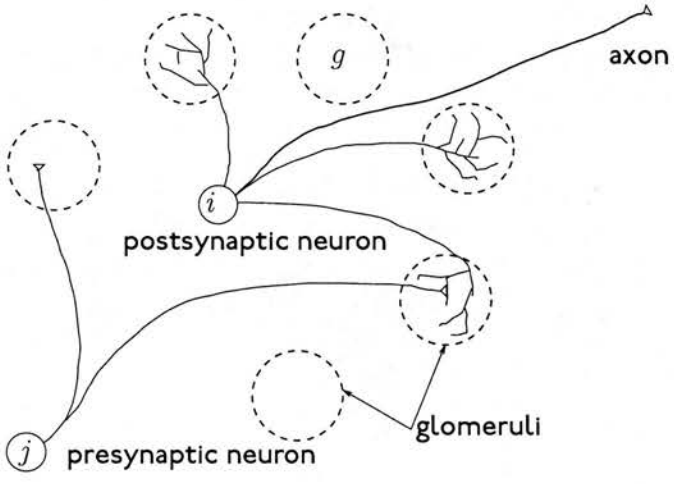

Figure 7.10: Connectivity of neurons via glomeruli.

$N_{\mathcal{G}X,Xi}$ of randomly-chosen glomeruli. We draw $N_{\mathcal{G}X,Xi}$ from a uniform distribution appropriate for that class of neuron. The numbers $\min(N_{\mathcal{G}X})$ and $\max(N_{\mathcal{G}X})$ specify the limits of the distribution and I shall denote its mean by $\langle N_{\mathcal{G}X,i} \rangle$. (Table 7.1 shows the default values for these and other anatomical parameters.)

It is useful to describe the allocation of a group of neurons to glomeruli by a matrix $\mathbf{G_X}$. In general, the matrix $\mathbf{G_X}$ defines the projection of XNs into glomeruli. Its elements are defined

$$G_{X,gXi} \begin{cases} = 1 & \text{with probability } \frac{N_{\mathcal{G}X,Xi}}{N_{\mathcal{G}}} \\ = 0 & \text{otherwise} \end{cases} . \tag{7.1}$$

If we assume that all neurons projecting into a glomerulus are fully connected, the binary expression

$$G_{X,gXi} G_{Y,gYj} \tag{7.2}$$

tells us whether neuron Xi synapses onto Yj via glomerulus g (see figure 7.10). Since we are assuming that all possible connections exist, it also tells us whether Yj synapses onto Xi, and that the neurons are therefore symmetrically connected. Summing over all the possible glomeruli, the total number of connections from Xi to Yj (and vice versa) is

$$\sum_{g=1}^{N_{\mathcal{G}}} G_{X,gXi} G_{Y,gYj} \ . \tag{7.3}$$

This expression shows that it is possible for a pair of neurons to have zero, one or more connections.

Within-glomerulus connectivity The second type of randomness, implies that the fact that two neurons innervate a common glomerulus does not mean that they synapse on one another. There is no quantitative data from the locust on the level of connectivity within glomeruli. However, we can estimate it by finding the density of connections in the glomeruli of another insect, making the assumption there is the same density in locust glomeruli, and then multiplying by the volume of the average locust glomerulus.

If we consider connections from LNs to LNs and PNs, from PNs to PNs and LNs and from RNs to LNs and PNs, then were there full connectivity, the expected number of connections in a glomerulus would be:

$$\begin{aligned}
&\left(N_{\mathrm{L}}\frac{\langle N_{\mathcal{G}\mathrm{L},i}\rangle}{N_{\mathcal{G}}} + N_{\mathrm{P}}\frac{\langle N_{\mathcal{G}\mathrm{P},i}\rangle}{N_{\mathcal{G}}}\right)^2 + N_{\mathrm{R}}\frac{\langle N_{\mathcal{G}\mathrm{R},i}\rangle}{N_{\mathcal{G}}}\left(N_{\mathrm{L}}\frac{\langle N_{\mathcal{G}\mathrm{L},i}\rangle}{N_{\mathcal{G}}} + N_{\mathrm{P}}\frac{\langle N_{\mathcal{G}\mathrm{P},i}\rangle}{N_{\mathcal{G}}}\right) \\
&= \left(300\frac{250}{1000} + 830\frac{15}{1000}\right)^2 + 50000\frac{2}{1000}\left(300\frac{250}{1000} + 830\frac{15}{1000}\right) \\
&= 7647 + 8745 = 16392 \ .
\end{aligned}$$

On the basis of morphological work by Gascuel and Masson (1991), Kerszberg and Masson (1995) estimate that there are 40000 synapses in a glomerulus in the AL of a worker honeybee. Given that the average volume of a bee glomerulus is about $15 \times 10^3\,\mu\mathrm{m}^3$ (Masson and Mustaparta, 1990), this gives a synaptic density of about $3\,\mu\mathrm{m}^{-3}$. If we assume that the synaptic density in the glomeruli of locusts is the same, there will be about 25000 synapses in the average locust glomerulus (given a diameter of $25\,\mu$m Ernst et al., 1977). Since this number is greater than the number of connections calculated above, it seems quite plausible that the neurons afferent on a glomerulus are fully connected.

Alternatively we could just assume that there is full connectivity of within the glomeruli. Certainly the connections within the glomerulus appear to be very dense

(Leitch and Laurent, 1996). I will therefore ignore random connectivity within glomeruli for now.

Random connection strength The final type of randomness is modelled by multiplying each element of the connectivity matrix by a random variable. Each element is then multiplied by a number $\hat{J}_{XiYj}$ chosen from a Gaussian distribution with mean $\langle \hat{J}_{XiYj} \rangle$ and a variance of 10%. (Section 7.4.2.2 deals with how to find $\langle \hat{J}_{XiYj} \rangle$.) The coupling of a Xi to Yj is now

$$G_{X,gXi} G_{Y,gYj} \hat{J}_{XiYj} \ . \tag{7.4}$$

Each connection between a pair of neurons via a different glomerulus can have a different delay. This means there can be up to $N_\mathcal{G}$ connections between each pair of neurons, depending on how many glomeruli they project into. To reduce the computational demands of the model I combine the connections to make one connection with one delay and a weight:

$$J_{XiYj} = \sum_{g=1}^{N_\mathcal{G}} G_{X,gXi} G_{Y,gYj} \hat{J}_{XiYj} \ . \tag{7.5}$$

7.4.2.2 Weights

For the "null hypothesis" model I decided to draw the weight for each connection from a Gaussian distribution with variance about 10% of the mean. Unfortunately there is not enough anatomical data to constrain the means for each type of connection (PNs to LNs, PNs to PNs and so on).

However, we do know that the PNs and LNs ought to fire alternately with a certain time period $T = 50\,\text{ms}$ and phase lag $\varphi = 0.25$. The mean weights for each type of connection will control whether PNs and LNs can fire alternately, and, if they can, the time period and phase that they will fire at for a given level of input.

It might be possible to indulge in some top-down modelling and use this information to constrain the weights. It turns out that with some mathematical analysis this is possible. Since the analysis is more generally applicable, I cover it in chapter 8 and leave setting the weights for now.

7.4.2.3 Delays

A rough calculation indicates that the axonal/dendritic delays should be small (order of 2 ms). In mammalian unmyelinated nerves the velocity of action potential conduction in metres per second is about two times the axonal width in micrometres (Kandel et al.,

1991). As the diameter of a PN neurite is around 1 μm (Leitch and Laurent, 1996), its conduction velocity is therefore about 2 ms^{-1}. Since the diameter of the AL is ~ 0.5 mm (Ernst et al., 1977), the approximate time of travel through a PN axon will be about 0.25 ms. The diameter of GABAergic neurites in the AL varies between 0.3 μm and 3 μm, so taking an average value gives a conduction velocity of about 4 ms^{-1} through the LN neurites, and a delay of about 0.125 ms. However passive conduction is slower, so these figures are underestimates. A factor of five slower would give a delay of 1.5 ms for PN to PN connections, about 1 ms for PN to LN connections and similar values for the other connections. Allowing for synaptic delays of the order of 0.5 ms (Kandel et al., 1991) and variability in path length, 2 ± 1 ms seems a reasonable estimate for all delays.

7.4.3 Physiology

This section describes how to translate the dynamics of the RNs, PNs and LNs into SRM neurons.

7.4.3.1 Receptor neurons

There are three main features of the RNs I believe are important to model. Firstly the firing frequency should depend roughly sigmoidally on the logarithm of the odour concentration and should have a maximum somewhere between 150 and 200 Hz (see figure 7.5). Secondly, there should be background firing rate in range 0–5 Hz, consistent with the evidence discussed earlier. Finally, some noise in the firing may help break down any accidental synchrony.

To model this, I use simple SRM neurons with the rectangular hyperbolic refractory function (2.22). Figure 7.11 shows the gain function of this type of neuron as a function of external input and for differing noise levels. We can take this input to be proportional to odour or molecule concentrations. Under this assumption, the curve produced by $\beta = 8$ with no adaptation ($F = 1$) seems a good qualitative fit to the experimental data (see figure 7.5).

To achieve the variable spontaneous firing rate we can set the threshold ϑ_{R} so that the spontaneous firing rate lies between 0 Hz and 5 Hz. The range 0.6–1 gives a suitable range of firing rates with no input. Table 7.2 summarises the parameters eventually settled on.

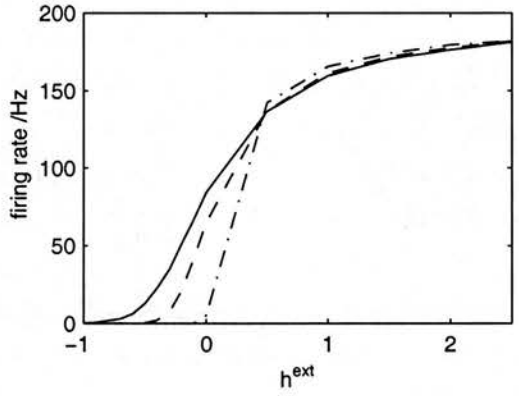

Figure 7.11: RN external input versus firing frequency for different noise levels and $\vartheta = 0$. Solid line: $\beta = 8$; dashed line: $\beta = 15$; dotted line: $\beta = 1000$. All other parameters as in table 7.2.

ϑ_R	0.6–1 mV	ϑ_P	3 mV	ϑ_L	3 mV
F_R	1	F_P	1	F_L	1
β_R	8	β_P	20	β_L	20
τ_R	10 ms	τ_P	10 ms	τ_L	15 ms
$\tau_{abs,R}$	5 ms				
η_R^0	1 mV				

Table 7.2: RN, PN and LN parameters.

7.4.3.2 Projection neurons

Inspired by the work of Kistler et al. (1997) in reducing the Hodgkin-Huxley equations to SRM neurons, I have attempted to model the PNs by fitting functions to their membrane potential traces, taken from the literature. Although I thought that it should be an easy matter to get the parameters from experimental traces of activity, it has turned out to be harder than I anticipated. The next few paragraphs describe my attempts to fix the parameters in this way.

The threshold ϑ_{P} is 3 mV as various traces from (Wehr and Laurent, 1999) and (Anton and Hansson, 1996) give values close to this value. The form of the PN EPSPs are difficult to find from the literature. However, figure 10a of Wehr and Laurent (1999) shows a trace which contains a likely candidate for a pure PN EPSP, unmixed with either an RN EPSP or an LN inhibitory postsynaptic potential (IPSP). The rise time of this EPSP is 10 ms, and it appears to be roughly the shape of an alpha function with time constant $\tau_{\mathrm{P}} = 10\,\mathrm{ms}$.

The refractory period of a PN looks to be 5 ms from Wehr and Laurent (1999) and the value of refractory function is $-7\,\mathrm{mV}$ at 5 ms after spiking (Anton and Hansson, 1996, figure 2). The time the refractory potential takes to get back to 0 mV is about 100 ms (Anton and Hansson, 1996, figure 2). The most straightforward way of modelling the refractory potential was to scan into a computer a suitably uncluttered trace (Wehr and Laurent, 1999, figure 11a, third panel) and fit a curve to it. The following equation seems to be a reasonable approximation:

$$\eta(t) = \begin{cases} 0 & t \leq 0 \\ -\exp(1.5 - t/12) & t > 0 \end{cases} . \tag{7.6}$$

Figure 7.12 shows the original trace and the approximation to it.

To add some noise to the firing patterns, the I set the parameter $\beta_{\mathrm{P}} = 20$.

7.4.3.3 Local neurons

The LNs are less straightforward than the PNs, as they do not spike with conventional, narrow action potentials. Rather, they produce so-called "graded action potentials" which can be initiated at several sites on the dendritic tree. There are several options for modelling the LNs:

- Model each LN as a single spiking neuron as do Rabinovich et al. (1998) with Hodgkin-Huxley neurons.

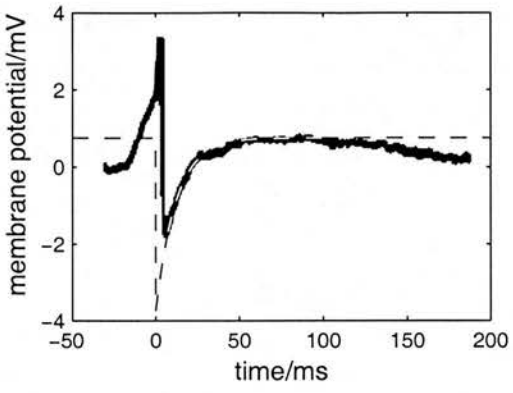

Figure 7.12: Part of the original trace from figure 11a, 3rd panel of Wehr and Laurent (1999) and the curve fitted to it.

- Model each LN as several conventionally spiking neurons. One could assume that there is one initiation site per glomerulus, in which case each LN would be modelled by about 250 SRM neurons.
- Model all of the LNs as a global inhibitor, claiming that their function is to regulate activity.

In the absence of any concrete information about exactly what the LNs are doing, I propose to take the first of the options above. Each LN can be modelled as an SRM neuron with the IPSP time constants and refractory functions inferred from experiment.

Laurent and Davidowitz (1994) show a recording of a PN membrane potential that suggests that the IPSP could be fitted by the alpha function with a time constant τ_{L} of about 15 ms. There appear to be no traces which indicate what form the refractory function might take; for want of better evidence I use the PN refractory function (7.6). I set the threshold to be 3 mV for the same reason. As with the PNs, $\beta = 20$.

7.5 Summary

One system in which both sequences and synchrony appear to play a role is the second stage of processing in the locust *Schistocerca's* olfactory system, the AL. The evidence found by Laurent and co-workers suggests that the temporal pattern of activation of the 830 excitatory PNs in the AL over a period of about 1 s encodes the identity of odours presented to the system. At the same time, the mass activity of the excitatory neurons and the 300 inhibitory LNs oscillates at 20 Hz, with the PNs leading by quarter

of a cycle. These oscillations seem to be functionally significant as when they are pharmacologically abolished honeybees find it harder to discriminate between similar odours. Although there are strong similarities between the olfactory system of the locust and other insects and vertebrates, the same types of spatiotemporal patterns do not appear to have been observed in other species.

A model of the AL could help explain the mechanism of the oscillations, the mechanism of the sequences and how the two interact. In this chapter I have constructed a network model of the AL. The SRM is used as the basic unit of the model as it is well suited to fitting the refractory properties of the neurons. The input is assumed to come from different groups of stochastically-firing RNs. The anatomy (in the form of connectivity) was chosen randomly within the known and estimated connectivity ratios. Unfortunately the mean magnitude of the weights cannot be constrained directly.

One unused constraint is the oscillation characteristics of the system. The next chapter will attempt to derive a constraint on the weights from the oscillation time period and the phase lead of the PNs over the LNs.

The major criticisms of the model built so far are that the LNs are not conventional spiking neurons and that it does not include the hypothesised slow inhibition. The counter to the second argument is that the model should be seen more as a "null hypothesis" to make sure that the observed temporal effects are not simply a product of a random structure.

Chapter 8

Synchronising oscillations in excitatory and inhibitory groups

As we have seen in chapter 4, the synchronisation properties of groups of spiking neurons connected by purely excitatory or purely inhibitory synapses have been extensively studied (for example Mirollo and Strogatz, 1990; van Vreeswijk et al., 1994; Smith et al., 1994). We have also seen that the Wilson-Cowan oscillator (Wilson and Cowan, 1972) has inspired a number of models of the dynamics of the mass activity of reciprocally connected groups of inhibitory and excitatory neurons. However, the dynamics of reciprocally connected groups of excitatory and inhibitory spiking neurons do not appear to have been studied, perhaps due to a lack of biological motivation.

As we saw in the previous chapter, the locust olfactory system provides the motivation for studying such a system. The main question it raised was how to set the mean weight for each type of connection in a network of excitatory and inhibitory neurons. A second question it raised is how the time period and phase of oscillation depend on the input strength to the system.

Thus the main problem is more general case of the problem addressed by the locking theorem of Gerstner et al. (1996a) introduced in chapter 4. There the problem was to find the conditions under which a *single* group of homogeneous neurons fire synchronously. Here the problem is to find the conditions under which *two* groups of homogeneous neurons fire regularly but with one group leading the other by a certain phase. The completely general case is for *multiple* groups of neurons where each group fires periodically and the different groups fire at different phases in the cycle.

In section 8.1, I give the mathematical form of the constraints for multiple groups and confirm that the locking theorem can be extended. In section 8.2, I present the implications of the constraints for the excitatory-inhibitory oscillator. In section 8.3, a network simulation with one set of parameters is consistent with most of the analytical

and numerical predictions but shows some differences, possibly due to the simulation method. Finally, in section 8.4, I discuss the conclusions and suggest some further work.

A version of this chapter is due to appear in the book originating from the "Emergent Neural Computational Architectures based on Neuroscience" workshop held in Edinburgh in September 1999 (Sterratt, 2001).

8.1 Constraints on stable synchronous oscillations

Suppose we have a network comprising N neurons organised into M groups defined by the connectivity, delays, thresholds, and PSP and refractory functions. I denote the set of neurons in the lth group by $\mathcal{G}_l$. The connectivity is such that the total presynaptic connection strength from each group is the same for all neurons in a group. We can express this mathematically by

$$\sum_{j \in \mathcal{G}_m} J_{ij} = \tilde{J}_{lm} \ , \tag{8.1}$$

where $\tilde{J}_{lm}$ denotes the total weight from the neurons of group m onto a neuron in group l. We further demand that the PSP functions and the weights are the same ($\varepsilon_{ij}(s) = \tilde{\varepsilon}_{lm}(s)$ and $\Delta_{ij} = \tilde{\Delta}_{lm}$) for all neurons $i \in \mathcal{G}_l$ and $j \in \mathcal{G}_m$. Finally, we require that the thresholds and refractory functions for neurons in a group be equal: $\vartheta_i = \tilde{\vartheta}_l$ and $\eta_i(s) = \tilde{\eta}_l(s)$ for $i \in \mathcal{G}_l$.

In a multi-group locked state the neurons of each group fire synchronously and periodically with a time period T. We assume that group l fires at $(k+\varphi_l)T$ for integer k where φ_l is a phase variable in the range [0,1). It is convenient to arrange the phases in ascending order and set $\varphi_1 = 0$ so that $0 = \varphi_1 < \varphi_2 < \ldots < \varphi_M$.

Now assume that the $l-1$th group has fired and that we are waiting for the lth group to fire (or that the Mth group has fired and we are waiting for the first group to fire). Although time is arbitrary, we will assume that we are in the first cycle after $t = 0$, that is that $\varphi_{l-1} < t < \varphi_l$ (or $\varphi_l < t < T$ if we are waiting for the first group). For any neuron $i \in \mathcal{G}_l$ the expected synaptic and refractory potentials are

$$h_i^{\text{syn}}(t) = \sum_{l=1}^{m-1} \tilde{J}_{lm} \sum_{k=0}^{1-F} \tilde{\varepsilon}_{lm}(t-(k+\varphi_m)T) + \sum_{l=m}^{M} \tilde{J}_{lm} \sum_{k=-1}^{-F} \tilde{\varepsilon}_{lm}(t-(k+\varphi_m)T) \tag{8.2}$$

and

$$h_i^{\text{ref}}(t) = \sum_{k=-1}^{-F} \tilde{\eta}_m(t-(k+\varphi_l)T) \ . \tag{8.3}$$

Group l should next fire when the membrane potential reaches the threshold $\tilde{\vartheta}_l$. If the threshold has been set correctly this will be at $t = \varphi_l T$, leading to the self-consistency or *threshold* condition:

$$\tilde{\vartheta}_l = h_i(\varphi_l T) \ . \tag{8.4}$$

A more precise requirement for the existence of coherent solutions is that for all $i \in \mathcal{G}_l$,

$$\varphi_l T = \inf(t > (\varphi_{l-1})T | h_i(t) = \tilde{\vartheta}_l) \ . \tag{8.5}$$

As $h_i(t)$ reaches $\tilde{\vartheta}_l$ from below, this implies that a necessary condition for stability is

$$\dot{h}_i(\varphi_l T) > 0 \ . \tag{8.6}$$

I refer to this as the *rising potential condition* (see also chapter 6).

Although these conditions show that synchronised solutions exist, they do not show that they are stable. In order to show this, we have to show that a small perturbation to the firing time of a neuron from the group firing in a cycle time will decrease in the next cycle. This linear perturbation analysis applied to a homogeneous network of neurons with standard dynamics yields the *locking theorem* (Gerstner et al., 1996b) mentioned in chapter 4. I will restate it here:

Theorem 8.1 *In a spatially homogeneous network of spiking neurons with standard dynamics, a necessary and, in the limit of a large number n of presynaptic neurons ($n \to \infty$), also sufficient condition for a coherent oscillation to be asymptotically stable is that firing occurs when the postsynaptic potential arising from all previous spikes is increasing in time.*

In a system with standard dynamics this is a stricter condition than the rising potential condition since the positive refractory derivative contributes to making the derivative of the membrane potential positive.

This result does not apply to more than one group of simultaneously firing neurons. However, it is straightforward to extend the proof to prove part of the the *infinite-limit extended locking theorem*:

Theorem 8.2 *In a network of spiking neurons with standard dynamics with M homogeneous groups of neurons such that all neurons in group l receive the same total postsynaptic weight from a large number of presynaptic neurons N_m in each group m a necessary and sufficient condition for constant phase, periodic, coherent oscillation to be asymptotically stable is that firing occurs when the postsynaptic potential arising from all previous spikes is increasing in time.*

Appendix A.2 contains the proof. The mathematical expression of the extended locking theorem is that

$$h_i^{\mathrm{syn}}(\varphi_l T) > 0 \quad \text{for } i \in \mathcal{G}_l \ . \tag{8.7}$$

8.2 Applying the constraints to excitatory and inhibitory groups

It is now a straightforward task to apply the extended locking theorem to one excitatory and one inhibitory group of neurons, a system that approximates the AL.

To abstract away from the locust AL, I will refer to the excitatory group as E and the inhibitory one as I. Later it will be convenient to work with positive weights, so I refer to the group connection weights which should be called $\tilde{J}_{\mathrm{EE}}$, $\tilde{J}_{\mathrm{EI}}$ and so on as $J_{\mathrm{EE}}, -J_{\mathrm{EI}}, J_{\mathrm{IE}}$ and $-J_{\mathrm{II}}$. (I drop the tildes from here on as there is no further need to refer to the weights between individual neurons.) I take the delays to be uniformly Δ. I assume that PSP functions do not depend on the postsynaptic neurons and denote the EPSP function by $\varepsilon_{\mathrm{E}}(t)$ and the IPSP function by $\varepsilon_{\mathrm{I}}(t)$. I will assume that they are zero until $t = \Delta$, rise monotonically to a maximum at time $t = \tau_{\mathrm{E}}$ or $t = \tau_{\mathrm{I}}$ and then fall monotonically back to zero. The refractory functions, denoted $\eta_{\mathrm{E}}(t)$ and $\eta_{\mathrm{I}}(t)$, both have positive derivatives so the network has standard dynamics.

To simplify the analysis I will assume that neurons only remember their last firing times, that is $F = 1$. This is reasonable if the membrane potential due to a second spike is much smaller than the membrane potential due to the first, which is true when the time period is long compared to the PSP time constant. In any case, it is straightforward to generalise to longer spike memories. I will also assume that the refractory function complies with the formal version of the threshold condition (8.5). This means the absolute refractory period is less than the desired period T and that it prevents multiple firing during a cycle.

Since with the standard dynamics the stability condition is stronger than the rising potential condition, we can ignore the rising potential condition. Of the two remaining conditions, the stability condition is the more fundamental, since it constrains only the weights, whereas the threshold condition also constrains the input levels. I therefore explore the consequences of the stability condition first, in section 8.2.1, before moving onto the consequences of the threshold condition in section 8.2.2.

8.2.1 Consequences of the stability constraint

In the alternating state, network activity oscillates with a time period of T and the excitatory group leads the inhibitory group by φT, where φ is a phase variable with the range [0,1). Applying the stability constraint (8.7) yields

$$J_{\mathrm{EE}}\dot{\varepsilon}_{\mathrm{E}}(T) - J_{\mathrm{EI}}\dot{\varepsilon}_{\mathrm{I}}\left((1-\varphi)T\right) > 0 \tag{8.8}$$

for the excitatory group and

$$J_{\mathrm{IE}}\dot{\varepsilon}_{\mathrm{E}}(\varphi T) - J_{\mathrm{II}}\dot{\varepsilon}_{\mathrm{I}}(T) > 0 \ . \tag{8.9}$$

for the inhibitory group.

The consequence of these inequalities is that there are combinations of time periods and phase for which there can be no stable firing, regardless of the size of the weights. This is because either inequality is not satisfied when the excitatory derivative is less than or equal to zero and the inhibitory derivative is greater than or equal to zero. For the condition on the excitatory group (8.8) this happens when $T < \Delta$ or $T \geq \tau_E + \Delta$ and $0 \leq (1-\varphi)T \leq \tau_{\mathrm{I}} + \Delta$. The condition on the inhibitory group (8.9) is violated when $T \leq \tau_{\mathrm{I}} + \Delta$ and $\varphi T \geq \tau_{\mathrm{E}} + \Delta$ or $\varphi T < \Delta$. As it is enough for one group to become unstable to plunge the whole system into instability, the forbidden combinations of T and φ are given by the union of the regions defined by the above inequalities. They can be displayed in a plot of φ versus T (referred to as T-φ space from now on) as in figure 8.1.

The second consequence of the inequalities (8.8) and (8.9) is that for those combinations of T and φ for which activity is not inherently unstable, stability depends on appropriate weights. Thus for any possible pair of T and φ there will be a region of the four-dimensional weight space that allows stable firing. We can make a major simplification by noting that the inequalities concern the *ratios* $\hat{J}_{\mathrm{EE}} := J_{\mathrm{EE}}/J_{\mathrm{EI}}$ and $\hat{J}_{\mathrm{IE}} := J_{\mathrm{IE}}/J_{\mathrm{II}}$ and finding the regions of a two-dimensional weight-ratio space that allow stable firing. Since the weights are by definition positive, the weight ratios are always greater than or equal to zero.

The stability condition (8.8) imposes different constraints on T, φ and the weight ratio $\hat{J}_{\mathrm{EE}}$ depending on the sign of $\dot{\varepsilon}_{\mathrm{E}}(T)$, and hence on the size of T compared to Δ and $\tau_{\mathrm{E}} + \Delta$.

1. For $T < \Delta$ or $T = \tau_E + \Delta$, $\dot{\varepsilon}_{\mathrm{E}}(T) = 0$ and from (8.8) we can deduce that

$$\dot{\varepsilon}_{\mathrm{I}}((1-\varphi)T) = 0 \ , \tag{8.10}$$

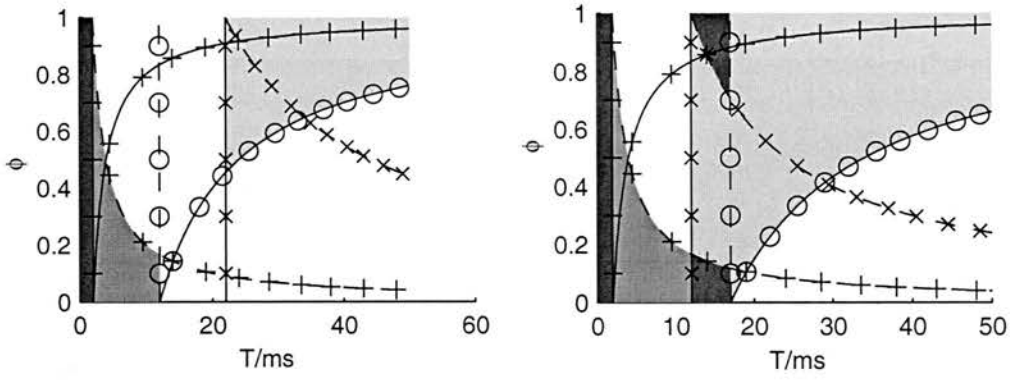

Figure 8.1: Forbidden regions of the T-φ plane for two sets of parameters. The light regions are unstable due to the excitatory group becoming unstable, medium-grey areas unstable due to the inhibitory group and the darkest areas unstable due to both groups. Dashed lines pertain to the excitatory group, dotted lines to the inhibitory group and dash-dotted lines to both. Plus signs indicate where condition (8.10) and its inhibitory counterpart become true. Crosses indicate zeros in the denominators and circles zeros in the numerators of equations (8.11) and (8.12) and their inhibitory counterparts. Left: $\Delta = 2\,\text{ms}$, $\tau_\text{E} = 20\,\text{ms}$ and $\tau_\text{I} = 10\,\text{ms}$. Right: $\Delta = 2\,\text{ms}$, $\tau_\text{E} = 10\,\text{ms}$ and $\tau_\text{I} = 15\,\text{ms}$ (estimated locust parameters).

so that stability condition is not satisfied. This is the region $T < \Delta$ where both conditions are violated (see figure 8.1).

2. If $\Delta < T < \tau_\text{E} + \Delta$, $\dot{\varepsilon}_\text{E}(T) > 0$ and

$$\hat{J}_\text{EE} > \frac{\dot{\varepsilon}_\text{I}((1-\varphi)T)}{\dot{\varepsilon}_\text{E}(T)} \quad . \tag{8.11}$$

When $\dot{\varepsilon}_\text{I}((1-\varphi)T) \leq 0$ (for $(1-\varphi)T \leq 0$ or $T \geq \tau_\text{I} + \Delta$) this equation is satisfied for any weight ratio $\hat{J}_\text{EE}$ (and thus any weights J_EE and J_EI) since weight ratios are always positive.

3. When $T > \tau_\text{E} + \Delta$, $\dot{\varepsilon}_\text{E}(T) < 0$ and equation (8.11) does not hold, since we have to reverse the sign of the inequality when rearranging (8.8). Instead,

$$\hat{J}_\text{EE} < \frac{\dot{\varepsilon}_\text{I}((1-\varphi)T)}{\dot{\varepsilon}_\text{E}(T)} \quad . \tag{8.12}$$

When $\varepsilon_\text{I} \geq 0$ (for $0 < (1-\varphi)T \leq \tau_\text{I} + \Delta$) the inequality cannot be satisfied for positive weight ratios. This corresponds to the forbidden region where $T > \tau_\text{E} + \Delta$.

We can derive similar inequalities for the inhibitory group from (8.9).

The third consequence of the inequalities (8.8) and (8.9) complements the second. Any pair of weight ratios limits the stable combinations of T and φ even more than the inherent stability. This follows from setting $\hat{J}_{\mathrm{EE}}$ in the inequalities (8.10), (8.11) and (8.12) and solving for T and φ. By contrast to the inherently unstable areas, the solution does depend on the exact form of the PSP functions; we cannot simply consider the signs of the PSP gradients.

With alpha function PSPs (defined in section 2.4.3) there appears to be no analytical solution to the inequalities (8.10), (8.11) and (8.12) and their inhibitory counterparts. We must solve both sets of inequalities numerically to find the regions each allow. The intersection of these regions is the allowable region. Figure 8.2 shows contour plots of the right hand sides of both sets of inequalities as a function of T and φ. Solving the inequalities is equivalent to slicing these functions at different heights and looking at the regions above or below the cut, depending on the sign of the denominator of the inequality. Thus the contours in figure 8.2 show the potential boundaries of regions of instability.

Figure 8.3 shows the regions of stability and instability for a particular pair of weight ratios. We can see how boundaries follow some of the contours shown in figure 8.2.

8.2.2 Consequences of the threshold constraint

The threshold condition (8.4) means that

$$\vartheta_{\mathrm{E}} = J_{\mathrm{EE}}\varepsilon_{\mathrm{E}}(T) - J_{\mathrm{EI}}\varepsilon_{\mathrm{I}}((1-\varphi)T) + \eta_{\mathrm{E}}(T) + h_{\mathrm{E}}^{\mathrm{ext}} \tag{8.13}$$

holds for the excitatory group and that

$$\vartheta_{\mathrm{I}} = J_{\mathrm{IE}}\varepsilon_{\mathrm{E}}(\varphi T) - J_{\mathrm{II}}\varepsilon_{\mathrm{I}}(T) + \eta_{\mathrm{I}}(T) + h_{\mathrm{I}}^{\mathrm{ext}} \tag{8.14}$$

holds for the inhibitory group.

These equations tell us directly how much activation is required to sustain activity in a stable region of T-φ space. Figure 8.4 shows the mapping of a grid in T-φ space into $h_{\mathrm{E}}^{\mathrm{ext}}$-$h_{\mathrm{I}}^{\mathrm{ext}}$ space for two sets of parameters. There are a few points to notice here.

1. As the excitatory or inhibitory external potential is increased, the time period decreases. It seems intuitive that more excitatory input should speed up the oscillations, but not that more inhibitory input should. The reason is this happens is that more excitatory input makes the inhibitory neurons fire earlier, which in turn release the excitatory neurons from their inhibition earlier.

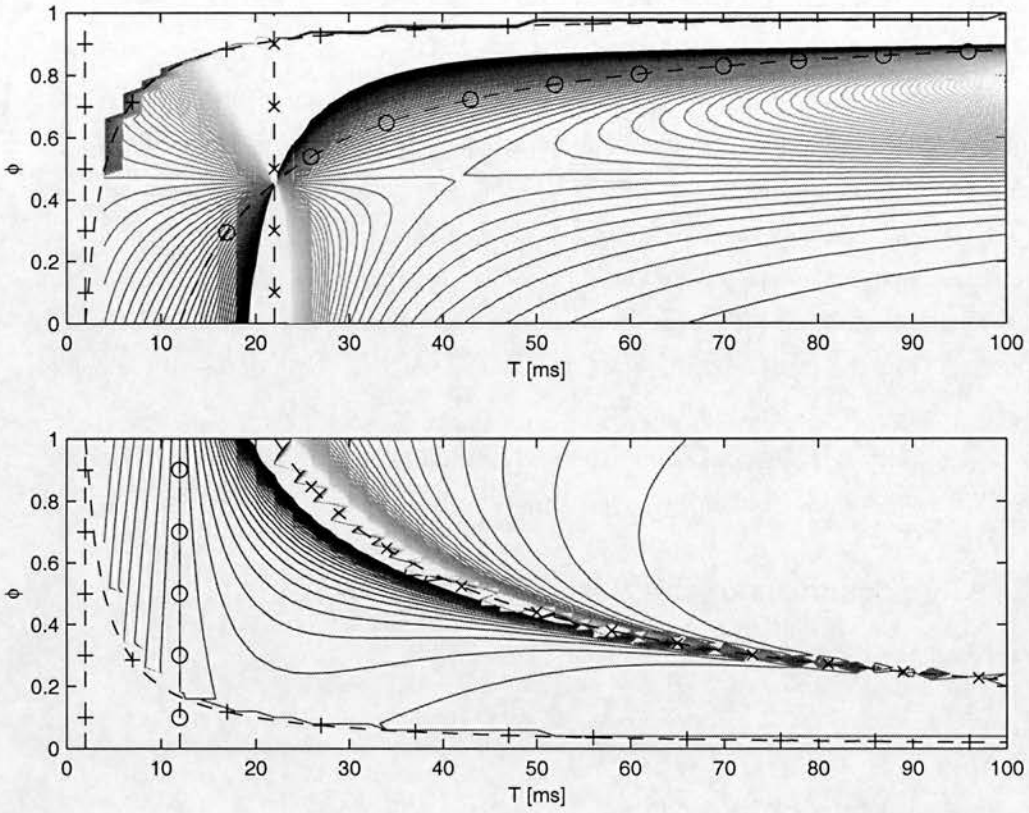

Figure 8.2: The right hand sides of the inequalities derived from the instability condition. The top panel shows a contour plot of the function defined by the right hand side of (8.10), (8.11) and (8.12) and the bottom panel shows the same plot for the inhibitory versions of (8.10), (8.11) and (8.12). Lighter contours indicate higher values and darker ones indicate lower ones. Dashed lines marked by crosses indicates asymptotes caused by the denominator going to zero. Dashed lines marked by circles indicate where the functions are zero. Dashed lines marked by plus signs indicate the boundaries of where the function is undefined because the argument of the denominator is negative.

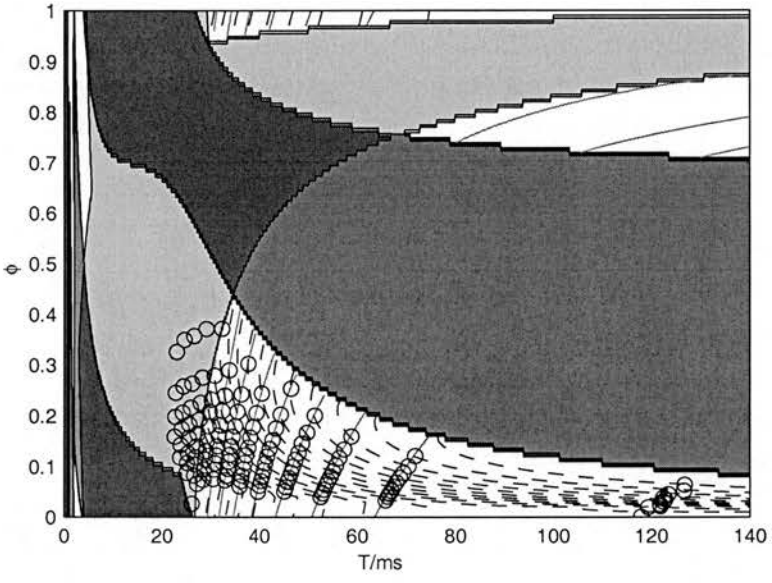

Figure 8.3: Unstable regions of T-φ space and mapping from $h_{\mathrm{E}}^{\mathrm{ext}}$-$h_{\mathrm{I}}^{\mathrm{ext}}$ space onto T-φ space for a pair of weight ratios. The shaded regions are unstable, with the shade representing the groups whose stability conditions are violated: the light region corresponds to the excitatory group, the intermediate region to the inhibitory group, and the darkest region to both groups. The unshaded regions with lines plotted in them are stable given the correct input. The lines represent the levels of external excitation required to produce the values of T and φ. Lighter shaded lines correspond to higher values. The solid lines represent constant $h_{\mathrm{E}}^{\mathrm{ext}}$ and the dashed lines represent constant $h_{\mathrm{I}}^{\mathrm{ext}}$. The circles represent simulation values obtained by setting the input levels to those of the lines. They agree well with the theoretical results, although they appear in the theoretically unstable area too. Parameters: τ_{E} =10 ms, τ_{I} =15 ms, Δ = 2 ms, $J_{\mathrm{EE}} = 0.5$, $J_{\mathrm{EI}} = 0.5$, $J_{\mathrm{IE}} = 1$, $J_{\mathrm{II}} = 1$ and $F = 3$. Refractory function given by (7.6).

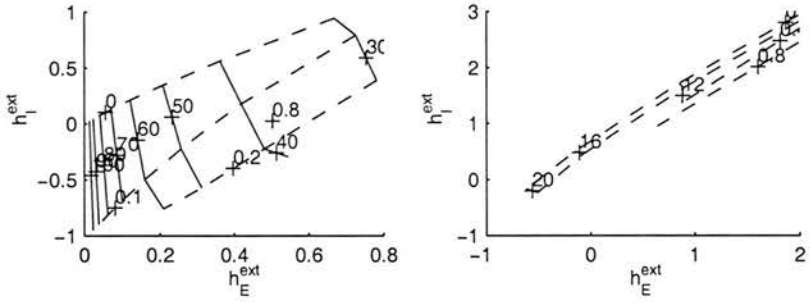

Figure 8.4: The mapping from T-φ space into $h_{\mathrm{E}}^{\mathrm{ext}}$-$h_{\mathrm{I}}^{\mathrm{ext}}$ space for two sets of parameters. Solid lines correspond to constant T and dashed lines to constant φ; numbers between 0 and 1 label some of the constant-T lines with the phase and multiples of 10 label some of the constant-φ lines. Left: τ_{E} =10 ms, τ_{I} =15 ms, Δ = 2 ms, $J_{\mathrm{EE}} = 0.5$, $J_{\mathrm{EI}} = 0.5$, $J_{\mathrm{IE}} = 1$, $J_{\mathrm{II}} = 1$, $F = 3$. Right: τ_{E} =20 ms, τ_{I} =10 ms, Δ = 3 ms, $J_{\mathrm{EE}} = 1$, $J_{\mathrm{EI}} = 0.5$, $J_{\mathrm{IE}} = 1$, $J_{\mathrm{II}} = 0.5$, $F = 3$.

2. More input to the excitatory neurons means they increase their lead over the inhibitory neurons. We would expect more excitatory input to make the excitatory neurons fire earlier, but without doing calculations we would not know whether it brings forward the inhibitory neurons' firing by more or less. By contrast, more input to the inhibitory neurons reduces the excitatory neurons' lead.

3. The input to both groups can be above or below threshold. It is somewhat surprising that the excitatory group can have below-threshold input as it requires above-threshold external input to start firing. However, once it is firing the self-excitation is sufficient to keep it firing and the external input can be reduced. So below-threshold input to the excitatory group is a hysteresis state.

To find the amount of external input required to obtain a particular time period and phase we must solve (8.13) and (8.14) numerically. The lines in figure 8.3 show a grid in $h_{\mathrm{E}}^{\mathrm{ext}}$-$h_{\mathrm{I}}^{\mathrm{ext}}$ space mapped into allowed regions of T-φ space. We can see that changes to either $h_{\mathrm{E}}^{\mathrm{ext}}$ or $h_{\mathrm{I}}^{\mathrm{ext}}$ change both T and φ.

8.3 Simulations

To test whether the analysis is correct, I simulated a network with 100 excitatory and 100 inhibitory neurons and the parameters in the caption of figure 8.3 for varying values of external input. I analysed the results to find whether there was stable firing, and if so, the time period and phase of oscillations. In order to make sure that the network did

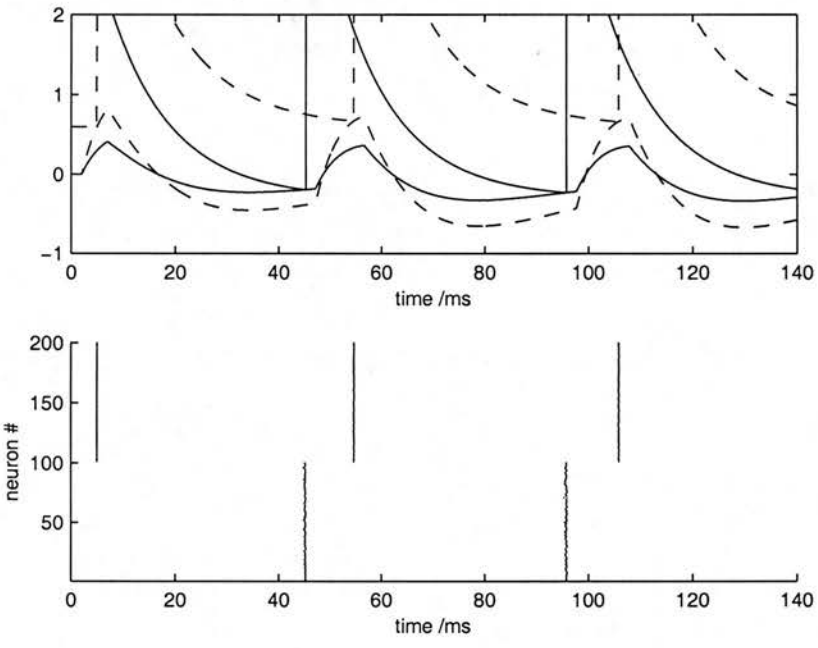

Figure 8.5: *Upper axes:* An example of the synaptic potentials (lower traces) and effective threshold $\vartheta - h^{\mathrm{ext}}(t) - h^{\mathrm{ref}}(t)$ (upper traces) of neurons in the excitatory (solid line) and inhibitory (dashed line) groups. Each neuron fires when its membrane potential crosses the effective threshold. *Lower axes:* The corresponding spike raster for excitatory neurons (numbers 1–100) and inhibitory neurons (numbers 101–200). The parameters are: $\tau_{\mathrm{E}} = 10\,\mathrm{ms}$, $\tau_{\mathrm{I}} = 15\,\mathrm{ms}$, $\Delta = 2\,\mathrm{ms}$, $J_{\mathrm{EE}} = 0.5$, $J_{\mathrm{EI}} = 0.5$, $J_{\mathrm{IE}} = 1$, $J_{\mathrm{II}} = 1$, $F = 3$, $\beta = 20$, $\vartheta = 0$, $h_{\mathrm{E}}^{\mathrm{ext}} = 0.3$ and $h_{\mathrm{I}}^{\mathrm{ext}} = -0.6$. The resulting time period and phase are $T = 51.3\,\mathrm{ms}$ and $\varphi = 0.200$. For the meaning of the parameters see section 8.2.

not stay in a stable state by chance, I added some noise to the firing times by making the firing probabilistic (Gerstner and van Hemmen, 1992). The simulation results are shown in figure 8.3, along with the theoretical results.

In the allowed regions they fit well with the theoretical predictions. However, the network appears to fire stably even when it should not according to the theory. It is not clear why this happens, though it is possible that the noise may stabilise the network in these areas.

Figure 8.5 shows an example of the time course of the excitatory and inhibitory synaptic potentials and the effective threshold, that is $\vartheta - h^{\text{ext}} - h^{\text{ref}}(t)$. Although both groups fire as their membrane potentials rise, as demanded by the stability condition, when the excitatory group fires it does so on the falling phase of both PSPs that contribute to it. To see this, note that at the time the excitatory group fires both spikes contributing to its membrane potential have been released longer ago than the their rise times, that is $(1-\varphi)T - \Delta > \tau_{\text{I}}$ and $T - \Delta > \tau_{\text{E}}$. Similarly, the inhibitory group in figure 8.5 is firing on the falling phase of the EPSP and IPSP since $\varphi T - \Delta > \tau_{\text{E}}$ and $T - \Delta > \tau_{\text{I}}$.

8.4 Discussion

This chapter started with a problem set by modelling the first stage of olfactory processing in the locust, the AL. This modelling work raised the problem of choosing weights in a network of excitatory and inhibitory spiking neurons that produce the right time period and phase of oscillation. In order to do this I had to extend the locking theorem (Gerstner et al., 1996b) slightly. By applying the extended locking theorem to a network comprising excitatory and inhibitory homogeneous groups I showed:

- that the excitatory and inhibitory neurons can only fire synchronously and alternately for certain time periods and phases of oscillation;
- how to find weights that produce a certain, allowed, time period and phase of oscillation;
- that oscillations are possible for below-threshold input to inhibitory neurons and, when the network is in a hysteresis state, for below-threshold input to excitatory neurons; and
- how the time period and phase depend on the input and vice versa.

Simulations confirm most of these results, but, puzzlingly, seem to be stable when the theory predicts they should not. This may be due to the symmetry-breaking noise included in the simulations.

I am not aware of the problem of the time period and phase of networks of spiking excitatory and inhibitory spiking neurons having been posed or analysed before. Although there is a sizeable literature on the dynamics of networks of spiking neurons, none of them appear to deal with networks comprising excitatory and inhibitory neurons (Mirollo and Strogatz, 1990; van Vreeswijk et al., 1994). While there has been much work on excitatory and inhibitory oscillators based on the population model of Wilson and Cowan (1972), this does not relate to spiking neurons, which allow different dynamics to continuous-valued population models (Gerstner, 2000). By contrast, my extension to the locking theorem is trivial — indeed it has been hinted at (Gerstner et al., 1996b). Nevertheless, I believe that it has been a worthwhile accomplishment to have put it on a firmer footing.

Perhaps the most surprising result is the forbidden values of time period and phase, independent of the values of the weights. These regions possibly act to limit the time periods at which neural systems can work, and so are perhaps responsible for the time periods observed in the locust. The results also indicate that it should be rather difficult for the locust to maintain the experimentally-observed constant oscillation time period, even if the excitatory and inhibitory inputs are proportional to each other. This implies that either the input is relatively constant or that the oscillation time period does actually change in the locust, perhaps as a function of odour concentration. It may be possible that there are parameter regimes that do give the desired characteristics, however. It may also be possible that a more complex neuron model with active channels is required to achieve a fairly constant oscillation time period.

In deriving the results I have assumed that the refractory potential is strong enough to prevent PNs firing before they are inhibited. If this is not true, firing may not be "correct" as neurons may fire more than once on each cycle. Another, more limiting assumption is that of the homogeneity of the groups, a condition unlikely to be found in the nervous system. Less homogeneous groups will introduce differences in the firing times of units of a group, thus making the locking less precise. However, an extension of the one-group locking theorem to noisy neurons suggests that moderate amounts of noise still allow reasonably precise, stable locking and there are arguments as to why noisy neurons might be equivalent to inhomogeneous connections (Gerstner, 2000).

Several questions remain. In particular the effect of noise and inhomogeneity on the locking is not well understood. There may be ways of setting parameters to make large stable regions or to minimise the dependence of the time period on the inputs. The behaviour as the external inputs are increased in proportion to each other is relevant to the locust and should be studied.

In conclusion, this simple model of excitatory and inhibitory spiking neurons is a useful tool in predicting and understanding the activity of real neural systems without going to complex simulations. It may have application beyond the locust in some of the many excitatory-inhibitory subnetworks of nervous systems that show oscillatory activity.

8.5 Summary

The locking theorem of Gerstner et al. (1996b) states that a necessary and sufficient condition for the synchronous, periodic firing of infinitely-large groups of homogeneously connected neurons is that the total synaptic input of every neuron is rising at the time that it fires. A generalised version of this problem is that of synchronising groups of neurons that are connected homogeneously within themselves but heterogeneously between each other. I have extended the locking theorem slightly to cover the general case, showing that the necessary and sufficient condition on each neuron is exactly the same as in the single-group version.

The problem of the previous chapter is the two group version of the general locking problem. From the extended locking theorem I have shown analytically that for a general form of PSP function the excitatory and inhibitory neuronal populations cannot fire alternately at certain time periods and phases, regardless of the size of the weights.

The equations derived from the locking theorem also allow us to find weights that produce an allowed time period and phase of oscillation. A particular set of weights will restrict the possible time periods and phases of oscillations; the restricted areas can be found numerically. Numerical methods also allow us to predict the time period and phase as a function of external input and vice versa.

I have shown that oscillations are possible with below-threshold input to the inhibitory neurons and that oscillations are also possible with below-threshold input to the excitatory neuron, but only if network is in a hysteresis state. A network simulation with one set of parameters shows is consistent with the analytical and numerical predictions.

Chapter 9

Synchronising *Schistocerca*

In this chapter I describe how to apply the theory developed in chapter 8 to the null hypothesis model developed in chapter 7 and present simulation results from the resulting model.

The theoretical results from the preceding chapter are given in terms of the total weight from all members of one group of neurons onto a neuron in another group. Therefore these values have to be scaled according to the average number of connections from neurons of one group onto a neuron of another. Section 9.1 describes how to do this.

In section 9.2 I carried out simulations where the PNs and LNs are stimulated directly rather than by the RNs. This is to assess the effects of the random connectivity matrix on the model. It seems that the effect is to alter the locked oscillations discovered in the previous chapter.

In section 9.3 the results are discussed and suggestions for further work are made.

The simulations described in this chapter represent a small proportion of the number that I have carried out. Many of these simulations were carried out with older versions of the model, which I now believe to be less parsimonious than the one presented in chapter 7. However, some of these models did appear to fit the oscillation data better than the current one.

9.1 Setting the weights

To derive the average weight per connection, we must take into account the fact that one neuron may synapse onto another via more than one glomerulus. To be precise, we would expect neurons Xi and Yj to be connected by

$$\frac{N_{\mathcal{G},Xi}}{N_{\mathcal{G}}} \cdot \frac{N_{\mathcal{G},Yj}}{N_{\mathcal{G}}} \cdot N_{\mathcal{G}} \tag{9.1}$$

synapses on average. Therefore we must normalise the total weight from one type of neuron onto another not only by the number of presynaptic neurons, but also by this value. For example,

$$\langle J_{\mathrm{P}i,\mathrm{R}j} \rangle = \frac{\tilde{J}_{\mathrm{PR}}}{N_{\mathrm{R}}} \cdot \frac{N_{\mathcal{G}}}{N_{\mathcal{G},Xi} N_{\mathcal{G},Yj}} \quad . \tag{9.2}$$

9.2 Simulations with the randomised connectivity matrix

A necessary condition for the full model to produce oscillations is for a cut-down version of the model comprising only the PNs and LNs connected by the random connectivity matrix to produce oscillations of the appropriate time period and frequency when fed with the correct external input. Input from the RNs will induce fluctuations in the inputs. I have run a number of simulations using values of the weights and external inputs that should support oscillations at a time period of $T = 50\,\mathrm{ms}$ and a phase of $\varphi = 0.25$. However, I have not yet found a point in weight space that produces the desired firing patterns. This section presents some of the simulation results in order to give an insight into why the model is not working as expected.

The first set of weights are those from the previous chapter, $\tilde{J}_{\mathrm{PP}} = 0.5$, $\tilde{J}_{\mathrm{PL}} = 1$, $\tilde{J}_{\mathrm{LP}} = 0.5$ and $\tilde{J}_{\mathrm{LL}} = 1$. With external inputs $h_{\mathrm{P}}^{\mathrm{ext}} - \vartheta_{\mathrm{P}} = 0.4$ and $h_{\mathrm{L}}^{\mathrm{ext}} - \vartheta_{\mathrm{L}} = -0.5$ the network with these (uniform) weight values should produce the correct behaviour. In all the simulations presented in this chapter, $F = 3$.

Using the randomised connectivity matrix generated as described in chapter 7 and from these mean weights generated as described in section 9.1 did not lead to the desired firing patterns. Figure 9.1 shows the spike raster of a selection of PNs and LNs. We can see that the PNs fire twice on each cycle before causing the LNs to spike, rather than causing the LNs to spike directly. The reason for this behaviour should be evident from representative PN and LN traces (figure 9.2) The problem is the PNs do not excite the LNs quite enough the first time they fire in a cycle, presumably because the EPSPs are not as synchronous as in the case with uniform connectivity studied in chapter 8 and therefore do not summate as effectively.

Another simulation where the desired time period and phase is pushed further into the stable area of $T - \varphi$ space shows similar results. The only change in the parameters were the weights: $\tilde{J}_{\mathrm{PP}} = 0.5$, $\tilde{J}_{\mathrm{PL}} = 0.5$, $\tilde{J}_{\mathrm{LP}} = 0.5$, $\tilde{J}_{\mathrm{LL}} = 2$. The external inputs were $h_{\mathrm{P}}^{\mathrm{ext}} - \vartheta_{\mathrm{P}} = 0.35$ and $h_{\mathrm{L}}^{\mathrm{ext}} - \vartheta_{\mathrm{L}} = 0.40$. Figure 9.4 shows the resulting spike raster. The results are less like the desired results than the first set of parameters, with the

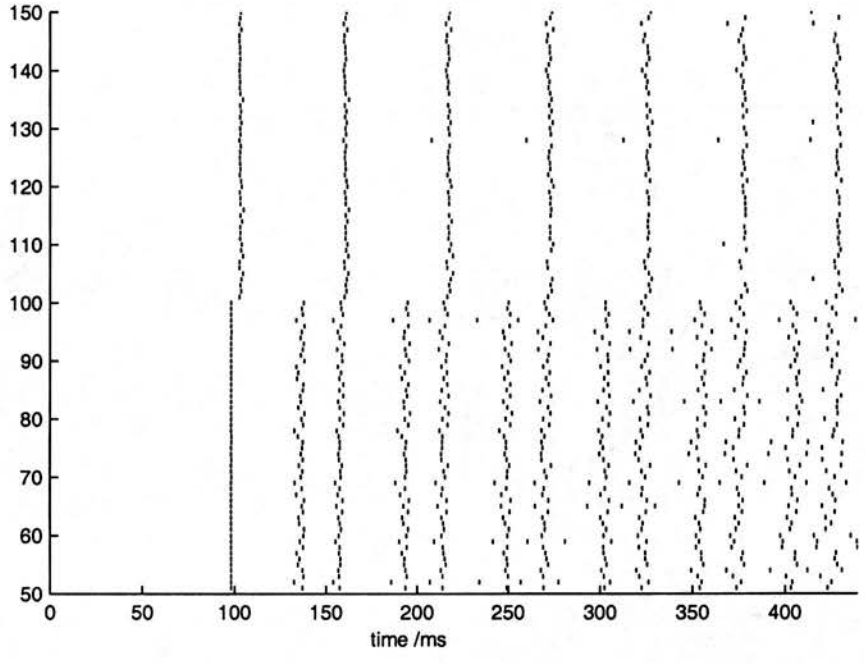

Figure 9.1: Spike raster of network activity. Neurons 50–100 are PNs and neurons 101–150 are LNs. Parameters: $\tau_{\mathrm{P}} = 10\,\mathrm{ms}$, $\tau_{\mathrm{L}} = 15\,\mathrm{ms}$, $\Delta = 2\,\mathrm{ms}$, $\tilde{J}_{\mathrm{PP}} = 0.5$, $\tilde{J}_{\mathrm{PL}} = 0.5$, $\tilde{J}_{\mathrm{LP}} = 1$, $\tilde{J}_{\mathrm{LL}} = 1$, $F = 3$, $\beta = 20$, $\vartheta = 0$, $h_{\mathrm{P}}^{\mathrm{ext}} = 0.3 + \vartheta_{\mathrm{P}}$ and $h_{\mathrm{L}}^{\mathrm{ext}} = -0.6 + \vartheta_{\mathrm{L}}$.

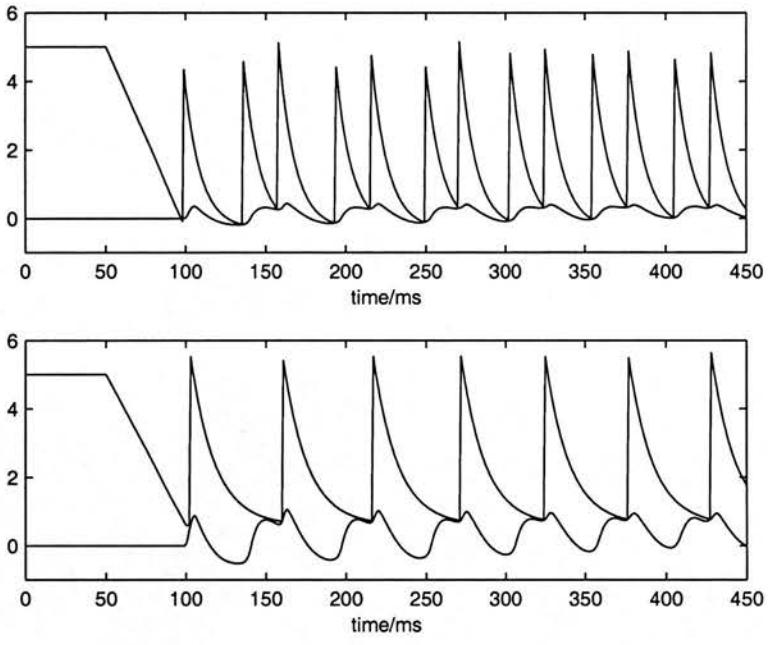

Figure 9.2: *Upper axes:* Synaptic potential (lower trace) and effective threshold (upper trace) from a PN. *Lower axes:* The same quantities for an LN in the same simulation. Parameters as in figure 9.1.

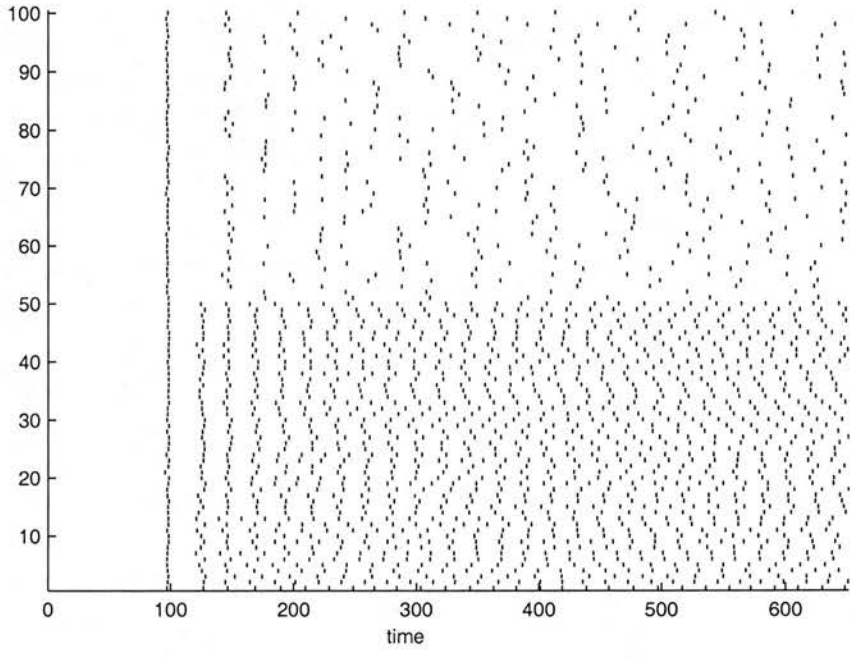

Figure 9.3: Spike raster of activity. Parameters: $\tilde{J}_{\mathrm{PP}} = 0.5$, $\tilde{J}_{\mathrm{PL}} = 0.5$, $\tilde{J}_{\mathrm{LP}} = 0.5$, $\tilde{J}_{\mathrm{LL}} = 2$. $h_{\mathrm{P}} = 0.35 + \vartheta_{\mathrm{P}}$ and $h_{\mathrm{L}} = 0.4 + \vartheta_{\mathrm{L}}$. Otherwise parameters are the same as the first simulation.

network degenerating into a fairly asynchronous state rather quickly. Figure 9.4 shows the membrane potentials obtained in the network. The theoretical trace (figure 9.5) shows that the weight values ought to work in a network with no weight variance. Again, the problem seems to be that the membrane potential to the LNs from the PNs is too variable.

This indicates weights from LNs onto PNs are rather variable. Figure 9.6 shows histograms of the different weight strengths. It does appear that the weights from LNs onto PNs are particularly variable.

Consideration of the inequalities in the previous chapter indicated that $\hat{J}_{\mathrm{PP}}$ should be small in the region of desired time period and phase and that $\hat{J}_{\mathrm{LP}}$ could be very small, since its value was immaterial in the desired region. If these ratios are small, the weights from the inhibitory neurons will be much stronger than the weights from the excitatory neurons. This should mean that the system will not be as sensitive to the firing times of the excitatory neurons as before. It will also mean that the synaptic potential is usually far below the effective threshold, apart from near firing times. This will prevent spurious firing due to the noise in the neurons causing them to fire because

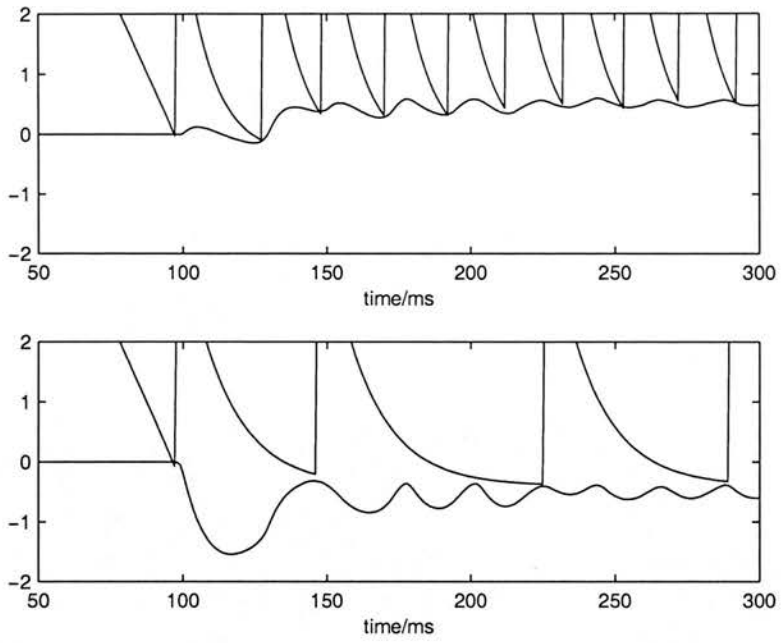

Figure 9.4: Effective thresholds and synaptic potentials for the second set of parameters. The top plot shows a typical PN and the lower plot shows a typical LN.

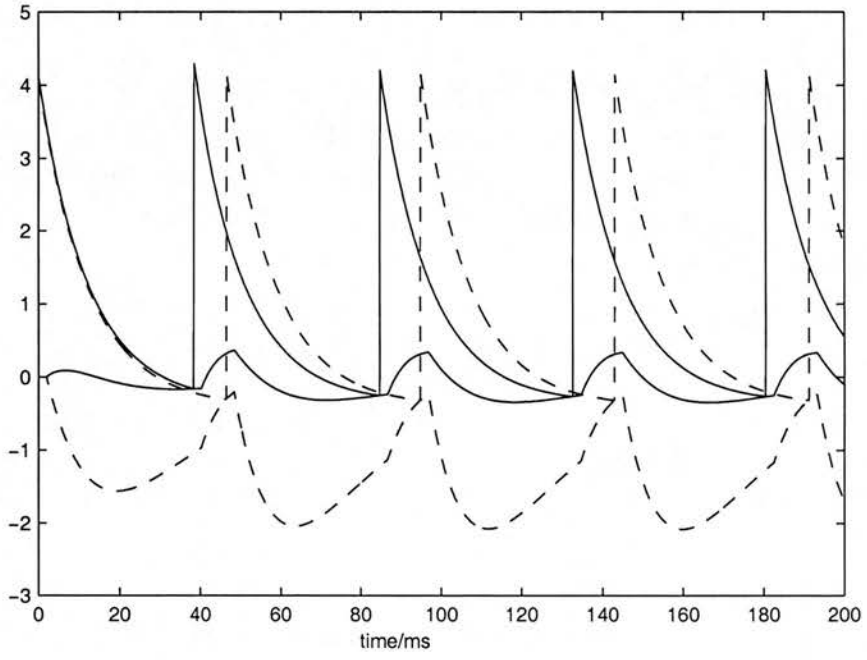

Figure 9.5: Predicted effective thresholds and synaptic potentials for the second set of parameters.

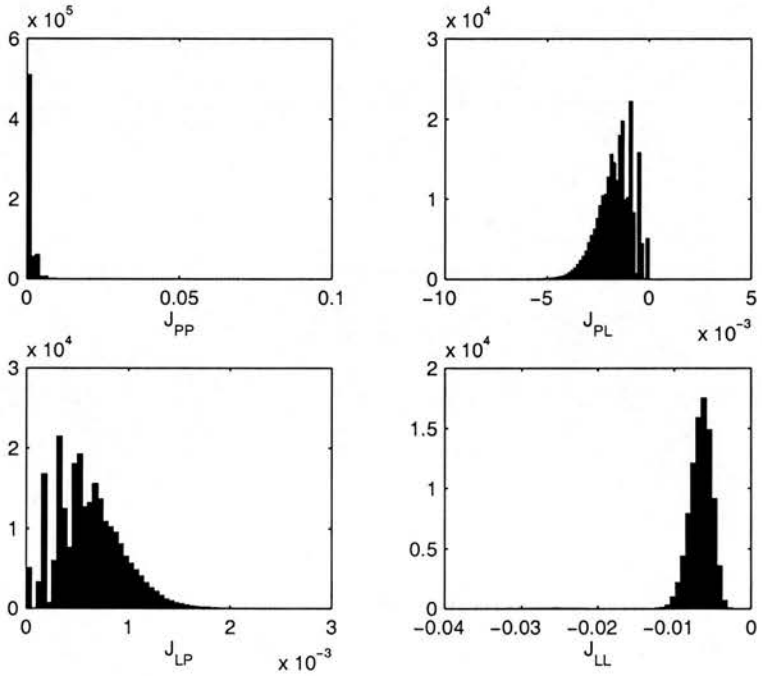

Figure 9.6: The connection statistics for the second set of parameters. Each histogram describes the distribution of the weights indicated by the label on the abscissa.

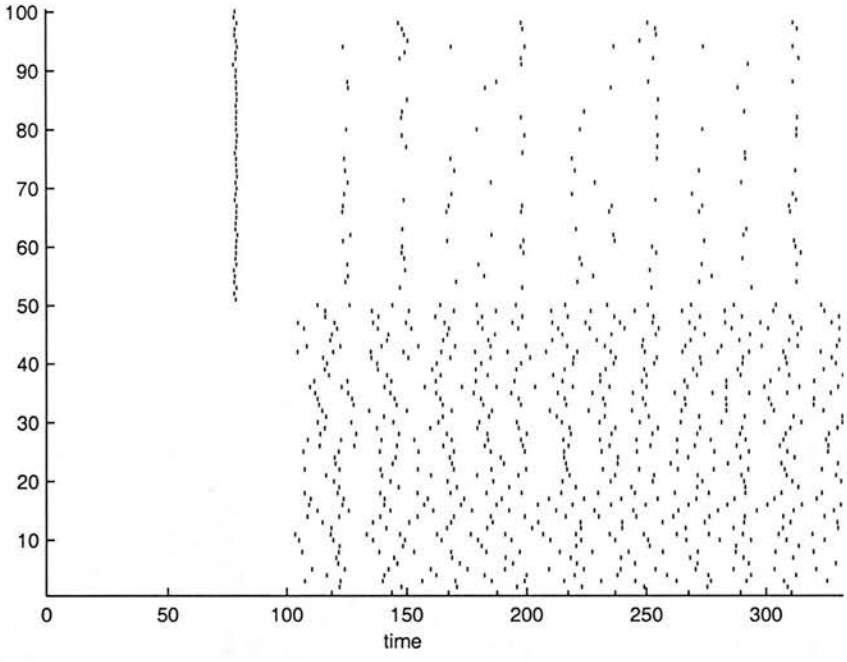

Figure 9.7: Spike raster of activity. Parameters: $\tilde{J}_{\mathrm{PP}} = 0.1$, $\tilde{J}_{\mathrm{PL}} = 10$, $\tilde{J}_{\mathrm{LP}} = 0.1$, $\tilde{J}_{\mathrm{LL}} = 5$. $h_{\mathrm{P}} = 3.0 + \vartheta_{\mathrm{P}}$ and $h_{\mathrm{L}} = 4.0 + \vartheta_{\mathrm{L}}$. Otherwise parameters are the same as the first simulation.

they are near the threshold for long periods of time. I therefore decided to try a simulation with $\tilde{J}_{\mathrm{PP}} = 0.1$, $\tilde{J}_{\mathrm{PL}} = 10$, $\tilde{J}_{\mathrm{LP}} = 0.1$ and $\tilde{J}_{\mathrm{LL}} = 5$.

Figure 9.7 shows the resulting spike raster and figure 9.8 shows representative synaptic potentials and the effective threshold. Again, the simulations did not compare well with the results predicted by the theory. There does however seem to be periodic activity among the LNs, though not in the PNs. Again, the problem seems to be that the LNs fail to fire, probably due to the weight variance. The theoretical firing membrane potential and effective threshold (figure 9.9) show that LN firing ought to occur on a fairly steeply rising part of the membrane potential and should therefore be stable.

Perhaps it could be that the noise in the firing is too large. In chapter 4 we saw that noise levels could make the difference between asynchrony and synchrony in a network. However, repeating the last experiment with $\beta_{\mathrm{P}} = \beta_{\mathrm{L}} = 1000$ produced similar results.

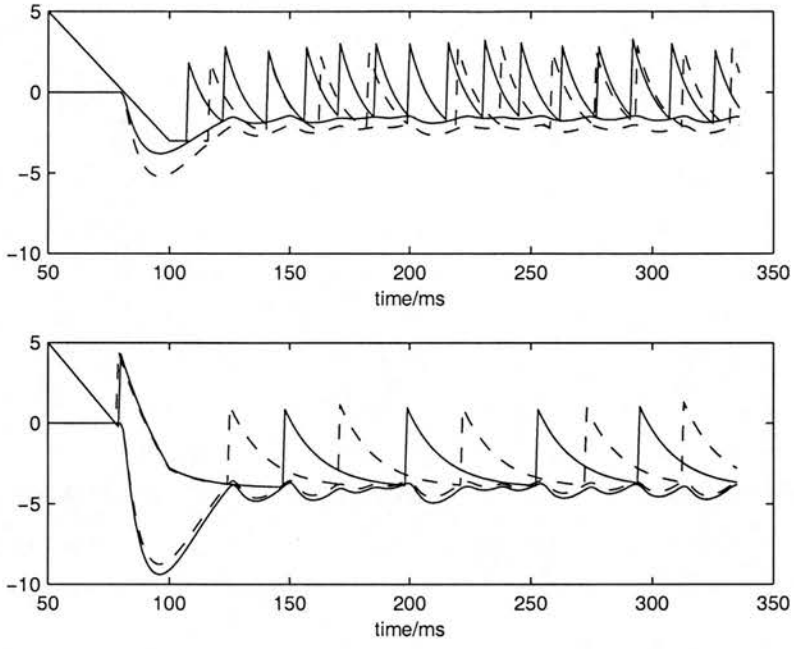

Figure 9.8: Effective thresholds and synaptic potentials for the third set of parameters. The top plot shows two PNs and the lower plot shows two LNs.

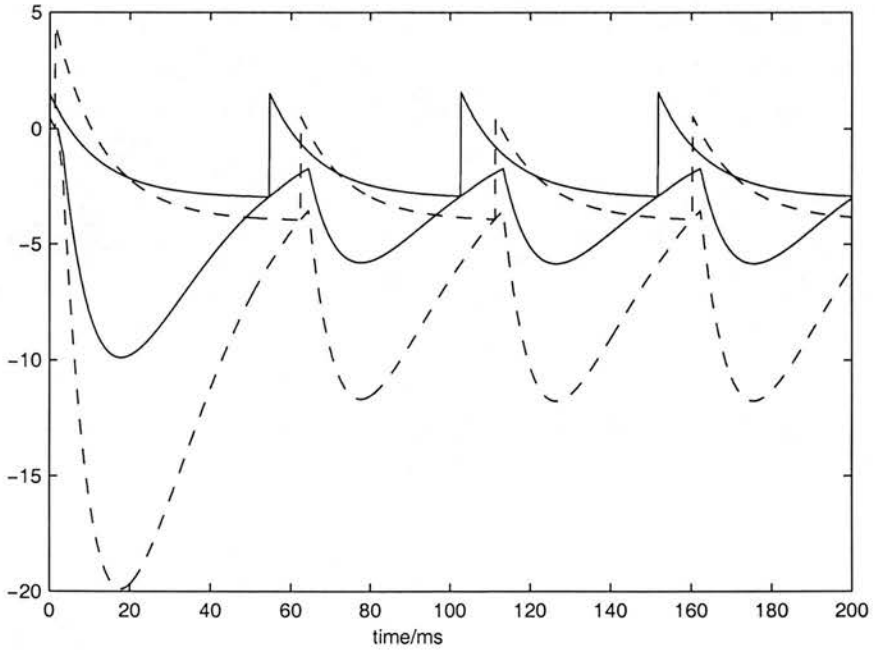

Figure 9.9: Predicted effective thresholds and synaptic potentials for the third set of parameters.

9.3 Discussion

From the simulations from various parts of parameter space presented here, it seems that the work of the last chapter in fixing the weights has not succeeded in producing a model that can reproduce the basic oscillation results. Nor has the model spontaneously produced spatiotemporal patterns, which indicates that other mechanisms besides fast inhibition and excitation coupled by a random weight matrix are at work.

There are a number of possible reasons for the failure to produce patterns and some possible ways forward. In section 9.3.1 I consider whether the results could be due to a failing in the model. I consider the possibility that I was trying to simulate the wrong data in section 9.3.2. If the model is a reasonably realistic approximation to reality a more extensive exploration of the parameter space might locate suitable weights. I consider method of doing this in section 9.3.3. It may be that other mechanisms need to be built into the model; I discuss these in section 9.3.4.

9.3.1 The antennal lobe model

It is possible that the model of the antennal lobe does not correspond well enough to reality. In this section I will discuss elements of the model in turn.

I am fairly confident that the connectivity structure and delays in the model are realistic. This is because the anatomical data is relatively unambiguous. However, it could be that the assumption of random connectivity is false, and that a more ordered connectivity would lead to less variance in the weights between groups, and would therefore be more likely to support synchronous oscillations.

I am less sure of the physiological parameters, such as the PSP functions and the refractory function. This is because there was not much data that I could use to fit them to. As chapter 8 shows, these parameters could have a profound effect on whether particular time periods and phases are stable or not.

Interestingly, previous simulations that were very similar to the current ones, apart from in the form of the refractory function (which I considered to be over-fitted), produced results that look more promising. Figure 9.10 shows a case where the older model almost worked. The weights were derived using the above equations with $T = 50\,\text{ms}$ and $\varphi = 90°$. The PNs are firing before the LNs in each cycle, though some are firing more than once (due to the refractory potential not being strong enough). The average phase looks to be about 90°. This is a further indication that the behaviour is very sensitive to the parameters of the model.

There is also a more fundamental concern about the neuron models. It could be

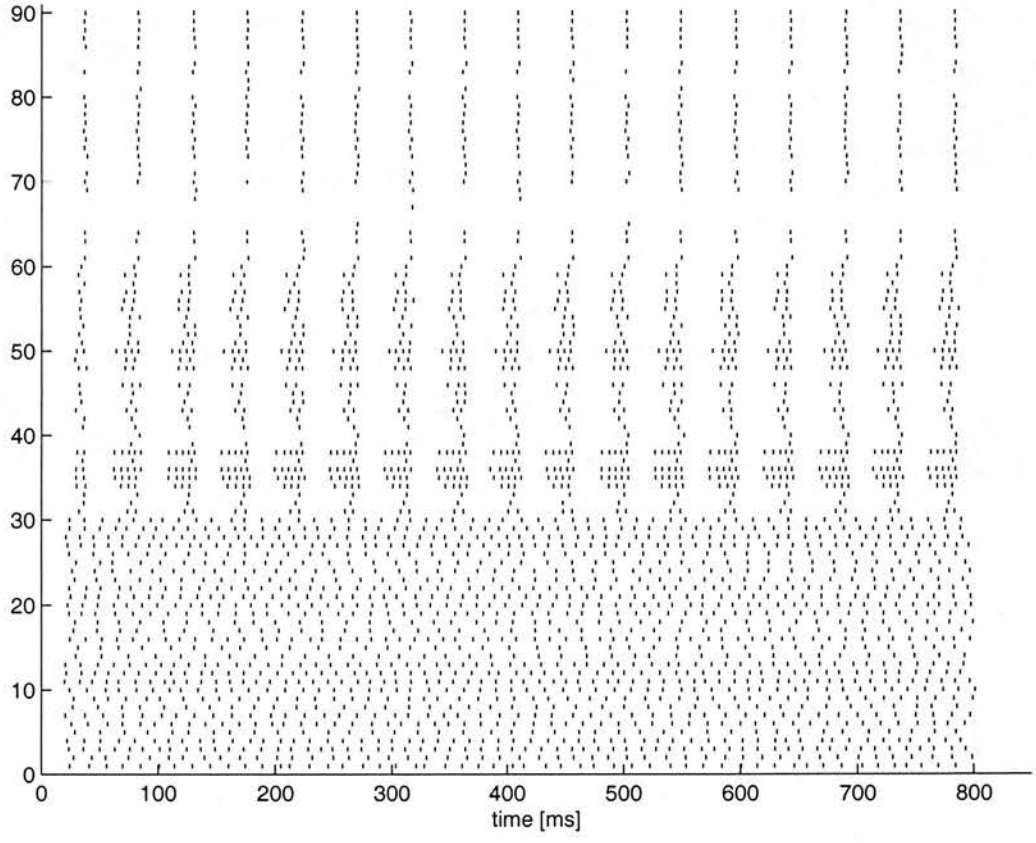

Figure 9.10: Oscillatory synchronisation of PNs and LNs in an older version of the model. Rasters 1–30 are from RNs; 31–60 are from PNs; and 61–90 are from LNs.

that ungated spiking neuron models (such as the SRM) are too simple to describe the dynamics of the locust AL. In particular, the LNs are extremely complex morphologically, and are not proper spiking neurons in the first place. It is possible that the dynamics would be easier to stabilise with conductance-based models that can incorporate shunting inhibition. The problem with using more complex neuronal models is that we do not know very much about the physiology of the PNs and LNs.

There is another reason why we might expect the neuronal model be inadequate. From the work done in chapter 8, it would appear that the time period and phase of oscillation will depend quite sensitively on the input. However, it seems that the time period and phase of oscillation is fairly constant when odours are present. It would thus appear that the simple voltage-based neurons may not be able to adapt.

9.3.2 Interpretation of the data

The data (for example, Laurent et al., 1996; figure 7.9) shows that the locking of the PN responses to the LFP oscillation is not very tight: their spikes are typically spread over quarter of a cycle. Perhaps, then, tight, synchronous locking is not the correct data to be modelling or estimating parameters by? In this case, some of the results obtained in this chapter, while not confirming that the analysis of chapter 8 extends well to variable parameters, does at least give more realistic results. In future work, the goal would be to reproduce more realistic distributions of PN spikes.

It may also be possible that the transient synchronisation of PNs is a more fundamental mechanism than the oscillations. Transient synchronisation of PNs could lead to the oscillitory activity observed. This would imply that the model should focus on the mechanism of transient oscillations. If the hypothesis is correct, the oscillations would emerge from the model. This is a possible direction for future research.

9.3.3 The parameter space

Although the work of the previous chapter tells us which regions of parameter space will not allow stable firing, it still leaves a lot of parameter space to explore, much of which is evidently unfriendly to synchronous oscillations. Assuming that the inputs are fixed by the weights $\tilde{J}_{\mathrm{PP}}$, $\tilde{J}_{\mathrm{PL}}$, $\tilde{J}_{\mathrm{LP}}$ and $\tilde{J}_{\mathrm{LL}}$, the space is four-dimensional. Although I have tried to explore part of it intelligently, I believe that it is possible that I may have missed a suitable region of parameter space. Two possible ways of locating the point in parameter space would be to improve the theory of chapter 8 or to use automated parameter space search techniques.

The theory developed in chapter 8 was not designed to deal with a large weight variance, as is present in the current model (see figure 9.6). It is possible that a more robust theory would narrow down the parameters still further, though it is also possible that the variance in the weights is insurmountable with the types of neurons and PSPs used in the model. One factor that was not considered in the theory was the relative gradients of the synaptic potential and the refractory potential. We might expect larger gradients in both potentials to lead to tighter locking. However, the theory is already fairly complicated, and I consider it unlikely that it could be extended in a useful way.

It might be worth using other techniques, such as genetic algorithms to explore the parameter space in more depth than I can. This would require a fitness function, which could be provided on the basis of automatic evaluation of spike train statistics, such as the cross- and auto-correlation functions. These should be relatively straightforward to construct. They could also be applied to more realistic data (see previous section).

9.3.4 Other mechanisms

It could be that other, non-conductance-dependent mechanisms are at work in the locust AL. For example, dynamic depressing synapses (Tsodyks and Markram, 1997) could provide a mechanism to keep the time period and phase of oscillation constant.

Depressing synapses might also have a role to play in the slow spatiotemporal patterns. Other mechanisms that might play a part in the spatiotemporal patterns are: more ordered, synfire-like connections between PNs; slow inhibition to regulate activity; and slow excitation.

9.4 Summary

From the simulations results in this chapter, it seems that applying the theoretical results of the previous chapter to the null hypothesis model of the locust AL developed in chapter 7 does not give the desired oscillations at a period of 50 ms and a phase lead of 0.25. Simulations from some areas of parameter space result in oscillations, but with multiple firing of PNs. Simulations from other areas lead to asynchrony.

There are a number of possible reasons for the failure to produce oscillations of the desired type. Firstly, the model could be intrinsically unable to oscillate in the desired fashion. This could be due to failings in extracting parameters from experimental data, mistaken assumptions, such as random connectivity, or, more fundamentally, due to using the wrong type of neuron model. Secondly, I may have not found the correct part of parameter space in which the model can produce oscillations. Possible ways around

this would be to improve or extend the analysis of chapter 8 or to use a method such as genetic algorithms to explore the parameter space more thoroughly. Finally, there may be additional mechanisms that need to be incorporated into the model for it to work. One candidate is depressing synapses and another is additional slow inhibitory neurons.

Another possibility is that the results from this chapter are in fact more realistic than tight locking would be anyway. In this case, the goal of future work should be to reproduce more realistic firing patterns.

Chapter 10

Conclusions

To conclude the thesis, I will summarise the main results in section 10.1 and outline ideas for further work in section 10.2. In section 10.3 I speculate about the future of understanding temporal phenomena in the nervous system

10.1 Contribution of the thesis

The contributions of this thesis can be divided into three categories: methodological, theoretical and modelling results.

10.1.1 Methodological results

The first methodological contribution was to simulate the network of Hansel et al. (1998) with interpolated and uninterpolated SRM neurons and compare the synchrony properties to the exact solution. This showed that a network of SRM neurons requires a smaller time step than IF neurons solved using RK2 in both the interpolated and uninterpolated cases. This is significant because it could allow faster simulation of networks of spiking neurons, especially with arbitrary PSP and refractory kernels. There is, however, a word of warning about this result. In practice, solving differential equations is faster than computing exponential functions. Thus if the network can be described by IF neurons with synaptic functions that are solutions of differential equations, this will be faster.

The second methodological achievement was to show how to simulate networks of noisy neurons with escape rate noise and interpolation. This should allow faster simulation of networks of noisy neurons. The main criticism of this work is that I have not evaluated it against a benchmark task, as I did with the deterministic network.

10.1.2 Theoretical results

The first theoretical results were to do with sequence-learning.

I derived equations for the threshold-speed relationship of a generalised synfire chain comprising discrete units that had been trained in a supervised fashion at a training speed with a temporal learning rule. I then derived a continuous approximation to it and applied both analyses to a realistic potentiation function. I showed that the discrete analysis corresponds better to physical reality than the continuous approximation to it previously studied. The novel part of this work was the idea of supervised training at a training speed and the discrete analysis. The main deficiency in this work is that it is only true in the case of perfectly uncorrelated patterns. Simulation results indicate that even small correlations have a large effect on pattern retrieval. Also, I have not taken account of weight saturation effects that would occur during the repeated presentation of a pattern sequence.

I also investigated the dynamical stability of spatiotemporal sequences learned in this way. In the discrete case the sequences are unstable at lower speeds. Thus, for low training speeds, the recall speed of chains will be higher than the speed at which they were trained. This could be of significance for (for example) motor sequences as they could be learned slowly and then speeded up.

I have applied the learning speed result to the realistic temporal potentiation function. Due to the asymmetric learning function the speed does not scale with the time constant of the potentiation function, as in previous work.

The second theoretical result has to do with synchrony. I formally extended the locking theorem of Gerstner et al. (1996b) to cover more than one group of neurons. This allows the stability of locking of groups of homogeneously connected neurons to be investigated.

I applied the extended locking theorem to neural networks comprising groups of excitatory and inhibitory neurons showing:

- that the excitatory and inhibitory neurons can only fire synchronously and alternately for certain time periods and phases of oscillation;
- how to find weights that produce a certain, allowed, time period and phase of oscillation;
- that oscillations are possible for below-threshold input to inhibitory neurons and, when the network is in a hysteresis state, for below-threshold input to excitatory neurons; and

- how the time period and phase depend on the input and vice versa.

10.1.3 Modelling results

I set up an anatomically and physiologically realistic model of the locust AL using SRM neurons. This is the first spiking neural network model of the locust AL, and should provide a basis for understanding the interplay between sequences and oscillations. I used the results from the excitatory and inhibitory groups of neurons to determine the average weight strengths.

I have implemented this model using a C++ program. However, I have not been able to get the model to reproduce some basic results from the locust olfactory system. In order to do this, I suspect that the model will have to be changed. Nevertheless, I believe that the formal description of the model may be useful to future modellers.

10.2 Further work

There are two main areas of work in this thesis that are unfinished.

The first is the learning of sequences. As the simulations showed, the theoretical results of chapter 6 only apply to network with patterns with no or very little overlap. The work that has been done on the capacity was with units with effectively square PSPs rather than smoothly-rising PSPs like alpha functions. Also, this work dealt with connections only between adjacent nodes in the synfire chain, whereas the experimentally-discovered temporal learning rule implies there ought to be connections between nodes further afield. I believe that extending the capacity calculations to more realistic networks would be a worthwhile enterprise.

The second item of unfinished business is the model of the locust AL. I have not yet succeeded in getting it to produce convincing oscillations or temporal patterns. I suspect that a reevaluation of the model will be more useful than a concerted search through parameter space to produce oscillations. More work should be done on investigating the ideas mentioned in section 7.3.1.2 in order to model the slow spatiotemporal patterns.

10.3 Outlook

Will we crack the cortical code, and if so, when? Being of cautious disposition, I am not about to hazard an answer to this question. However, I would be so bold to predict that if the cortical code is cracked, it will be as much by dint of understanding the dynamics of networks of neurons and learning in them as by postulating directly how

neurons code for things. In any case, until the cortical code is cracked, the future is bright for research into all things temporal in the nervous system.

Appendix A

Mathematical asides

A.1 Why we should expect to see more triplets

We can see this from the following calculation. We want to know what the conditional probability of finding a one unit (1-U), two unit (2-U) or three unit (3-U) triplet is, given that we have already found a triplet. Equations of the form

$$P[\text{record 1-U triplet}|\text{record triplet}] = \frac{P[\text{record 1-U triplet}]}{P[\text{record triplet}]} \tag{A.1}$$

give these conditional probabilities. In fact it is really the ratios of the conditional probabilities, so since the denominator is the same in all cases, we can concentrate on finding the numerators. The numerators are all products of the probability of impaling one, two or three neurons and the probability of the impaled neuron or neurons appearing enough times in the chain to produce a triplet, given that the chain is already impaled. The probability of a neuron being impaled is relatively easy. If there are n neurons in each node of a synfire chain with P nodes, in a network with N neurons and we record from N_R neurons we expect to record from $x = N_R nP/N$ neurons. The Poisson formula gives the number of neurons impaled:

$$P[y \text{ neurons impaled}] = e^{-x}\frac{x^y}{y!}. \tag{A.2}$$

The probability of the neurons appearing often enough in the chain so that a triplet is recorded is not so regular. When we have managed to record from three neurons from the same chain, all the neurons by definition appear once in the chain, and so the probability is 1 and When recording from one neuron we must find at least two other neurons in the chain, so

$$P[\text{record 3-U triplet}] = \frac{e^{-x}}{3!}\left(\frac{N_R nP}{N}\right)^3. \tag{A.3}$$

When two neurons are impaled, at least one of them must appear more than once in the chain, so

$$P[\text{record 2-U triplet}] = \frac{e^{-x}}{2!}\left(\frac{N_R nP}{N}\right)^2 \times 2\left(\frac{nP}{N} + \left(\frac{nP}{N}\right)^2 + \ldots\right). \tag{A.4}$$

Finally, for a 1-U triplet, the same neuron must occur at least two more times in the chain, so

$$P[\text{record 1-U triplet}] = \frac{e^{-x}}{1!}\frac{N_R nP}{N} \times \left(\left(\frac{nP}{N}\right)^2 + \left(\frac{nP}{N}\right)^3 + \ldots\right). \tag{A.5}$$

Dividing each equation by $e^{-x}(nP/N)^3$ and ignoring terms of order (nP/N), we find the ratio of these probabilities to be

$$P[\text{record 1-U triplet}] : P[\text{record 2-U triplet}] : P[\text{record 3-U triplet}] = \frac{N_R}{N^2} : \frac{N_R^2}{N} : \frac{N_R}{6}. \tag{A.6}$$

Since the total number of neurons N is much bigger than the number of neurons recorded from N_R, it is clear that we should expect to see many more repeating triplets from three different neurons than from two different neurons than from one different neuron.

A.2 Proof of the Extended Locking Theorem

To show whether the group firing times are stable to small perturbations, we can perform a linear stability analysis. Suppose that the firing times before $\varphi_l T$ are perturbed by small times $\delta_i^{(k)} \ll T \min_l \varphi_l$. The firing times are now $(k+\varphi_l)T + \delta_i^{(k)}$ for $k = 0, -1, -2, \ldots$ for a neuron in group $m < l$ and $(k+\varphi_l)T + \delta_i^{(k)}$ for $k = -1, -2, \ldots$ for a neuron in group $m \geq l$.

The slight changes in firing times will change the membrane potential slightly. An increase in membrane potential when it is near the threshold makes a neuron fire earlier. The change in firing time is greater when the rate of change of the membrane potential is small. Mathematically,

$$\delta_i^{(0)} = -\frac{\delta h_i(\varphi_l T)}{\dot{h}(\varphi_l T)} \tag{A.7}$$

where $\delta h_i(\varphi_l T)$ is the change in membrane potential due to the perturbations in the previous firing times.

We can linearise so that:

$$\eta_l(\varphi_l T - (k+\varphi_l)T - \delta_i^{(k)}) \approx \eta_l(-kT) - \dot{\eta}_{l,k}\delta_i^{(k)} \tag{A.8}$$

and

$$\varepsilon_{lm}(\varphi_l T - (k+\varphi_m)T - \delta_i^{(k)}) \approx \varepsilon_{lm}((\varphi_l - \varphi_m - k)T) - \dot{\varepsilon}_{lm,k}\delta_i^{(k)} \tag{A.9}$$

where

$$\dot{\eta}_{l,k} = \dot{\eta}_l(-kT) \text{ and } \dot{\varepsilon}_{lm,k} = \dot{\varepsilon}_{lm}((\varphi_l - \varphi_m - k)T) \ .$$

To find the small change in membrane potential $\delta h_i(\varphi_l T)$, we substitute the perturbed times for the unperturbed times in (8.2) and (8.3) and substitute the linearised expressions for the refractory, synaptic and membrane potential terms. Substituting the result in a rearranged version of (A.7) yields

$$\dot{h}_i(\varphi_l T)\delta_i^{(0)} = \tag{A.10}$$
$$\sum_{k=-1}^{-F} \dot{\eta}_{l,k}\delta_i^{(k)} + \sum_{m=1}^{l-1}\sum_{j\in\mathcal{G}_m} J_{ij}\sum_{k=0}^{1-F}\dot{\varepsilon}_{lm,k}\delta_j^{(k)} + \sum_{m=l}^{M}\sum_{j\in\mathcal{G}_m} J_{ij}\sum_{k=-1}^{-F}\dot{\varepsilon}_{lm,k}\delta_j^{(k)} \ .$$

By the law of large numbers it is reasonable to assume that mean time shifts vanish, that is $(1/N)\sum_i \delta_i^{(k)} \approx 0$. In order to simplify the problem to make it tractable we must further assume that

$$\sum_{j\in\mathcal{G}_m} J_{ij}\delta_j^{(k)} \approx 0 \ . \tag{A.11}$$

Note that this is a stricter condition than (8.1) as it implies that the weights and perturbations are uncorrelated and that the weights sample the perturbations fairly well. For example, $J_{ij} = J_0\delta_{ij}$ (where δ is here the Dirac delta) satisfies (8.1) but does not necessarily lead to (A.11).

The assumption (A.11) allows us to neglect the last two summations in (A.10) so that the only delays influencing the 0th delay of neuron $i \in \mathcal{G}_l$ are the previous delays of neuron i itself:

$$\delta_i^{(0)} = \sum_{k=-1}^{-F} A_l^{(k)}\delta_i^{(k)} \text{ where } A_l^{(k)} = \frac{\dot{\eta}_{l,k}}{\sum_{k=-1}^{-F}\dot{\eta}_{l,k} + \dot{h}_i^{\text{syn}}(\varphi_l T)} \ . \tag{A.12}$$

We can recast (A.12) in matrix form:

$$\begin{pmatrix} \delta_i^{(0)} \\ \vdots \\ \delta_i^{(1-F)} \end{pmatrix} = \mathbf{F}_l \begin{pmatrix} \delta_i^{(-1)} \\ \vdots \\ \delta_i^{(-F)} \end{pmatrix} \text{ where } \mathbf{F}_l = \begin{pmatrix} A_l^{(-1)} & A_l^{(-2)} & A_l^{(-3)} & \cdots & A_l^{(-F)} \\ 1 & 0 & 0 & \cdots & 0 \\ 0 & 1 & 0 & \cdots & 0 \\ \vdots & \vdots & \vdots & \ddots & \vdots \\ 0 & 0 & 0 & \cdots & 0 \end{pmatrix} \ .$$

The condition for stability is that as $t \to \infty$, $\delta_i^{(k)} \to 0$. In the matrix notation, this is equivalent to $\lim_{n\to\infty} \mathbf{F}_l^n(\vec{\delta}) = 0$ for an arbitrary delay vector $\vec{\delta}$. A sufficient condition for this to happen is that the eigenvalues of $\mathbf{F}_l$ all lie within the unit circle.

Gerstner et al. (1996b) use various matrix theorems to prove that $\sum_k A_l^{(k)} < 1$ is a necessary and sufficient condition for the modulus of the maximum eigenvalue to be less than one. Substituting (A.12) into this condition yields

$$\frac{\sum_{k=-1}^{-F} \dot{\eta}_{l,k}}{\sum_{k=-1}^{-F} \dot{\eta}_{l,k} + \dot{h}_i^{\text{syn}}(\varphi_l T)} < 1 \ . \tag{A.13}$$

As, in the standard dynamics, $\dot{\eta}_{l,k} > 0$, the second part of the denominator must be positive, yielding the stability condition (8.7).

Bibliography

Abbott, L. F. and Song, S. (1999). Temporally asymmetric Hebbian learning, spike timing and neuronal response variability. In Kearns, M. S., Solla, S. A., and Cohn, D. A., editors, *Advances in Neural Information Processing Systems*, volume 11. MIT Press, Cambridge, Massachusetts.

Abeles, M. (1991). *Corticonics: neural circuits of the cerebral cortex.* Cambridge University Press, Cambridge.

Abeles, M., Bergman, H., Margalit, E., and Vaadia, E. (1993). Spatiotemporal firing patterns in the frontal cortex of behaving monkeys. *Journal of Neurophysiology*, 70:1629–1638.

Abeles, M. and Gerstein, G. L. (1988). Detecting spatiotemporal firing patterns among simultaneously recorded single neurons. *Journal of Neurophysiology*, 60:909–924.

Abeles, M., Prut, Y., Bergman, H., and Vaadia, E. (1994). Synchronization in neuronal transmission and its importance for information processing. *Progress in Brain Research*, 102:395–404.

Adrian, E. D. (1928). *The Basis of Sensation: The Action of the Sense Organs.* Christophers, London.

Aertsen, A., Diesmann, M., and Gewaltig, M.-O. (1996). Propagation of synchronous spiking activity in feedforward neural networks. *Journal of Physiology (Paris)*, 90:243–247.

Amari, S.-I. (1972). Learning patterns and pattern sequences by self-organising nets of threshold elements. *IEEE Transactions on Computers*, C-21:1197–1206.

Amit, D. J. (1995). The Hebbian paradigm reintegrated: Local reverberations as internal representations. *Behavioral and Brain Sciences*, 18:617–657.

Amit, D. J. (1997). Is synchronisation necessary and is it sufficient? *Behavioral and Brain Sciences*, 20. 683.

Amit, D. J. and Brunel, N. (1997). Dynamics of a recurrent network of spiking neurons before and following learning. *Network: Computation in Neural Systems*, 8:373–404.

Amit, D. J., Gutfreund, H., and Sompolinsky, H. (1985a). Spin-glass models of neural networks. *Physical Review A*, 32:1007–1018.

Amit, D. J., Gutfreund, H., and Sompolinsky, H. (1985b). Storing infinite numbers of patterns in a spin-glass model of neural networks. *Physical Review Letters*, 55:1530–1533.

Anton, S. and Hansson, B. S. (1996). Antennal lobe interneurons in the desert locust *Schistocerca gregaria* (Forskal): processing of aggregation pheromones in adult males and females. *Journal of Comparative Neurology*, 370:85–96.

Arnoldi, H. M. R. and Brauer, W. (1996). Synchronization without oscillatory neurons. *Biological Cybernetics*, 74:209–223.

Barlow, H. B. (1972). Single units and sensation: A neuron doctrine for perception. *Perception*, 1:371–394.

Bennett, L. V. (1975). Development of a desert locust plague. *Nature*, 256:486–487.

Bi, G.-q. and Poo, M.-m. (1998). Synaptic modifications in cultured hippocampal neurons: Dependence on spike timing, synaptic strength, and postsynaptic cell type. *Journal of Neuroscience*, 18:10464–10472.

Bialek, W., Rieke, F., de Ruyter van Steveninck, R. D., and Warland, D. (1991). Reading a neural code. *Science*, 252:1854–1857.

Bienenstock, E. (1995). A model of neocortex. *Network: Computation in Neural Systems*, 6:179–224.

Bliss, T. V. P. and Collingridge, G. L. (1993). A synaptic model of memory: long-term potentiation in the hippocampus. *Nature*, 361:31–39.

Boeckh, J. (1967). Reaktionsschwelle, Arbeitsbereich und Spezifität eines Geruchsrezeptors auf der Heuschreckenantenne. *Zeitschrift für vergleichende Physiologie*, 55:378–406.

Braitenberg, V. (1978). Cell assemblies in the cerebral cortex. In Heim, R. and Palm, G., editors, *Theoretical Approaches to Complex Systems*, volume 21 of *Lecture Notes in Biomathematics*, pages 171–188. Springer-Verlag, Berlin.

Brodal, P. (1992). *The central nervous system: Structure and function.* Oxford University Press, New York.

Bugmann, G. (1997). Binding by synchronisation: A task-dependence hypothesis. *Behavioral and Brain Sciences*, 20:685.

Bullock, T. H. (1993). Integrative systems research on the brain. *Annual Review of Neuroscience*, 16:1–15.

Campbell, S. R. and Wang, D. L. (1996). Synchronization and desynchronization in a network of locally coupled Wilson-Cowan oscillators. *IEEE Transactions on Neural Networks*, 7:541–554. Description of the Wang-style relaxation oscillators for visual binding and segregation.

Carr, C. E. (1993). Processing of temporal information in the brain. *Annual Review of Neuroscience*, 16:233–43.

Christensen, T. A., Pawlowski, V. M., Lei, H., and Hildebrand, J. G. (2000). Multi-unit recordings reveal context-dependent modulation of synchrony in odor-specific neural ensembles. *Nature Neuroscience*, 3:927–931.

Crick, F. and Koch, C. (1990). Some reflections on visual awareness. *Cold Spring Harbour Symposia on Quantitative Biology*, 55:953–962.

Dayan, P. and Abbott, L. F. (2001). *Theoretical Neuroscience: Computational and Mathematical Modeling of Neural Systems*. MIT Press, Cambridge, Massachusetts.

Dayhoff, J. E. and Gerstein, G. L. (1983a). Favored patterns in spike trains. I. Detection. *Journal of Neurophysiology*, 49:1334–1348.

Dayhoff, J. E. and Gerstein, G. L. (1983b). Favored patterns in spike trains. II. Application. *Journal of Neurophysiology*, 49:1349–1363.

deCharms, R. C. and Merzenich, M. M. (1996). Primary cortical representation of sounds by the coordination of action-potential timing. *Nature*, 381:610–613.

Destexhe, A., Mainen, Z. F., and Sejnowski, T. J. (1994). An efficient model for computing synaptic conductances based on a kinetic model of receptor binding. *Neural Computation*, 6:14–18.

Diesmann, M., Gewaltig, M.-O., and Aertsen, A. (1996). Characterisation of synfire activity by propagating "pulse packets". In Bower, J. M., editor, *Computational Neuroscience: Trends in Research 1995*. Academic Press, San Diego, London.

Diesmann, M., Gewaltig, M.-O., and Aertsen, A. (1999). Stable propagation of synchronous spiking in cortical neural networks. *Nature*, 402:529–533.

Eckhorn, R., Bauer, R., Jordan, W., Brosch, M., Kruse, W., Munk, M., and Reitboeck, H. J. (1988). Coherent oscillations: a mechanism of feature linking in the visual cortex — Multiple electrode and correlation analyses in the cat. *Biological Cybernetics*, 60:121–130.

Engel, A. K., König, P., Gray, C. M., and Singer, W. (1990). Stimulus-dependent neuronal oscillations in cat visual cortex: Inter-columnar interaction as determined by cross-correlation analysis. *European Journal of Neuroscience*, 2:588–606.

Engel, A. K., König, P., Kreiter, A. K., Schillen, T. B., and Singer, W. (1992). Temporal coding in the visual cortex: new vistas on integration in the nervous system. *Trends in Neurosciences*, 15:218–226.

Ermentrout, B. (1998). The analysis of synaptically generated travelling waves. *Journal of Computational Neuroscience*, 5:191–208.

Ernst, K. D., Boeckh, J., and Boeckh, V. (1977). A neuroanatomical study on the organization of the central antennal pathways in insects: II. Deutocerebral connections *Locusta migratoria* and *Periplaneta americana*. *Cell and Tissue Research*, 176:285–308.

Faber, T., Jorges, J., and Menzel, R. (1999). Associative learning modifies neural representations of odors in the insect brain. *Nature Neuroscience*, 2:74–78.

FitzHugh, R. (1961). Impulses and physiological states in theoretical models of nerve membrane. *Biophysical Journal*, 1:445–466.

Freeman, W. J. and Skarda, C. A. (1985). Spatial EEG patterns, non-linear dynamics and perception: the Neo-Sherringtonian view. *Brain Research*, 357:147–175.

Galizia, C. G. and Menzel, R. (2000a). Odour perception in honeybees: coding information in glomerular patterns. *Current Opinion in Neurobiology*, 10:504–510.

Galizia, C. G. and Menzel, R. (2000b). Probing the olfactory code. *Nature Neuroscience*, 3:853–854.

Galizia, C. G., Sachse, S., Rappert, A., and Menzel, R. (1999). The glomerular code for odor representation in species specific in the honeybeen *Apis mellifera*. *Nature Neuroscience*, 2:473–478.

Gao, Q., Yuan, B., and Chess, A. (2000). Convergent projections of *Drosophila* olfactory neurons to specific glomeruli in the antennal lobe. *Nature Neuroscience*, 3:780–785.

Gascuel, J. and Masson, C. (1991). A quantitative ultrastructural study of the honeybee antennal lobe. *Tissue and Cell*, 23:341–355.

Gerstner, W. (1991). Associative memory in a network of 'biological' neurons. In Lippmann, R. P., Moody, J. E., and Touretzky, D. S., editors, *Advances in Neural Information Processing Systems*, volume 3, pages 84–90. Morgan Kaufmann Publishers, Inc.

Gerstner, W. (1995). Time structure of the activity in neural network models. *Physical Review E*, 51:738–758.

Gerstner, W. (1996). Rapid phase locking in systems of pulse-coupled oscillators with delays. *Physical Review Letters*, 76:1755–1758.

Gerstner, W. (1998). Spiking neurons. In Maass, W. and Bishop, C. M., editors, *Pulsed Neural Networks*, pages 3–54. MIT Press, Reading, Massachusetts.

Gerstner, W. (2000). Population dynamics of spiking neurons: Fast transients, asynchronous states, and locking. *Neural Computation*, 12:43–89.

Gerstner, W., Kempter, R., van Hemmen, J. L., and Wagner, H. (1996a). A neuronal learning rule for sub-millisecond temporal coding. *Nature*, 383:76–78.

Gerstner, W., Ritz, R., and van Hemmen, J. L. (1993a). A biologically motivated and analytically soluble model of collective oscillations in the cortex I. Theory of weak locking. *Biological Cybernetics*, 68:363–374.

Gerstner, W., Ritz, R., and van Hemmen, J. L. (1993b). Why spikes? Hebbian learning of time-resolved excitation patterns. *Biological Cybernetics*, 69:503–515.

Gerstner, W. and van Hemmen, J. L. (1992). Associative memory in a network of 'spiking' neurons. *Network: Computation in Neural Systems*, 3:139–164.

Gerstner, W. and van Hemmen, J. L. (1993). Coherence and incoherence in a globally coupled ensemble of pulse-emitting units. *Physical Review Letters*, 71:312–315.

Gerstner, W. and van Hemmen, J. L. (1994a). Coding and information processing in neural networks. In Domany, E., van Hemmen, J. L., and Shulten, K., editors, *Models of Neural Networks II: Temporal aspects of Coding and Information Processing in Biological Systems*, pages 1–94. Springer-Verlag, New York.

Gerstner, W. and van Hemmen, J. L. (1994b). How to describe neuronal activity: Spikes, rates or assemblies? In Cowan, J. D., Tesauro, G., and Alspector, J., editors, *Advances in Neural Information Processing Systems*, volume 6, pages 463–470. Morgan Kaufmann Publishers, Inc.

Gerstner, W., van Hemmen, J. L., and Cowan, J. D. (1996b). What matters in neuronal locking. *Neural Computation*, 8:1689–1712.

Golledge, H. D. R., Hilgetag, C. C., and Tovée, M. J. (1996). Information processing: A solution to the binding problem? *Current Biology*, 6:1092–1095.

Gray, C. M. (1994). Synchronous oscillations in neuronal systems: Mechanisms and functions. *Journal of Computational Neuroscience*, 1:11–38.

Gray, C. M. (1999). The temporal correlation hypothesis of visual feature integration: Still alive and well. *Neuron*, 24:31–47.

Gray, C. M., König, P., Engel, A. K., and Singer, W. (1989). Oscillatory responses in cat visual cortex exhibit inter-columnar synchronization which reflects global stimulus properties. *Nature*, 338:334–337.

Hammer, M. (1993). An identified neuron mediates the unconditioned stimulus in associative olfactory learning in honeybees. *Nature*, 366:59–63.

Hansel, D., Mato, G., Meunier, C., and Neltner, L. (1998). On numerical simulations of integrate-and-fire neural networks. *Neural Computation*, 10:467–483.

Hansson, B. S., Ochieng', S. A., Grosmaitre, X., Anton, S., and Njagi, P. G. N. (1996). Physiological responses and central nervous projections of antennal olfactory receptor neurons in the adult desert locust, *Schistocerca gregaria* (Orthoptera: Acrididae). *Journal of Comparative Physiology A*, 179:157–167.

Hebb, D. O. (1949). *The Organization of Behavior.* Wiley, New York.

Herrmann, M., Hertz, J. A., and Prügel-Bennett, A. (1995). Analysis of synfire chains. *Network: Computation in Neural Systems*, 6:403–414.

Hertz, J. and Prügel-Bennett, A. (1996). Learning short synfire chains by self-organization. *Network: Computation in Neural Systems*, 7:357–363.

Hertz, J. A. (1999). Modelling synfire chains. In Burdet, G., Combe, P., and Parodi, O., editors, *Neuronal Information Processing: From Biological Data to Modelling and Applications*, volume 7 of *Series in Mathematical Biology and Medicine.* World Scientific, Singapore. Proceedings of the Summer School *Traitement Neuronal de l'Information*, 30 June – 12 July 1997, Cargèse, France.

Hertz, J. A., Krogh, A. S., and Palmer, R. G. (1991). *Introduction to the Theory of Neural Computation.* Addison-Wesley, Reading, Massachusetts.

Herz, A., Sulzer, B., Kühn, R., and van Hemmen, J. L. (1988). The Hebb rule: Storing static and dynamic objects in an associative neural network. *Europhysics Letters*, 7:663–669.

Herz, A. V. M. and Hopfield, J. J. (1995). Earthquake cycles and neural reverberations: Collective oscillations in systems with pulse-coupled threshold elements. *Physical Review Letters*, 75:1222–1225.

Hildebrand, J. G. and Shepherd, G. M. (1997). Mechanisms of olfactory discrimination: Converging evidence for common principles across phyla. *Annual Review of Neuroscience*, 20:595–631.

Hodgkin, A. L. and Huxley, A. F. (1952). A quantitative description of membrane current and its application to conduction and excitation in nerve. *Journal of Physiology*, 117:500–544.

Hopfield, J. (1995). Pattern recognition using action potential timing for stimulus representation. *Nature*, 376:33–36.

Hopfield, J. J. (1982). Neural networks and physical systems with emergent collective computational abilities. *Proceedings of the National Academy of Sciences of the USA*, 79:2554–2558.

Hopfield, J. J. (1984). Neurons with graded response have collective computational properties like those of two-state neurons. *Proceedings of the National Academy of Sciences of the USA*, 81:3088–3092.

Hopfield, J. J. and Herz, A. V. M. (1995). Rapid local synchronization of action potentials: Toward computation with coupled integrate-and-fire neurons. *Proceedings of the National Academy of Sciences of the USA*, 92:6655–6662.

Kafka, W. A. (1970). Molekulare Wechselwirkungen bei der Erregung einzelner Riechzellen. *Zeitschrift für vergleichende Physiologie*, 70:105–143.

Kandel, E. R., Schwartz, J. H., and Jessell, T. M. (1991). *Principles of Neural Science.* Prentice-Hall International, London, third edition.

Kandel, E. R., Schwartz, J. H., and Jessell, T. M. (1995). *Essentials of Neural Science and Behaviour.* Prentice-Hall International, London.

Kandel, E. R., Schwartz, J. H., and Jessell, T. M., editors (2000). *Principles of Neural Science.* McGraw-Hill, New York, fourth edition.

Kepler, T. B., Abbott, L. F., and Marder, E. (1992). Reduction of conductance-based neuron models. *Biological Cybernetics*, 66:381–387.

Kerszberg, M. and Masson, C. (1995). Signal-induced selection among spontaneous oscillatory patterns in a model honeybee olfactory glomeruli. *Biological Cybernetics*, 72:487–495.

Kiang, N. Y. S. (1980). Processing of speech by the auditory nervous system. *Journal of the Acoustical Society of America*, 68:830–835.

Kistler, W. M., Gerstner, W., and van Hemmen, J. L. (1997). Reduction of the Hodgkin-Huxley equations to a single-variable threshold model. *Neural Computation*, 9:1015–1045.

Koch, C. and Segev, I., editors (1998). *Methods in Neuronal Modelling: From Ions to Networks.* MIT Press, Cambridge, Massachusetts, second edition.

König, P. and Schillen, T. B. (1991). Stimulus-dependent assembly formation of oscillatory responses: I. Synchronisation. *Neural Computation*, 3:155–166.

Lapicque, L. (1907). Recherches quantitatives sur l'excitation électrique des nerfs traitée comme une polarisation. *Journal of Physiology (Paris)*, 9:620–635.

Laurent, G. (1996). Dynamical representation of odors by oscillating and evolving neural assemblies. *Trends in Neurosciences*, 19:489–496.

Laurent, G. and Davidowitz, H. (1994). Encoding of olfactory information with oscillating neural assemblies. *Science*, 265:1872–1875.

Laurent, G. and Naraghi, M. (1994). Odorant-induced oscillations in the mushroom bodies of the locust. *Journal of Neuroscience*, 14:2993–3004.

Laurent, G., Stopfer, M., Friedrich, R. W., Rabinovich, M. I., Volkovskii, A., and Abarbanel, H. D. I. (2001). Odor encoding as an active, dynamical process: Experiments, computation and theory. *Annual Review of Neuroscience*, 24:263–297.

Laurent, G., Wehr, M., and Davidowitz, H. (1996). Temporal representations of odors in an olfactory network. *Journal of Neuroscience*, 16:3837–3847.

Leitch, B. and Laurent, G. (1996). GABAergic synapses in the antennal lobe and mushroom body of the locust olfactory system. *Journal of Comparative Neurology*, 372:487–514.

Lestienne, R. and Strehler, B. L. (1987). Time structure and stimulus dependence of precisely replicating patterns present in monkey cortical neuronal spike trains. *Brain Research*, 437:214–238.

Levy, W. B. (1996). A sequence predicting CA3 is a flexible associator that learns and uses context to solve hippocampal-like tasks. *Hippocampus*, 6:579–590.

Li, Z. (1990). A model of olfactory adaptation and sensitivity enhancement in the olfactory bulb. *Biological Cybernetics*, 62:349–361.

Li, Z. (1994). Modelling the sensory computation of the olfactory bulb. In Domany, E., van Hemmen, J. L., and Shulten, K., editors, *Models of Neural Networks II: Temporal aspects of Coding and Information Processing in Biological Systems*. Springer-Verlag, New York.

Li, Z. and Hertz, J. (2000). Odour regonition and segmentation by a model olfactory bulb and cortex. *Network: Computation in Neural Systems*, 11:83–102.

Li, Z. and Hopfield, J. J. (1989). Modelling the olfactory bulb and its neural oscillatory processings. *Biological Cybernetics*, 61:379–392.

Linster, C. and Hasselmo, M. (1997). Modulation of inhibition in a model of olfactory bulb reduces overlap in the neural representation of olfactory stimuli. *Behavioural Brain Research*, 84:117–127.

Linster, C. and Masson, C. (1996). A neural model of olfactory sensory memory in the honeybee's antennal lobe. *Neural Computation*, 8:94–114.

Linster, C., Masson, C., Kerszberg, M., Personnaz, L., and Dreyfus, G. (1993). Computational diversity in a formal model of the insect olfactory macroglomerulus. *Neural Computation*, 5:228–241.

Linster, C. and Smith, B. H. (1997). A computational model of the response of honey bee antennal lobe circuitry to odour mixtures: overshadowing, blocking and unblocking can arise from lateral inhibition. *Behavioural Brain Research*, 97:1–14.

Little, W. A. (1974). The existence of persistent states in the brain. *Mathematical Biosciences*, 19:101–120.

Little, W. A. and Shaw, G. L. (1978). Analytic study of the memory storage capacity of a neural network. *Mathematical Biosciences*, 39:281–290.

Maass, W. (1996). Networks of spiking neurons: The third generation of neural network models. Technical Report NC-TR-96-045, ESPRIT Working Group in Neural and Computational Learning.

Maass, W. (1997). Fast sigmoidal networks via spiking neurons. *Neural Computation*, 9:279–304.

MacKay, D. M. (1962). Self-organization in the time domain. In Yovits, M. C., Jacobi, G. T., and Goldstein, G. D., editors, *Self-Organising Systems 1962*, pages 37–48. Spartan Books, Washington.

MacLeod, K. and Laurent, G. (1996). Distinct mechanisms for synchronization and temporal patterning of odor-encoding neural assemblies. *Science*, 274:976–979.

Marczynski, T. J., Burns, L. L., and Marczynski, G. T. (1980). Neuronal firing patterns in the feline hippocampus during sleep and wakefulness. *Brain Research*, 185:139–160.

Marczynski, T. J. and Sherry, C. J. (1971). A new analysis of trains of increasing or decreasing interspike intervals treated as self-adjusting sets of ratios. *Brain Research*, 35:533–538.

Markram, H., Lübke, J., Frotscher, M., and Sakmann, B. (1997). Regulation of synaptic efficiency by coincidence of postsynaptic APs and EPSPs. *Science*, 275:213–215.

Masson, C. and Mustaparta, H. (1990). Chemical information processing in the olfactory system of insects. *Physiological Reviews*, 70:199–245.

McClelland, J. L., McNaughton, B. L., and O'Reilly, R. C. (1995). Why there are complementary learning systems in the hippocampus and neocortex: Insights from the successes and failures of connectionist models of learning and memory. *Psychological Review*, 102:419–457.

Meddis, R. (1986). Simulation of mechanical to neural transduction in the auditory receptor. *Journal of the Acoustical Society of America*, 79:702–711.

Milner, P. M. (1974). A model for visual shape recognition. *Psychological Review*, 81:521–535.

Mirollo, R. E. and Strogatz, S. H. (1990). Synchronization of pulse-coupled biological oscillators. *SIAM Journal of Applied Mathematics*, 50:1645–1662.

Mori, K., Nagao, H., and Sasaki, Y. F. (1998). Computation of molecular information in mammalian olfactory systems. *Network: Computation in Neural Systems*, 9:R79–R102.

Murlis, J., Elkinton, J. S., and Cardé, R. T. (1992). Odour plumes and how insects use them. *Annual Review of Entomology*, 37:505–532.

Neuenschwander, S. and Singer, W. (1996). Long-range synchronization of oscillatory light responses in the cat retina and lateral geniculate-nucleus. *Nature*, 379:728–733.

Nishimori, H., Nakamura, T., and Shiino, M. (1990). Retrieval of spatio-temporal sequence in asynchronous neural network. *Physical Review A*, 41:3346–3354.

Oram, M. W., Wiener, M. C., Lestienne, R., and Richmond, B. J. (1999). Stochastic nature of precisely timed spike patterns in visual system neuronal responses. *Journal of Neurophysiology*, 81:3021–3033.

Palm, G. (1990). Assoziatives Gedächtnis und Gehirntheorie. *Spektrum der Wissenschaft*, "Gehirn und Kognition", Artikelsammlung, pp. 164–174.

Perkel, D. A., Gerstein, G. L., and Moore, G. P. (1967a). Neuronal spike trains and stochastic point processes: I. The single spike train. *Biophysical Journal*, 7:391–418.

Perkel, D. A., Gerstein, G. L., and Moore, G. P. (1967b). Neuronal spike trains and stochastic point processes: II. Simultaneous spike trains. *Biophysical Journal*, 7:419–440.

Phillips, W. A. and Singer, W. (1997). In search of common foundations for cortical computation. *Behavioral and Brain Sciences*, 20:657–682.

Press, W. H., Teukolsky, S. A., Vetterling, W. T., and Flannery, B. P. (1992). *Numerical Recipes in C.* Cambridge University Press, Cambridge, second edition.

Prut, Y., Vaadia, E., Bergman, H., Haalman, I., Slovin, H., and Abeles, M. (1998). Spatiotemporal structure of cortical activity: Properties and behavioral relevance. *Journal of Neurophysiology*, 79:2857–2874.

Rabinovich, M., Bazhenov, M., Heurta, R., Abarbanel, H. D. I., and Laurent, G. (1998). A model of transient synchronization in locust antennal lobe circuits. In *Society for Neuroscience Abstracts*, volume 24, page 910.

Richmond, B. J., Optican, L. M., Podell, M., and Spitzer, H. (1987). Temporal encoding of two-dimensional patterns by single units in primate inferior temporal cortex. I. Response characteristics. *Journal of Neurophysiology*, 57:133–146.

Rieke, F., Warland, D., de Ruyter van Steveninck, R., and Bialek, W. (1997). *Spikes: Exploring the neural code.* MIT Press, Cambridge, Massachusetts.

Rumelhart, D. E., McClelland, J. L., and Williams, R. J. (1986). Learning internal representation by error propagation. In Rumelhart, D. E., McClelland, J. L., and the PDP Research Group, editors, *Parallel Distributed Processing*, volume 1, chapter 8. MIT Press, Cambridge, Massachusetts.

Schillen, T. B. and König, P. (1991). Stimulus-dependent assembly formation of oscillatory responses: II. Desynchronisation. *Neural Computation*, 3:167–178.

Schillen, T. B. and König, P. (1994). Binding by temporal structure in multiple frequency domains of an oscillatory neuronal network. *Biological Cybernetics*, 70:397–405.

Shadlen, M. N. and Newsome, W. T. (1994). Noise, neural codes and cortical organization. *Current Opinion in Neurobiology*, 4:569–579.

Shepherd, G. M. (1994). *Neurobiology.* Oxford University Press, New York, third edition.

Shepherd, G. M., editor (1998). *The Synaptic Organization of the Brain.* Oxford University Press, New York, fourth edition.

Singer, W. (1994). The role of synchrony in neocortical processing and synaptic plasticity. In Domany, E., van Hemmen, J. L., and Shulten, K., editors, *Models of Neural Networks II: Temporal aspects of Coding and Information Processing in Biological Systems*, pages 141–174. Springer-Verlag, New York.

Singer, W. and Gray, C. M. (1995). Visual feature integration and the temporal correlation hypothesis. *Annual Review of Neuroscience*, 18:555–586.

Smith, L. S., Cairns, D. E., and Nischwitz, A. (1994). Synchronization of integrate-and-fire neurons with delayed inhibitory connections. In Marinaro, M. and Morasso, P. G., editors, *Proceedings of ICANN94*, pages 142–145. Springer-Verlag.

Spiridon, M. and Gerstner, W. (1999). Noise spectrum and signal transmission through a population of spiking neurons. *Network: Computation in Neural Systems*, 10:257–272.

Spruston, N., Schiller, Y., Stuart, G., and Sakmann, B. (1995). Activity-dependent action potential invasion and calcium influx into hippocampal CA1 dendrites. *Science*, 268:297–300.

Sterratt, D. C. (1999). Is a biological temporal learning rule compatible with learning synfire chains? In *ICANN99: Ninth International Conference on Artificial Neural Networks*, pages 551–556. Institute of Electrical Engineers, London.

Sterratt, D. C. (2001). Locust olfaction: Synchronous oscillations in excitatory and inhibitory groups of spiking neurons. In Wermter, S., Austin, J., and Willshaw, D., editors, *Emergent Neural Computational Architectures Based on Neuroscience*, volume 2036 of *Lecture Notes in Artificial Intelligence*. Springer-Verlag, Berlin Heidelberg.

Stopfer, M., Bhagavan, S., Smith, B. H., and Laurent, G. (1997). Impaired odour discrimination on desynchronization of odour-encoding neural assemblies. *Nature*, 390:70–74.

Stopfer, M. and Laurent, G. (1999). Short-term memory in olfactory network dynamics. *Nature*, 402:664–668.

Strausfeld, N. J., Hansen, L., Li, Y., Gomez, R. S., and Ito, K. (1998). Evolution, discovery and interpretations of arthropod mushroom bodies. *Learning and Memory*, 5:11–37.

Stuart, G. J. and Sakmann, B. (1994). Active propagation of somatic action potentials into neocortical pyramidal cell dendrites. *Nature*, 367:69–72.

Theunissen, F. and Miller, J. P. (1995). Temporal encoding in nervous systems: A rigorous definition. *Journal of Computational Neuroscience*, 2:149–162.

Tsodyks, M., Mitkov, I., and Sompolinsky, H. (1993). Pattern of synchrony in inhomogeneous networks of oscillators with pulse interactions. *Physical Review Letters*, 71:1280–1283.

Tsodyks, M. V. and Feigel'man, M. V. (1988). The enhanced storage capacity in neural networks with low activity level. *Europhysics Letters*, 6:101–105.

Tsodyks, M. V. and Markram, H. (1997). The neural code between neocortical pyramidal neurons depends on transmitter release probability. *Proceedings of the National Academy of Sciences of the USA*, 94:719–723.

Tuckwell, H. C. (1988a). *Introduction to theoretical neurobiology: volume 1, linear cable theory and dendritic structure*, volume 8 of *Cambridge studies in mathematical biology*. Cambridge University Press, Cambridge, UK.

Tuckwell, H. C. (1988b). *Introduction to theoretical neurobiology: volume 2, nonlinear and stochastic theories*, volume 8 of *Cambridge studies in mathematical biology*. Cambridge University Press, Cambridge, UK.

Vaadia, E., Haalman, I., Abeles, M., Bergman, H., Prut, Y., Slovin, H., and Aertsen, A. (1995). Dynamics of neuronal interactions in monkey cortex in relation to behavioural events. *Nature*, 373:515–518.

van Vreeswijk, C. (1996). Partial synchronisation in populations of pulse-coupled oscillators. *Physical Review E*, 54:5522–5537.

van Vreeswijk, C., Abbott, L. F., and Ermentrout, G. B. (1994). When inhibition not excitation synchronises neural firing. *Journal of Computational Neuroscience*, 1:313–321.

Vickers, N. J., Christensen, T. A., Baker, T. C., and Hildebrand, J. G. (2001). Odour-plume dynamics influence the brain's olfactory code. *Nature*, 410:466–470.

Villa, A. E. P. and Abeles, M. (1990). Evidence for spatiotemporal firing patterns within the auditory thalamus of the cat. *Brain Research*, 509:325–327.

von der Malsburg, C. (1981). The correlation theory of brain function. Technical Report 81–2, Max Planck Institute for Biophysical Chemistry. Reprinted in E. Domany, J. L. van Hemmen, and K. Shulten, editors (1994), *Models of Neural Networks II: Temporal aspects of Coding and Information Processing in Biological Systems*, pages 95–120. Springer-Verlag, New York.

von der Malsburg, C. and Buhmann, J. (1992). Sensory segmentation with coupled neural oscillators. *Biological Cybernetics*, 67:233–242.

von der Malsburg, C. and Schneider, W. (1986). A neural cocktail-party processor. *Biological Cybernetics*, 54:29–40.

Waloff, Z. and Green, S. M. (1975). Regularities in duration of regional desert locust plagues. *Nature*, 256:484–485.

Wang, D. (1996). Synchronous oscillations based on lateral connections. In Sirosh, J., Miikkulainen, R., and Choe, Y., editors, *Lateral Interactions in the Cortex: Structure and Function.* The UTCS Neural Networks Research Group, Austin, TX. Electronic book, ISBN 0-9647060-0-8, http://www.cs.utexas.edu/users/nn/web-pubs/htmlbook96.

Wang, D. L. L. and Brown, G. J. (1999). Separation of speech from interfering sounds based on oscillatory correlation. *IEEE Transactions on Neural Networks*, 10:684–697.

Wehr, M. and Laurent, G. (1996). Odour encoding by temporal sequences of firing in oscillating neural assemblies. *Nature*, 384:162–166.

Wehr, M. and Laurent, G. (1999). Relationship between afferent and central temporal patterns in the locust olfactory system. *Journal of Neuroscience*, 19:381–390.

Wennekers, T. (1999a). Analysis of spatio-temporal patterns in associative networks of spiking neurons. In *ICANN99: Ninth International Conference on Artificial Neural Networks.* Institute of Electrical Engineers, London.

Wennekers, T. (1999b). *Synchronisation und Assoziation in Neuronalen Netzen.* Berichte aus der Informatik. Shaker Verlag, Aachen. PhD Thesis.

Wennekers, T. and Palm, G. (1996). Controlling the speed of synfire chains. In v. d. Malsburg, C., v. Seelen, W., Vorbrüggen, J. C., and Sendhoff, B., editors, *Artificial Neural Networks — ICANN96*, volume 1112 of *Lecture Notes in Computer Science.* Springer-Verlag, Berlin, Heidelberg, New York.

Wennekers, T. and Palm, G. (2000). Cell assemblies, associative memory and temporal structure in brain signals. In Miller, R., editor, *Time and the Brain*, volume 3 of *Conceptual Advances in Brain Research.* Harwood Academic Publishers.

Willshaw, D. J., Buneman, O. P., and Longuet-Higgins, H. C. (1969). Non-holographic associative memory. *Nature*, 222:960–962.

Wilson, H. R. and Cowan, J. D. (1972). Excitatory and inhibitory interactions in localized populations of model neurons. *Biophysical Journal*, 12:1–24.

Wilson, M. and Bower, J. M. (1992). Cortical oscillations and temporal interactions in a computer simulation of piriform cortex. *Journal of Neurophysiology*, 67:981–995.

Wilson, M. A. and Bower, J. M. (1988). A computer simulation of olfactory cortex with functional implications for storage and retrieval of olfactory information. In Anderson, D., editor, *Advances in Neural Information Processing Systems*, volume 0, pages 114–126. American Institute of Physics.

Wilson, M. A. and Bower, J. M. (1991). A computer simulation of oscillatory behavior in primary visual cortex. *Neural Computation*, 3:498–509.

Zhang, L. I., Tao, H. W., Holt, C. E., Harris, W. A., and Poo, M. M. (1998). A critical window for cooperation and competition among developing retinotectal synapses. *Nature*, 395:37–44.

List of Citations

Abbott and Song (1999), 43
Abeles and Gerstein (1988), 63
Abeles et al. (1993), 60, 64–66
Abeles et al. (1994), 61, 62
Abeles (1991), 47, 53–57, 61, 67, 113, 144
Adrian (1928), 1, 14, 15
Aertsen et al. (1996), 57
Amari (1972), 48
Amit and Brunel (1997), 54, 78
Amit et al. (1985a), 6
Amit et al. (1985b), 6, 7
Amit (1995), 25
Amit (1997), 78
Anton and Hansson (1996), 125, 132, 136, 137, 152
Arnoldi and Brauer (1996), 59, 103
Barlow (1972), 15, 39, 78
Bennett (1975), 115
Bi and Poo (1998), 41–43, 113
Bialek et al. (1991), 21–23
Bienenstock (1995), 25, 58, 59, 61, 112
Bliss and Collingridge (1993), 40, 43
Boeckh (1967), 133
Braitenberg (1978), 50
Brodal (1992), 12, 13
Bugmann (1997), 75
Bullock (1993), 23
Campbell and Wang (1996), 79
Carr (1993), 72
Christensen et al. (2000), 125
Crick and Koch (1990), 77
Dayan and Abbott (2001), 20, 21
Dayhoff and Gerstein (1983a), 63
Dayhoff and Gerstein (1983b), 63
Destexhe et al. (1994), 98
Diesmann et al. (1996), 57
Diesmann et al. (1999), 57, 58
Eckhorn et al. (1988), 75
Engel et al. (1990), 19, 75
Engel et al. (1992), 75, 76
Ermentrout (1998), 30, 31, 39, 59, 103, 107, 110–112
Ernst et al. (1977), 120–122, 131–133, 148, 150
Faber et al. (1999), 122, 127, 142
FitzHugh (1961), 29
Freeman and Skarda (1985), 124, 125
Galizia and Menzel (2000a), 119, 124, 126
Galizia and Menzel (2000b), 126
Galizia et al. (1999), 124, 127
Gao et al. (2000), 123, 124
Gascuel and Masson (1991), 148
Gerstner and van Hemmen (1992), 32, 37, 38, 60, 166
Gerstner and van Hemmen (1993), 83, 85
Gerstner and van Hemmen (1994a), 32, 37
Gerstner and van Hemmen (1994b), 34, 80
Gerstner et al. (1993a), 32, 38, 85
Gerstner et al. (1993b), 41, 43, 52, 144
Gerstner et al. (1996a), 155
Gerstner et al. (1996b), 4, 79, 85, 157, 166–168, 184, 190
Gerstner (1991), 29, 32
Gerstner (1995), 35, 36, 38, 39, 85
Gerstner (1996), 82
Gerstner (1998), 16, 32, 36, 39
Gerstner (2000), 35, 36, 38, 44, 83, 167
Golledge et al. (1996), 78
Gray et al. (1989), 62, 75

Gray (1994), 62, 72
Gray (1999), 78
Hammer (1993), 127, 129
Hansel et al. (1998), 89–101, 183
Hansson et al. (1996), 131, 133
Hebb (1949), 6, 39, 40
Herrmann et al. (1995), 49, 57–59, 113
Hertz and Prügel-Bennett (1996), 67, 113
Hertz et al. (1991), 4, 6, 33, 50
Hertz (1999), 57, 58, 68, 113
Herz and Hopfield (1995), 84
Herz et al. (1988), 52
Hildebrand and Shepherd (1997), 115–117, 119, 121–123
Hodgkin and Huxley (1952), 26–28
Hopfield and Herz (1995), 82, 83
Hopfield (1982), 5, 6, 40, 44, 49
Hopfield (1984), 5, 44
Hopfield (1995), 139
König and Schillen (1991), 44, 80, 81
Kafka (1970), 133, 134, 145
Kandel et al. (1991), 149, 150
Kandel et al. (1995), 11
Kandel et al. (2000), 127
Kepler et al. (1992), 29
Kerszberg and Masson (1995), 129, 148
Kiang (1980), 72, 73
Kistler et al. (1997), 38, 152
Koch and Segev (1998), 16, 19
Lapicque (1907), 26, 29
Laurent and Davidowitz (1994), 23, 125, 135–137, 139, 141, 153
Laurent and Naraghi (1994), 125, 144
Laurent et al. (1996), 125, 136, 139–141, 180
Laurent et al. (2001), 121, 122, 125
Laurent (1996), 23, 119, 122, 123, 125, 126, 136, 139
Leitch and Laurent (1996), 119, 132, 149, 150
Lestienne and Strehler (1987), 63
Levy (1996), 47, 50, 51, 60
Li and Hertz (2000), 130
Li and Hopfield (1989), 123, 130, 142
Linster and Hasselmo (1997), 130
Linster and Masson (1996), 128, 129, 142
Linster and Smith (1997), 129
Linster et al. (1993), 128, 131, 142, 146
Little and Shaw (1978), 5
Little (1974), 5
Li (1990), 130
Li (1994), 130
Maass (1996), 25
Maass (1997), 25
MacKay (1962), 1
MacLeod and Laurent (1996), 125, 132, 136–139, 141
Marczynski and Sherry (1971), 63
Marczynski et al. (1980), 63
Markram et al. (1997), 41
Masson and Mustaparta (1990), 119, 121, 131, 132, 148
McClelland et al. (1995), 68, 103
Meddis (1986), 30
Milner (1974), 74
Mirollo and Strogatz (1990), 82, 83, 155, 167
Mori et al. (1998), 117, 118, 121, 123, 124
Murlis et al. (1992), 117, 126–128
Neuenschwander and Singer (1996), 75
Nishimori et al. (1990), 50
Oram et al. (1999), 64, 66
Palm (1990), 50
Perkel et al. (1967a), 16, 17, 19, 37
Perkel et al. (1967b), 19
Phillips and Singer (1997), 77, 78
Press et al. (1992), 89, 92
Prut et al. (1998), 64–66
Rabinovich et al. (1998), 152
Richmond et al. (1987), 16
Rieke et al. (1997), 14–16, 19, 21, 23
Rumelhart et al. (1986), 8, 40
Schillen and König (1991), 44, 80, 81
Schillen and König (1994), 80
Shadlen and Newsome (1994), 25, 65
Shepherd (1994), 10, 13, 48

Shepherd (1998), 118, 121, 123
Singer and Gray (1995), 75
Singer (1994), 77
Smith et al. (1994), 83–85, 155
Spiridon and Gerstner (1999), 44
Spruston et al. (1995), 43
Sterratt (1999), 104
Sterratt (2001), 156
Stopfer and Laurent (1999), 127, 142
Stopfer et al. (1997), 79, 125, 141
Strausfeld et al. (1998), 119
Stuart and Sakmann (1994), 43
Theunissen and Miller (1995), 21, 24
Tsodyks and Feigel'man (1988), 58
Tsodyks and Markram (1997), 30, 68, 144, 181
Tsodyks et al. (1993), 83, 84
Tuckwell (1988a), 29
Tuckwell (1988b), 28, 29
Vaadia et al. (1995), 19, 20
Vickers et al. (2001), 117
Villa and Abeles (1990), 64
Waloff and Green (1975), 115
Wang and Brown (1999), 80
Wang (1996), 79
Wehr and Laurent (1996), 125, 137, 138
Wehr and Laurent (1999), 136, 139, 152, 153
Wennekers and Palm (1996), 59, 103, 104, 108, 111–113
Wennekers and Palm (2000), 60
Wennekers (1999a), 56, 58
Wennekers (1999b), 59, 60, 62
Willshaw et al. (1969), 40
Wilson and Bower (1988), 130
Wilson and Bower (1991), 77, 78
Wilson and Bower (1992), 130
Wilson and Cowan (1972), 44, 79, 155, 167
Zhang et al. (1998), 41, 42, 53, 104, 108, 112
deCharms and Merzenich (1996), 74
van Vreeswijk et al. (1994), 31, 83, 84, 155, 167
van Vreeswijk (1996), 83, 84
von der Malsburg and Buhmann (1992), 80
von der Malsburg and Schneider (1986), 79
von der Malsburg (1981), 74, 79